ADDIS ABABA UNIVERSITY
SCHOOL OF GRADUATE STUDIES

Electrochemical and Optical Studies of Electronically Conducting Polymers for Use in Electronic Devices

by

Shimelis Admassie

A thesis submitted in partial fulfillment of
the requirements for the degree of

Doctor of Philosophy

Addis Ababa University

May 2006

CONTENT

Acknowledgment....iv
List of Figures....vi
List of Tables....xiv
List of Appendices....xv
Abstract....xvi

1. Introduction to Electronically Conducting Polymers......1
1.1.History of Conducting Polymers....1
1.2. Chemical and Electronic Structure of ECPs....2
1.3. Electrochemical and Spectroscopic Concepts and Techniques....8
1.3.1. Electrochemical Cells and Reactions 8
1.3.2. Cyclic Voltammetry, Chronoampereometry and
Square Wave Voltammetry....11
1.3.3. Absorption and Emission Spectroscopy 18
1.4. Electrochemical Spectroscopy of Electronically Conducting Polymers....22
1.5. Polymer Photovoltaic Cells....27
1.5.1 Introduction....27
1.5.2. Working Principles of Polymer Solar Cells 28
1.5.3. Preparation of Polymer Solar Cells....30
1.5.4. Characterization of Polymer Solar Cells 31
1.5.5. Optimization of the Efficiencies of Polymer Solar Cells....32
1.5.5.1. Light Absorption....32
1.5.5.2. Charge Separation....34
1.5.5.3. Charge Transport....35
1.5.5.4. Charge Collection....36
1.6. Polymer Light Emitting Diodes....37
1.6.1 Introduction....37
1.6.2 The Basic Operational Principles of Polymer Light Emitting
Diodes....38
1.6.3 Preparation and Characterization of Polymer Light Emitting

Diodes.....39
1.6.4 Some Strategies to Optimize the Efficiencies of Polymer Light Emitting Diodes.....41
1.6.4.1. Low work function cathode.....41
1.6.4.2. Bilayer Devices.....41
1.6.4.3. Blend Devices.....42
1.6.4.4. Single layers with electron transporting units.....43
1.7. Chromism in Electronically Conducting Polymers.....44
1.7.1. Polymeric Electrochromism.....44
1.7.1.1. Introduction.....44
1.7.1.2 Types of Electrochromic Materials.....44
1.7.1.3 Polythiophenes as Electrochromic Materials.....45
1.7.1.4 Origin of Electrochromism in Conjugated Polymers.....47
1.7.1.5 Characterization Parameters of Electrochromic Materials.....48
1.7.1.6 Characterization Methods of Electrochromic Materials.....50
1.7.2. Polymeric Thermochromism and Solvatochromism.....52
1.8 Objectives of the Study and Organization of Subsequent Chapters.....58
1.9 References.....59

2. Electrochemical Studies of Electronically Conducting Polymers.....67
2.1.Background.....67
2.2.Experimental.....68
2.3. Results and Discussion.....69
2.3.1. Electrochemical and optical studies of the band gaps of alternating polyfluorene copolymers.....69
2.3.2. Characterization of electronically conducting polymers designed for polymer solar cells.....81
2.3.2.1. Structure-property relationships in low band gap alternating polyflourene copolymers designed for polymer solar cells.....81
2.3.2.2. Structure-property relationships in low band gap

homopolymers designed for polymer solar cells.....87
2.3.2.3. Optical and electrochemical properties of conjugated polymers incorporating oxadiazole units.....91
2.3.3. Characterization of electronically conducting polymers designed for polymer light emitting diodes.....95
2.3.3.1. Characterization of alkoxyphenyl-substituted polyfluorenes with hole transporting triphenyl amine units.....95
2.3.3.2. Characterization of anthracene and benzothiadiazole containing polyflourene copolymers.....97
2.4. Conclusions.....101
2.5. References.....102

3. Vapour Phase Polymerized (VPP) PEDOT as Electrode Material for Polymer Solar Cells.....105
3.1. Background.....105
3.2. Experimental.....108
3.3. Results and Discussion.....111
3.3.1. A polymer photodiode using VPP PEDOT as an anode.....111
3.3.2. A polymer photodiode using VPP PEDOT as a cathode.....116
3.4. Conclusions.....119
3.5. References.....119

4. Chromism in Electronically Conducting Polymers.....122
4.1.Background.....122
4.2. Experimental.....124
4.3 Results and Discussions.....126
4.3.1. Electrochromism in Diffractive Conducting Polymer Gratings.....126
4.3.2. Electrochromism in Conducting Polymer Bilayer System.....134
4.3.3. Chromic Transitions in Phenyl-Substituted Polythiophenes.....143
4.4. Conclusions.....149
4.5. References.....151

Acknowledgment

I have no words to express my gratitude to my God who opened the various doors giving me the wisdom, energy and health to carry out this research work and endure all the hardships.

I am greatly indebted to my research advisors Prof. Theodros Solomon and Dr. Teketel Yohannes for their continuous guidance and encouragements to carry out this research work under difficult circumstances and with the very limited material and financial support. Dr. Wendimagegn Mamo has earned my deepest gratitude and sincere respect for supplying almost all of the polymers used in this research work and for the knowledge and experience I gained from him through a friendship relationship.

This research work would not have reached this stage without the unreserved help of Prof. Olle Inganäs of the University of Linköping (LiU) and his research group who guided me for most of the work and allowed me to work in his research group with great freedom covering all the financial costs related to the research work. I want to say thank you very much to Drs. F. Zhang, X. Wang and Abay Gadissa for their help in preparing and characterizing the PSCs and PLEDs devices. I am thankful to the Center of Organic Electronics at LiU for covering my living expenses for six months in Sweden. Moreover, I am greatly indebted to the Organization for the Prohibition of Chemical Weapons (OPCW) for covering my travel and living expenses during my six months stay in Sweden. I am also grateful for the Addis Ababa University for allowing me to join the PhD program, granting me the study leave and the financial help to cover my travel and living expenses during my six months stay in Sweden and to buy some locally available materials.

I have also been specially privileged to get different kinds of assistances and guidance from almost all staff members of the Department of Chemistry, AAU and many friends elsewhere. I would like to specially thank Drs. Ghirma Moges, Bernd Hundhammer, Tarekegn G/Yesus, Ahmed Mustefa, Mesfin Reddi, Regien Stomphorst, Profs. Berhanu M. Abegaz, Ermias Dagne, Negussie Retta, Ato Terefe Getaneh, Abay Gadisa, Sefiu Belew, Tarekegn Berhanu and Ahmed Hussien for their many help and encouragements.

I am deeply grateful to the support, prayer and guidance I enjoyed from the members of the Sharholmen Church, particularly Mengesha, Sisay, Yohannes and their families. Tigist Aberra and Muluken Tafesse deserve my special thank you for all you did and it is my prayer for God to meet all your needs. I cannot forget the encouragement and prayer support of Evan. Bekele G/Michael, Yonas Beyene, Fekede Teferra, Abera Mitiku, Nigatu Abera and many others and may God also hear your prayers and bless you richly!

My wife, Tewab, endured a preoccupied husband without compliant and took the full responsibility of managing the home and caring our children. May God grant her His reward in this life and the life after for everything she sacrificed for our home as a godly woman! Tibarek, Nathnael, Salem and all our family members, I want to say thank you very much and God bless you for understanding and helping your Mom during those difficult times.

List of Figures

1.1 Conductivity of conducting polymers....2

1.2 The chemical structure of examples of conjugated polymers....3

1.3 Calculated energy levels of oligothiophenes with n = 1-4 and of polythiophene, where E_g is the band gap....4

1.4 Trans- and cis-polyacetylene....5

1.5 Neutral, positive, and negative solitons and their corresponding energy band diagrams....5

1.6 The aromatic and quinoid forms of ECPs....6

1.7 (a) Structure of a conjugated polymer at increasing levels of oxidation. (b) Electronic band structure of the conjugated polymer (i) polymer in insulating state, (ii) partially oxidized polaron state; (iii) fully oxidized bipolaron state....7

1.8 Schematic diagram of a cell for voltammetric measurements: w.e., working electrode; r.e., reference electrode; c.e., counter electrode. The electrodes are inserted through holes in the cell cover....8

1.9 A complete cell stand....9

1.10 Representation of (a) reduction and (b) oxidation process of a species, A, in solution. The molecular orbitals (MO) of species A shown are the highest occupied MO and the lowest vacant MO....10

1.11 Potential-time signal in cyclic voltammetric experiment....12

1.12 Typical cyclic voltammogram for a reversible O + ne- = R redox process....12

1.13 Cyclic voltammetry of C_{60} and C_{70} in an acetonitrile-toluene solution....14

1.14 Cyclic voltammograms for irreversible (curve A) and quasi-reversible (curve B) redox processes....14

1.15 (a) Potential-time waveform and (b) the resulting current flow *vs* time for chronoamperometric experiment....15

1.16 Double potential step chronoamperometry. (a) Typical wave form. (b) current response....16

1.17 Wave form and measurement scheme for square wave voltammetry....17

1.18 A typical current *vs* potential response curve in square wave voltammetry....17

1.19 Energy levels of molecular orbitals in formaldehyde and possible electronic transitions....18
1.20 Distinction between singlet and triplet states, using formaldehyde as an example....19
1.21 Perrin-Jablonski diagram and illustration of the relative positions of absorption, fluorescence and phosphorescence spectra....21
1.22 Cyclic voltammograms of regioregular poly(3-octylthiophene) recorded in 0.1 M Bu_4NBF_4 solution in acetonitrile (E measured *vs* Ag/AgC1 reference electrode)....24
1.23 Uv-vis-nir spectroelectrochemical curves recorded for regioreguiar poly(3-octylthiophene) in 0.1M Bu_4NBF_4 solution in acetonitrile: (a) E = 0 mV; (b) E = 500 mV; (c) E = 800 mV; (d) E = 900 mV; (e) E = 1000 mV; (f) E = 1200 mV; (g) E =1400 mV (E measured *vs* Ag/AgC1 reference electrode)....24
1.24 Relationship between the electrochemically measured onset potentials, E'_{ox} and E'_{red}, and the ionization potential, IP, and the band gap, E_g....25
1.25 Schematic illustration of (a) the device structure of an polymer solar cell, (b) flow chart showing the steps involved in the conversion of light to an electric current, and (c) the energy levels and light harvesting. Upon irradiation an electron is promoted to the LUMO leaving a hole behind in the HOMO. Electrons are collected at the Al electrode and holes at the ITO electrode, Φ: workfunction, χ: electron affinity, IP: ionisation potential, E_g: optical band gap 29
1.26 Schematic diagram of an polymer solar cell design....30
1.27 I–V curves of an polymer solar cell under dark (a) and illuminated (b) conditions. The open-circuit voltage (V_{OC}) and the short-circuit current (I_{SC}) are shown. The maximum output is given by the square $I_{max}V_{max}$....31
1.28 Solar irradiance spectrum (broad curve) and the cumulative integral of the irradiance (thin curve)....33
1.29 Dissociation of electron-hole pair at the donor-acceptor interface. The electron goes to the acceptor while the hole stays on the donor....35
1.30 (a) Schematic drawing of a single-layer electroluminescent device, (b) photoluminescence and (c) electroluminescence process in polymer LED....39

1.31 Typical variations of the current density J and of the luminance L with applied voltage V in an OLED. Insert: Typical absorption (ABS), photoluminescence (PL) and electroluminescence (EL) spectra of an organic material.....40
1.32 Chemical structures of some polymers used in bilayer devices.....42
1.33 Chemical structures of some polymers and small molecules used in blend devices.....42
1.34 Chemical structures of some polymers used in single layer devices.....43
1.35 Baytron P (Bayer AG, Leverkusen, Germany), which is a dispersion of the oxidized polymer PEDOT and the polyanion PSS in water.....46
1.36 Optical absorption spectra of a PEDOT/PSS cell for different voltages, i.e. different oxidation levels..... 47
1.37 Electrochromic switching of PEDOT/PSS.....48
1.38 Schematic diagram of a solid-state electrochromic device (ECD) suitable for a transmissive light-modulation application.....51
1.39 Temperature-dependent UV-vis absorption spectrum of sodium poly(2-(4-methyl-3-thienyloxy)ethanesulfonate) in water, upon heating.....53
1.40 Temperature-dependent UV-vis absorption spectrum of sodium poly(2-(3-thienyloxy)ethanesulfonate) in water, upon heating.....54
1.41 Temperature-dependent (A) and solvent-dependent (v/v) (B) UV-vis absorption spectra of poly(1,4-(2,5-dioctyloxyphenylene)-2,5-thiophene).....55
1.42 Ground-state potential energy surfaces of 1-(2,5-dimethoxyphenylene)-2'-thiophene (DMOPT) and 1-(2,5-diethylphenylene)-2'-thiophene (DIETPT).....56
1.43 Temperature-dependent (A) and solvent-dependent (v/v) (B) UV-Vis absorption spectra of poly(1,4-(2,5-dioctylphenylene)-2,5-thiophene).....57
2.1. Chemical structures of the polymers investigated.....69
2.2. UV-Vis absorption spectrum of (■) APFO 1, (●) APFO 2, (▲) APFO 3, (▼) APFO 8, (♦) APFO 5, (◄) APFO 9, and (►) APFO 10 polymer films coated on a glass substrate.....70
2.3. UV-Vis absorption spectrum of (■) APFO-Green 2, (●) APFO 11, (▲) APFO 12, (▼) APFO 13, and (♦) APFO-Green 1 polymer films coated on a glass substrate.....70
2.4. Cyclic voltammogram (first scans) of APFO 1-3, APFO 5, APFO 8-10,

APFO-Green 1 and APFO-Green 2 films casted on a platinum disk electrode in Bu_4NBF_4/AcN supporting electrolyte/solvent system at a scan rate of 100 mV/s.....71
2.5. Cyclic voltammogram (first scans) of (a) background; (b) APFO 13; (c) APFO 12 and (d) APFO 11 polymer films casted on a platinum disk electrode in Bu_4NBF_4/AcN supporting electrolyte/solvent system at a scan rate of 100 mV/s.....71
2.6. Cyclic voltammogram (○) background; (▲) first scan; (●) second scan and (♦) third scan for APFO 3 polymer films casted on a platinum disk electrode in Bu_4NBF_4/AcN supporting electrolyte/solvent system at a scan rate of 100 mV/s. The insert shows the n-doping region separately drawn to show the clear resolution of the first reduction peaks on the second and third scans.....72
2.7. Cyclic voltammogram (a) background; (third scans) of (b) APFO 3, (d) APFO-Green 2 and (e) APFO-Green 1 polymer films casted on a platinum disk electrode in Bu_4NBF_4/AcN supporting electrolyte/solvent system at a scan rate of 100 mV/s.....73
2.8. A diagram showing the method used to estimate onset values for oxidation and reduction potentials.....74
2.9. A plot of the electrochemical band gap determined from onset (●) and peak averages (■) against the optical band gap determined from maximum absorption wavelength.....76
2.10. A plot of the energies of HOMO from peak averages (▲), from onset (■) and LUMO from peak average (▼) and onset (●) for the polymers investigated.....76
2.11. Square wave voltammograms (third scans) for (a) APFO 3, (b) APFO-Green 2 and (d) APFO-Green 1 films casted on a platinum disk electrode in Bu_4NBF_4/AcN supporting electrolyte/solvent system.....77
2.12. Repeating units used in the MNDO calculations.....80
2.13. MNDO calculated energies of HOMO and LUMO of the various repeating units.....80
2.14. The chemical structure of the low band gap alternating polyfluorene copolymers APFO 14, APFO 15, APFO-Green 4, APFO-Green 5, and APFO-Green 6.....81
2.15. The optical absorption spectrum of the low band gap polymers (▲)APFO 14,

(○)APFO-Green 5, (★)APFO-Green 6, (△)APFO 15, and (▽)APFO-Green 4.....82
2.16. Cyclic voltammograms for the p-doping region of polymers (▲) APFO 14, (○) APFO-Green 5, (★)APFO-Green 6, (△)APFO 14, and (▽)APFO-Green 4 films solvent casted on Pt disk electrode in 0.1 M TBATFB/AcN supporting electrolyte.....83
2.17. Cyclic voltammograms for the n-doping region of polymers (▲) APFO 14, (○) APFO-Green 5, (★)APFO-Green 6, (△)APFO 14, and (▽)APFO-Green 4 films solvent casted on Pt disk electrode in 0.1 M TBATFB/AcN supporting electrolyte.....83
2.18. Square wave voltammograms of polymers (▲) APFO 14, (○) APFO-Green 5, (★)APFO-Green 6, (△)APFO 14, and (▽)APFO-Green 4 films solvent casted on Pt disk electrode in 0.1 M TBATFB/AcN supporting electrolyte.....84
2.19. The chemical structure of the low band gap homo polymers P1-P5.....87
2.20. The optical absorption spectrum of the low band gap polymers (▲) P1, (○) P2, (★) P3, (△) P4, and (▽) P5.....88
2.21. Cyclic voltammograms of polymers P1-P5 films solvent casted on Pt disk electrode in 0.1 M TBATFB/AcN supporting electrolyte.....89
2.22. The chemical structures of oxadiazole containing polymers P6-P9.....91
2.23. Absorption and emission spectra for polymers (•) P6, (□) P7, (▲) P8 from chloroform solution and (★) P6, (△) P7, (○) P8 from films casted on glass from a chloroform solution.....92
2.24. Cyclic voltammograms of polymers (△) P6, (▲) P7, (○) P8 and (•) P9 films solvent casted on Pt disk electrode in 0.1M TBATFB/AcN supporting electrolyte.....93
2.25. Cyclic voltammograms of P7 on Pt disk electrode in 0.1 M TBATFB/can supporting electrolyte at a sweep rate of 5, 10, 20, 50 and 100 mV/s. The insert shows a plot of the peak current as a function of sweep rate.....94
2.26. Chemical structures of polymers P10-P13. Polymers P11, P12 and P13 contains 10, 25% and 50% of the triphenylamine-substituted fluorene units respectively.....95
2.27. UV-Vis absorption together with PL- and EL-emission spectra for P11.....96
2.28. Chemical Structures of Polymers P14-P16.....97
2.29. UV-Vis absorption spectrum of polymers (□) P14, (★) P15 and

(▲) P16; photoluminescence emission of polymers (△) P14, (▽) P15 and (•) P16; and electroluminescence emission of polymers (○) P14, (◁) P15 and (▼) P16.....98
2.30. Cyclic voltammogram of (○) background, polymers (□) P14, (△) P15 and (■) P16 casted on a glassy carbon disk electrode in Bu_4NFB_4/AcN supporting electrolyte/solvent system at 100 mV/s..... 99
2.31. Current density-voltage characteristics of polymers (■) P14, (▲) P15 and (•) P16…...100
2.32. Electroluminescence intensity versus the applied potential of polymers (■) P14, (▲) P15 and (•) P16..... 100
3.1. The chemical structures used in the device fabrication.....109
3.2. Solar cell device structure made of glass/conductive anode/active layer/LiF/Al.....109
3.3. The schematic illustration of the top and bottom components of the solar cells device where VPP PEDOT is used as a cathode.....110
3.4. General schematic diagram for photovoltaic measurements. (a) Power supply, (b) lamp housing, (c) monochromator, (d) sample holder and (e) an output measuring instrument.....110
3.5. Transparencies of the various anodes used in the device in the range 350-800 nm.....111
3.6. AFM image of VPP PEDOT films.....112
3.7. IPCE of photodiodes with different anode materials.....113
3.8. I-V characteristics of photovoltaic devices with different anodes under AM1.5 illumination without LiF layer.....113
3.9. I-V characteristics of photovoltaic devices with different anodes under AM1.5 illumination with LiF layer.....114
3.10. Semi-log of I-V characteristics of photovoltaic devices with different anodes in the dark without LiF layer.....114
3.11. Semi-log of I-V characteristics of photovoltaic devices with different anodes in the dark with LiF layer.....115
3.12. The photocurrent image of a typical device.....116
3.13. The incident photon to current conversion efficiency (IPCE) of a typical device.....117
3.14. The current-voltage characteristics measured under dark conditions.....118
4.1. Schematic diagram of apparatus used for spectroelectorchemical switching measurements.....125

4.2. Inverted microscopic images of (a) patterned PEDOT-PSS film formed with the 300 lines/mm gratings with 4.3 μm gap width, (b) patterned PEDOT-PSS film formed with the 600 lines/mm gratings with 1.6 μm gap width.....126
4.3. AFM images of patterned PEDOT-PSS film formed with the (a) 300 lines/mm: height of the ridges about 410 nm and the period is about 3.164 μm, (b) 600 lines/mm: height of the ridges about 140 nm and the period is about 1.494 μm.....128
4.4. Ex-situ static spectroelectrochemistry of unpatterned PEDOT-PSS film on ITO/glass electrode in 0.1 M TEATFB in acetonitrile at (a) +0.2, (b) –0.2, (c) –0.6 and (d) –1.2 V.....129
4.5. Ex-situ static spectroelectrochemistry of patterned PEDOT-PSS film on ITO/glass electrode in 0.1 M TEATFB in acetonitrile at (a) +0.2, (b) –0.2, (c) –0.6 and (d) –1.2 V.....129
4.6. Comparison of the ex-situ static spectroelectrochemistry of unpatterned and patterned PEDOT-PSS film on ITO/glass in 0.1 M TEATFB in acetonitrile: (a) patterned film at +0.2 V, (b) unpatterned film at +0.2 V, (c) unpatterned film at –0.6 V and (d) patterned film at –0.6 V.....130
4.7. Comparison of the in-situ static spectroelectrochemistry of PEDOT-PSS film on ITO/glass electrode in 0.1 M TEATFB in acetonitrile (i) unpatterned at (a) +0.2 V, (b) –0.2 V, (c) –0.6 V and (ii) patterned at (d) +0.2 V, (e) –0.2 V, (f) –0.6 V.....131
4.8. Comparison of the change in % transmittance vs time of (a) unpatterned and (b) patterned PEDOT-PSS film on ITO/glass in TEATFB in acetonitrile when the potential is stepped between –0.6 and +0.6 V. at 610 nm.....132
4.9. The change in current vs time of (a) unpatterned and (b) patterned PEDOT-PSS film on ITO/glass in TEATFB in acetonitrile when the potential is stepped between –0.6 and +0.6 V, simultaneously measured with the optical measurement shown in Figure 4.8.....132
4.10. Chemical structures of the polymers used to make bilayer.....135
4.11. Effect of supporting electrolyte/solvent system on the absorption behavior of Polymer I coated on ITO: (a) in the dry state, (b) dipped into $LiCLO_4$/MeOH, (c) TEAP/AcN supporting electrolyte/solvent system.....135
4.12. Effect of supporting electrolyte/solvent system on the absorption behavior of

Polymer II coated on ITO: (a) in the dry state, (b) dipped into $LiClO_4$/MeOH supporting electrolyte/solvent system.....136
4.13. Static ex-situ spectroelectrochemistry of polymer I spin-coated on PEDOT-PSS/ITO/glass electrode in 0.1 M TEATFB in acetonitrile at (a) +0.8 V (b) +0.4 V, (c) 0.0 V, (d) –0.4 V (e) –1.2 v and (f) –1.8 V.....136
4.14. Static ex-situ spectroelectrochemistry of polymer II spin-coated on PEDOT-PSS/ITO/glass electrode in 0.1 M TEATFB in acetonitrile at (a) +0.4 V (b) +0.0 V, (c) –0.4 V, (d) –1.0 V (e) –1.4 V and (f) –1.8 V.....137
4.15. Static ex-situ spectroelectrochemistry of polymer I coated on PEDOT-PSS/ITO/glass at (a) +0.8 V; (b) –1.8 V and (c) +0.8 V after going to –1.8 V showing the reversibility in the color of the polymer.....138
4.16. Static ex-situ spectroelectrochemistry of polymer II coated on PEDOT-PSS/ITO/glass at (a) +0.8 V; (b) –1.8 V, (c) +0.8 V after going to –1.8 V and (d) –1.8 V after going to +0.8 V, showing the reversibility.....138
4.17. Comparison of the Absorbance vs wavelength for (i) single layer of Polymer I at (a) +0.2 V, (b) –0.2 V, (c) –0.6 V; (ii) single layer of PEDOT-PSS at (d) +0.2 V, (e) –0.2 V, (f) –0.6 V; (iii) bilayer of PEDOT-PSS with Polymer I at (g) +0.2 V, (h) –0.2 V, (i) –0.6 V.....139
4.18. Absorbance *vs* wavelength plot for glass/ITO/Polymer II in $LiClO_4$/MeOH at two different potentials showing (a) the neutral and (b) doped state.....140
4.19. Comparison of the % transmittance *vs* time plots for (a) glass/ITO/PEDOT-PSS/Polymer II, (b) glass/ITO/PEDOT-PSS/Polymer I bilayer in TEATFB/acetonitrile.....141
4.20. % transmittance *vs* time plots for glass/ITO/Polymer II, in $LiClO_4$/MeOH supporting electrolyte/solvent system when the potential is switched between –0.2 and +0.8 V *vs* Ag/Ag^+ at 515 nm.....142
4.21. % transmittance *vs* time plots for glass/ITO/PEDOT-PSS/Polymer I, in TEAFB/AcN supporting electrolyte/solvent system when the potential is switched between –0.6 and +0.6 V *vs* Ag/Ag^+ at 630 nm.....142
4.22. Chemical structures of polymers 1-9.....144
4.23. UV-Vis optical absorption spectra of polymer 6 at: (a) 18^{o}C, (b) 85^{o}C,

and (c) 150^{o}C.....145
4.24. UV-Vis optical absorption spectra of polymer 8 at: (a) 18^{o}C, (b) 85^{o}C,
and (c) 150^{o}C.....146
4.25. UV-Vis optical absorption spectra of polymer 1 in chloroform/methanol
mixtures at different mole fractions of methanol: (a) 0.0, (b) 0.36, and
(c) 0.64.....147
4.26. UV-Vis optical absorption spectra of polymer 7 in chloroform/methanol
mixtures at different mole fractions of methanol: (a) 0.0, (b) 0.36, (c) 0.64, (d) 0.85,
and (e) 0.96.....147
4.27. Potential energy curve (a) polymer 1, (b) polymer 2, (c) polymer 3, (d) polymer 4,
and (e) polymer 5.....148
4.28. Potential energy curve (a) polymer 6, (b) polymer 7, (c) polymer 8, and
(d) polymer 9.....148

List of Tables

1.1. Electrochromic transition in some polythiophenes.....46
2.1.Summary of the electrochemical and optical data of the series of alternating polyfluorene copolymers determined from peak values.....74
2.2. Summary of the electrochemical and optical data of the series of alternating polyfluorene copolymers determined from onset values.....75
2.3. The onset-potentials and the corresponding LUMO and HOMO values as a function of sweep rate for APFO 3.....78
2.4. The onset-potentials and the corresponding LUMO and HOMO values as a function of sweep rate for APFO-Green 2.....78
2.5. The onset-potentials and the corresponding LUMO and HOMO values as a function of sweep rate for APFO-Green 1.....79
2.6. Optical properties of polymers APFO 14, APFO 15, APFO-Green 4, APFO-Green 5, and APFO-Green 6.....82
2.7. Onset potential values (*vs* Ag/AgCl), estimated HOMO and LUMO levels and comparison with open circuit potential for APFO 14, APFO 15, APFO-Green 4, APFO-Green 5, and APFO-Green 6.....85
2.8. Half-wave potential values (*vs* Ag/AgCl) and estimation of HOMO and LUMO levels for APFO 14, APFO 15, APFO-Green 4, APFO-Green 5, and APFO-Green 6.....85
2.9. Optical properties of polymers P1-P5.....88
2.10. Peak and half wave potentials (*vs* Ag/AgCl) of polymers P1-P5.....89
2.11. Onset potential values (vs Ag/AgCl), estimation of HOMO and LUMO levels and comparison with open circuit potential for polymers P1-P5.....89
2.12. Absorption and emission maxima of the polymers P1-P4 in solution and films.....92
2.13. Peak and half-wave potentials (*vs* Ag/AgCl) of polymers P6-P9.....93
2.14. Onset potential values (*vs* Ag/AgCl) and estimation of HOMO and LUMO levels for polymers P6-P9.....94
2.15. Electrochemical properties of polymers P10-P13.....96
2.16. Photoluminescence efficiencies (ϕ_{PL}) in chloroform solution and external

quantum efficiencies (EQE) of the devices.....97
2.17. Optical absorption and emission properties of polymers P14-P16.....99
2.18. Summary of the electrochemical data for polymers P14-P16.....99
3.1. Summary the anode conductivities and transmission values.....111
3.2. Summary of the photovoltaic characteristics of the devices made without LiF.....115
3.3. Summary of the photovoltaic characteristics of the devices made with LiF.....116
4.1. Effect of Potential Limits on the Electrochromic Properties for Patterned PEDOT-PSS Film.....133
4.2. The electrochromic properties of spin-coated PEDOT-PSS on ITO glass without patterning and patterned PEDOT-PSS film when the potential is scanned between –0.6 to + 0.6 V.....134
4.3. Comparison of the absorption maxima in the solution and condensed phase for the polymers investigated.....143
4.4.Comparison of the absorption maxima at two different temperatures for the polymers investigated.....145
4.5. Summary of the energy barrier to rotation to a planar structure for the dimer molecules of the polymers whose structures are shown in Figure 4.21.....149

List of Appendices

Appendix A: Computational Methods Employed.....I

Abstract

The electrochemical and optical properties of a series of low band gap alternating polyfluorene copolymers and polythiophene derivatives with quinoxaline units were characterized optically and electrochemically for use in polymer solar cells. The polymers have band gaps ranging from 2.1-0.8 eV. A structure-property correlation, which sheds light on the design of efficient devices, was observed. Oxadiazole-containing polymers were also optically and electrochemically characterized for polymer/polymer blend devices. Most of the polymers gave good electrochemical reversible reduction behavior with very high ionization potential (> 6.1 eV) and very high electron affinities (3.5-3.6 eV). A series of alkoxyphenyl-substituted fluorene units together with different amounts of a hole-transporting triphenylamine-substituted fluorene units designed for light-emitting devices were characterized. All polymers show high photoluminescence efficiency and light emission in the blue spectral region. Electrochemical studies shows more pronounced reversible behaviour and hence, improved hole-transport, as the ratio of the hole-transporting unit is increased. The electroluminescence quantum efficiencies of the devices increase six times going from **P10** to **P11**. Compared with **P11**, polymers **P12** and **P13** show lower efficiencies in devices. These findings indicate the presence of an optimal polymer composition, where balance between the charge-carrier mobilities has been reached. Anthrancene and benzothiadiazole containing polyfluorene copolymers (**P14-P16**) were also characterized. Polymers **P15** and **P16** show high photoluminescence efficiency while polymer **P15** does not show any significant light emission up to 8.0 V. The results also show the need for balance of electron and hole injection and transport in polymer light emitting diodes. The photovoltaic properties of devices made using a highly conducting polymer electrode, from vapor-phase polymerized poly(3,4-ethylenedioxy)thiophene (VPP PEDOT) on glass substrate as an anode and a polyfluorene copolymer, **APFO-3**, mixed with PCBM as the active layer. The device performance was compared with that of devices made with PEDOT-PSS on glass substrates. The device performance of solar cells constructed from the VPP PEDOT made on a flexible and transparent substrate as a cathode material and ITO/ PEDOT:PSS films supported on glass substrates as anode were characterized. The devices have shown good electrical and optical responses. The electrochromic polymer PEDOT-PSS spin coated on ITO/glass was patterned with soft lithographic method in order to diffract the incident light, and thereby modify absorption of light by the film to improve the electrochromic efficiency of the polymer. The absorbance peak at around 610 nm was found to be much higher in the patterned PEDOT-PSS film than the one observed in the unpatterned film. Values of coloration efficiencies varying from 107 to 174 cm^2/C were obtained for three different unpatterned PEDOT-PSS films, where as for three different patterned PEDOT-PSS films higher values ranging from 204 to 371 cm^2/C were found. These increased values of the electrochromic efficiencies are attributed to diffraction. The electrochromic behaviours of some polythiophenes were also investigated in bilayer system. The solvatochromic and thermochromic behaviors of phenyl-substituted polythiophenes were studied. The pristine polymers, upon dissolution in chloroform, exhibited blue-shifted absorption. The solid films of the polymers showed significant blue-shifted as well as red-shifted absorptions when heated. While the addition of methanol to the chloroform solutions of the polymers caused dramatic chromic changes and development of red-shifted spectra for many of the polymers investigated, the symmetrically phenyl-substituted and sterically hindered polymer (polymer **P1**) does not show significant changes. These chromic behaviors have been examined in terms of substituent effects and attempt has been made to explain these effects by calculating the energy barrier for rotation to a planar structure using the HF SCF method and 3-21G* basis set.

1 Introduction to Electronically Conducting Polymers

1.1. History of Conducting Polymers

Polymers are substances consisting of large molecules also known as macromolecules. The molecules are built up of many subunits called monomers which are linked together, usually by covalent bonds. In a polymer, the number of subunits is larger than 100 [1]. Assemblies of less than 100 subunits are often referred to as oligomers. Polymers are traditionally known for electrically insulating properties. Since the first report of doping of polyacetylene in 1977 by A. J. Heeger, A.G. MacDiarmid and H. Shirakawa (Nobel prize in 2000) [2-4], conducting polymers, i.e., polymers with alternating single and double bonds, have been studied extensively as a novel class of electronic materials. One of the common features of conducting polymers as compared to conventional sigma (σ)-bonded nonconducting polymers is that they have small band gaps, relatively large electron affinities and small ionization potentials, which result in low energy excitations. As a consequence, conducting polymers are suitable for a wide range of electronic and optical applications. Another exciting common features of conducting polymer is that the conductivity can be increased by over 10 orders of magnitude upon doping, undergoing an insulator to metal transition. For example, the room temperature conductivity of polyacetylene changes from ~ 10^{-13} – 10^{-5} S/cm to greater than 10^{5} S/cm upon doping with iodine [5-8], a value close to the conductivity of copper (~ $5x10^{5}$ S/cm) (Figure 1.1). Combining the novel electronic and optical properties of modern solid-state materials with the strength of flexibility and conventional processability of polymers, conducting polymers have shown a tremendous potential for technological application. Conducting polymers have been used successfully as active materials in thin film transistors (TFT) [9-11], light emitting devices (LED) [12-15], photovoltaics (PV) [17-19] and integrated circuits (IC) [20-22].

The discovery of electroluminescence (EL) in 1990 from a non-doped conducting polymer thin film [12], sandwiched between electrodes, motivated many researchers to

study the semiconducting properties of the conjugated polymer even though polymer diodes were fabricated and characterized in the 1980s.

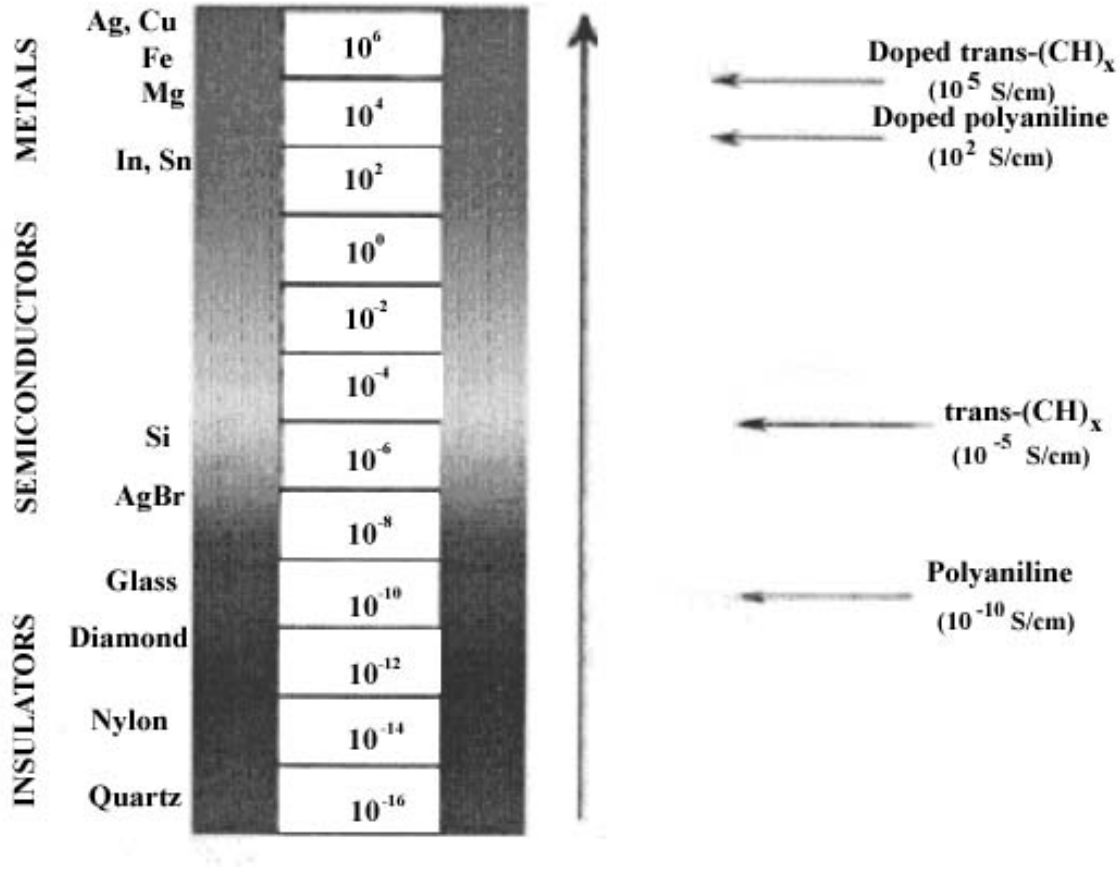

Figure 1. 1 *Conductivity of conducting polymers*.

1.2. Chemical and Electronic Structure of ECPs

Conducting polymers can be divided into two classes: redox polymers and π-conjugated polymers or electronically conducting polymers. The redox polymers have one or more redox groups attached to the main chain. This redox group may be oxidised and an ion in the electrolyte will compensate that charge. Then, the next redox group is oxidised while the former one is reduced and an electron is transferred. In this way a charge moves from redox site to redox site, yielding an electrical current. This current, however, is small and the material gives a low conductivity [23].

π-conjugated polymers or electronically conducting polymers, consist of alternate single and double carbon–carbon bonds (Figure 1.2).

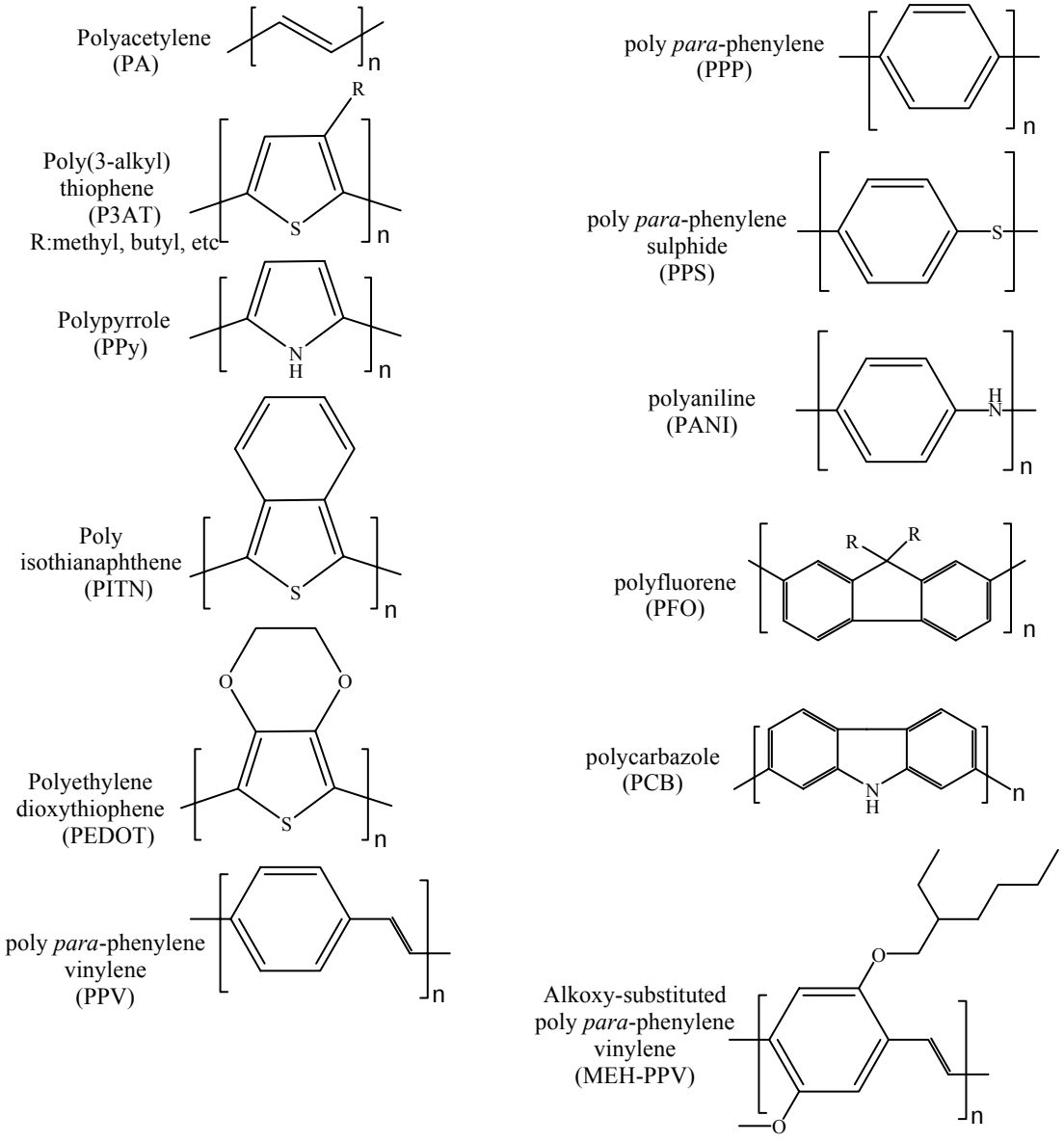

Figure 1. 2 *The chemical structure of examples of conjugated polymers.*

The band structure of a conjugated polymer originates from the interaction of the π-orbitals of the repeating units throughout the chain. This is exemplified in Figure 1.3 where the calculated energy levels of oligothiophenes with n = 1- 4 and of polythiophene are shown as a function of oligomer length [24]. The addition of every new thiophene unit causes hybridization of the energy levels yielding more and more levels until a point

is reached at which there are bands rather than discrete levels. Interaction between the π-electrons of neighboring molecules leads to a three-dimensional band structure.

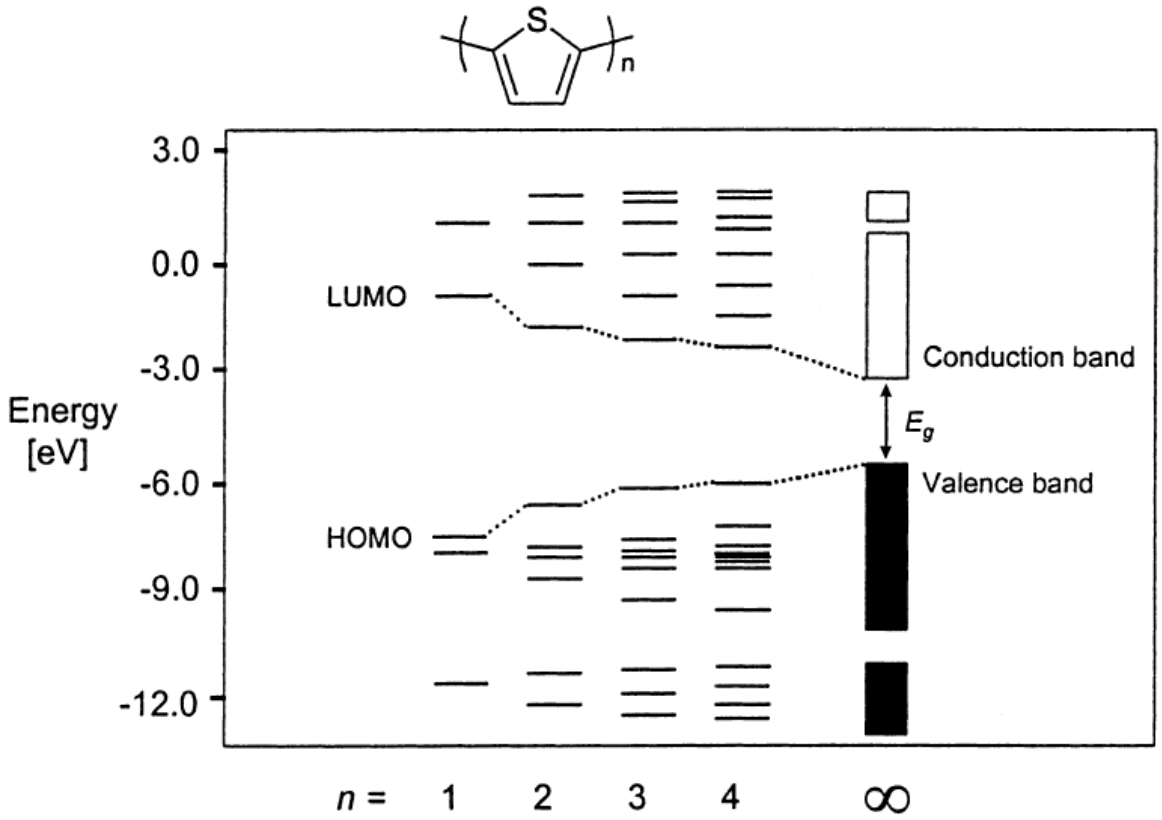

Figure 1.3 *Calculated energy levels of oligothiophenes with n = 1-4 and of polythiophene, where E_g is the band gap.*

Analogous to semiconductors, the highest occupied band (which originates from the HOMO of a single thiophene unit) is called the valence band, while the lowest unoccupied band (originating from the LUMO of a single thiophene unit) is called the conduction band. The difference in energy between these levels is called the band gap (E_g). Since π-conjugated polymers allow virtually endless manipulation of their chemical structure, control of the band gap of these semiconductors is a research issue of ongoing interest. This band gap engineering gives the polymer its desired electrical and optical properties, and reduction of the band gap to approximately zero is expected to afford an intrinsically conducting polymer [25-26].

Polyacetylene has two *trans* and two *cis* structures (Figure 1.4). The two *trans* structures are energetically degenerate. On the other hand the two *cis* structures are not energetically equivalent and therefore have a non-degenerate ground state. The quinoid *cis* structure is of higher energy than the aromatic *cis* structure.

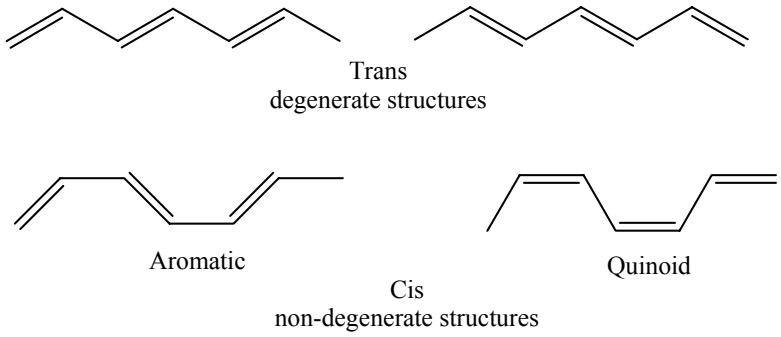

Figure 1.4 *Trans- and cis-polyacetylene.*

If the two degenerate structures of *trans*-polyacetylene are on the same chain, they will be separated by a defect in the bond alternation as shown in Figure 1.5.

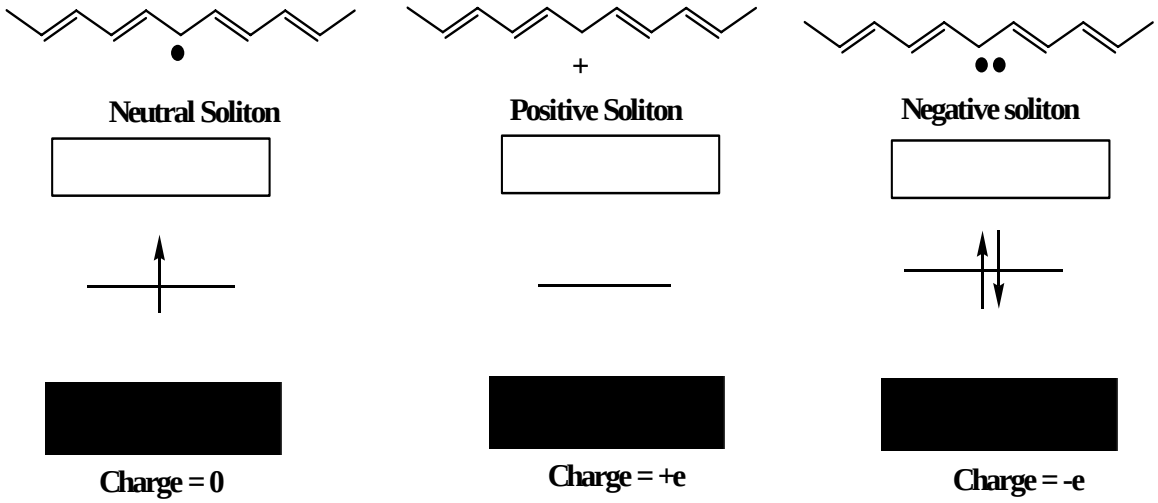

Figure 1.5 *Neutral, positive, and negative solitons and their corresponding energy band diagrams.*

The carbon atom between the conjugated segments will be sp^3-hybridized and contains one unpaired electron although the overall charge remains zero. As a result, a new localized electronic state is created at the middle of the forbidden gap, i.e., the unpaired

electron resides in a non-bonding orbital. These conformational defects are called solitons. The soliton is positively charged with spin zero when the electron is removed and negatively charged with spin zero when electron is added. The band diagrams and the three different types of solitons are shown schematically in Figure 1.5.

In other ECPs, there are two different non-degenerate structures known as aromatic and quinoid (Figure 1.6). The energy of the aromatic form is lower than the energy of the quinoid form and the ground state of a non-degenerate conjugated polymer corresponds to the aromatic structure. One therefore cannot utilize the concept of soliton in these kinds of ECPs. The charge carriers are known as polarons and bipolarons.

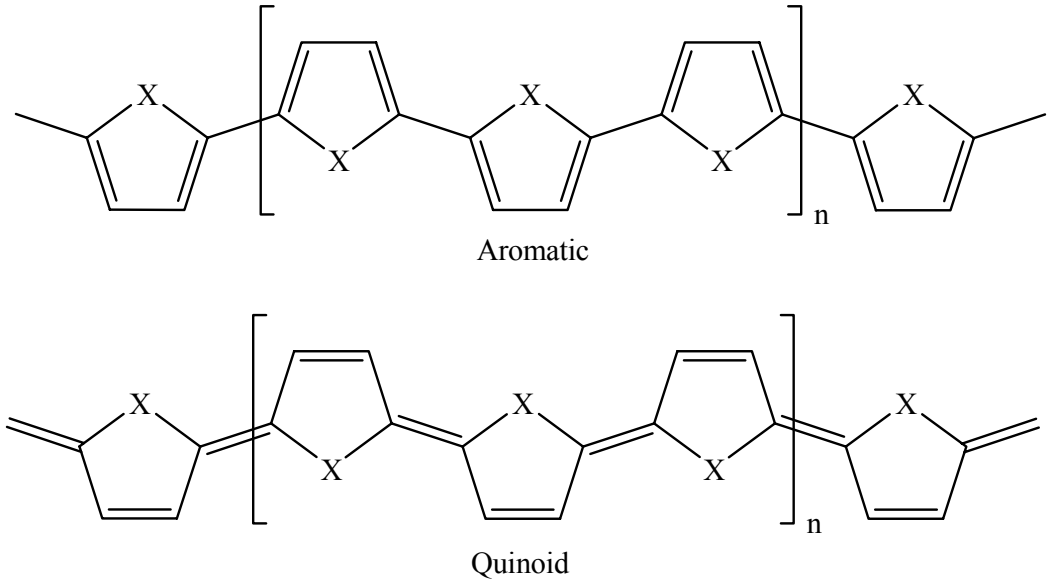

Figure 1.6 *The aromatic and quinoid forms of ECPs.*

These species are formed when the neutral insulating polymer is oxidized (Figure 1.7). The change in the band structure during the oxidation process is illustrated in Figure 1.7b, showing the transition of the insulating polymer (a) to a state of low (b) and finally high oxidation (c). New electronic levels are introduced between the conduction band and the valence band. The lower level is occupied by one electron. This corresponds to a radical cation. The new levels lead to newly allowed electronic transitions. This explains the higher electrical conductivity. State (c) is the bipolaron state. Overoxidation of

conducting polymer leads to structures that carry one positive charge on every monomeric unit. This situation makes the polymer insulating again [27].

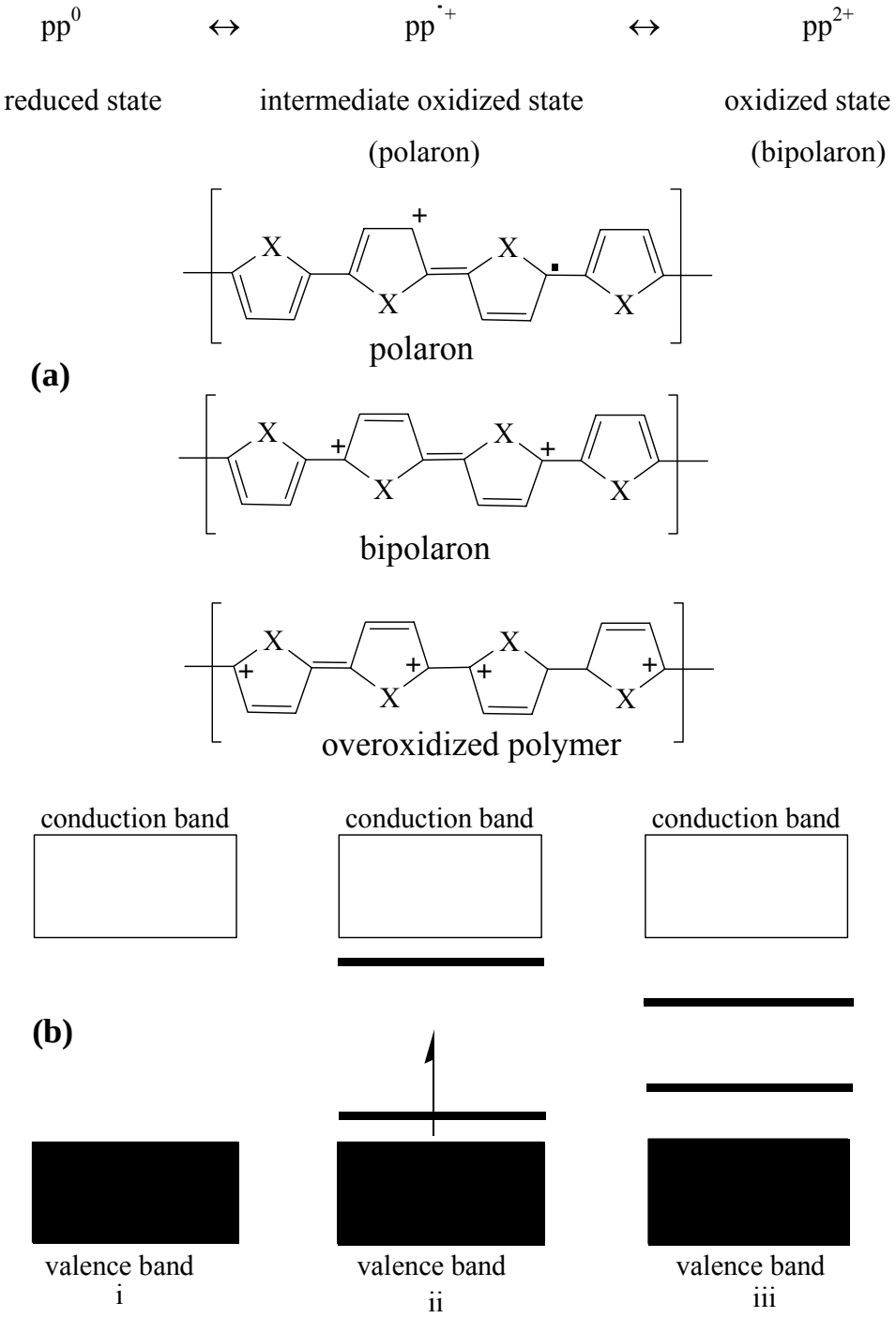

Figure 1.7 *(a) Structure of a conjugated polymer at increasing levels of oxidation. (b) Electronic band structure of the conjugated polymer (i) polymer in insulating state, (ii) partially oxidized polaron state; (iii) fully oxidized bipolaron state.*

1.3. Electrochemical and Spectroscopic Concepts and Techniques

1.3.1. Electrochemical Cells and Reactions [28-30]

Three-electrode cells (e.g., Figure 1.8) are commonly used in electrochemical experiments. The cell is usually a covered beaker of 5-50 mL, and contains the three electrodes (working, reference, and auxiliary), which are immersed in the sample solution. The three electrodes, as well as the tube used for bubbling the deoxygenating gas, are supported in five holes in the cell cover. Complete systems, integrating the three-electrode cell, built-in gas control, and magnetic stirrer, along with the proper cover, are available commercially (e.g., Figure 1.9).

Working Electrode. Solid electrodes such as glassy carbon, gold or platinum disks have been used over the past decades replacing the dropping mercury electrode. Electrodes made from these materials have a wider positive potential range than Hg. However, they require frequent cleaning of the surface by polishing to remove adsorbed species, in order to obtain reproducible results.

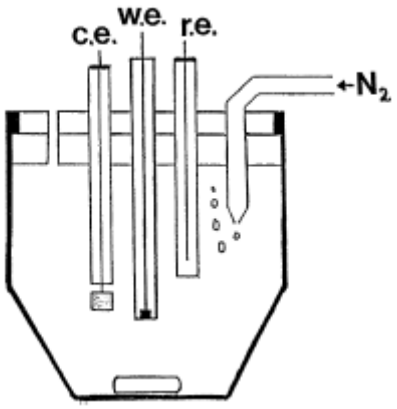

Figure 1.8 *Schematic diagram of a cell for voltammetric measurements: w.e., working electrode; r.e., reference electrode; c.e., counter electrode. The electrodes are inserted through holes in the cell cover.*

Reference Electrode. The internationally accepted primary reference is the standard hydrogen electrode (SHE), or normal hydrogen electrode (NHE), which has all components at unit activity:

$Pt/H_2(a = 1)/H^+$ (a = 1, aqueous)

Potentials are often measured and quoted with respect to reference electrode other than the NHE, which is not very convenient from an experimental standpoint. Commonly used reference electrodes are the saturated calomel electrode (SCE), which is $Hg/Hg_2Cl_2/KCl$(saturated in water) with a potential of 0.242 V *vs* NHE and the silver-silver chloride electrode, Ag/AgCl/KCl (saturated in water) with a potential of 0.197 V *vs* NHE. In organic solvents, commonly the Ag/Ag^+ redox couple is employed, which is achieved by dipping a silver wire into a Ag^+ solution of known concentration using the same solvent as the bulk solution.

Figure 1.9 *A complete cell stand*.

Since the reference electrode has a constant makeup, its potential is fixed. The potential of the working electrode is controlled with respect to the reference and that is equivalent to observing or controlling the energy of electrons within the working electrode. By driving the working electrode to more negative potentials (e.g., by connecting a battery of power supply to the cell with its negative side attached to the working electrode), the energy of the electrons is raised. They can reach a level high enough to transfer into

vacant electronic states on species in the electrolyte. In that case, a flow of electrons from electrode to solution (a reduction current) occurs (Figure 1.10a). Similarly, the energy of the electrons can be lowered by imposing a more positive potential, and at some point electrons on solutes in the electrolyte will find more favorable energy on the electrode and will transfer there. Their flow, from solution to electrode, is an oxidation current (Figure 1.10b).

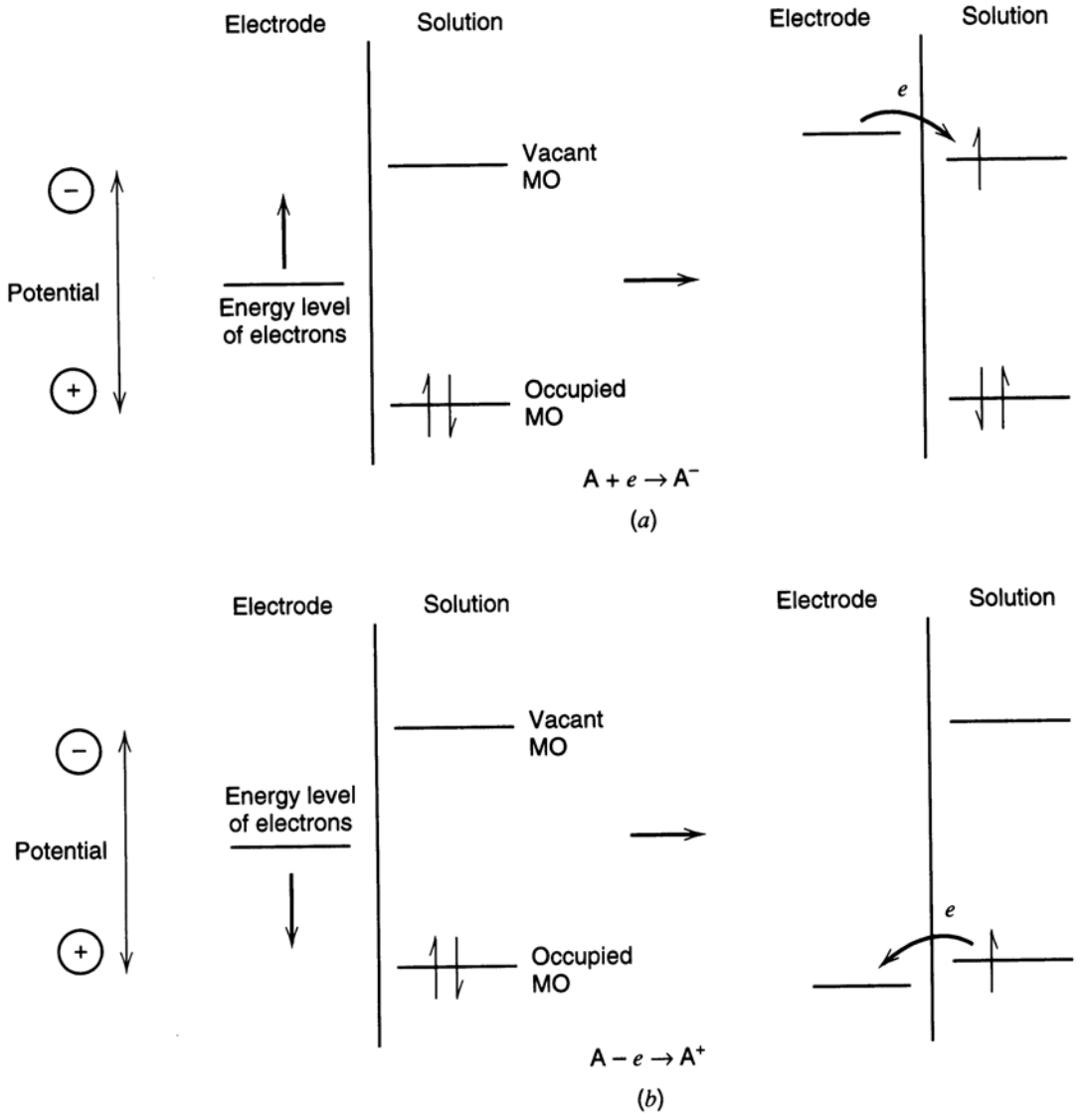

Figure 1.10 *Representation of (a) reduction and (b) oxidation process of a species, A, in solution. The molecular orbitals (MO) of species A shown are the highest occupied MO and the lowest vacant MO.*

Counter Electrode. An inert conducting material, such as platinum wire or graphite rod of sufficiently large electrode area is usually used as the current-carrying counter or auxiliary electrode.

Solvents and supporting electrolytes. Electrochemical experiments are commonly carried out in a medium that consists of a solvent containing a supporting electrolyte. The choice of the solvent is dictated primarily by the solubility of the analyte and its redox activity, and by the solvent property such as electrical conductivity, electrochemical activity, and chemical reactivity. The solvent should not react with the analyte (or products) and should not undergo electrochemical reactions over a wide potential range. While water has been used as a solvent more than any other media, nonaqueous solvents [e.g., acetonitrile, propylene carbonate, dimethyformamide, dimethyl sulfoxide, or methanol) have also been used. Supporting electrolytes are used to decrease the resistance of the solution, to eliminate electromigration effects, and to maintain a constant ionic strength. The supporting electrolyte should be prepared from highly purified reagents and should not be easily oxidized or reduced. The usual electrolyte concentration is 0.1 – 1.0 M, in other words, in large excess of the concentration of the electroactive species.

Oxygen removal. The background current occurring from the electrochemical reduction of oxygen interferes with the measurement of many reducible species. In addition, the products of the oxygen reduction may affect the electrochemical process under investigation. The most common method to remove dissolved oxygen is purging the solution with an inert gas (usually purified nitrogen) for 10 – 20 min prior to recording the voltammogram. To prevent oxygen from re-entering, the cell should be blanketed with the inert gas while the voltammogram is recorded.

1.3.2. Cyclic Voltammetry, Chronoampereometry and Square Wave Voltammetry [28-30].

Cyclic voltammetry (CV) is the most widely used technique for acquiring qualitative information about electrochemical reactions. It is often the first experiment performed in

electrochemical study for it offers a rapid location of redox potentials of the electroactive species and is convenient to evaluate the effect of media upon the redox species. CV employs a triangular wave form as shown in Figure 1.11 and the current (both cathodic and anodic) is measured during the complete sweep of the applied triangular voltage. The resulting current-potential curve (cyclic voltammogram) has the form shown in Figure 1.12.

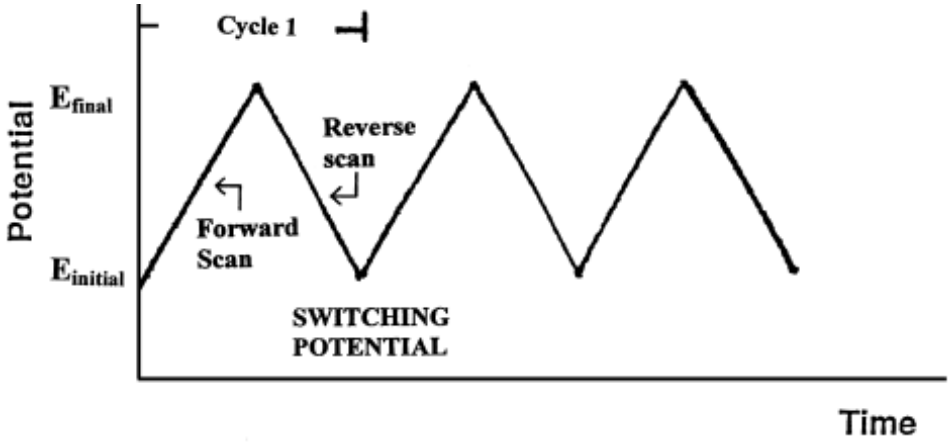

Figure 1.11 *Potential-time signal in cyclic voltammetric experiment.*

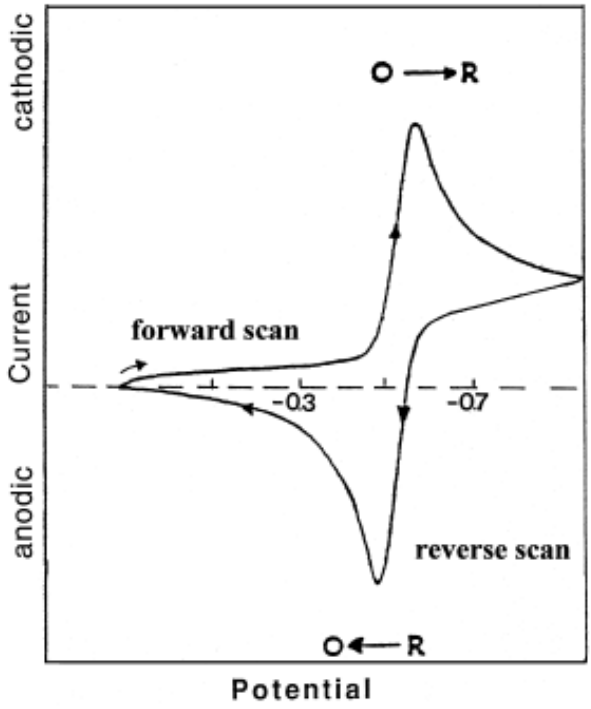

Figure 1.12 *Typical cyclic voltammogram for a reversible O + ne- = R redox process.*

The peak potentials and peak currents are used to interpret the resulting cyclic voltammmogram. The peak current for a reversible couple under diffusion control (at 25°C), is given by the Randles-Sevick equation:

$$i_p = (2.69 \times 10^5) n^{3/2} A C D^{1/2} v^{1/2} \qquad (1.1)$$

where n is the number of electrons, A is the electrode area (in cm^2), C is the concentration (in mol cm^{-3}), D is the diffusion coefficient (in $cm^2\ s^{-1}$), and *v* is the scan rate (in $V\ s^{-1}$). Accordingly, the current is directly proportional to the concentration and increases with the square root of the scan rate. The ratio of the reverse-to-forward peak currents, $i_{p,r}/i_{p,f}$, is unity for a simple reversible couple.

The position of the peaks on the potential axis (E_p) is related to the formal potential of the redox process. The formal potential for a reversible couple is centred between $E_{p,a}$ and $E_{p,c}$:

$$E^o = \frac{E_{p,a} + E_{p,c}}{2} \qquad (1.2)$$

The separation between the peak potentials (for a reversible couple) is given by

$$\Delta E_p = E_{p,a} - E_{p,c} = \frac{0.059}{n}\ V \qquad (1.3)$$

Thus, the peak separation can be used to determine the number of electrons transferred, and as a criterion for a Nernstian behaviour. Accordingly, a fast one-electron process exhibits a ΔE_p of about 59 mV. Both the cathodic and anodic peak potentials are independent of the scan rate.

For multielectron-transfer (reversible) processes, the cyclic voltammogram consists of several distinct peaks if the E^o values for the individual steps are successively higher and are well separated. An example of such a mechanism is the six-tep reduction of the fullerenes C_{60} and C_{70} to yield the hexaanion products C^{6-}_{60} and C^{6-}_{70}. Such six successive reduction peaks are observed in Figure 1.13.

For irreversible processes (those with sluggish electron exchange), the individual peaks are reduced in size and widely separated (Figure 1.14, curve A). Totally irreversible

systems are characterized by a shift of the peak potential with the scan rate. The voltammograms for a quasi-reversible system are also more drawn-out and exhibit a larger separation in peak potentials compared to those of a reversible system (Figure 1.14, curve B.)

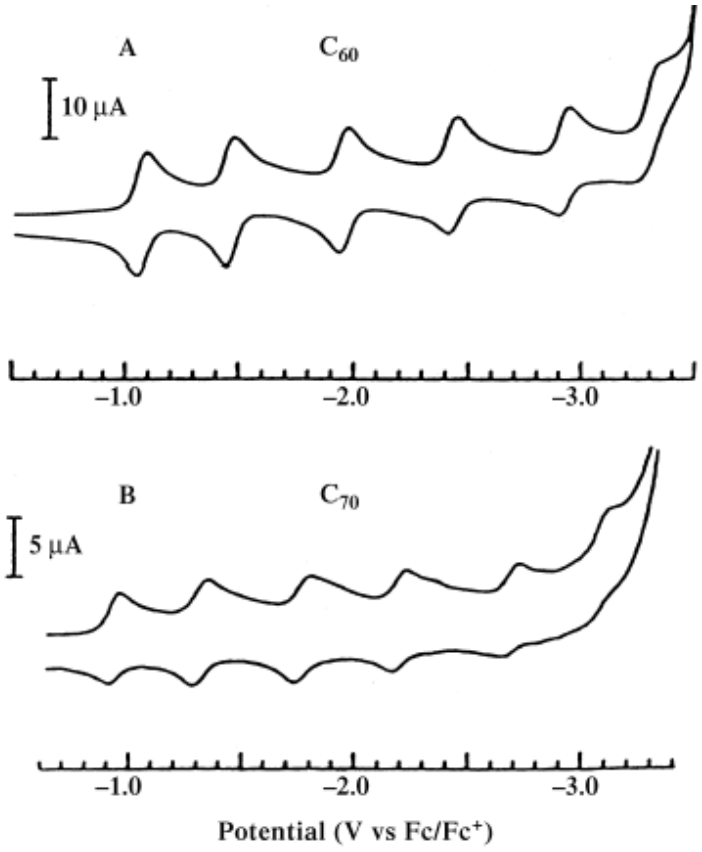

Figure 1.13 *Cyclic voltammetry of C_{60} and C_{70} in an acetonitrile-toluene solution.*

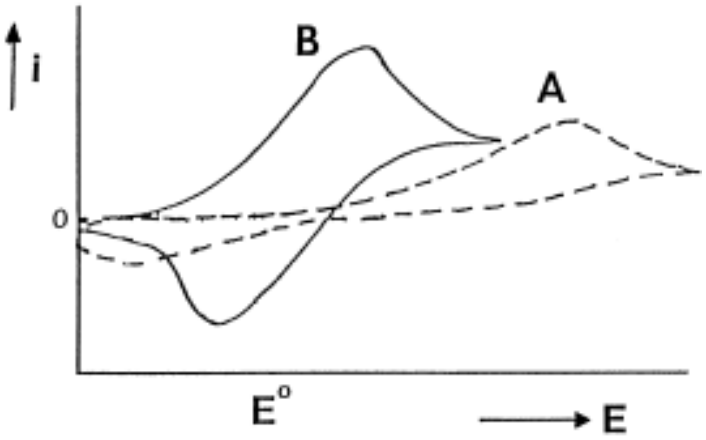

Figure 1.14 *Cyclic voltammograms for irreversible (curve A) and quasi-reversible (curve B) redox processes.*

Chronoamperometry (CA) involves stepping the potential of the working electrode from a value at which no faradaic reaction occurs to a potential at which the surface concentration of the electroactive species is effectively zero (Figure 1.15). A stationary working electrode and unstirred solution are used. The resulting current-time dependence is monitored. The current decays with time and is given by the Cottrell equation:

$$i(t)=\frac{nFACD^{\frac{1}{2}}}{\pi^{\frac{1}{2}}t^{\frac{1}{2}}}=kt^{-\frac{1}{2}} \qquad (1.4)$$

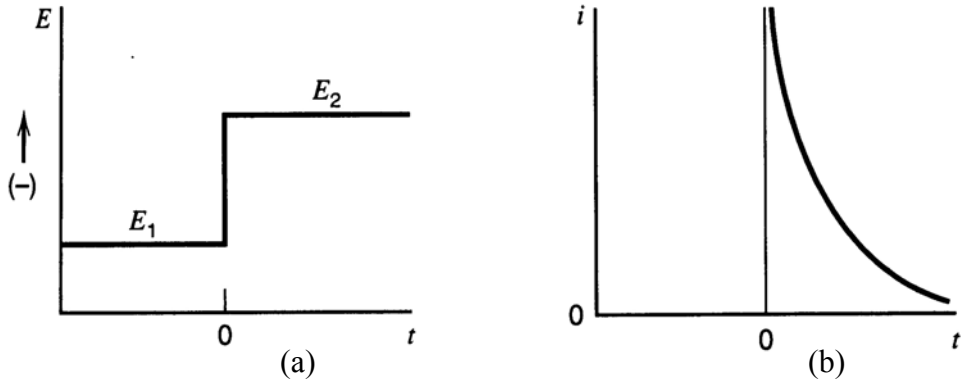

Figure 1.15 (a) *Potential-time waveform and (b) the resulting current flow vs time for chronoamperometric experiment.*

CA is often used for measuring the diffusion coefficient of electroactive species or the surface area of the working electrode. The potential-step experiment can also be used to record the charge *versus* time dependence in chronocoulometric experiment. If the potential E_2 is reversed back to E_1 as shown in Figure 1.16a, the electroactive species that was reduced initially by going from E_1 to E_2 in the forward step will now be oxidized. Integrating the area under the curve (Figure 1.16b) in the positive and negative current axis gives the charge injected and ejected during the reduction and oxidation processes. These oxidation and reduction process can be repeated several times in cyclic chronoamperometry experiments and is frequently used in the study of electrochromism.

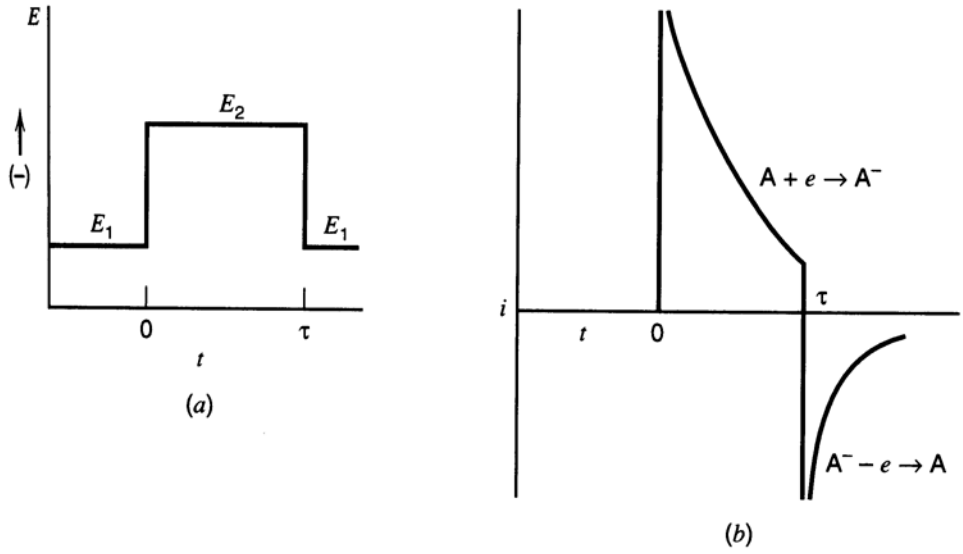

Figure 1.16 *Double potential step chronoamperometry. (a) Typical wave form. (b) current response.*

Square Wave Voltammetry (SWV), popularized by Janet G. Osteryoung, has proved to be a useful method to investigate redox reactions with overlapping waves. In SWV a square wave potential superimposed to a staircase potential is applied as shown in Figure 1.17. The line shown in bold is the actual potential waveform applied to the working electrode. The light intervening lines indicate the underlining staircase onto which the square wave can be regarded as having been superimposed. In each cycle, a forward current sample is taken at the time indicated by the solid dot, and a reverse current sample is taken at the time marked by the shaded dot. The method takes advantage of computer timing to repeatedly sample current signals at two points relative to the time of application of a square wave voltage signal to the electrode. The difference between the two current values is plotted as a function of the applied DC potential. The resultant is a peak rather than voltammetric wave, corresponding to the electroactivity of the species in the electrochemical cell. The major component of this difference current is the faradaic current, which flows due to an oxidation or reduction at the electrode surface. The capacitive or charging current component, due to electrical charging of electrode double layer, is largely eliminated. This increases the signal to noise ratio. Trace analyses of metallic ions and of organic pharmaceutical compounds are common applications for these pulse techniques.

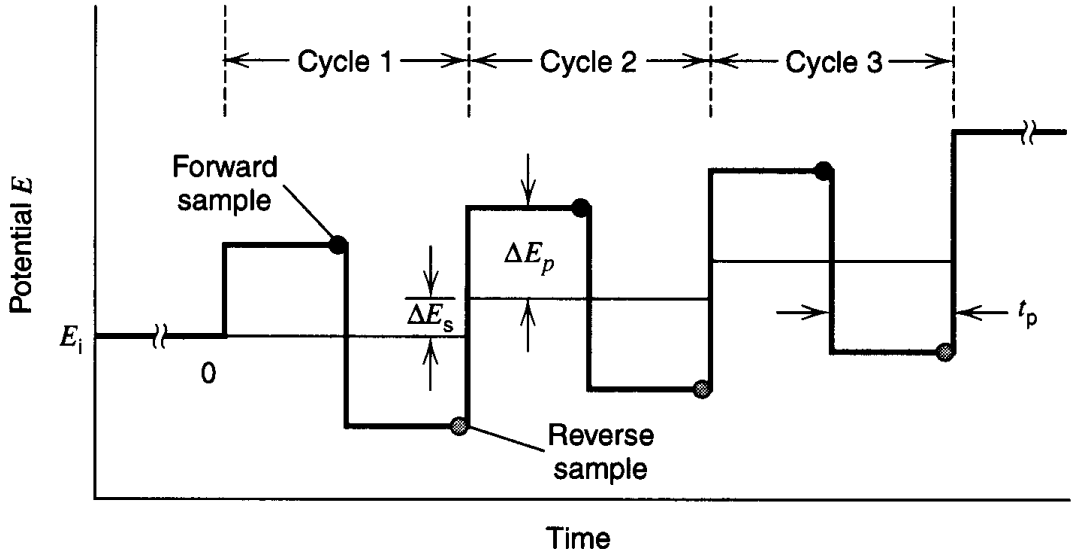

Figure 1.17 *Wave form and measurement scheme for square wave voltammetry.*

The square wave is characterized by a pulse height, ΔE_p, measured with respect to the corresponding tread of the staircase, and a pulse width, t_p. Alternatively, the pulse width can be expressed in terms of the square wave frequency, $f = 1/2t_p$. The staircase shifts by ΔE_s at the beginning of each cycle, thus the scan rate $v = \Delta E_s/2t_p = f\Delta E_s$. The scan begins at an initial potential, E_i, which can be applied for an arbitrary time to initialize the system as desired. Figure 1.18 shows the resulting response curve (i *vs* E).

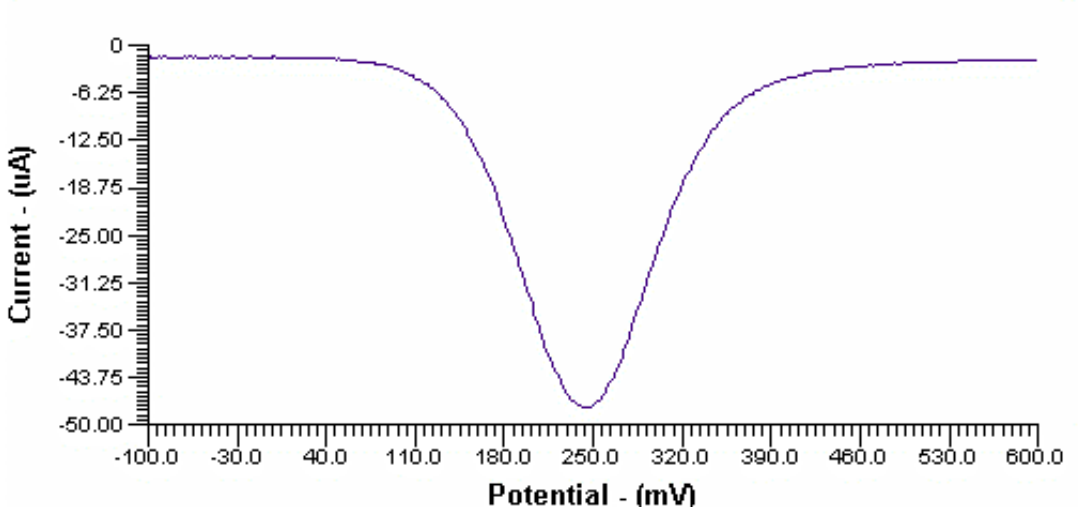

Figure 1.18 *A typical current vs potential response curve in square wave voltammetry.*

1.3.3. Absorption and Emission Spectroscopy [31-32]

An electronic transition consists of the promotion of an electron from an orbital of a molecule in the ground state to an unoccupied orbital by absorption of a photon. Electrons in a molecule can be classified into three different types:

1. Electrons in a single covalent bond (σ-bond) are tightly bound and radiation of high energy (short wavelength) is required to excite them.
2. Electrons may be attached to atoms as lone pairs, e.g., in chlorine, oxygen and nitrogen. These non-bonding electrons can be excited at a lower energy (longer wavelength) than tightly bound bonding electrons.
3. Electrons in double or triple bonds (π-orbitals) can be excited relatively easily. In molecules containing a series of alternating double bonds (conjugated systems); the π-electrons are delocalized and require less energy for excitation, so the absorption rises to higher wavelengths.

To illustrate these transitions and energy levels, Figure 1.19 shows formaldehyde as an example, with all the possible transitions.

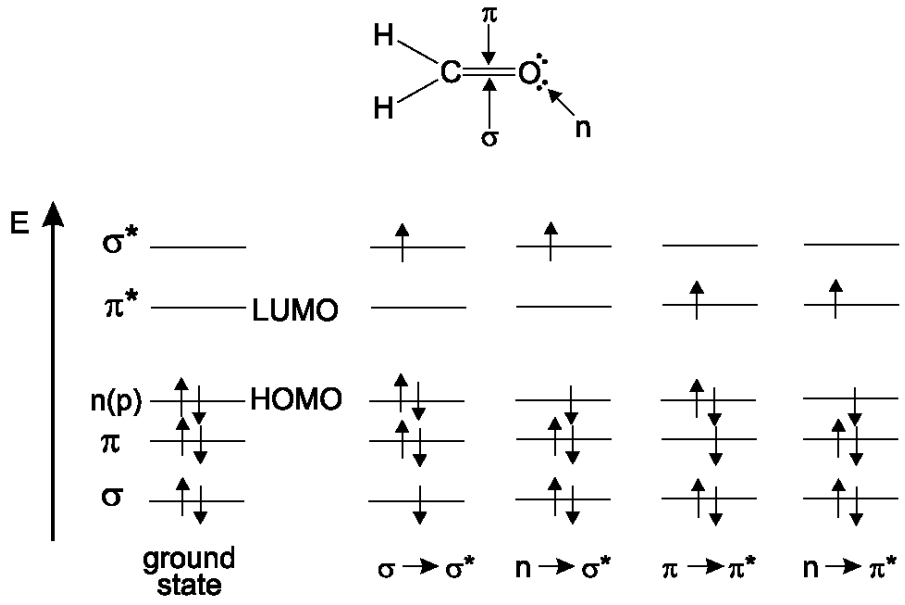

Figure 1.19 *Energy levels of molecular orbitals in formaldehyde and possible electronic transitions.*

Luminescence is an emission of ultraviolet, visible or infrared photons from an electronically excited species. Fluorescence and phosphorescence are particular cases of luminescence where the mode of excitation is absorption of a photon, which brings the absorbing species into an electronic excited state. The emission of photons accompanying deexcitation is then called photoluminescence (fluorescence or phosphorescence), which is one of the possible physical effects resulting from interaction of light with matter.

In absorption and emission spectroscopy, two important types of orbitals are considered: the Highest Occupied Molecular Orbitals (HOMO) and the Lowest Unoccupied Molecular Orbitals (LUMO). Both of these refer to the ground state of the molecule. For instance, in formaldehyde, the HOMO is the n orbital and the LUMO is the π* orbital (see Figure 1.20).

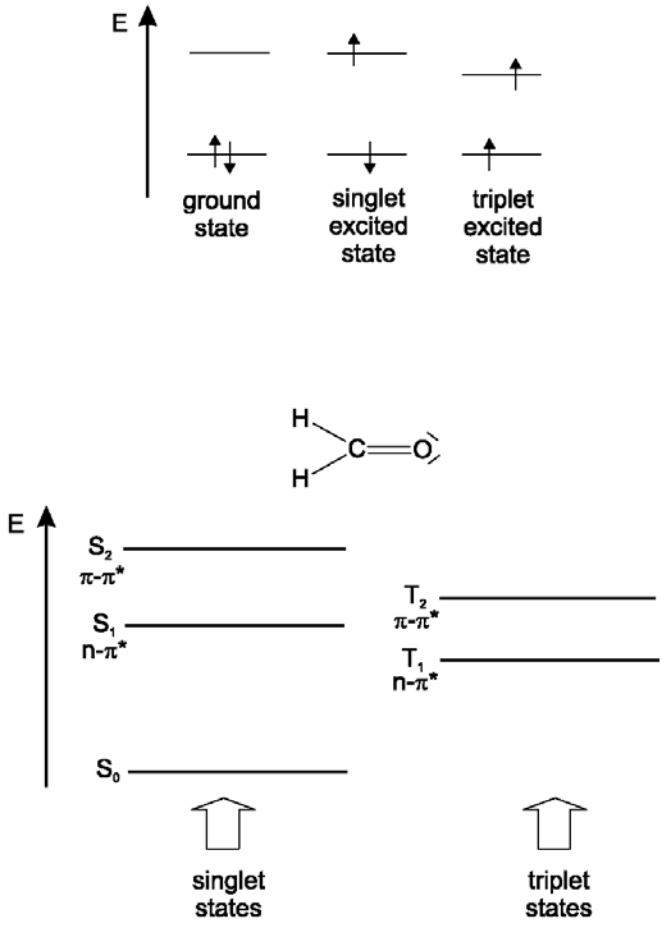

Figure 1.20 *Distinction between singlet and triplet states, using formaldehyde as an example.*

When one of the two electrons of opposite spins (belonging to a molecular orbital of a molecule in the ground state) is promoted to a molecular orbital of higher energy, its spin is in principle unchanged so that the total spin quantum number ($S = \Sigma s_i$, with $s_i = +½$ or $-½$) remains equal to zero. Because the multiplicities of both the ground and excited states ($M = 2S + 1$) is equal to 1, both are called singlet state (usually denoted S_0 for the ground state, and S_1; S_2; . . . for the excited states) (Figure 1.20). The corresponding transition is called a singlet–singlet transition. A molecule in a singlet excited state may undergo conversion into a state where the promoted electron has changed its spin; because there are then two electrons with parallel spins, the total spin quantum number is 1 and the multiplicity is 3. According to Hund's Rule, the triplet state has a lower energy than that of the singlet state of the same configuration.

Experimentally, the efficiency of light absorption at a wavelength λ by an absorbing medium is characterized by the absorbance A(λ) or the transmittance T(λ), defined as

$$A(\lambda) = \log \frac{I_\lambda^o}{I_\lambda} = -\log T(\lambda) \qquad (1.5)$$

$$T(\lambda) = \frac{I_\lambda}{I_\lambda^o} \qquad (1.6)$$

where I^0_λ and I_λ are the light intensities of the beams entering and leaving the absorbing medium, respectively. In many cases, the absorbance of a sample follows the Beer–Lambert Law

$$A(\lambda) = \log \frac{I_\lambda^o}{I_\lambda} = \varepsilon(\lambda) l c \qquad (1.7)$$

where ε(λ) is the molar absorption coefficient (commonly expressed in L mol^{-1} cm^{-1}), c is the concentration (in mol L^{-1}) of absorbing species and *l* is the absorption path length (thickness of the absorbing medium) (in cm). The molar absorption coefficient, ε(λ), expresses the ability of a molecule to absorb light in a given solvent.

When a molecule absorbs a photon of light, an energetically excited state is formed. The fate of this species is varied, depending upon the exact nature of the molecule and its

surroundings, but the end result is deactivation (loss of energy) and return to the ground state. The main deactivation processes which occur are fluorescence (loss of energy by emission of a photon), internal conversion and vibrational relaxation (non-radiative loss of energy as heat to the surroundings), and intersystem crossing to the triplet manifold and subsequent non-radiative deactivation. The Perrin–Jablonski diagram (Figure 1.21) is convenient for visualizing in a simple way these processes.

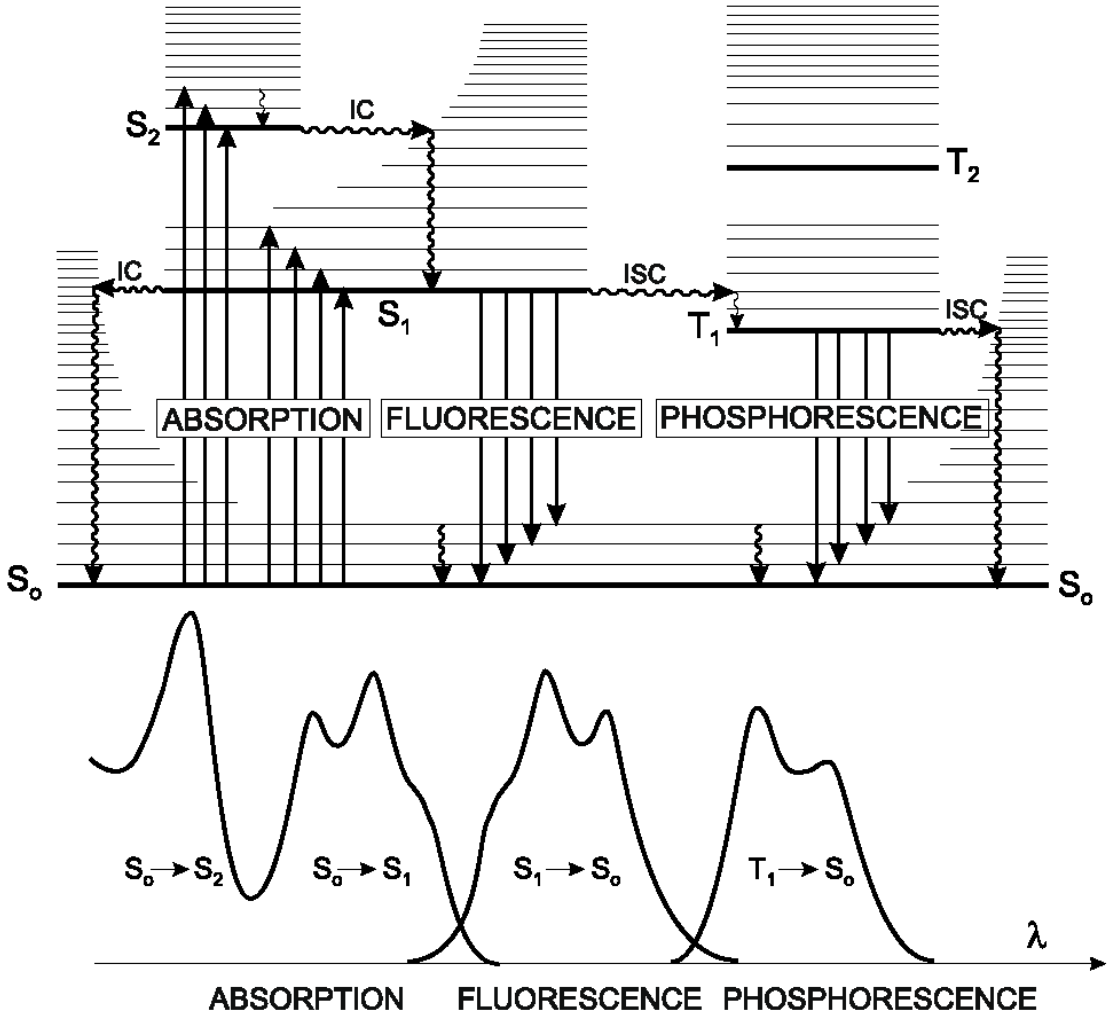

Figure 1.21 *Perrin-Jablonski diagram and illustration of the relative positions of absorption, fluorescence and phosphorescence spectra.*

The fluorescence quantum yield (Φ_F) is the ratio of photons absorbed to photons emitted through fluorescence. In other words the quantum yield gives the probability of the

excited state being deactivated by fluorescence rather than by another, non-radiative mechanism. Relative values of quantum yields are calculated using the standard samples which have a fixed and known fluorescence quantum yield value, according to the following equation [33-34]:

$$\phi_{unk} = \phi_{std}\left(\frac{I_{unk}}{A_{unk}}\right)\left(\frac{A_{std}}{I_{std}}\right)\left(\frac{\eta_{unk}}{\eta_{std}}\right)^2 \qquad (1.8)$$

where ϕ_{unk} is the fluorescence quantum yield of the sample, ϕ_{std} is the quantum yield of the standard, I_{unk} and I_{std} are the integrated emission intensities of the sample and the standard, respectively, A_{unk} and A_{std} are the absorbances of the sample and the standard at the excitation wavelength, respectively, and η_{unk} and η_{std} are the refractive indexes of the corresponding solutions (pure solvents were assumed).

1.4. Electrochemical Spectroscopy of Electronically Conducting Polymers

Cyclic voltammetry is used for studying the electroactivity of electronically conductive polymer films synthesised electrochemically or casted on electrode surfaces. Although the CV of ECPs varies in shape on type and polymerization conditions, some common features can often be observed. Generally, with thin polymer films, the peak current varies linearly with the sweep rate as if the charges were adsorbed on the surface of the polymer film. When thicker films are used, the peak current varies with the square-root of the sweep rate, indicating that the charge transfer is limited by the diffusion of electrons and/or ions in the polymer matrix. By comparing the injected charge during the anodic wave with the charge withdrawn during the cathodic wave upon repeated cycling, the electrochemical stability of the polymer can be determined. The position of the peaks has been shown to depend on conjugation length. With increasing conjugation length the respective oxidation and reduction potentials shifts towards lower energies [35]. Also, substitution influences the position of the peaks. Electron-donating substituents lower the oxidation potential, and the electron-withdrawing substituents raise them [36].

In the ideal case, reversible cyclic voltammograms of redox-active monolayer films should show completely symmetrical and mirror-image cathodic and anodic waves with identical peak potentials and current levels. The width of the oxidation peak is often larger than expected for a surface reaction with a true Nernstian behavior. This has been attributed to interaction among charged sites [37-38], differences between the conformation of the neutral and doped states, transport properties and the distribution of conjugation lengths of the chain segments [39]. In the case of p-doping, the charging is shown as a steep anodic wave followed by a broad, flat plateau as the potential increases. It has been suggested that the plateau is related to capacitive charging of double layers of the system [40-42]. In the reverse scan a potential shifted cathodic wave appears at the low-energy end of the plateau with a peak height of about half the value of the anodic peak.

Uv-vis-nir spectroelectrochemical experiments can be carried out using commercially available ITO (indium tin oxide) transparent electrodes inside a conventional cuvette or specially designed optically transparent thin layer electrolysis cell containing a three-electrode arrangement. In Figures 1.22 and Figure 1.23 cyclic voltammograms and uv-vis-nir spectroelectrochemical curves recorded for different electrode potentials are shown for poly(3-octylthiophene). The spectroelectrochemical behaviour of other ECPs such as polypyrrole or poly(*p*-phenylene) is similar so the conclusions presented here can be generalized. Cyclic voltammograms of poly(3-octylthiophene) indicate that oxidative doping of this polymer is a two-step phenomenon since two overlapping redox couples are clearly seen [43].

This two-step oxidation is also manifested in Uv-vis-nir spectroelectrochemical studies. The spectra recorded for increasing potentials (i.e., for increasing doping levels) show gradual bleaching of the π-π^* transition with simultaneous growth of two peaks at 1.6 eV (780 nm) and 0.7 eV (1780 nm) usually ascribed to the formation of bipolaron sub-gap states. At E = 800 mV, i.e., in between the maxima of both oxidation peaks, the absorption at 2.39 eV (520 nm) is still rather strong, indicating that the oxidative doping is not completed yet at this potential. In order to achieve complete doping, manifested by

total bleaching of the π-π* transition, the electrode must be polarized at potentials higher than those corresponding to the second oxidation peak.

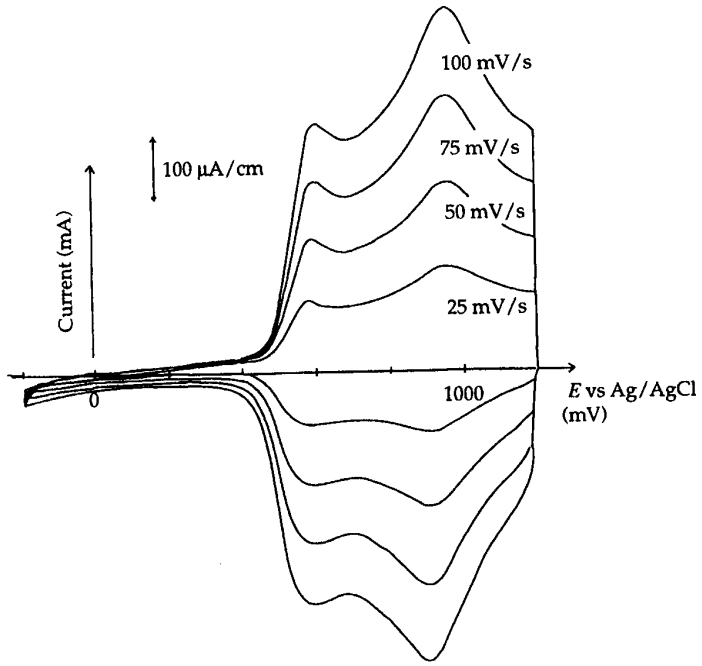

Figure 1.22 *Cyclic voltammograms of regioregular poly(3-octylthiophene) recorded in 0.1 M Bu_4NBF_4 solution in acetonitrile (E measured vs Ag/AgC1 reference electrode).*

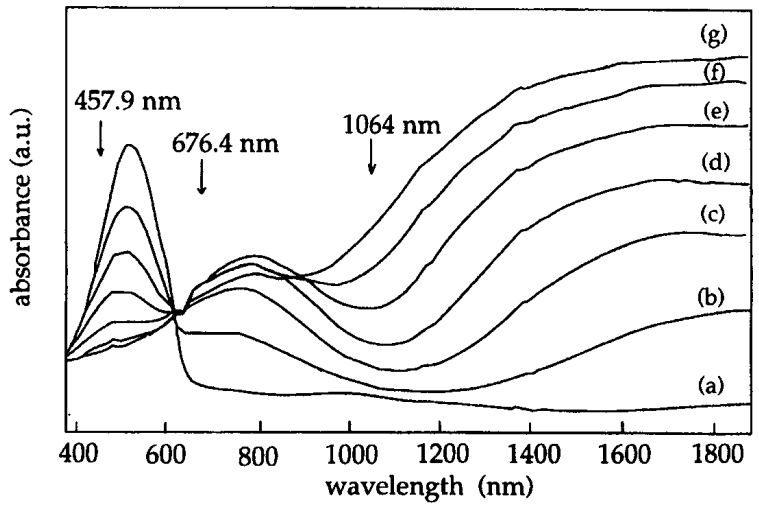

Figure 1.23 *Uv-vis-nir spectroelectrochemical curves recorded for regioreguiar poly(3-octylthiophene) in 0.1M Bu_4NBF_4 solution in acetonitrile: (a) E = 0 mV; (b) E = 500 mV; (c) E = 800 mV; (d) E = 900 mV; (e) E = 1000 mV; (f) E = 1200 mV; (g) E =1400 mV (E measured vs Ag/AgC1 reference electrode).*

Parameters such as ionization potential (IP), electron affinity (EA) and energy gap (Eg) are important to understand and control the electrical and optical properties as well as the doping process of conducting polymers. These parameters are useful to construct the energy level diagrams of conducting polymers. Methods to determine the energy diagram are important in order to develop a further understanding of, and to optimize, device performance. Both IP and EA are of crucial importance when device applications are considered because IP and EA are the polymer-related major factors determining electrode/polymer interfacial energy barriers, despite the fact that the contribution of other factors cannot be neglected [44].

The relationship between electrochemical parameters considering a simplified energy level structure for the polymers is shown schematically in Figure 1.24.

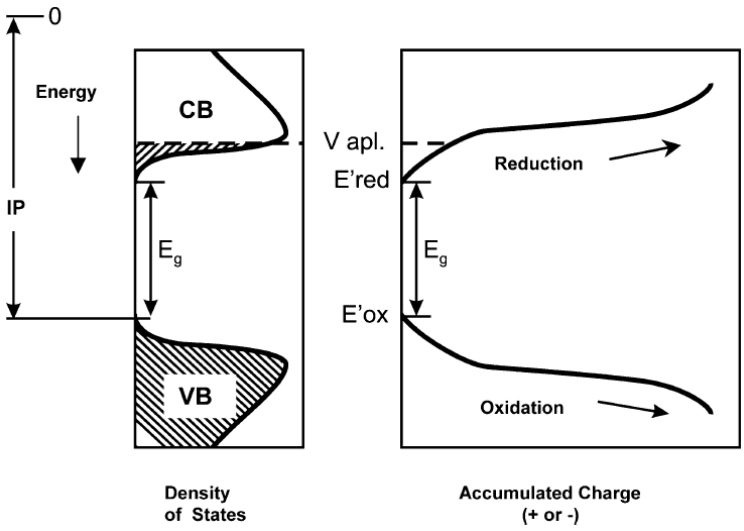

Figure 1.24 *Relationship between the electrochemically measured onset potentials, E'_{ox} and E'_{red}, and the ionization potential, IP, and the band gap, E_g.*

On the left hand side, the density of states is drawn for two relevant bands, the valence band (VB) and the conduction band (CB). The band gap (Eg) is then the energy difference between the top of valence band and the bottom of the conduction band, and the ionization potential (IP) is the energy from the valence band edge to the vacuum level. On the right-hand side of Figure 1.24 the potentials for a reduction or oxidation

cycle as a function of accumulated charge are schematically shown. In the case of the oxidation process, no charges will be removed from the polymer electrode until the applied voltage reaches an onset value, which corresponds to the highest occupied states in the valence band. As the voltage is further increased, more and more states are emptied. The opposite is true for the reduction cycle [44].

If one is able to do both oxidation and reduction in the same electrolyte system, the difference between the two onset potentials should closely correspond to the energy gap and can be directly compared to the optical band gap [45]. This has not generally been the case for conjugated polymers, where often only reduction or oxidation is observed, or where only one process is found to be reversible. Moreover, in order to correlate the oxidation and reduction potentials to IP and EA values, respectively, the electrochemical processes must keep the molecular structure of the polymer, i.e. no degradation of the polymer chain can occur. In this case, the oxidation or reduction potential will be related not only to the loss or capture of an electron, but to the overall chemical processes like bond dissociation. The injection of charge must only convert the polymer chain into an ion.

This method of estimation is mainly based on the detailed quantum chemical calculations of Bredas *et al.* [46] who found a linear correlation between ionization potential (I_p) and oxidation potential (E_{ox}) and also between electron affinity (E_a) and reduction potentials (E_{red}). They also indicated that these values refer to the first oxidation and reduction potentials (for removing or adding one electron), which correspond to the onset values of the electrochemical process. However, such deduction might be possible at very slow scan rates where all the adsorbed species can be reduced or oxidized. In their work the gas phase IP and EA of polymers were related with E^{ox}_{on} and E^{red}_{on} values using:

$$IP = E^{ox}_{on} + 6.3 \quad (1.9)$$

$$EA = E^{red}_{on} + 6.3 \quad (1.10)$$

The correlation factor of 6.3 eV was said to be consisting of a scale factor of 4.7 eV relating SCE to vacuum and a factor of 1.5 – 2.0 eV for polarization energy correction to adjust gas phase values to solid-state values. Most authors [47-49] take a value of 1.9 eV

for the polarization energy and subtract from 6.3 to obtain the most frequently used and recommended [50] method for a reasonable estimate as:

$$EA\ (E_{LUMO}) = (E'_{red} + 4.4)\ eV \quad (1.11)$$

$$IP\ (E_{HOMO}) = (E'_{ox} + 4.4)\ eV \quad (1.12)$$

Where, E'_{red} and E'_{ox} are onset reduction and oxidation potential versus the Ag/AgCl reference electrode.

Even though determination of optical as well as electrochemical band gap from onset values is widely used by many authors, peak values rather than the ill-defined onset values is argued to have a strong theoretical basis [51]. Some authors [51-55] prefer to estimate HOMO, LUMO and band gap values from the well-defined electrochemical parameter of the formal potential and peak potential values. The formal potential is taken as the average of the anodic and cathodic peak potentials for p-and n-doping. However, it is not always possible to get well-defined peaks, particularly in the cathodic n-doping. To convert the formal potential values to vacuum scale, the absolute potential for the Standard Hydrogen Electrode (SHE) is taken as 4.43 eV [56] and the potential difference between the Ag/AgCl and SHE is taken to be 0.22 V. However, there is still uncertainty in converting the electrochemical oxidation and reduction values measured against ferrocene as internal standard to vacuum level. Inganäs and co-workers have discussed these ambiguities in detail [57].

1.5. Polymer Solar Cells (PSCs)

1.5.1 Introduction

Traditional fossil fuel energy sources are finite, and release waste products into the atmosphere, such as NO_2 and CO_2, which are harmful to the earth's global environment. As a result, alternative energy sources are receiving increasing attention. Examples include wind, hydroelectric, and solar power. In particular, solar power is attractive due to the abundance and consistency of sunlight. Development of the standard silicon solar cell occurred in the 1950s. This technology is based on the p-n junction physics of

semiconductors. Absorption of light generates electron-hole pairs that diffuse until they reach the junction where they are collected. Researchers at Bell Laboratories developed the first crystalline silicon solar cell in the 1950s with a solar power conversion efficiency of 6%. Modern solar power conversion efficiencies are between 15 and 20%. However, the relatively high cost of manufacturing these silicon cells has prevented them from widespread use. Another disadvantage of silicon cells is the use of toxic chemicals in their manufacture. These aspects prompted the search for environmentally friendly and low cost solar cell alternatives based on organic semiconductors [58].

Motivated by the low cost of production which would open the way for wide spread application and the infinite variability of organic compounds which can be tailored to meet individual needs, photovoltaic devices based on organic materials has been investigated intensively during the last couple of decades. Such studies have focused on dye sensitized solar cells and organic solar cells made from relatively small organic molecules and electronically conductive polymers. In 1991, O'Regan and Gratzel [59] developed what is now known as the dye-sensitized nanocrystalline solar cell, which is a potentially low cost alternative to the standard silicon solar cell. A nanocrystalline film of TiO_2 is sensitized with a dye known as $Ru(II)L_2(NCS)_2$ with L = 4,4'-dicarboxy-2,2'-bipyridyl to absorb solar radiation. These types of cells have reached solar power conversion efficiencies up to 10%. [59,60]. Since a 1%-efficient thin-film organic solar cell based on a single donor-acceptor (D-A) heterojunction was reported by Tang [61], the power conversion efficiencies of both small organic molecules and electronically conducting polymers based photovoltaic devices have steadily improved through the use of new materials and device structures. The power conversion efficiencies of these devices at light intensity of 100 mW/cm^2 have reached up to 5 % [62-63].

1.5.2. Working Principles of Polymer Solar Cells [64-65]

In a typical polymer solar cell, a thin film (~100nm) of the active organic layer is sandwiched between two planar electrodes, as illustrated in Figure 1.25a. One of the

electrodes must be semi-transparent, often indium–tin-oxide (ITO). The other electrode is very often a metal like aluminium, calcium, magnesium or gold.

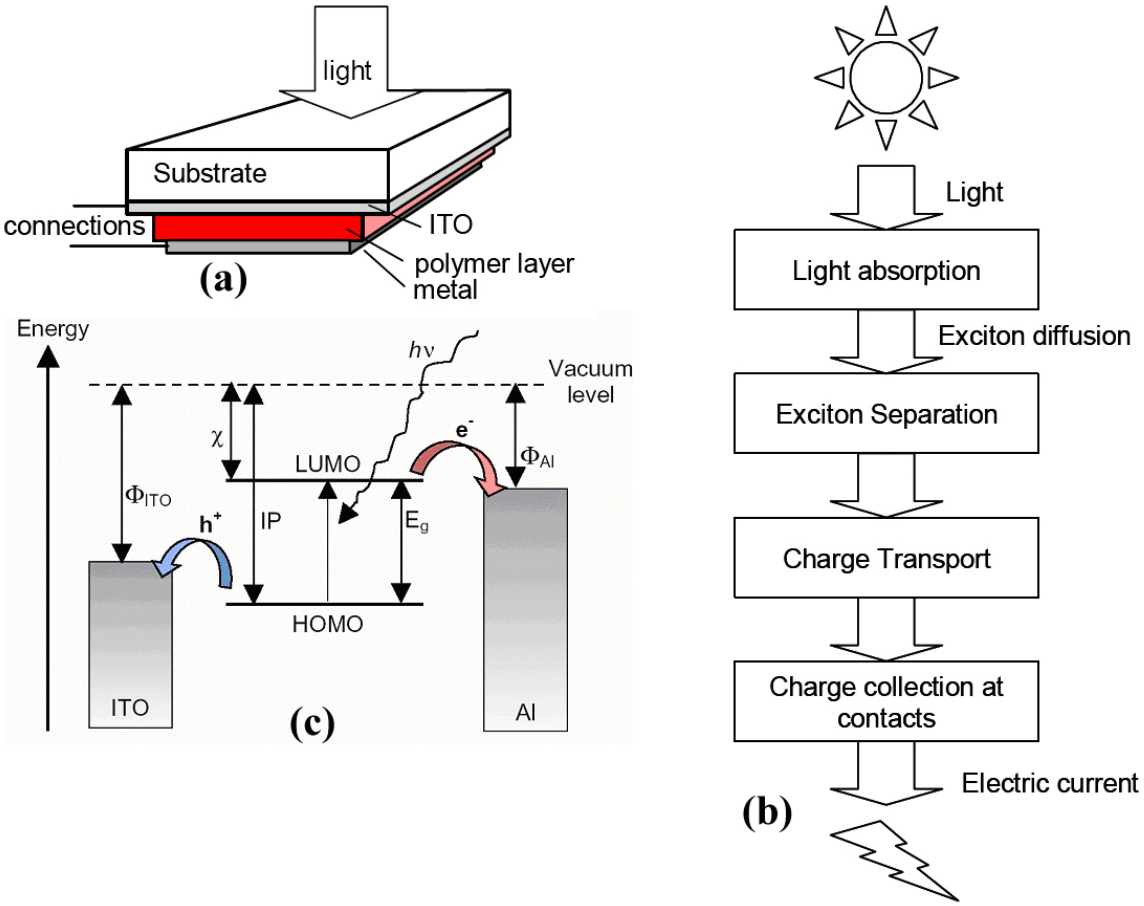

Figure 1.25 *Schematic illustration of (a) the device structure of a polymer solar cell, (b) flow chart showing the steps involved in the conversion of light to an electric current, and (c) the energy levels and light harvesting. Upon irradiation an electron is promoted to the LUMO leaving a hole behind in the HOMO. Electrons are collected at the Al electrode and holes at the ITO electrode, Φ: workfunction, χ: electron affinity, IP: ionisation potential, E_g: optical band gap [64].*

The production of electrical energy from sunlight is the result of a series of processes (Figure 1.25b). First, when light is absorbed an electron is promoted from the highest occupied molecular orbital (HOMO) to the lowest unoccupied molecular orbital (LUMO) forming an electron-hole pair (see Figure 1.25c). This process must be followed by the dissociation of the electron-hole pair. The electron must then reach one electrode while

the hole must reach the other electrode. In order to achieve charge separation, an electrical field is needed, which is provided by the differences in the ionisation energy or work functions of the electrodes. This difference in the work functions is the reason why electron-flow is more favored from the low work function electrode to the high work function electrode. The light harvesting process along with the positioning of energy levels is depicted in Figure 1.25c.

1.5.3. Preparation of Polymer Solar Cells

To construct a polymer solar cell based on conjugated polymers, part of the transparent conducting layer, indium tin oxide (ITO) is first etched away using a mixture of concentrated hydrochloric and nitric acid and water in the ratio of 4.6:0.4:5. This creates a contacting area for the cathode without shortcutting the thin film device. Then a thin layer of PEDOT-PSS is spin coated followed by removal of part of the PEDOT-PSS layer with water to allow a good contact for the anode layer. After drying it for sometime, the active layer (i.e. a polymer donor/and acceptor fullerene derivative mixture) is spin coated from a chloroform solution. Part of the active layer is again wiped out with chloroform to create good contact for the anode electrode. After drying the film, the back contact is applied by evaporating aluminium or LiF/Al in a vacuum chamber. A schematic diagram of the resulting device is shown in Figure 1.26.

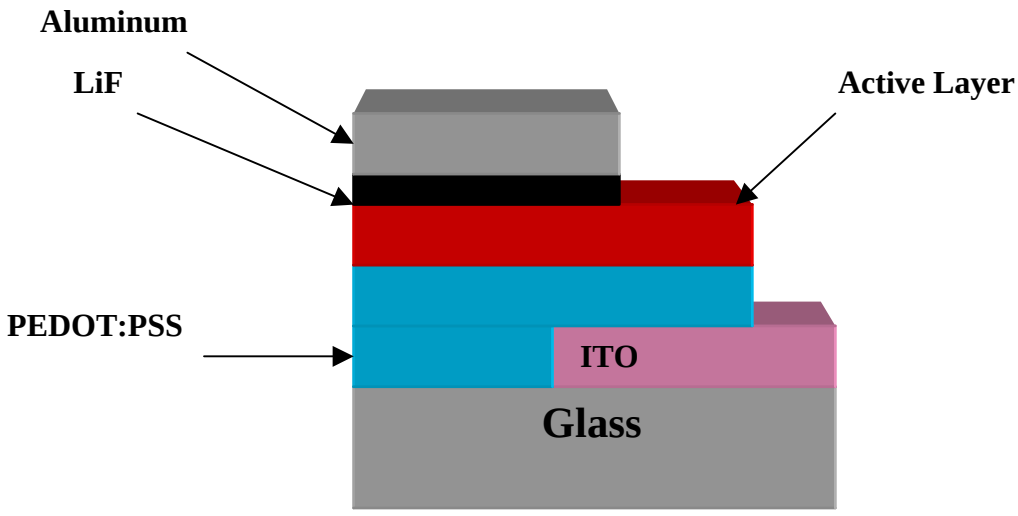

Figure 1.26 *Schematic diagram of an organic solar cell design.*

1.5.4. Characterization of Polymer Solar Cells [65]

Experimentally, a polymer cell is characterized by obtaining a power curve, that is, a plot of the cell voltage, V, *versus* cell current, I (Figure 1.27). The dotted lines (a) show I–V curve of the cell in the dark. When a cell is illuminated, the I–V curve is shifted down by the short-circuit current, I_{SC} (Fig.1.27b)

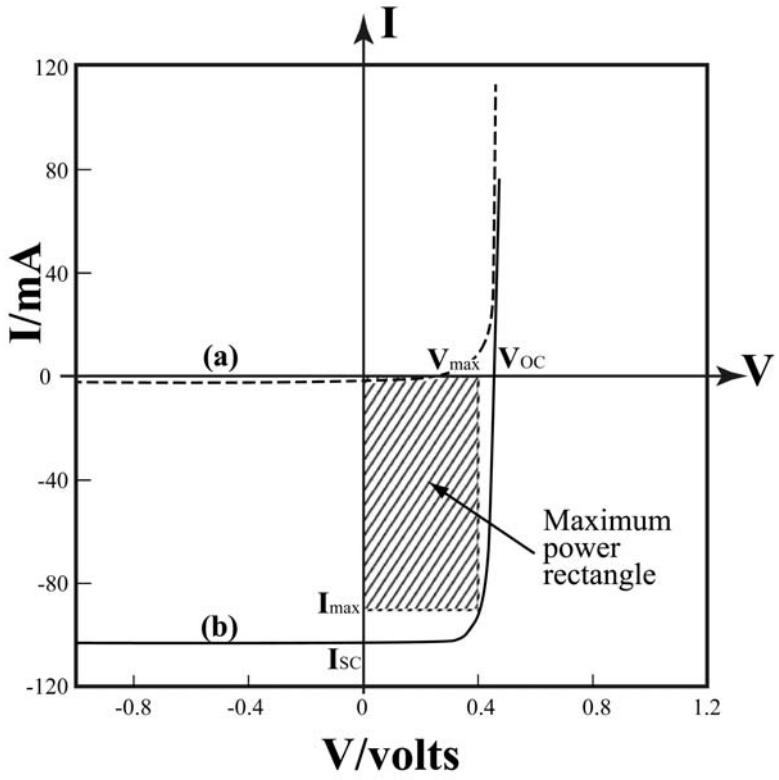

Figure 1.27 *I–V curves of a polymer solar cell under dark (a) and illuminated (b) conditions. The open-circuit voltage (V_{OC}) and the short-circuit current (I_{SC}) are shown. The maximum output is given by the square $I_{max}V_{max}$.*

The open-circuit voltage (V_{OC}) is the maximum voltage attainable in a solar energy conversion device and is typically around 1 V or higher in a good organic device. It is determined from the IV curve as the point at which the curve crosses the voltage axis (I = 0), as marked on Figure 1.27 above. The maximum current is the short-circuit photocurrent, I_{SC}, that flows when the two electrodes are shorted together. The power output of the cell, P, is given by I x V, so under both open-circuit and short-circuit conditions, P = 0. The maximum power out put of the cell occurs at a particular point on

the curve I_{max}-V_{max} and is related to the open and short circuit parameters by the fill factor (FF) and is given by:

$$FF=\frac{I_{max}V_{max}}{V_{OC}I_{SC}} \qquad (1.13)$$

The power conversion efficiency of the cell (PCE) in percent, is given by:

$$PCE\%=\frac{I_{max}V_{max}}{P_r}x100=\frac{I_{SC}V_{OC}FF}{P_r}x100 \qquad (1.14)$$

where P_r is the radiant power of intensity 80-100 mW/cm^2 input to the cell.

The effectiveness of a cell to convert incident photons of a given wavelength into photocurrent is measured by the incident monochromatic photon to current conversion efficiency (IPCE), which is defined as the number of electrons generated per number of incident photons. It can be obtained using:

$$IPCE\%=\frac{(\#\text{of electrons})_{out}}{(\#\text{of photons})_{in}}x100=\frac{1240I_{SC}}{\lambda I_i} \qquad (1.15)$$

where I_{sc} is the short circuit current (μA cm^{-2}), λ the excitation wavelength (nm) and I_i the photon flux (W m^{-2}) measured with a standard silicon diode.

1.5.5. Optimization of the Efficiencies of PSCs.

Better efficiencies in polymer solar cells can be achieved by optimizing the various steps involved in the generation of current from the incident light. These include improving the light absorption, the charge separation, transport and collection process. Some of the attempts towards this goal are described below.

1.5.5.1. Light Absorption

One strategy to improve light absorption demonstrated by Inganäs's group [66] is to trap light inside the active layer by creating a grated structure in the polymer layer using soft lithographic techniques. Much of this work was based on bilayer devices, in which a planar heterojunction is formed between a layer of polymer (the hole acceptor) and

evaporated fullerene (C_{60}). In these devices, pattering the polymer layer with periodic grooves increases the trapping of light and absorption path length in the structure, as well as increasing the surface area of the donor-acceptor interface. This technique has also been used in this thesis work to increase the electrochromic property of PEDOT-PSS (see Chapter 4).

In most organic solar cell devices only a small portion of the incident light is absorbed because the bandgap is too high. Even in the most efficient device made so far from P3HT/PCBM, they only cover wavelengths up to 600 nm [67-68]. Below 600 nm, only about 30% of the solar energy can be collected (see Figure 1.28). However, if the absorption is extended to 1100 nm, about 80% of the solar energy could be utilized. To construct solar cell devices reaching into the NIR and IR regions, polymers with narrow band-gaps that absorb light at the longer wavelengths are needed.

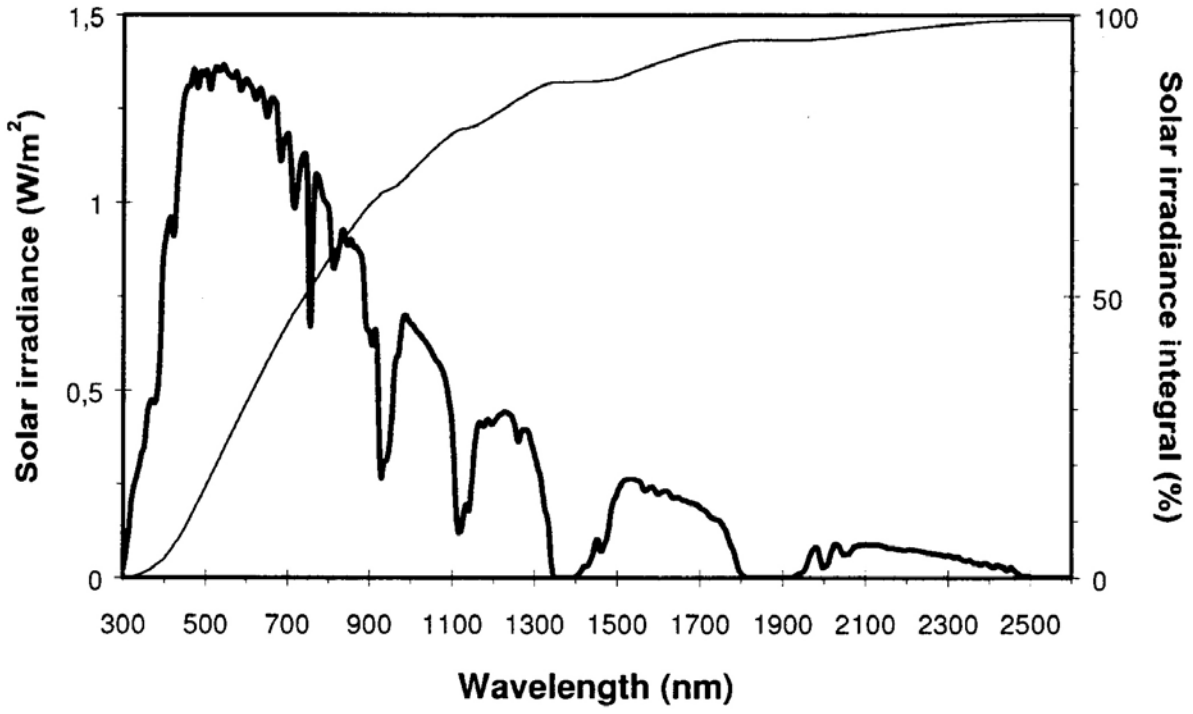

Figure 1.28 *Solar irradiance spectrum (broad curve) and the cumulative integral of the irradiance (thin curve).*

However, at least two challenges could be identified with low band-gap polymers to harvest long wavelength photons. One is the reduction of open-circuit voltage (V_{OC})

compared with high band-gap polymers, because the V_{OC} is related to the energy difference of LUMO of the electron acceptor and HOMO of the electron donor [69-70]. The other challenge is to have large enough driving force for electron transfer from the polymer to the electron acceptor. This means that the LUMO of the electron donor must be closer in energy to vacuum than the LUMO of the electron acceptor in order to have enough driving force for exciton dissociation at the interface of electron donor and acceptor [71-72]. When decreasing the band-gap of a polymer both the LUMO level and the HOMO level are affected. The LUMO position of the polymers might be shifted away from the vacuum level so much that the use of new electron acceptors with lower LUMO than the commonly used PCBM is needed for preparing an efficient solar cell [71-72]. To the best of our knowledge, the J_{SC} of 8.88 mA/cm^2, V_{OC} of 0.59 V and PCE of 2.2% with spectral response extended to 800 nm obtained from the recently synthesized alternating polyfluorene copolymer, APFO-Green5 (see Chapter 2) are the highest published values among low band-gap polymer solar cells [72-77].

1.5.5.2. Charge Separation

Charge separation is known to occur at organic semiconductor/metal interfaces, at impurities such as oxygen or between materials with sufficiently different electron affinities (EA) and ionisation potentials (IP). In the latter, one material can act as electron acceptor (A) while the other keeps the positive charge and is referred to as electron donor (D). If the difference in IP and EA is not sufficient, the exciton may just hop onto the material with the lower band gap without splitting up its charges. Eventually it will recombine without contributing charges to the photocurrent. At present the highest overall efficiency of polymer based organic solar cell is based on the concept of bulk hetrojunction, where the active layers are made up of blends of a conjugated polymer, poly(3-hexylthiophene) (P3HT) and a derivative of the Buckminster fullerene called PCBM (Figure 1.29).

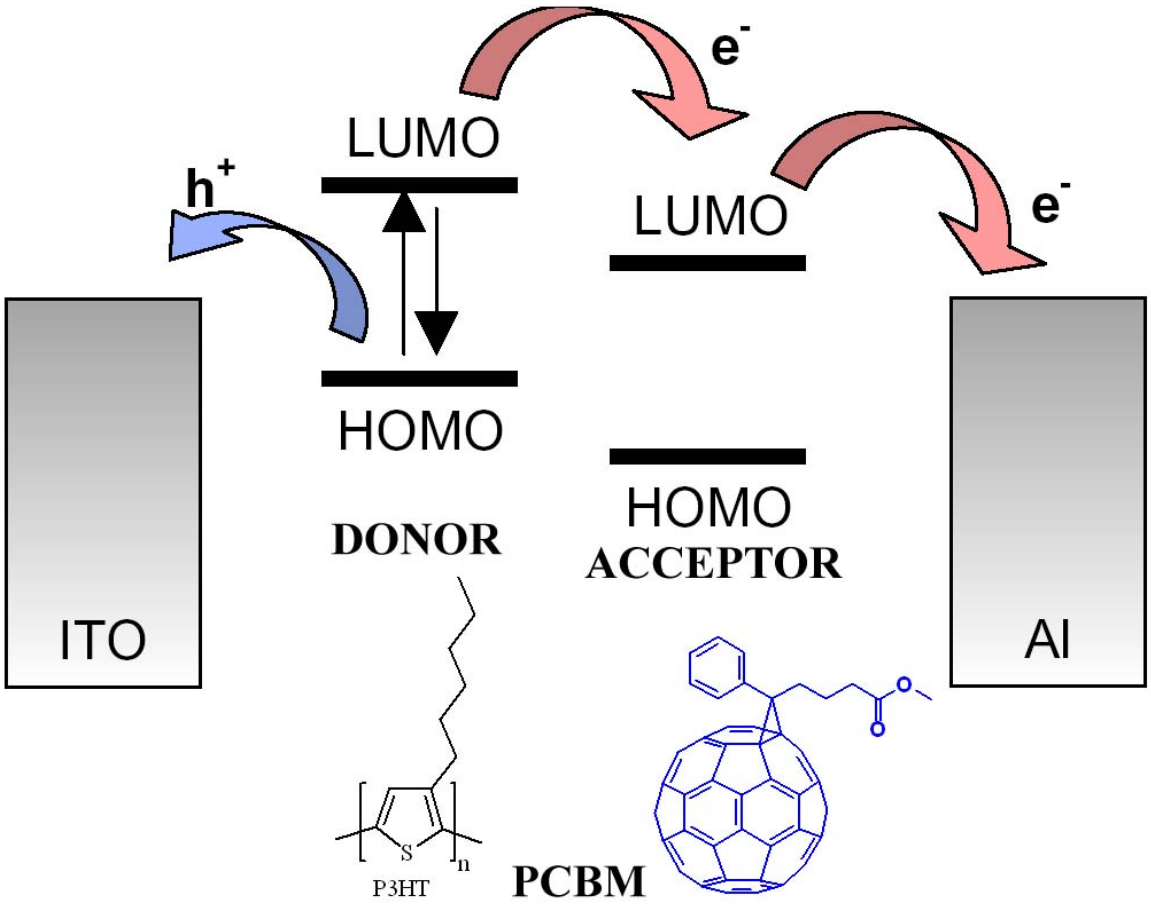

Figure 1.29 *Dissociation of electron-hole pair at the donor-acceptor interface. The electron goes to the acceptor while the hole stays on the donor.*

As depicted in Figure 1.29, when the donor molecule is excited (upward arrow); the electron is promoted from HOMO to LUMO leaving a hole behind. The electron and hole can recombine (downward arrow), yielding, e.g., luminescence, or they can dissociate. If the acceptor LUMO is sufficiently lower than the donor LUMO, the excited electron will relax into the acceptor LUMO and in this way separate from the hole.

1.5.5.3. Charge Transport

The morphology of conjugated polymer/fullerene mixture in bulk heterojunction solar cells is known to have an important influence on charge transport. One way to control the

morphology is by a proper choice of the solvent used for dissolving the mixture. Sariciftci's group showed that the photocurrent and open circuit voltage of the diodes depends on the solvent used to dissolve the components. They demonstrated that the power conversion efficiency of the solar cells could be improved dramatically by manipulating the morphology of the blend. A device made from a chlorobenzene solution showed a threefold increase in efficiency compared to the device made from a toluene solution. They attributed the resulting enhancement in the organic solar devices as originating from the improved mobility of the charge carriers [78]. Postproduction heat treatment was also found to have an influence on the morphology of the film. Very recently, Heeger's group demonstrated polymer based organic solar cells with PCE approaching 5% after postproduction thermal annealing at 150^{o}C. They attributed the higher efficiency to thermally induced morphological modification, thermally induced crystallization and improved transport across the interface [79].

1.5.5.4. Charge Collection.

When a pristine conjugated polymer is brought into contact with electropositive metals typically used as electrodes like aluminium, an insulating layer is formed at the interface between the aluminium and the polymer. For instance in the case of aluminium on poly(p-phenylene vinylene) (PPV), X-ray Photoelectron Spectroscopy (XPS) studies reveals the formation of a 30 Ă thick insulating layer. This layer is thought to be formed as Al atoms diffuse into the polymer matrix where Al reacts with the vinyl groups and disrupt the conjugation. The effect of this layer is to increase the electron injection barrier at the interface. Naturally, as the layer becomes thicker and thicker electron extraction becomes impossible rendering the device useless. Different strategies have been investigated to overcome this problem. In LEDs a thin protective layer between an Al-electrode and the organic layer has been found effective and increasing overall performance. Hung *et al.* [80] demonstrated that a 5–10 Ă thin LiF or MgO layer improved efficiency of the Al-electrode by lowering the electron-injection barrier. LiF does not dissociate and react chemically, but rather serves as a protecting layer between the electrode and the organic material. Also, Al_2O_3 has been shown to have favourable

properties as a protective layer reducing drive voltage and increasing device performance in LEDs [81]. LiF has been reported to increase the FF and stabilise the V_{OC} in PV cells.

Transparent ITO is the material most used as the high-work function material in PV devices and LEDs. The ITO–polymer interface is not well understood or well controlled. There are large variations of the ITO morphology and work function from manufacturer to manufacturer and from batch-to-batch [64]. Similar to the cathode interface, atoms from the anode can react with the organic material. Also, indium was found to diffuse into the organic layer where it acts as trapping site for charge carriers [82]. One strategy used to minimize indium and oxygen diffusion is to place an interfacial hole-transporting layer, such as PEDOT-PSS [64], between ITO and the active material. This layer also serves to smooth out the uneven surface of ITO.

1.6. Polymer Light Emitting Diodes

1.6.1 Introduction

A light-emitting diode (LED) is a solid-state device that emits light upon the application of a forward-biasing current. It is different from the incandescent light bulb, in which heating a filament to a very high temperature generates light. A LED is a cold lamp, which converts electric energy directly into optical energy without the intermediate step of thermal conversion. This luminescent mechanism, called electroluminescence, has an emission wavelength in the visible or infrared region [83].

The initial discovery of such a phenomenon in 1936 [84] for inorganic materials has attracted a great deal of attention. Since then, a series of inorganic light emitting diodes (LEDs) have been developed, capable of emitting light of the whole visible spectra. The materials used to fabricate inorganic LEDs are compounds of elements from groups III and V of the periodic table such as GaAs, GaP, AlGaAs, InGaP, GaAsP, GaAsInP, and AlInGaP. Hence, the fabrication processes of inorganic LEDs are complicated making the fabrication cost of inorganic LEDs very high [85].

Electroluminescence from organic materials was already known from 1963, when it was first observed for anthracene single crystal [86]. Nevertheless, the research remained focused on inorganic devices, due to the weaker performance and the disadvantageous operation durability of organic devices. With the widespread use of organic functional materials in every field of electronic and opto-electronic applications during the 1980s, the researches on OLEDs have gained increasing attention. The main reason why organic materials have gained so much attention in the field of light emitting diodes is the possibility of producing low cost, large area, and flexible films of organic compounds for applications such as roll-up TV screens and displays [87].

The basic requirements for organic electroluminescent materials are the capability to undergo charge transfer to an electrode, the ability to transport charge and to fluoresce efficiently. A variety of organic materials including metal chelates, simple oxadizoles, triarylamines and various ECPs have been investigated as active components in order to optimize device performance [88].

1.6.2 The Basic Operational Principles of Polymer Light Emitting Diodes

In a light emitting diode (LED) or electroluminescent device (Figure 1.30a), the thin film of light-emitting material is sandwiched between two electrodes, one of which has to be semitransparent [89]. Under an applied bias (voltage), oppositely charged carriers (electrons and holes) are injected into the emissive layer(s) from the opposing contacts, and are swept through the device by the high ($> 10^5$ V/cm) electric field. Some of the electrons and holes combine within the emissive material to form triplet and singlet excited states. The singlets are indistinguishable from the excited states of photoluminescence (PL), the fluorescence process resulting from photoexcitation of the ground state, where irradiation of a fluorescent polymer excites an electron from HOMO to LUMO. In a typical conjugated polymer, two new energy states are generated upon relaxation within the original HOMO-LUMO energy gap and each filled with one electron of opposite sign (singlet excited state). The excited state polymer may then relax to the ground state with emission of light at a longer wavelength than that absorbed (photoluminescence) (Figure 1.30b). In a PLED, electrons are injected into the LUMO

(to form a radical anion) and holes into the HOMO (to form a radical cation) of the electroluminescent polymer. The resulting charges migrate from polymer chain to polymer chain under the influence of the applied electric field. When a radical anion and a radical cation combine on a single conjugated segment, singlet and triplet excited states are formed, of which the singlets emit light (Figure 1.30c).

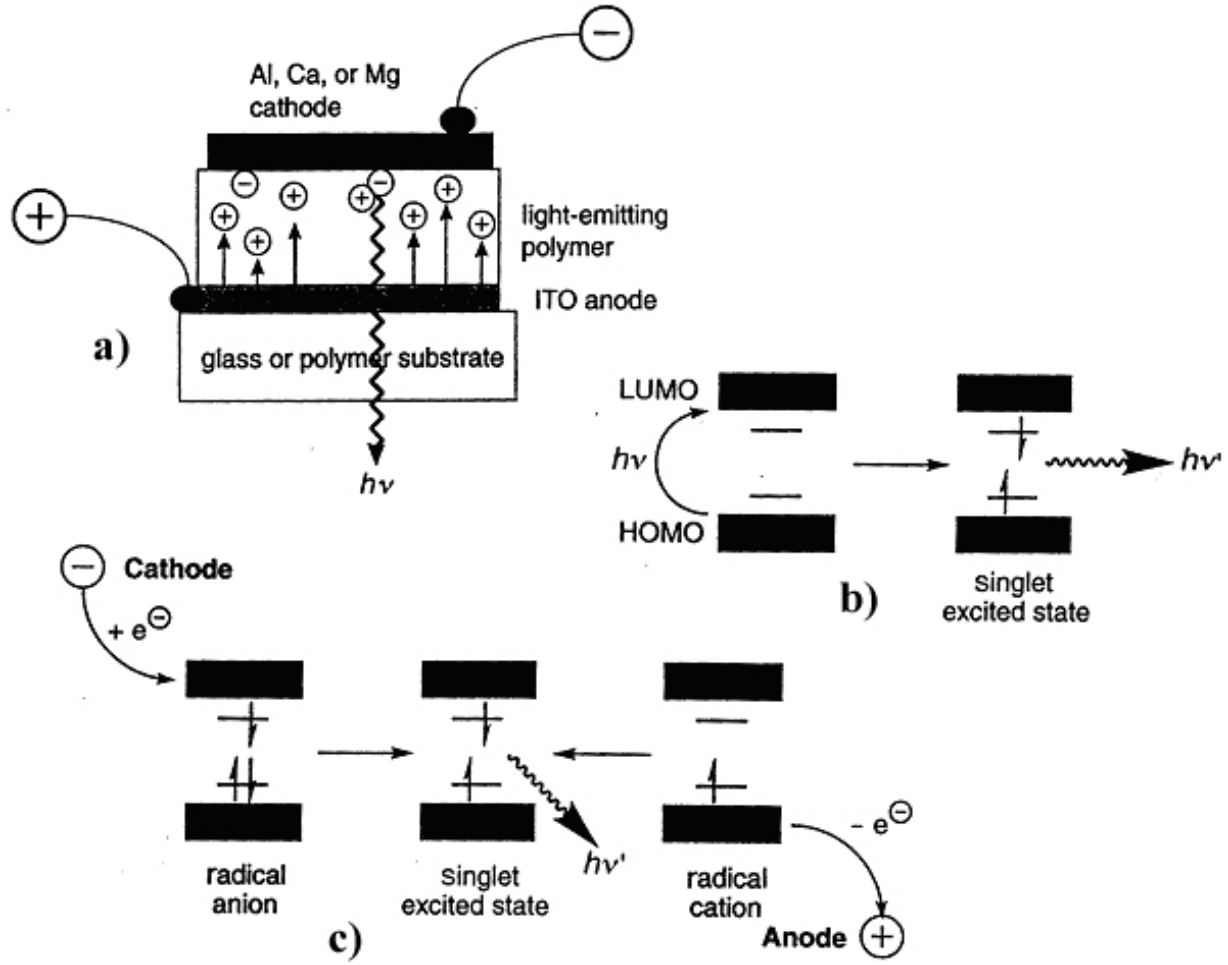

Figure 1.30 *(a) Schematic drawing of a single-layer electroluminescent device, (b) photoluminescence and (c) electroluminescence process in polymer LED.*

1.6.3 Preparation and Characterization of PLEDs

The device preparation procedures for single layer polymer based light emitting diodes are similar to that of polymer based organic solar cells described in section 1.5.3 except that the electron acceptor PCBM is not added in the active layer.

Organic light emitting diodes are characterized by recording absorption, photoluminescence and electroluminescence spectra as well as the current-voltage and luminance-voltage curves. Typical results are shown in Figure 1.31. Below a so-called 'threshold voltage', typically 2 to 5 V, the current is small and no light is emitted. Above it, emission appears and both L and J increase rapidly together with V. The EL emission spectrum is nearly identical to that of photoexcited fluorescence of the emitting material, indicating that the emitting state is the same in EL and ordinary fluorescence. The emission spectrum is generally fairly broad. Cyclic voltammetry is used to estimate the HOMO and LUMO levels of the active materials.

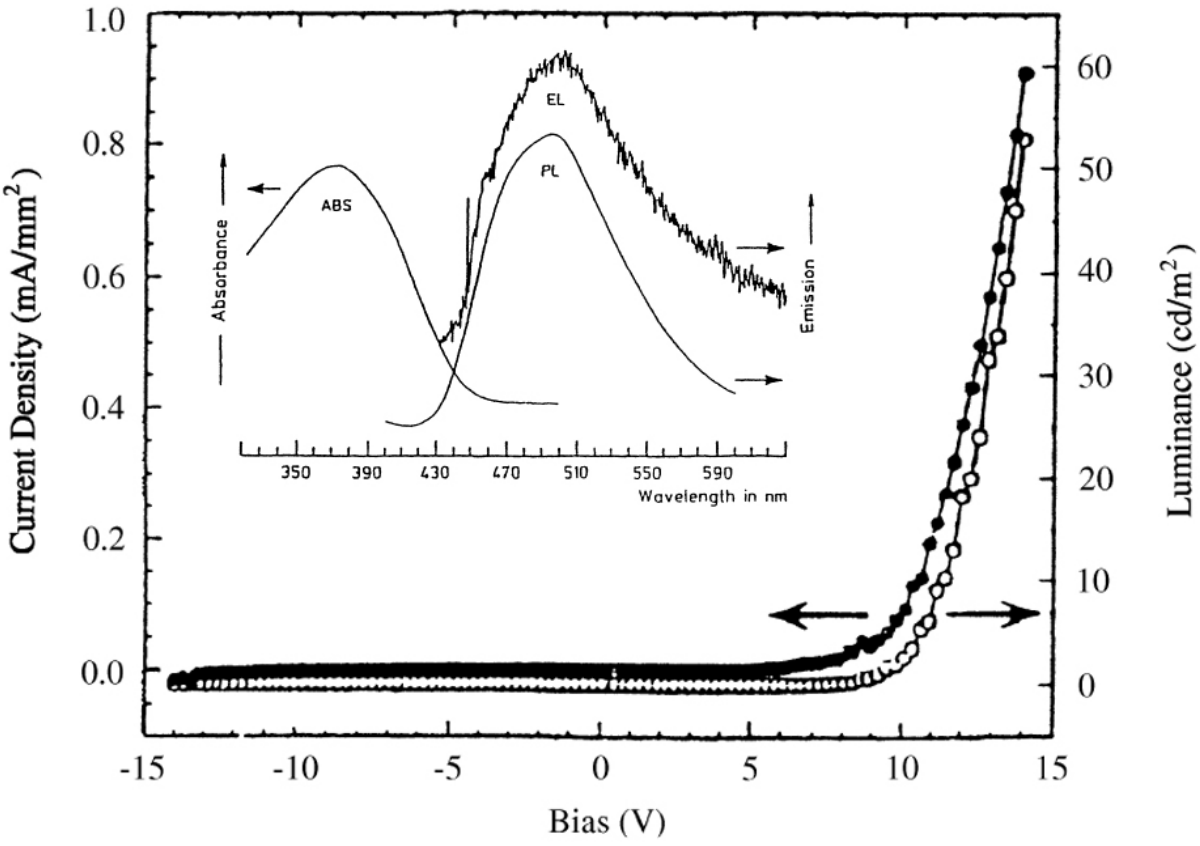

Figure 1.31 *Typical variations of the current density J and of the luminance L with applied voltage V in an OLED. Insert: Typical absorption (ABS), photoluminescence (PL) and electroluminescence (EL) spectra of an organic material [90].*

External quantum efficiency (EQE) is commonly used in evaluating the emission property of OLEDs. It is defined as the ratio of the number of photons emitted by the

OLED into the viewing direction to the number of electrons injected [91]. Another measure of the efficiencies of OLEDs is the internal quantum efficiency (IQE), which is defined as the ratio of the total number of photons generated within the structure to the number of electrons injected.

1.6.4 Some Strategies to Optimize the Efficiencies of PLEDs.

To achieve improved EQEs, it is crucial for charge injection and transport to be balanced. At least four kinds of strategies have been reported in the literature and are briefly described below with some illustrative examples.

1.6.4.1. Low work function cathode

A low work function metal, such as calcium, can be used as the cathode to lower the energy barrier to electron injection into the polymer film. For example the EQEs of MEH-PPV based deviced increased from 0.002% to 0.36% when the cathode is changed from Al to Ca. [92]. The drawback of this strategy is that such metals are highly reactive and are unstable in the atmosphere.

1.6.4.2. Bilayer Devices

Improvements in device performance of PLED were reported by assembling an electron transporting layer (ETL) in a multilayer structures. Pei et al [92] demonstrated that the EQE of the single layer device consisting of ITO/MEH-PPV/Al is improved from 0.002% to 0.08% by introducing the electron transporting oxadaizole containing polymer **P1** in the bilayer device consisting of ITO/MEH-PPV/P1/Al. The EQEs of a single layer OLEDs prepared by poly(p-phenylene vinylene) (PPV) is usually in the range of 0.0005% and 0.002% [93]. Chen et al [94] increased the EQE to 0.1% by using **P2** as an electron transport layer in the bilayer structure of ITO/PPV/**P2**/Al. Dailey *et al.* [95] also reported an improved EQE of 0.25% using PPY as electron transport layer in the device structure ITO/MEH-PPV/PPY/Al. The ETL is placed on top of the emissive polymer film

(by spin-coating or thermal evaporation) before deposition of the cathode. This approach requires more complex fabrication procedures than those used for single-layer devices.

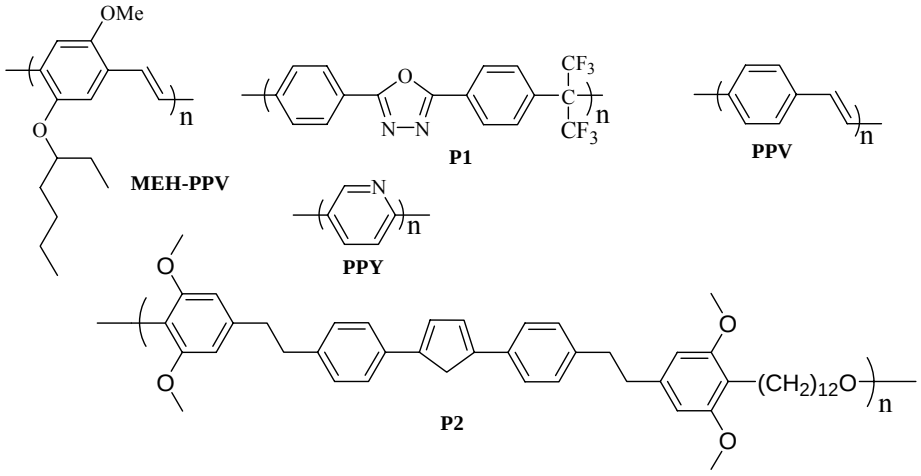

Figure 1.32 *Chemical structures of some polymers used in bilayer devices.*

1.6.4.3. Blend Devices

Blends of donor and acceptor conjugated polymers with favorable electronic structures (HOMO/LUMO levels) represent one option to achieve balanced charge injection and transport in polymer light emitting diodes. Alam *et al.* [96] used poly(2,2'-(3,3'-dioctyl-2,2'-bithienylene)-6,6'-bis(4-phenylenequinolene)) (POBTPQ) as n-type conjugated polymer blended with MEH-PPV and reported an EQE of 0.70% for 70% (by wt.) composition of MEH-PPV.

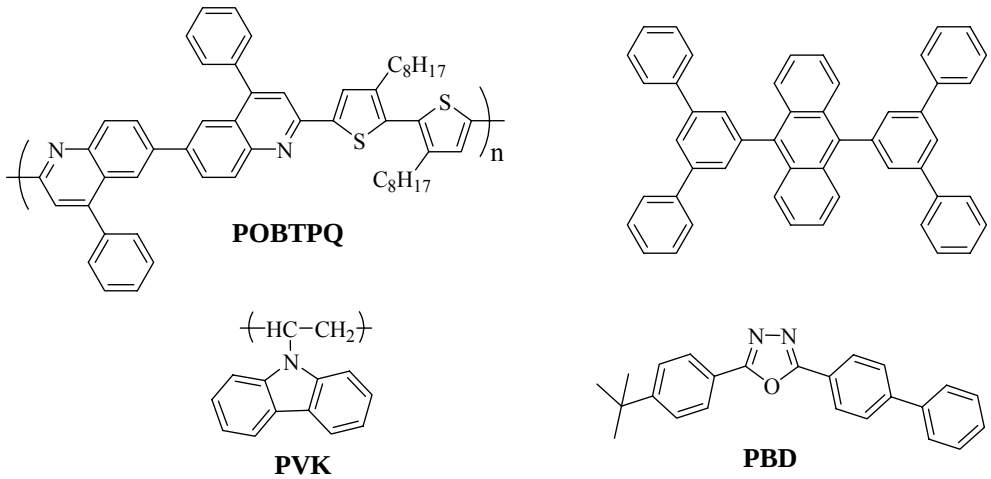

Figure 1.33 *Chemical structures of some polymers and small molecules used in blend devices.*

Recently, Niu *et al.* [97] reported a highly efficient single-layer LEDs by blending 9,10-bis(3',5'-diaryl)phenyl anthracene (DPPA) in poly(N-vinylcarbazole) (PVK) with an electron-transporting molecule 2-tert-butylphenyl-5-biphenyl-1,3,4-oxadiazole (PBD) with an EQE of 1.5%.

1.6.4.4. Single layers with electron transporting units.

Electron-deficient segments can be covalently bound to the emissive polymer, either by insertion into the main-chain, as end-capping groups, or as pendant side-groups. The synthesis of these polymers can be very challenging, often requiring multi-step routes and/or specific cross-coupling reactions.

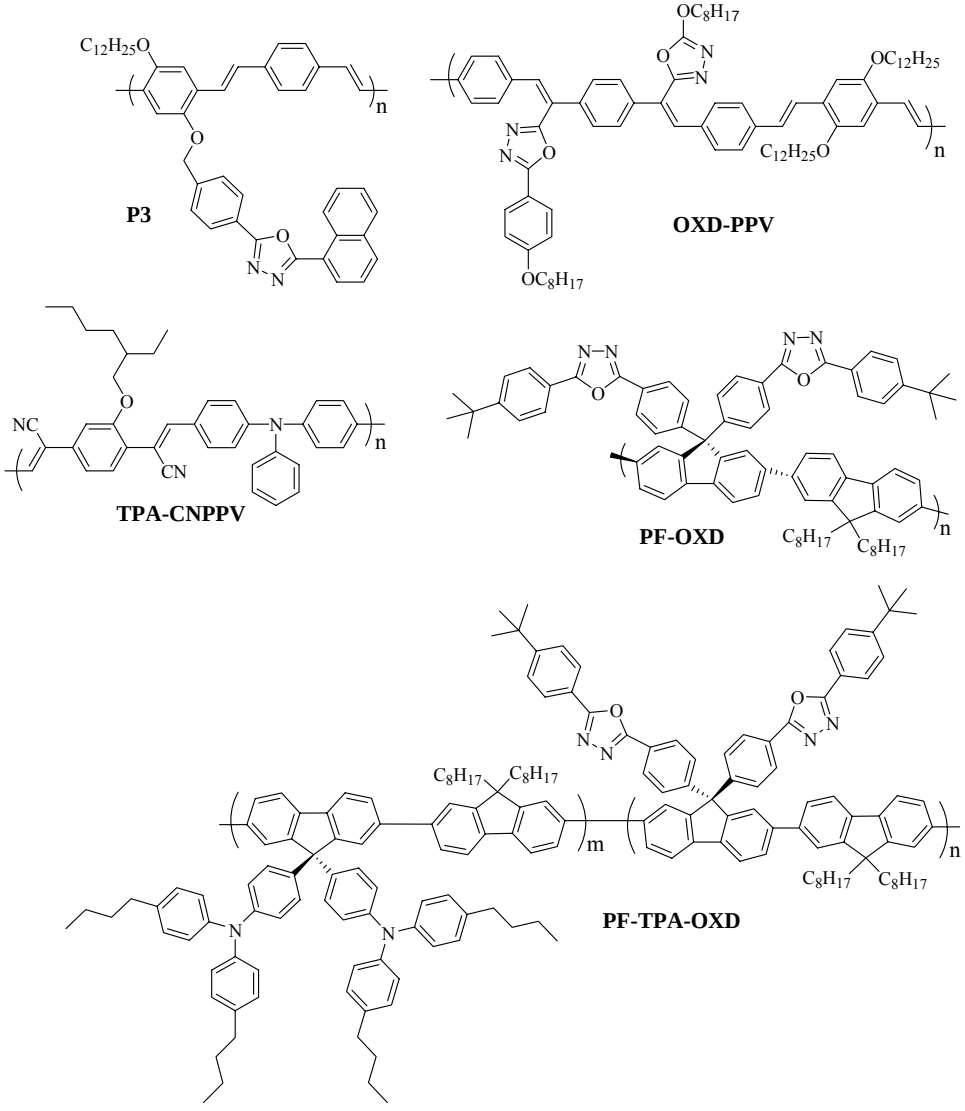

Figure 1.34 *Chemical structures of some polymers used in single layer devices.*

Bao *et al.* [98] prepared an organic soluble PPV derivative (**P3**) bearing an electron transporting pendant and an alkoxy group in the phenylene ring and also placed an oxymethylene spacer between the pendant and the backbone. This polymer emits light at 580 nm, and the ITO/**P3**/Al device exhibited an EQE of 0.02%. Li *et al.* [99] synthesized a PPV derivative with both hole and electron injecting units having an EQE of 0.1% and luminance of 2100 cd/m^2 in ITO/TPA-CNPPV/Al. Kim *et al.* [100] reported a highly efficient PPV derivative with oxadiazole pendant unit (OXD-PPV) with an EQEs of 0.34% and 1457 cd/m^2 for Al cathode. Oxadiazole containing polyfluorenes are also widely investigated. Shu *et al.* [101-102] reported an EQE of 0.52% at a brightness of 537 cd/m^2 for PF-OXD and 1.21% at a brightness of 354 cd/m^2 for PF-TPA-OXD in a single layer device.

1.7. Chromism in Electronically Conducting Polymers

1.7.1. Polymeric Electrochromism

1.7.1.1. Introduction

Chemical species that can be electrochemically switched between different colours are said to be electrochromic. Electrochromism results from the generation of different visible region electronic absorption bands on switching between redox states. Major applications of electrochromic materials are in displays and in the fabrication of smart windows. Smart windows are active glazing devices that can be used to control the amount of visible and solar radiation entering a building, in order to minimise the building's energy load normally associated with heating, cooling and lighting [103-110].

1.7.1.2 Types of Electrochromic Materials

There are three main types of electrochromic materials in terms of their electronically accessible optical states. The first type includes materials with at least one colored and one bleached state. These materials are especially useful for absorption/transmission-type

device applications such as smart windows and optical shutters. Typical examples of this area are metal oxides, viologens, and polymers such as poly(3,4-ethylenedioxythiophene) (PEDOT). A second class of materials consists of electrochromes with two distinctive colored states. These EC materials lack a transmissive state but are useful for display-type applications where different colors are desired in different redox states. Polythiophene is a good example of this type, where the thin films of this polymer switch from red to blue upon oxidation. A third class includes the growing interest in the electrochromic field, where more than two color states are accessible depending on the redox state of the material. This is the area where conjugated polymers have found the most interest due to their versatility for making blends, laminates, and copolymers. Additionally, there are inherently multicolor EC polymers such as PANI or poly(3,4-propylenedioxypyrrole) (PProDOP). Whilst many types of chemical species exhibit electrochromism, only those with favourable electrochromic performance parmeters are potentially useful in commercial applications. Thus most applications require electrochromic materials with a high contrast ratio, colouration efficiency (absorbance change/charge injected per unit area) and cycle life. Whereas displays need fast response times, by contrast smart windows can tolerate response times of up to several minutes [104]. Some of the important parameters in identifying and characterizing the electrochromic materials are outlined in section 1.7.1.5.

1.7.1.3 Polythiophenes as Electrochromic Materials

Polythiophene are among the several conducting polymers investigated in electrochromism. Thin films of conducting polythiophenes may be prepared by the electrochemical oxidation of solution monomer via the thiophene radical cation. The electrochromic properties of polythiophene and of the polymers of several substituted thiophenes are shown in Table 1.1. These polymers are inherently electrochromic, and they can be switched electrochemically or chemically between different colored states. Most of the well-studied conjugated polymers are anodically coloring, meaning they are more deeply colored in their oxidized form. Polythiophene (PT) and its 3-substituted derivatives fall into this category. These polymers are red to purple in their reduced or neutral form, and dark blue to black in their oxidized form. Although this type of color

change can be useful, a more desirable color change would be one where the polymer switches from a highly colored state to a highly transmissive state [104].

Table 1.1. Electrochromic transition in some polythiophenes.

Monomer	Polymer λ_{max}/nm and color	
	Oxidised	Reduced
Thiophene	730	470
	Blue	Red
3-methylthiophene	750	480
	Deep blue	Red
3,4-Dimethylthiophene	750	620
	Dark blue	Pale brown

Of the conducting polymers available, poly(3,4-ethylenedioxythiophene) (PEDOT) and its derivatives exhibit the most promising EC properties. When compared to PT, PEDOT exhibits more rapid switching, lower oxidation potentials, and greater stability at ambient and elevated temperatures. In addition, PEDOT is a cathodically coloring polymer that is a dark opaque blue in its reduced form and a very transmissive light blue in its oxidized form [111].

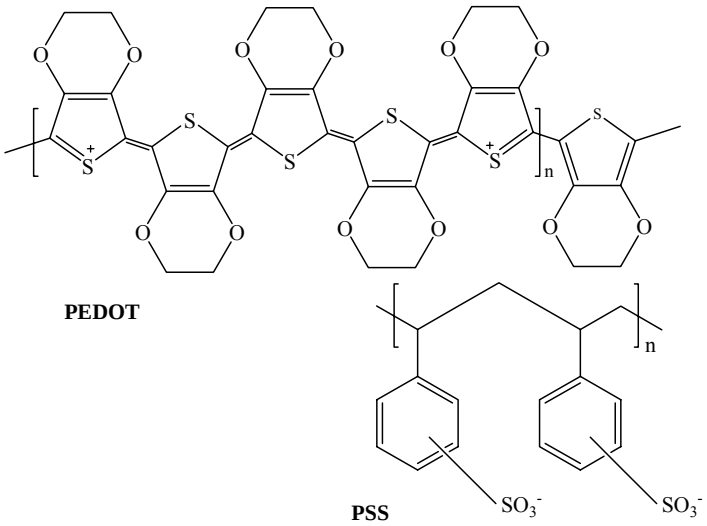

Figure 1.35 *Baytron P (Bayer AG, Leverkusen, Germany), which is a dispersion of the oxidized polymer PEDOT and the polyanion PSS in water.*

The conducting polymeric complex of poly(3,4-ethylenedioxythiophene) and poly(styrene sulfonate) (PEDOT/PSS) forms a dispersion of the oxidized polymer PEDOT and the polyanionic PSS. This dispersion is commercially available from Bayer under the trade name Baytron P (Figure 1.35) [112-113].

1.7.1.4 Origin of Electrochromism in Conjugated Polymers

Electrochromism in conjugated polymers occurs through changes in the conjugated polymer's π-electronic character accompanied by reversible insertion and extraction of ions through the polymer film upon electrochemical oxidation and reduction. In their neutral (insulating) states, these polymers show semiconducting behavior with a band gap (Eg) between the valence band (HOMO) and the conduction band (LUMO). Upon electrochemical or chemical doping, the band structure of the neutral polymer is modified, generating lower energy intraband transitions and creation of charged carriers (polarons and bipolarons), which are responsible for increased conductivity and optical modulation. The doping process, and the resulting optical changes in conjugated polymers, can most vividly be illustrated through spectroelectrochemical experiments such as the one shown in Figure 1.36-1.37 for a thin film of poly(3,4-ethylenedioxythiophene)–poly(styrene sulfonate) [39, 114] .

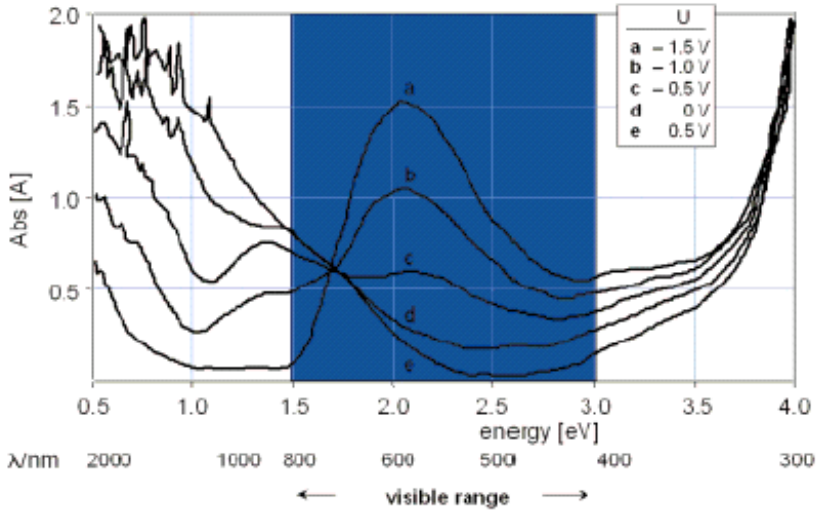

Figure 1.36 *Optical absorption spectra of a PEDOT/PSS cell for different voltages, i.e. different oxidation levels.*

This polymer is deep blue in the neutral state, and upon electrochemical oxidation switches to a transmissive sky blue in the oxidized (conducting) state. The neutral (colored) state of PEDOT-PSS has a strong π–π* absorption in the visible region with a maximum wavelength at about 610 nm. Initial oxidation (p-doping) results in a new absorption band in the near-IR region (~900 nm), forming at the expense of the π–π* transitions, which is attributed to polarons (radical cations) generated along the polymer chain. Upon complete electrochemical oxidation, the π–π* transitions are fully depleted and the polaron absorption peaks are lost, while a lower energy transition, peaked in the near-IR region increases. This absorption is assigned to the bipolaronic (dication) state of the conjugated polymer. Such optical and structural changes are reversible through repeated doping and dedoping over many redox cycles.

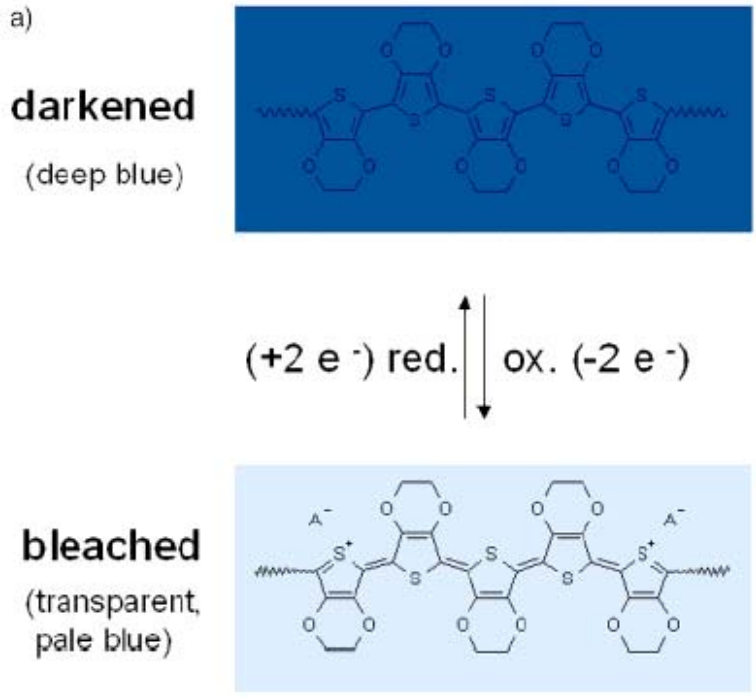

Figure 1.37 *Electrochromic switching of PEDOT/PSS.*

1.7.1.5 Characterization Parameters of Electrochromic Materials [115-116]

Electrochromic Contrast. Electrochromic contrast is probably the most important factor in evaluating an electrochromic material. It is often reported as a percent

transmittance change ($\Delta\%T$) at a specified wavelength where the electrochromic material has the highest optical contrast. For some applications, it is more useful to report a contrast over a specified range rather than a single wavelength.

Coloration Efficiency. The coloration efficiency (also referred to as electrochromic efficiency), η, is a practical tool to measure the power requirements of an electrochromic material. In essence, it determines the amount of optical density change (ΔOD) induced as a function of the injected/ejected electronic charge (Q_d), i.e., the amount of charge necessary to produce the optical change. It is given by the equation:

$$\eta = (\Delta OD)/Q_d = \log[T_b/T_c]/Q_d \qquad (1.16)$$

where η (cm^2/C) is the coloration efficiency at a given λ and T_b and T_c are the bleached and colored transmittance values, respectively. The relationship between η and the charge injected to the EC material can be used to evaluate the reaction coordinate of the coloration process, or the η values can be reported at a specific degree of coloration for practical purposes.

Coulombic efficiency. The coulombic efficiency, η', which is defined as the ratio between the reduction and oxidation charges is also used to characterize an electrochromic material. Values near to 100% indicate that the charge consumed in the reduction and oxidation are very close and indicate an efficient coloring/bleaching process.

Switching Speed. Switching speed is often reported as the time required for the coloring/bleaching process of an EC material. It is important especially for applications such as dynamic displays and switchable mirrors. The switching speed of electrochromic materials is dependent on several factors such as the ionic conductivity of the electrolyte, accessibility of the ions to the electroactive sites (ion diffusion in thin films), magnitude of the applied potential, film thickness, and morphology of the thin film. Today subsecond switching rates are easily attained using polymers and composites containing small organic electrochromes.

Stability. Stability is usually associated with electrochemical stability since the degradation of the active redox couple results in the loss of electrochromic contrast and hence the performance of the EC material. Common degradation paths include irreversible oxidation or reduction at extreme potentials, *iR* loss of the electrode or the electrolyte, side reactions due to the presence of water or oxygen in the cell, and heat release due to the resistive parts in the system. Although current reports include switching stabilities of up to 10^6 cycles without significance performance loss, the lack of durability (especially compared to LCDs) is still an important drawback for commercialization of ECDs. Defect-free processing of thin films, careful charge balance of the electroactive components, and air free sealing of devices are important factors for long term operation of ECDs.

Optical Memory. One of the benefits of using an electrochromic material in a display as opposed to a light-emitting material is its optical memory (also called open-circuit memory), which is defined as the time the material retains its absorption state after the electric field is removed. In solution-based electrochromic systems such as viologens, the colored state quickly bleaches upon termination of current due to the diffusion of soluble electrochromes away from the electrodes (a phenomenon called self-erasing). In solid-state ECDs, where the electrochromes are adhered to electrodes, the electrochromic memory can be as long as days or weeks with no further current required. In reality, however, ECDs may require small refreshing charges to maintain the charge state because side reactions or short circuits change the desired color.

1.7.1.6 Characterization Methods of Electrochromic Materials

Electrochromic materials are generally first studied at a single working electrode, under potentiostatic or galvanostatic control, using three-electrode circuitry. Traditional techniques such as cyclic voltammetry, coulometry, chronoamperometry, all with, as appropriate, *in situ* spectroscopic measurements are employed for characterization. Cyclic voltammetry studies helps to locate the potential range for the oxidation and reduction processes. Integrating the area under the i *vs* t curve obtained in the

chronoampereometric study helps to extract the charge injected/ejected during the redox process. The absorption *vs* time experiments carried out simultaneously with the chronoamperometry helps to find the transmission of the colored and bleached state.

For electrochromic device (ECD) investigations a simple two-electrode system is constructed in a sandwich configuration (Figure 1.38). In such devices, the 'electrochromic electrode' (where the colour switching takes place) is separated from a charge-balancing counter electrode by a solid (often polymeric) or liquid electrolyte [104-105].

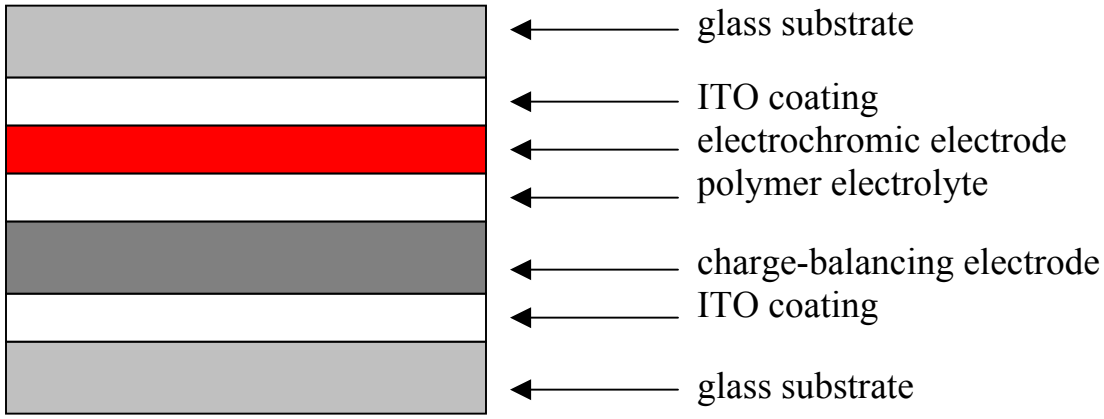

Figure 1.38 *Schematic diagram of a solid-state electrochromic device (ECD) suitable for a transmissive light-modulation application.*

Colour changes in the ECD occur by charging/discharging the electrochemical cell on application of an electric potential. The electrochemical electrode is generally glass coated with an electrically conducting film such as tin-doped indium oxide (ITO), onto which is deposited the electrochromic material. In variable light transmissive devices the counter electrode substrate also has to be transparent ITO glass, with the counter electrode chemical species being either colourless in both its redox forms or electrochromic in a complementary mode to the primary electrochromic material [104].

1.7.2. Polymeric Thermochromism and Solvatochromism

The chromic properties of polymers have been investigated by several groups in order to explain the relationship between optical properties and chemical structure [117-122]. These studies have also opened new possibilities for applications in chemical and biochemical sensors [123-126]. The chromic behaviour of these substituted polythiophenes depends on conformational transitions of the polythiophene backbone caused by changes in temperature (thermochromism) or solvent (solvatochromism). The transitions are believed to be between a coplanar (highly conjugated) form and a nonplanar (less conjugated) conformational structure of the backbone [127]. In order to understand the effect of substituents on molecular conformations and subsequently on their physical properties, theoretical calculations have been of great importance. *Ab inito* calculations performed on many substituted bithiophenes have provided rotational barriers that have been correlated with the thermochromism and solvatochromism observed on the parent polymers.

The first example [123] of transduction of physical information (temperature) into an optical signal from conjugated polymers was related to the so-called thermochromic effect. This intriguing effect has been extensively studied and has led to the development of various thermochromic polythiophene. As an example of thermochromism reported for some neutral conjugated polymers in solution, Figure 1.39 shows the temperature-dependent UV-vis spectrum of sodium poly(2-(4-methyl-3-thienyloxy)ethanesulfonate), in water. At low temperatures, this polymer is highly conjugated with an absorption maximum centered around 545 nm. Upon heating, an important color change (from red-violet to yellow) takes place, which is related to the shift of the maximum of absorption from 545 nm to 425 nm. These optical effects are thermally reversible (although some hysteresis is sometimes observed).

To a first approximation, these interesting optical effects have been attributed to a transition between a planar (highly conjugated) form and a non-planar (less conjugated) conformational structure of the backbone. These assumptions are based on the fact that

there is a close relationship between the backbone conformation and the electronic structure of conjugated macromolecules. Any twisting of the main chain from a planar conformation leads to a decrease of the effective conjugation length, which is associated with a blue shift of the absorption in the UV-Vis range.

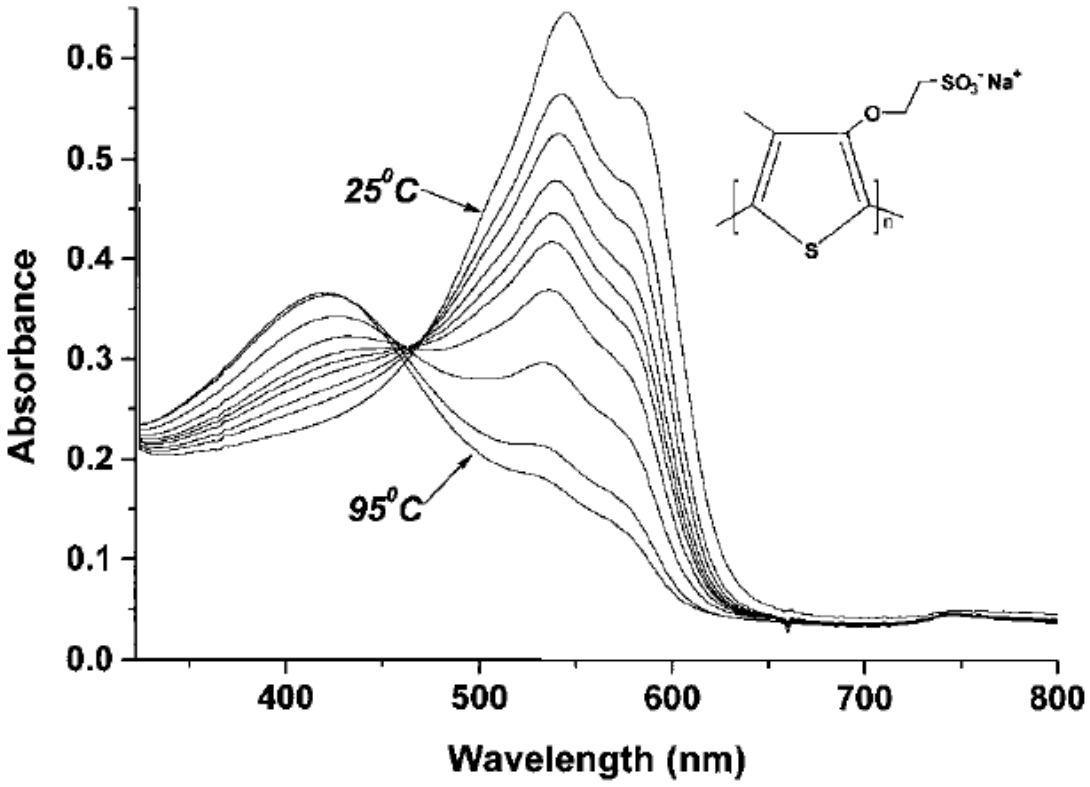

Figure 1.39 *Temperature-dependent UV-vis absorption spectrum of sodium poly(2-(4-methyl-3-thienyloxy)ethanesulfonate) in water, upon heating.*

Although the chromic effects are the consequence of the main-chain conformation (and/or interchain interactions), it has also been found that these thermochromic properties are strongly dependent upon the nature and the position of the side chains along the backbone. More precisely, it has been suggested that these optical effects are driven by a delicate balance between repulsive steric interactions and attractive interchain interactions; the latter being necessary to get a planar conformation in the case of thermochromic polythiophenes. For instance, comparisons between Figures 1.39 and

1.40 clearly show that subtle changes in the repeat unit of conjugated polymers can lead to completely different chromic behaviors. In both polymers, side-chain disordering can be thermally induced in the alkoxy substituents but conformational flexibility of the backbone is made possible by the adequate steric hindrance created by the methyl group at the 4-position, which forces the formation of a non-planar conformation when highly conjugated (co-planar) polythiophene assemblies are disrupted. The totally different chromic behaviour one observes by small changes in the structures of the repeating unit can also clearly be seen from the following example [120]. Poly(1,4-(2,5-dialkoxyphenylene)-2,5-thiophene) undergoes a reversible thermochromic transition. When heated, the color of the polymer changes from red to yellow, returning to red when it is cooled to room temperature.

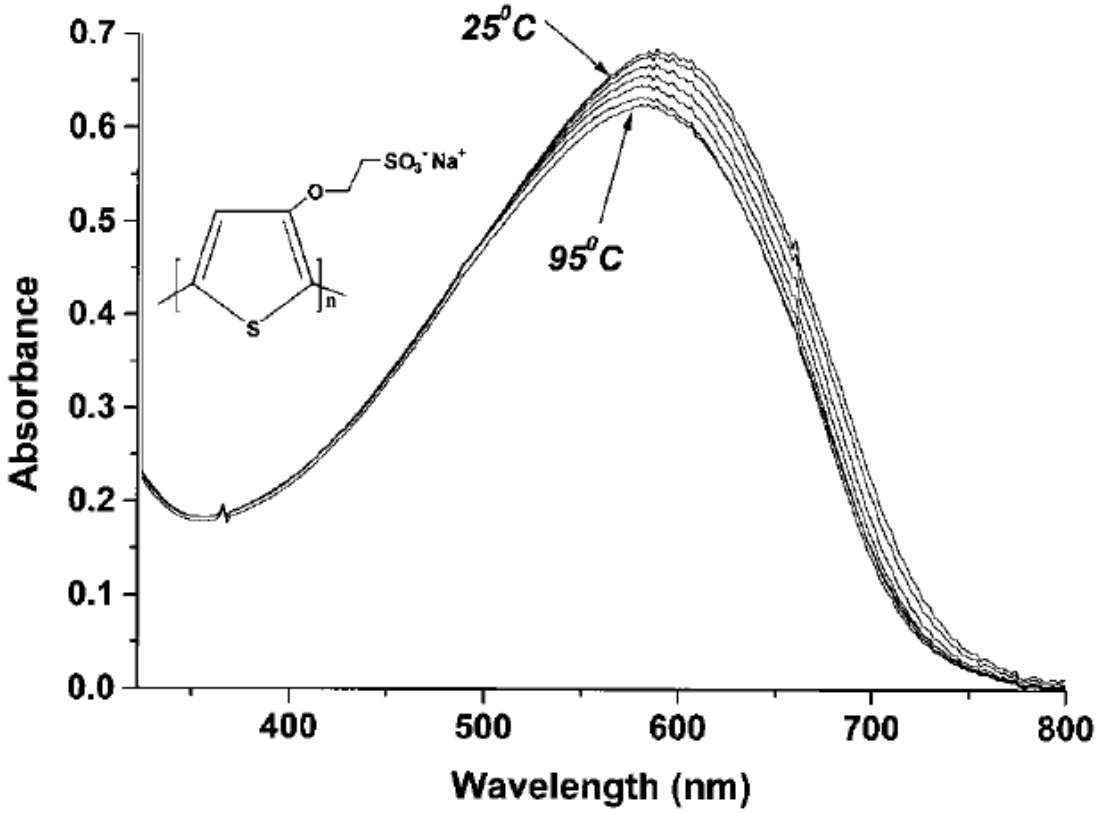

Figure 1.40 *Temperature-dependent UV-vis absorption spectrum of sodium poly(2-(3-thienyloxy)ethanesulfonate) in water, upon heating.*

As shown in Figure 1.41A, the maximum of absorption of poly(1,4-(2,5-dioctyloxyphenylene)-2,5-thiophene) varying from 495 nm at room temperature to 466 nm at 150 °C.

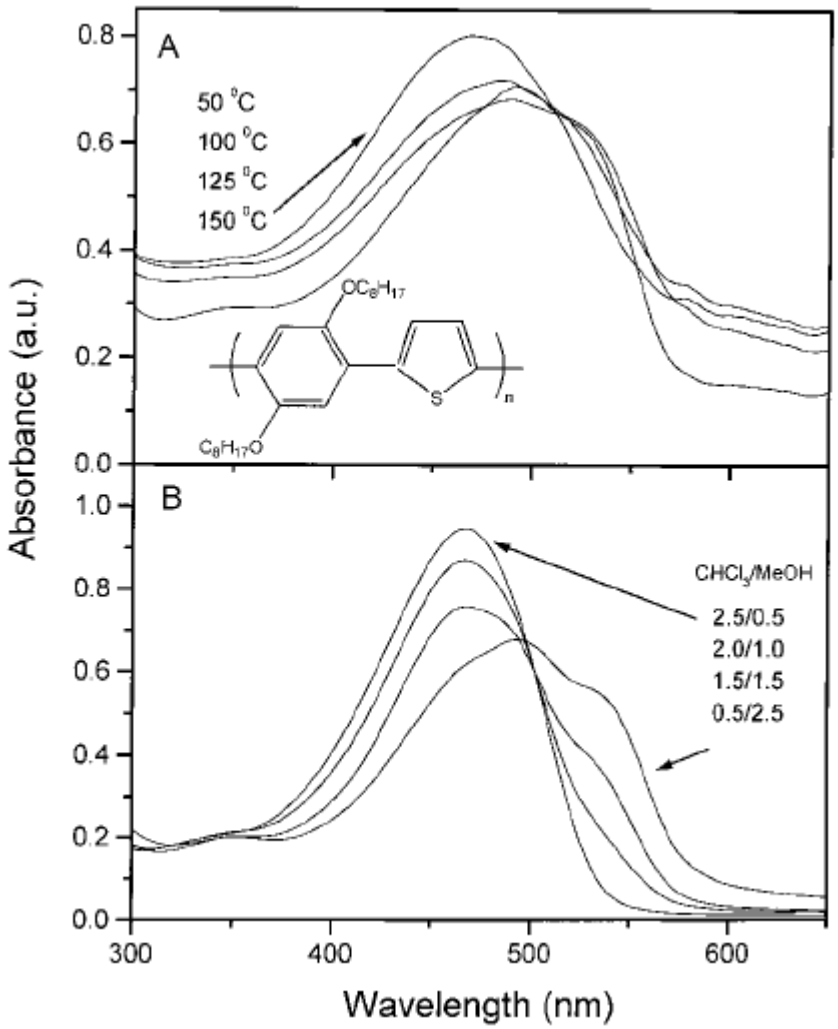

Figure 1.41 *Temperature-dependent (A) and solvent-dependent (v/v) (B) UV-vis absorption spectra of poly(1,4-(2,5-dioctyloxyphenylene)-2,5-thiophene).*

Similarly, solvatochromic studies in mixtures of chloroform (good solvent) and methanol (poor solvent) have revealed a shift of the maximum of absorption from 468 to 495 nm upon decreasing the quality of the solvent (Figure 1.41B). In both cases, it can be assumed that a more delocalized structure is created upon aggregation or cooling which leads to a red shift of the UV-vis absorption spectrum.

Quantum chemical theoretical analysis of the potential energy surfaces of dimer model compounds can be useful to understand these chromic effects. Planarization of twisted repeat units may occur upon stacking when the energy barrier against planarity is relatively small. In this regard, the potential energy surface of 1-(2,5-dimethoxyphenylene)-2'-thiophene (DMOPT) is reported in Figure 1.42.

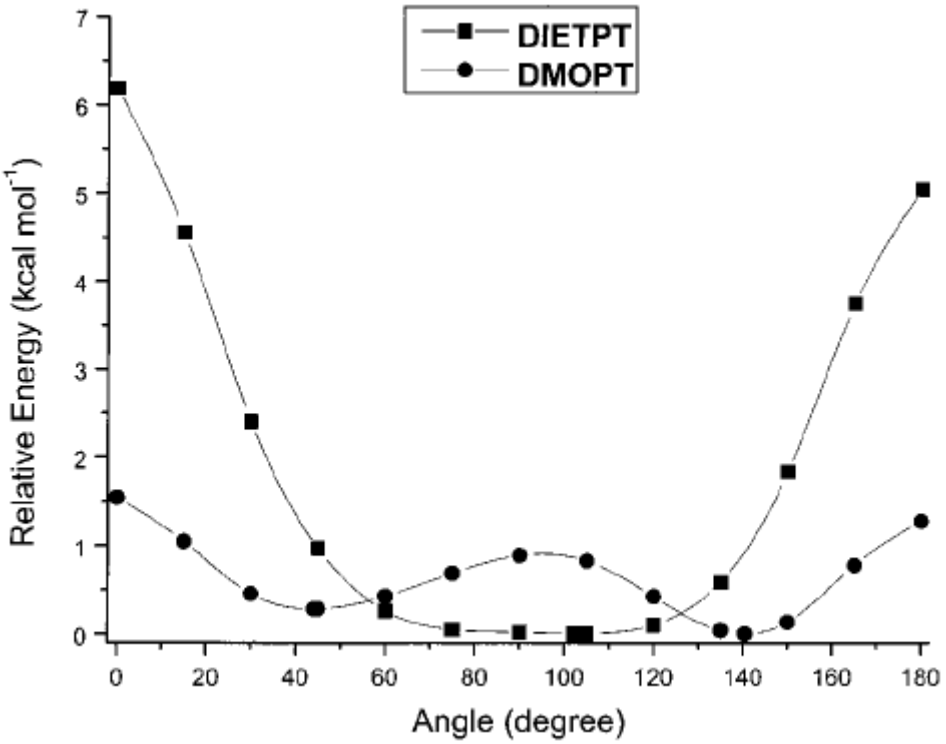

Figure 1.42 *Ground-state potential energy surfaces of 1-(2,5-dimethoxyphenylene)-2'-thiophene (DMOPT) and 1-(2,5-diethylphenylene)-2'-thiophene (DIETPT).*

In all cases, the dimeric model compound is the repeating unit of the related polymer with an anti (θ = 180°) conformation corresponding to the structure shown in Figure 1.41. Moreover, to reduce the time of calculations, octyloxy side chains were replaced by methoxy side groups for studies have shown that the side chain length does not significantly influence the conformation of the backbone. Therefore, for 1-(2,5-dimethoxyphenylene)-2'-thiophene (DMOPT), the global energy minimum is located at 140° whereas a local minimum is observed near 45°. One can see that the energy barrier against planarity (180°) is only 1.3 kcal/mol. This small energy barrier should be compensated through interchain interactions, and a coplanar structure is assumed to take

place in the related polymer in the solid state at low temperatures or upon aggregation in a poor solvent.

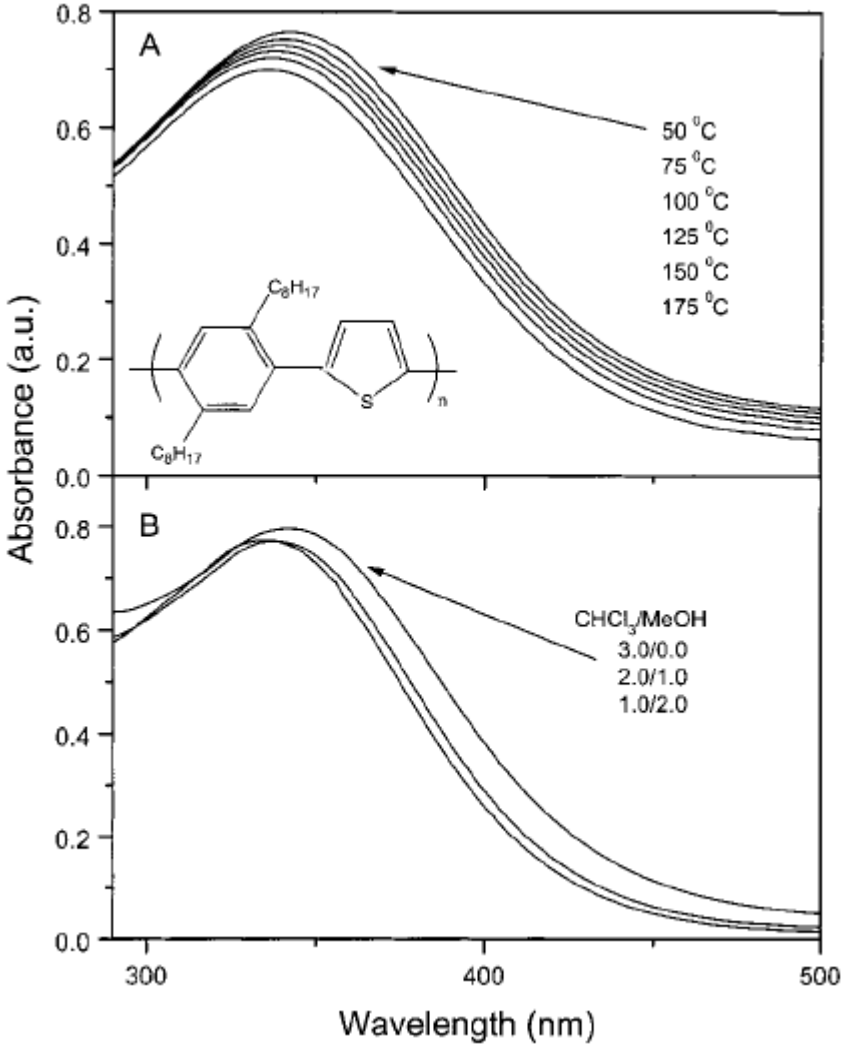

Figure 1.43 *Temperature-dependent (A) and solvent-dependent (v/v) (B) UV-vis absorption spectra of poly(1,4-(2,5-dioctylphenylene)-2,5-thiophene).*

In Figure 1.42, conformational analysis of 1-(2,5-diethylphenylene)-2'-thiophene (DIETPT) is also shown, and from these results, it is predicted that this dimer (and presumably, the related polymer) would adopt a highly twisted conformation (100°) with an energy barrier against planarity (180°) of 5.0 kcal/mol. This relatively high energy barrier should inhibit the formation of a coplanar structure. Accordingly, this twisted molecule (polymer) should remain twisted upon aggregation and, therefore, should not show any significant modification of its optical absorption spectrum as a function of

temperature or solvent quality. As shown in Figure 1.43, these assumptions have been confirmed: poly(1,4-(2,5-dioctylphenylene)-2,5-thiophene) exhibiting an absorption maximum at a relatively short wavelength (342 nm, both in the solid state and in solution) which does not significantly vary with temperature or solvent changes.

All these results on alternating conjugated polymers based on thiophene and 2,5-disubstituted phenylene units clearly show that minor modifications (the change of the oxygen atom next to the phenylene ring for a methylene group) in the structure of the repeat units may dramatically modify the chromic properties of the resulting polymers. Such important effects on the electrical and optical properties were already observed with various alkyl- and alkoxy-substituted conjugated polymers, and were tentatively explained by the different van der Waals radius of these two chemical species and by their different electron-donating effects.

1.8 Objectives of the Study and Organization of Subsequent Chapters

The general objective of this study was to design and characterize conducting polymer materials for use in electrochromic, photovoltaic and light emitting devices. The specific objectives include:

(i) To characterize conducting polymers specifically designed for photovoltaic and light emitting devices using electrical, electrochemical and optical techniques.
(ii) To design and manufacture photovoltaic cells using conducting polymers with acceptor molecules such as fullerene or its derivatives.
(iii) To micropattern electrochromic materials and analyse the electrochemical and optical properties that are necessary for improved performance.
(iv) To study the chromic properties of specifically designed conducting polymers.

The second chapter of this thesis deals with the electrical, optical and electrochemical characterization of several electronically conducting polymers designed for photovoltaic and light emitting devices. Using both cyclic voltammetry and square wave

voltammetry, the HOMO, LUMO and bang gap values were extracted. An attempt has also been made to study structure-property relationship in order to get insights for further improvement of device performance. Chapter 3 contains the work on synthesis and design of a highly conducting vapor phase polymerized (VPP) PEDOT for use as anode and cathode in photovoltaic devices to replace ITO and aluminium. The electrochromic properties of diffractive polymer grating prepared using soft lithographic techniques and bilayer consisting of conjugated polymers is presented in Chapter 4. This chapter also presents the solvatochromic and thermochromic properties of several undoped conjugated polymers.

1.9 References

1. P.J. Flory, Principles of Polymer Chemistry, Cornell University Press, New York, 1953, p. 3.
2. A. J. Heeger, *Rev. Mod. Phys.*, **73** (2001) 681.
3. A. G. MacDiarmid, *Rev. Mod. Phys.,* **73** (2001) 701.
4. H. Shirakawa, *Rev. Mod. Phys.,* **73** (2001) 713.
5. H. Shirakawa, E. J. Louis, A. G. Madiarmid, C. K. Chiang and A. J. Heeger, *J. Chem. Soc. Comm.,* (1977) 578.
6. C. K. Chiang, C. R. Jr. Fincher, Y. W. Park, A. J. Heeger, H. Shirakawa and E. J. Louis, *Phys. Rev. Lett.,* **39** (1977) 1098.
7. S. Roth and H. Bleier, *Adv. Phys.,* **36** (1987) 386.
8. Handbook of Conducting Polymers, 2nd ed. (Eds: T. A. Skotheim, R. L. Elsenbaumer, J. R. Reynolds), Marcel Dekker, New York 1998.
9. A. Tsumura, H. Koezuka and T. Ando, *Appl. Phys. Lett.,* **49** (1986) 1210.
10. A. Assadi, G. Svesson, M. Willander and O. Inganäs, *Appl. Phys. Lett.,* **53** (1988) 195.
11. J. H. Burroughs, C. A. Jones and R. H. Friend, *Nature,* **335** (1988) 137.
12. J. H. Burroughes, D. D. C. Bradley, A. R. Brown, R. N. Marks, K. Mackay, R. H. Friend, P. L. Burn and A. B. Holmes, *Nature,* **347** (1990) 539.

13. G. Gustafsson, Y. Cao, G. M. Treacy, F. Klavetter, N. Colaneri and A. J. Heeger, *Nature,* **357** (1992) 477.
14. P. L. Burns, A. B. Holmes, A. Kraft, D. D. C. Bradley, A. R. Brown, R. H. Friend and R. W. Gymer, *Nature,* **356** (1992) 47.
15. R. H. Friend, R. W. Gymer, A. B. Holmes, J. H. Burroughs, R. N. Marks, C. Taliani, D. D. C. Bradley, D. A. Dos Santos, J. L. Bredas, M. Logdlund and W. R. Salaneck, *Nature,* **397** (1999) 121.
16. G. Dennler and N.S. Sariciftci, *Proceedings of the IEEE,* **93** (2005)1429.
17. C. J. Brabec, N. S. Sariciftci and J. C. Hummelen, *Adv. Funct. Mater.,* **11** (2001) 15.
18. N. S. Sariciftci, *Curr. Opin. Sol. Sta. Mater. Sci.,* **4** (1999) 373.
19. J. Nelson, *Curr. Opin. Sol. Sta. Mater. Sci.,* **6** (2002) 87.
20. C. J. Drury, C. M. J. Mutsaers, C. M. Hart, M. Matters and D. M. de Leeuw, *Appl. Phys. Lett.,* **73** (1998) 108.
21. G. H. Gelinck, T. C. T. Geuns and D. M. de Leeuw, *Appl. Phys. Lett.,* **77** (2000) 1487.
22. H. Sirringhaus, N. Tessler and R. H. Friend, *Science,* **280** (1998) 1741.
23. Edwin W. H. Jager, PhD Thesis, Linköping, 2001.
24. H.A.M. van Mullekom, J.A.J.M. Vekemans, E.E. Havinga, E.W. Meijer, *Mater. Sc. and Eng.,* **32** (2001) 1.
25. J. Roncali, *Chem. Rev.,* **97** (1997) 173.
26. S.J. Higgins, *Chem. Soc. Rev.,* **26** (1997) 247.
27. C.J. Zhong, Z.Q. Tian, and Z.W. Tian, *J. Phys. Chem.,* **94** (1990) 2171.
28. A.J. Bard and L.R. Faulkner, Electrochemical Methods: Fundamentals and Applications, 2nd Ed., John Wiley & Sons, USA, 2001.
29. J. Wang, Analytical Electrochemistry, 2nd Ed., John Wiley & Sons, New York, 2000.
30. Christopher M.A. Brett and Ana Maria Olivera Brett, Electrochemistry: Principles, Methods and Applications; Oxford University Press, New York; 1994.

31. Bernard Valeur, Molecular Fluorescence: Principles and Applications; Wiley-VCH Verlag GmbH, 2001.
32. J. Mendham, R.C. Denney, J.D. Barnes, M.J.K. Thomas, VOGEL'S Textbook of Quantitative Analysis, 6th Ed., Prentice Hall, New York, 2000.
33. J. N. Demasa and G. A. Crosby, *J. Chem. Phys.,* **75** (1971) 991.
34. Hima S. Joshi, Ramin Jamshidi, and Yitzhak Tor, *Angew. Chem. Int. Ed.,* **38** (1999) 2722.
35. A.F. Diaz, J. Crowley, J. Bartgon, G.P. Gardini, J.B. Torrance, *J. Electroanal. Chem.,* **121** (1981) 355.
36. G. Tourillon, F. Garnier, *J. Electroanal. Chem.,* **161** (1984) 51.
37. P. Marque, and J. Roncali, *J. Phys Chem.,* **94** (1990) 8614.
38. A.F. Diaz, J.L. Castillo, J.A. Logan, W.Y. Lee, *J. Electroanal. Chem.,* **129** (1981) 115.
39. C. Carlberg, PhD thesis, University of Linkoping, Sweden, 1996.
40. S.W. Feldberg, *J. Amer. Chem. Soc.,* **106** (1984) 4671.
41. N. Mermilloid, J. Tanguy, F. Petiot, *J. Electrochem. Soc.,* **133** (1986) 1073.
42. T. Tanguy, N. Mermilliod, M. Hoclet, *J. Electrochem. Soc.,* **134** (1987) 795.
43. M. Zagorska and A. Pron and S. Lefrant, in Handbook of Organic Conductive Molecules and Polymers, Vol. 3, Conductive Polymers: Spectroscopy and Physical Properties, H.S. Nalwa (Ed.), Wiley, New York, 1997, pp.183-218.
44. L. Micaroni, F.C. Nart, I.A. Hummelgen, *J Solid State Electrochem.,* **7** (2002) 55.
45. H. Eckhardt, L.W. Shacklette, K.Y. Jen and R.L. Elsenbaumer, *J Chem Phys.,* **91** (1989) 1303.
46. J.L. Bredas, R. Silbey, D.S. Boudreaux, R.R. Chance, *J. Am. Chem. Soc.,* **105** (1983) 6555.
47. S. Janietz, D.D.C. Bradley, M. Grell, and C. Giebeler, M. Inbasekaran, E. P. Woo, *Appl. Phys. Lett.,* **73** (1998) 73.
48. A. Charas, J. Morgado, J.M.G. Martinho, L. Alcacer, S.F. Lim, R. H. Friend, C. Cacialli, *Polymer,* **44** (2003) 1843.

49. J. Pei, W.L. Yu, J. Ni, Y.H. Lai, W. Huang, A.J. Heeger *Macromolecules,* **34** (2001) 7241.
50. A.P. Kulkarni, C.J. Tonzola, A. Babel, S.A. Jenekhe, *Chem. Mater.,* **16** (2004) 4556.
51. A. Berlin, G. Zotti, S. Zecchin, G. Schiavon, B. Vercelli, A. Zanelli, *Chem. Mater.,* **16** (2004) 3667.
52. P.G. Pickup, in: R.E. White, J.O. Bockris, B.E. Conway, editors. Modern Aspects of Electrochemistry, No. 33, New York: Plenum Publishers, 1999. pp. 549-597.
53. M. Helbig and H.H. Hörhhold, *Makromol. Chem.,* **194** (1993) 1607.
54. K. Loganathan, E.G. Cammisa, B.D. Myron and P.G. Pickup, *Chem. Mater.,* **15** (2003) 1918.
55. J. N. Wilson, P.M. Windscheif, U. Evans, M.L. Myrick and U.H.F. Bunz, *Macromolecules,* **35** (2002) 8681.
56. H. Reiss, A. Heller, *J. Phys. Chem.,* **89** (1985) 4207.
57. T. Johansson, W. Mammo, M. Svensson, M.R. Anderson, O. Inganäs *J. Mater. Chem.,* **13** (2003) 1316.
58. C. D. Grant, A. M. Schwartberg, G. P. Smestad, J. Kowalik, L. M. Tolbert and J. Z. Zhang, *J. Electroanal. Chem.*, **522** (2002) 40.
59. B. Oregan and M Gratzel, *Nature*, **353** (1991) 737.
60. M.K. Nazeeruddin, A. Kay, I. Rodicio, R. Humphry-Baker, E. Muller, P. Liska, N. Vlachopoulos and M. Gratzel, *J. Am. Chem. Soc*., **115** (1993) 6382.
61. C.W. Tang, *Appl. Phys. Lett.,* **48** (1986) 183.
62. M. Reyes-Reyes, K. Kim and D.L. Carroll, *Appl. Phys. Lett.,* **87** (2005) 083506.
63. G. Li, V. Shrotriya, J. S. Huang, Y. Yao, T. Moriarty, K. Emery and Y. Yang, *Nature Mater.,* **4** (2005) 864.
64. H. Spanggaard and F.C. Krebs, *Solar Energy Materials & Solar Cells,* **83** (2004) 125.

65. J.J.M. Halls and R. Friend, Organic Photovoltaic Devices, in Clean electricity from Photovoltaics: Series on Photoconversion of Solar Energy-Vol, 1, M.D. Archer and R. Hill Eds. Imperial College Press, UK, pp377-445, 2001.
66. L. S. Roman, O. Inganas, T. Granlund, T. Nyberg, M. Svenson, M. R. Anderson and J. C. Hummelen, *Adv. Mater.,* **12** (2000)189.
67. P. Schilinsky, C. Waldauf and C.J. Barbec, *Appl. Phys. Lett.,* **81** (2002) 3885.
68. F. Padinger, R.S. Rittberger and N.S. Sariciftci, *Adv. Funct. Mater.,* **13** (2003) 85.
69. C. J. Brabec, A. Cravino, D. Meissner, N. S. Sariciftci, M. T. Rispens, L. Sanchez, J. C. Hummelen, T. Fromherz, *Thin Solid Films,* **403** (2002) 368.
70. A. Gadisa, M. Svensson, M. R. Andersson, O. Inganäs, *Appl. Phys. Lett.,* **84** (2004) 1609.
71. X. J. Wang, E. Perzon, J. L. Delgado, P. de la Cruz, F. L. Zhang, F. Langa, M. R. Andersson and O. Inganäs, *Appl. Phys. Lett.,* **85** (2004) 5081.
72. X. Wang, E. Perzon, F. Oswald, F. Langa, S. Admassie, M. R. Andersson and O. Inganäs, *Adv. Funct. Mater.,* **15** (2005) 1665.
73. F. L. Zhang, E. Perzon, X. J. Wang, W. Mammo, M. R. Andersson and O. Inganäs, *Adv. Funct. Mater.,* **15** (2005) 745.
74. S. E. Shaheen, D. Vangeneugden, R. Kiebooms, D. Vanderzande, T. Fromherz, F. Padinger, C. J. Brabec and N. S. Sariciftci, *Synth. Met.,* **121** (2001) 1583.
75. C. J. Brabec, C. Winder, N. S. Sariciftci, J. C. Hummelen, A. Dhanabalan, P. A. van Hal and R. A. J. Janssen, *Adv. Funct. Mater.,***12** (2002) 709.
76. L. M. Campos, A. Tontcheva, S. Gunes, G. Sonmez, H. Neugebauer, N. S. Sariciftci and F. Wudl, *Chem. Mater.,* **17** (2005) 4031.
77. C. Winder and N. S. Sariciftci, *J. Mater. Chem.,* **14** (2004) 1077.
78. S. E. Shaheen, C. J. Brabec, N. S. Sariciftci, F. Padinger T. Fromherz and J.C. Hummelen, *Appl. Phys. Lett.,* **78** (2001) 841.

79. W. Ma, C.Y. Yang, X. Gong, K. Lee and A. J. Heeger, *Adv. Funct. Mater.,* **15** (2005) 1617.
80. L.S. Hung, C.W. Tang, M.G. Mason, *Appl. Phys. Lett.,* **70** (1997) 152.
81. H. Tang and J. Shinar, *J. Appl. Phys. Lett.*, **71** (1997) 2560.
82. A.R. Schlatman, D.W. Floet, A. Hilberer, F. Garten, P.J.M. Smulders, T.M. Klapwijk and G. Hadziioannou, *Appl. Phys. Lett.,* **69** (1996) 1764.
83. Edward S. Yang, Microelectronic devices, McGraw-Hill, USA, 1988, pp 387- 413.
84. U. Mitschke and P. Bäuerle, *J. Mater. Chem.,* **10** (2000) 1471.
85. K. Wongpurk, MSc Thesis, Linköping, Sweden, 2001.
86. R. H. Friend and N.C. Greenham, in Handbook of Conducting Polymers, Eds. T.A. Skotheim, R.L Elsenbaumer and J.R Reynolds, Marcel Dekker, New York, 1988; pp 823-845.
87. S.R. Forrest, *Organic Electronics,* **4** (2003) 45.
88. U. Mitschke and P. Bauerle, *J. Mater. Chem.*, **10** (2000) 1471.
89. A. Kraft, A. C. Grimsdale, and A.B. Holmes, *Angew. Chem. Int. Ed.,* **37** (1998) 402.
90. M. Schott, *C. R. Acad Sci. Paris Sér. IV*, (2000) 381.
91. S.R. Forrest, D.D.C. Bradley and M.E. Thompson, *Adv. Mater.,* **15** (2002) 1043.
92. Q. Pei and Y. Yang, *Chem. Mater.,* **7** (1995) 1568.
93. M. Herold, J. Gmeiner, W. Rieβ and M. Schwoerer, *Synth. Met.,* **76** (1996) 109.
94. Y.Z. Lee and S.-A. Chen, *Synth. Met.,* **105** (1999) 185.
95. S. Dailey, M. Halim, E. Rebourt, L.E. Horsburgh, I.D.W. Samuel and A.P. Monkman, *J. Phys.: Condens. Matter,* **10** (1998) 5171.
96. M.M. Alam, C.J. Tonzola and S.A. Jenekhe, *Macromolecules,* **36** (2003) 6577.
97. Y.-H. Biu, B. Chen, T.-D. Kim, M.S. Liu and A. K.-Y Jen, *Appl. Phys. Lett.,* **85** (2004) 5433.

98. Z. Bao, Z. Peng, M.E. Galvin, E.A. Chandross, *Chem. Mater.,* **10** (1998) 1201.
99. X.-C. Li, Y. Liu, M.S. Liu, and A. K.-Y. Jen, *Chem. Mater.,* **11** (1999) 1568.
100. J.H. Kim, J.H. Park and H. Lee, *Chem. Mater.,* **15** (2003) 3414.
101. F.-I. Wu, D.S. Reddy and C.-F. Shu, *Chem. Mater.,* **15** (2003) 269.
102. C.-F. Shu , R. Dodda and F.-I. Wu, *Chem. Mater.,* **15** (2003) 6698.
103. P.M.S. Monk, R.J. Mortimer, and D.R. Rosseinky, Electrochromism: Fundamentals and Applications, VCH, Weinheim, 1995.
104. R.J. Mortimer, *Chem. Soc. Rev.,* **26** (1997) 147.
105. R. J. Mortimer, *Electrochim. Acta,* **44** (1999) 2971.
106. R. J. Mortimer, *Science Progress,* **85** (2002) 243.
107. R. D. Rauh, *Electrochim. Acta,* **44** (1999) 3165.
108. H. J. Byker, *Electrochim. Acta,* **46** (2001) 2015.
109. K. Gurunathan, A. V. M., R. Marimuthu, U. P. Mulik and D. P. Amalnerkar, *Materials Chemistry and Physics,* **61** (1999) 173.
110. R. Prakash and S. R. Somani, *Materials Chemistry and Physics*, **77** (2002) 117.
111. A. Kumar, D. M. W., Mark, C. Morvant, F. Piroux, K. A. Abboud, and J.R. Reynolds, *Chem. Mater.,* **10** (1998) 896.
112. L. B. Groenendaal, F. J. D. Freitag, H. Pielartzik, and J. R. Reynolds, *Adv. Mater.,* **12** (2000) 481.
113. L. B.Gronendaal, G. Z., Pierre-Henri Aubert, S. M. Waybright, and J. R. Reynolds, *Adv. Mater.,* **15** (2003) 855.
114. J.C. Gustafsson, B. Liedberg and O. Inganäs, *Solid State Ionics,* **69** (1994) 145.
115. A. A. Argun, P.-H. Aubert, B.C. Thompson, I. Schwendeman, C.L. Gaupp, J. Hwang, N.J. Pinto, D.B. Tanner, A.G. MacDiarmid and J.R. Reynolds, *Chem. Mater.,* 16 (2004) 4401.
116. L.-M. Haung, T.-C. Wen and A.G. Gopalan, *Synth. Met.,* **130** (2002) 155.

117. O. Inganäs, in Handbook of Organic Conductive Molecules and Polymers, Vol. 3, Conductive Polymers: Spectroscopy and Physical Properties, H.S. Nalwa (Ed.), Wiley, New York, 1997, p.787.
118. O. Inganäs, *Trends Polym. Sci.,* **2** (1994) 189.
119. P. Blondin, J. Bouchard, S. Beaupre, M. Belletete, G. Durocher, and M. Leclerc, *Macromolecules,* **33** (2000) 5874.
120. G. Dufresene, J. Bouchard, M. Belletete, G. Durocher, and M. Leclerc, *Macromolecules,* **33** (2000) 8252.
121. F. Bertinelli, P. Costa-Bizzarri, C. Della-Casa, and M. Lanzi, *Spectrochimica Acta Part A,* **58** (2002) 583.
122. K.P.R. Nilsson, M.R. Aandersson and O. Inganäs, *J. Phys.: Condens. Matter,* **14** (2002) 10011.
123. M. Leclerc, *Adv. Mater.,* **11** (1999) 1491.
124. L. M. Goldenberg, M. B. Bryce and M. C. Petty, *J. Mater. Chem.,* **9** (1999) 1957.
125. G. Mauthner, F.P. Wenzl, M. Collon, M. Bougettaya, J.R. Reynolds, G. Leising and E.J.W. List, *Synth. Met.,* **139** (2003) 613.
126. H.A. Ho and M. Leclerc, *J. Am. Chem. Soc.,* **125** (2003) 4412.
127. M. Leclerc and K. Faid, in Handbook of Conducting Polymers, 2nd Ed.; Marcel Dekker: New York, 1998; p695.

2 Electrochemical Studies of Electronically Conducting Polymers

2.1 Background

There have been several studies in the past three decades in the area of electronically conjugated polymers (ECPs) to replace inorganic materials in electronic devices. The research is growing rapidly, motivated by the low cost, ease of processability and fabrication including large area applications of ECPs in devices such as light emitting diodes [1-5], photovoltaics [6-10], field effect transistors (FET) [11-15] and electrochromism [16-20].

Some progresses in the performances of these devices were also reported by lowering the band-gap of ECPs [21]. For instance, the use of new low band gap ECPs absorbing in the red and near infrared part of the spectrum-where the maximum photon flux of the sun is located-is used as one strategy to improve the performance of photovoltaic devices [22-23]. Such low band gap ECPs are also very attractive due to their high intrinsic electrical conductivity, stability in the doped states, transparency in the neutral state and infrared absorption when p-doped [24-26]. Several strategies such as raising or lowering the HOMO or LUMO levels by using electron donating or withdrawing groups [27-28], introducing quinoid character into the ECP backbone and synthesizing ECPs containing alternating donor-acceptor-donor (D-A-D) units [29-32] have been used to lower the band gaps. Based on this DAD strategy, a series of low band gap alternating polyfluorene copolymers have been designed and characterized for solar cells with power conversion efficiencies well above 2% [33]. Motivated by these potentials of low band gap ECPs, a new series of alternating D-A-D polymers were characterized and their optical and electrochemical properties are presented in this chapter.

A desired requirement in all PLED is the simultaneous supply of electrons and holes to the active light emitting polymer layer sandwiched between two electrodes. Most electroactive conjugated polymers studied are either electron transporting (n-type) or hole transporting (p-type) and do not combine the required property of balanced electron and hole transport. Hence, several studies were done to solve this problem. One approach is to use a low work function metal such as calcium to improve the electron injection. However, the drawback in such devices is the instability of low work function metals such as calcium towards air [34].

Another approach is to use a bilayer or a multilayer structure where an electron transport or hole transporting polymer or both are introduced in a bilayer or multilayer configuration [35]. Such devices gave improved performances, even though the fabrication procedures are difficult. In this work, several polyfluorene copolymers with different hole injection and electron accepting properties were characterized and their PLEDs characteristics were compared to get insights for balanced electron and hole injection and improved performance.

2.2 Experimental

Absorption spectra were recorded using a Lambda 9 Spectrophotometer (Perkin-Elmer). PL and EL spectra were recorded using a FluoroMax-2 Spectrofluorometer. The quantum yield of fluorescence was determined by the relative method by comparing the areas of the fluorescence spectra of the standard and the sample. 9,10-Diphenylanthracene and quinine sulfate were used as reference substances.

Cyclic and square wave voltammetry experiments were carried out using an Autolab PGStat 10 (EchoChemie, the Netherlands). Typical values for the square wave voltammetric experiments were a step potential of 10 mV, frequency of 25 Hz and an amplitude of 0.01995 V. A conventional three-electrode system consisting of a platinum disk (1.6 mm in diameter) or glassy carbon disk (3.0 mm in diameter) as a working electrode, a silver wire quasi-reference electrode directly placed into the electrolyte solution and a platinum wire as counter electrode were used. The polymer films were deposited on working electrodes by solvent casting. The glassy carbon electrode was polished and rinsed with water, acetone, and acetonitrile. A 0.1 M solution of tetrabutylammonium tetrafluoroborate (Bu_4NBF_4) in acetonitrile was used as supporting electrolyte. Nitrogen gas was bubbled through the solution for about 20 minutes and bubbled over the solution throughout the experiment. The potential of the quasi-reference electrode was corrected to the Ag/AgCl reference electrode by measuring the ferrocene/ferrocenium redox couple in the supporting electrolyte-solvent system, which was 0.433 V *vs* Ag/AgCl.

Semi-empirical SCF MO calculations were carried out using Gaussian 98 program [36] using the MINDO method.

2.3 Results and Discussions

2.3.1 Electrochemical and optical studies of the band gaps of alternating polyfluorene copolymers

The chemical structures of the alternating polyfluorenes copolymers investigated in this work are shown in Figures 2.1.

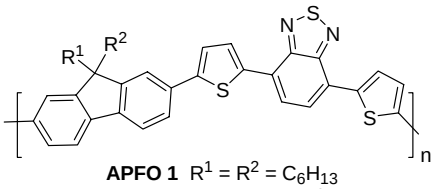

APFO 1 $R^1 = R^2 = C_6H_{13}$
APFO 2 $R^1 = C_6H_{13}$, $R^2 = CH_2CH(C_2H_5)C_4H_9$
APFO 3 $R^1 = R^2 = C_8H_{17}$
APFO 8 $R^1 = R^2 = C_2H_4OC_2H_4OCH_3$

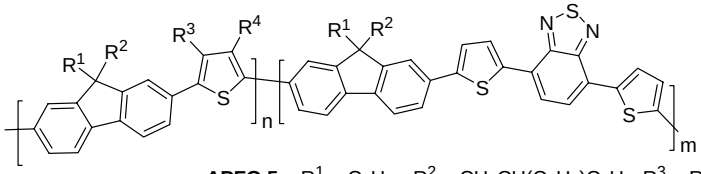

APFO 5 $R^1 = C_6H_{13}$, $R^2 = CH_2CH(C_2H_5)C_4H_9$, $R^3 = R^4 = H$
APFO 9 $R^1 = R^2 = C_2H_4OC_2H_4OCH_3$, $R^3 = R^4 = H$
APFO 10 $R^1 = R^2 = C_2H_4OC_2H_4OCH_3$, $R^3 = R^4 = NO_2$

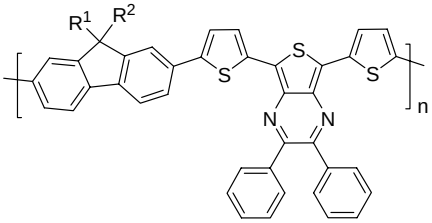

APFO-Green 2 $R^1 = R^2 = C_8H_{17}$
APFO 11 $R^1 = R^2 = C_2H_4OC_2H_4OCH_3$

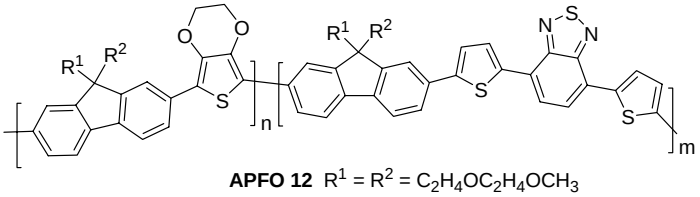

APFO 12 $R^1 = R^2 = C_2H_4OC_2H_4OCH_3$

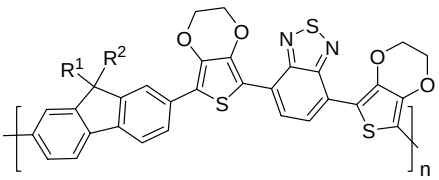

APFO 13 $R^1 = R^2 = C_2H_4OC_2H_4OCH_3$

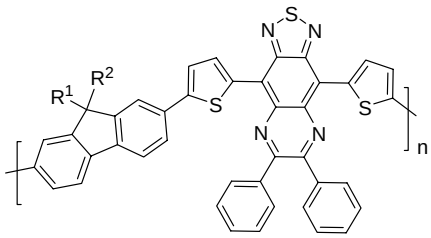

APFO-Green 1 $R^1 = R^2 = C_8H_{17}$

Figure 2.1 *Chemical structures of the polymers investigated.*

The UV-Vis absorption spectra of all the polymers display two maxima of absorption between 380 - 417 nm and 535 - 817 nm as shown in Figures 2.2 and 2.3. Both the onset wavelength and the maximum absorption wavelength for the peak at the higher maximum absorption were used to estimate the minimum and maximum optical band gaps.

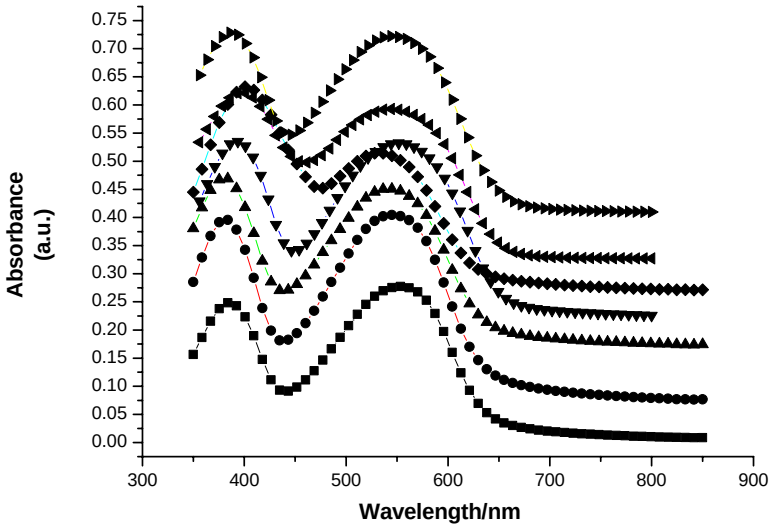

Figure 2.2 *UV-Vis absorption spectrum of (■) APFO 1, (●) APFO 2, (▲) APFO 3, (▼) APFO 8, (♦) APFO 5, (◄) APFO 9, and (►) APFO 10 polymer films coated on a glass substrate.*

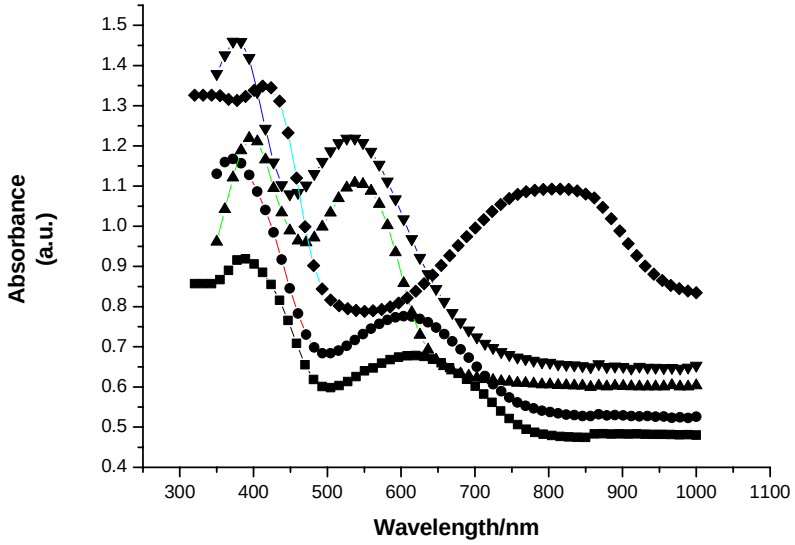

Figure 2.3 *UV-Vis absorption spectrum of (■) APFO-Green 2, (●) APFO 11, (▲) APFO 12, (▼) APFO 13, and (♦) APFO-Green 1 polymer films coated on a glass substrate.*

The cyclic voltammograms for the first cycle of the polymers, which were obtained from solvent-casted materials on a platinum disk electrode, are shown in Figures 2.4 and 2.5.

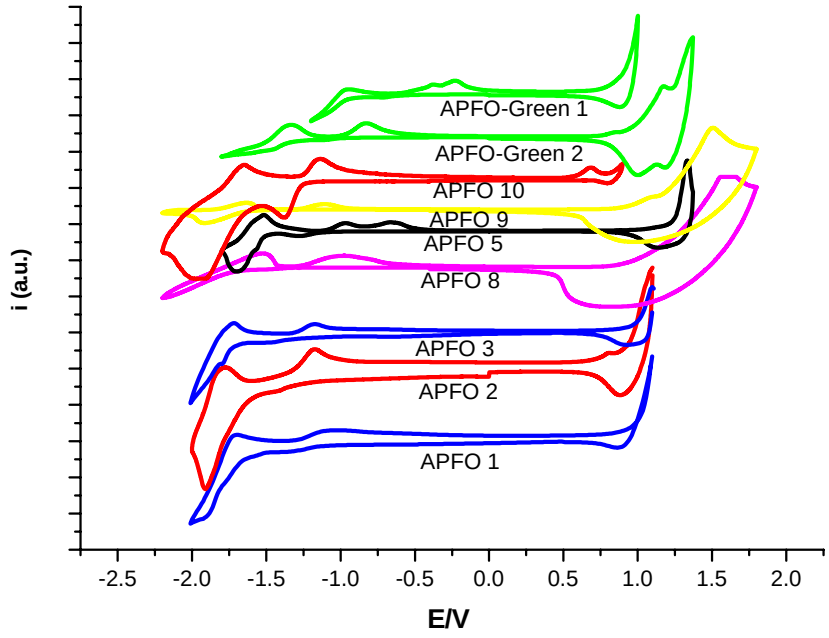

Figure 2.4 *Cyclic voltammogram (first scans) of APFO 1-3, APFO 5, APFO 8-10, APFO-Green 1 and APFO-Green 2 films casted on a platinum disk electrode in Bu_4NBF_4/AcN supporting electrolyte/solvent system at a scan rate of 100 mV/s.*

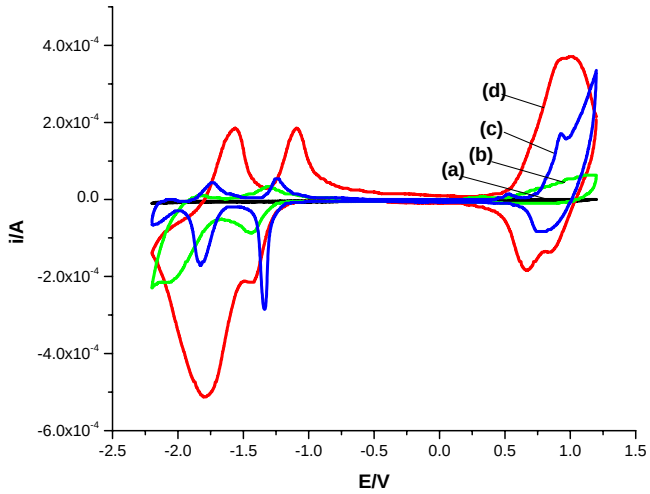

Figure 2.5 *Cyclic voltammogram (first scans) of (a) background; (b) APFO 13; (c) APFO 12 and (d) APFO 11 polymer films casted on a platinum disk electrode in Bu_4NBF_4/AcN supporting electrolyte/solvent system at a scan rate of 100 mV/s.*

It is not always possible to get well-defined peaks, particularly in the cathodic n-doping. We observed well-defined peaks in the n-doping regions for some of the alternating polyfluorenes with ethylenedioxythiophene in the back bone and oligoethylene oxide side chains (APFO 10, APFO 11, APFO 12, and APFO 13). However, the other polymers did not show such behavior. Hence, formal potentials from the first cycle are not always an experimentally accessible parameter in electroactivity studies. In the subsequent scans, the first reduction peak in the n-doping region becomes more clearly resolved like the other polymers as shown in Figure 2.6.

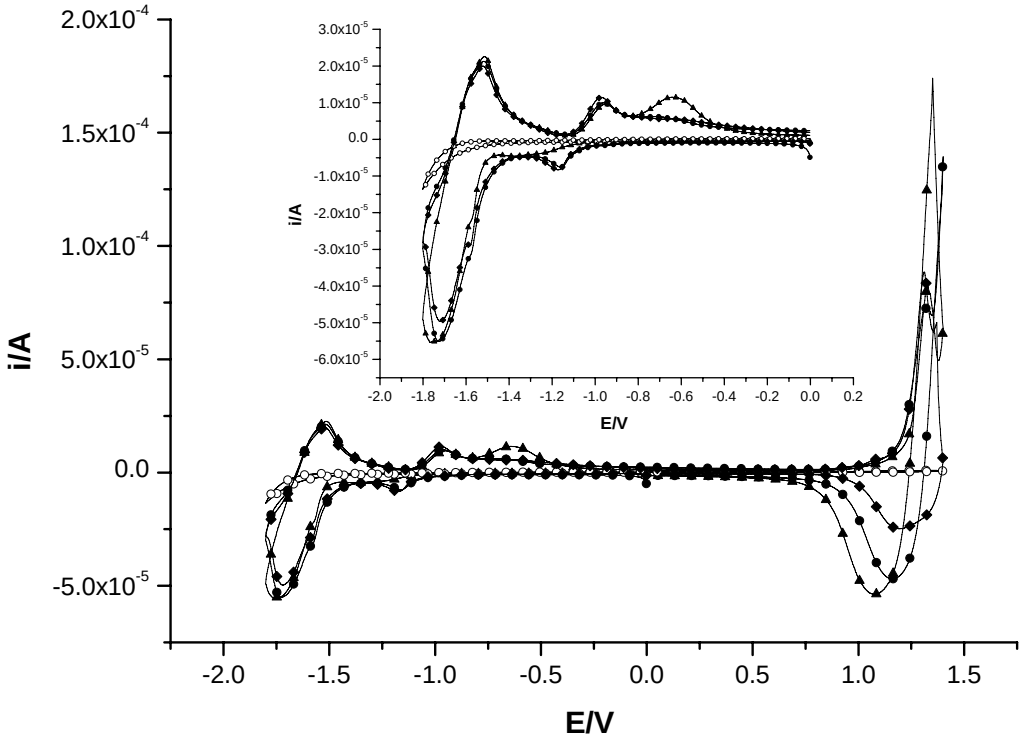

Figure 2.6 *Cyclic voltammogram (○) background; (▲) first scan; (●) second scan and (♦) third scan for APFO 3 polymer films casted on a platinum disk electrode in Bu_4NBF_4/AcN supporting electrolyte/solvent system at a scan rate of 100 mV/s. The insert shows the n-doping region separately drawn to show the clear resolution of the first reduction peaks on the second and third scans.*

Therefore, the third scans were used for such polymers to estimate the formal potentials. Selected cyclic voltammograms for the third scans of APFO 3, APFO-Green 2 and APFO-Green 1 are shown in Figure 2.7.

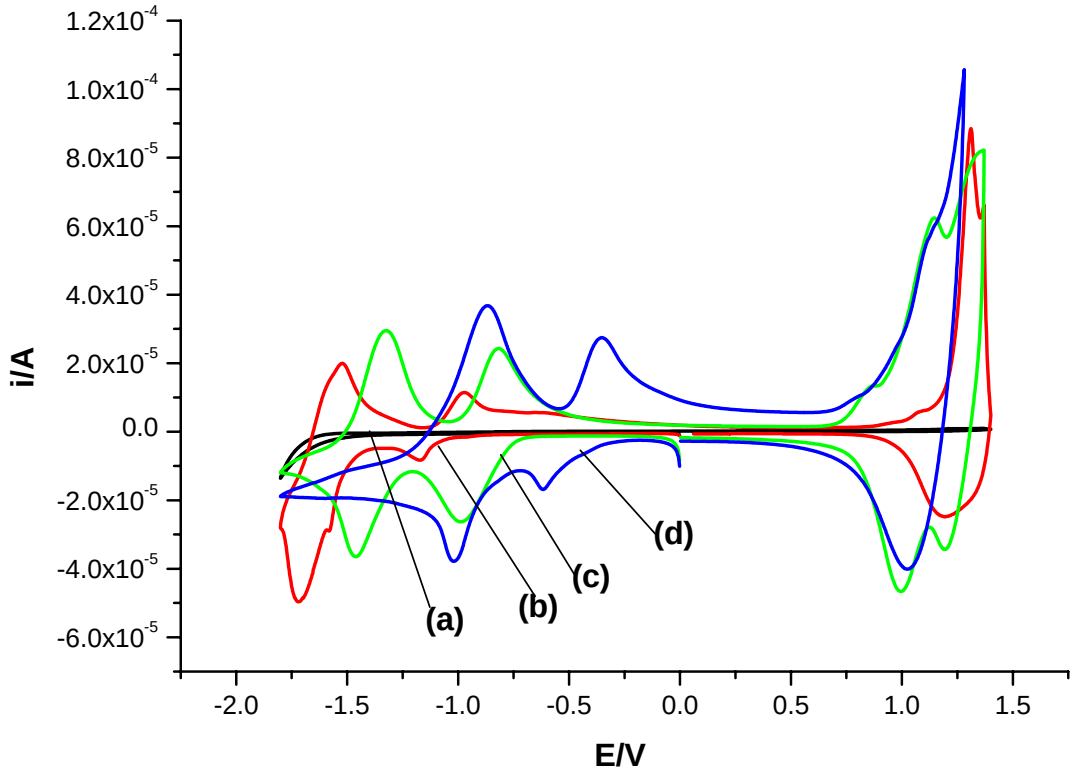

Figure 2.7 *Cyclic voltammogram (a) background; (third scans) of (b) APFO 3, (d) APFO-Green 2 and (e) APFO-Green 1 polymer films casted on a platinum disk electrode in Bu_4NBF_4/AcN supporting electrolyte/solvent system at a scan rate of 100 mV/s.*

The optical and electrochemical data obtained using the method of peak averages are summarized in Table 2.1. The onset method has also been used in this work to estimate HOMO-LUMO values and compare the electrochemical and optical band gap values estimated from onset.

Table 2.1 *Summary of the electrochemical and optical data of the series of alternating polyfluorene copolymers determined from peak values.*

Polymer	λ_{max} (nm)	E^g_{op} (eV)	E^o_{ox} (eV)	E^o_{red} (V)	-HOMO (eV)	-LUMO (eV)	E^g_{ec} (eV)
APFO 1	380, 543	2.28	1.17	-1.13(-1.07)	5.82	3.52(3.58)	2.30
APFO 2	381, 547	2.26	1.17	-1.14(-1.13)	5.82	3.51(3.52)	2.31
APFO 3	386, 554	2.23	1.19	-1.12(-1.14)	5.84	3.53(3.49)	2.34
APFO 8	398, 542	2.28	1.09	-1.06(-1.04)	5.74	3.59(3.61)	2.15
APFO 5	402, 535	2.31	1.25	-1.14(-1.16)	5.90	3.51(3.51)	2.39
APFO 9	392, 551	2.24	1.02	-1.13(-1.14)	5.67	3.52(3.51)	2.15
APFO 10	389, 545	2.26	1.05	-1.15(-1.12)	5.70	3.50(3.53)	2.20
APFO–Green 2	386, 616	2.00	1.02	-0.95(-0.98)	5.67	3.70(3.67)	1.97
APFO 11	373, 609	2.03	1.09	-1.01(-0.97)	5.74	3.64(3.68)	2.10
APFO 12	398, 543	2.28	1.10	-1.05(-1.07)	5.75	3.60(3.58)	2.15
APFO 13	377, 533	2.32	--		--		--
APFO–Green 1	417, 817	1.51	1.10	-0.54(-0.51)	5.75	4.11(4.14)	1.64

The onset values were estimated by taking the intersection point between the baseline and the tangent line drawn to the rising portion of the current as illustrated in Figure 2.8.

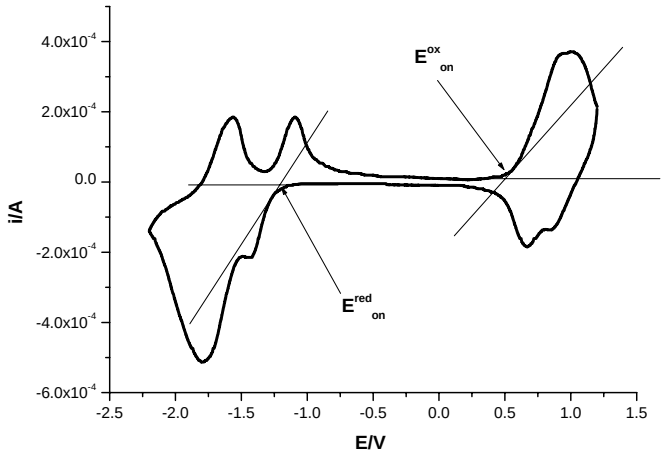

Figure 2.8 *A diagram showing the method used to estimate onset values for oxidation and reduction potentials.*

The optical and electrochemical data evaluated from these studies are summarized and compared in Table 2.2.

Table 2.2 *Summary of the electrochemical and optical data of the series of alternating polyfluorene copolymers determined from onset values.*

Polymer	λ_{max} (nm)	λ_{on} (nm)	E^{g}_{op} (eV)	E^{ox}_{on} (V)	E^{red}_{on} (V)	-HOMO (eV)	-LUMO (eV)	E^{g}_{ec} (eV)
APFO 1	380, 543	651	1.9	0.95	-1.11	5.4	3.3	2.1
APFO 2	381, 547	656	1.9	0.84	-1.10	5.2	3.3	1.9
APFO 3	386, 554	663	1.8	0.93	-1.12	5.3	3.3	2.0
APFO 8	398, 542	657	1.9	1.01	-1.09	5.4	3.3	2.1
APFO 5	402, 535	642	1.9	0.97	-1.07	5.4	3.3	2.1
APFO 9	392, 551	659	1.9	0.92	-1.07	5.3	3.3	2.0
APFO 10	389, 545	650	1.9	0.58	-1.22	5.0	3.2	1.8
APFO–Green 2	386, 616	788	1.6	0.58	-0.92	5.0	3.5	1.5
APFO 11	373, 609	774	1.6	0.66	-1.02	5.1	3.4	1.7
APFO 12	398, 543	680	1.8	0.86	-1.00	5.3	3.4	1.9
APFO 13	377, 533	718	1.7	0.64	-1.08	5.0	3.3	1.7
APFO–Green 1	417, 817	975	1.3	0.66	-0.60	5.1	3.8	1.3

The electrochemical band gaps determined from both onset and peak averages are plotted as a function of the optical band gap determined from the maximum absorption wavelength in Figure 2.9. In both the onset and peak average methods, there is a good correlation between the optical and electrochemical band gaps even if in most cases the electrochemical band gap is slightly higher than the optical band gap. The differences do not exceed ± 0.15 eV. In Figure 2.10, we compared the HOMO-LUMO values estimated from the onset and peak average methods. As expected in all cases the onset method gives lower estimates of HOMO-LUMO values than the peak average method. The differences in the estimates from the two methods are more pronounced in their HOMO values.

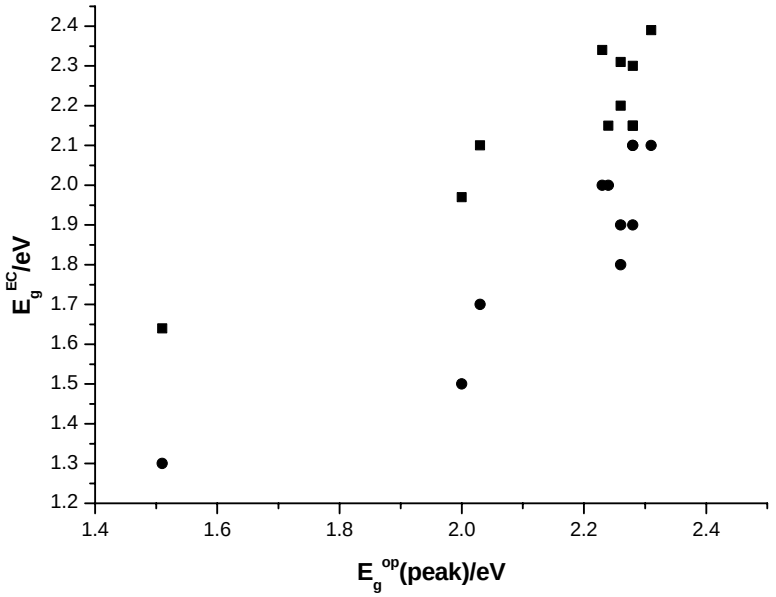

Figure 2.9 *A plot of the electrochemical band gap determined from onset (●) and peak averages (■) against the optical band gap determined from maximum absorption wavelength.*

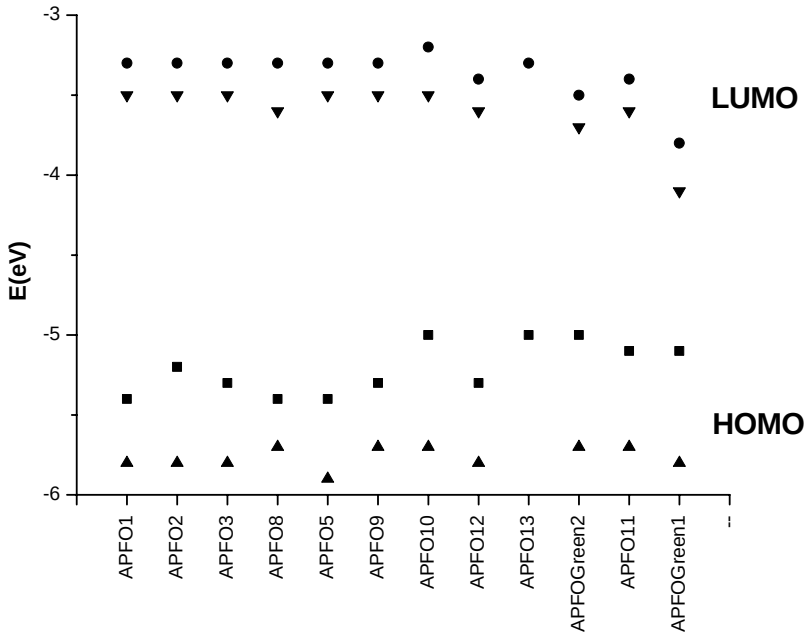

Figure 2.10 *A plot of the energies of HOMO from peak averages (▲), from onset (■) and LUMO from peak average (▼) and onset (●) for the polymers investigated.*

One common feature of these polymers is the accessibility of the n-doping regions at less cathodic potentials, which makes the estimation of the LUMO much simpler. Because of this we investigated the square wave voltammetric behavior of the polymers and also extracted the half wave potentials and the corresponding LUMO values. Square wave voltammetry (SWV) has an additional advantage of increased sensitivity and suppression of the background current. Typical square wave voltammograms for three polymers (APFO 3, APFO Green 2 and APFO Green 1) are shown in Figure 2.11 and the values extracted are shown in parenthesis in Table 2.1. There is a good agreement between the values obtained from the two methods.

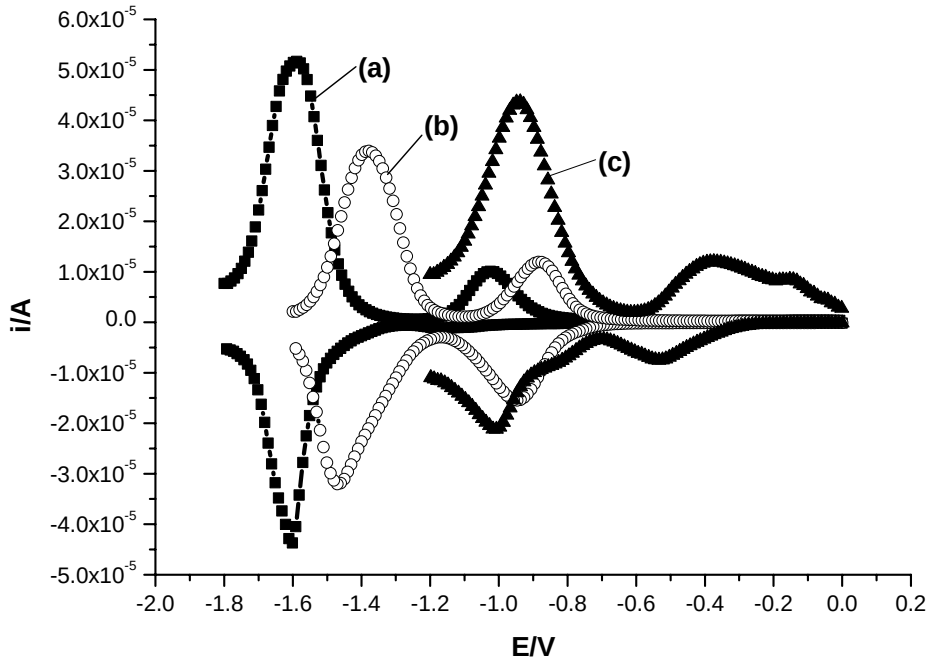

Figure 2.11 *Square wave voltammograms (third scans) for (a) APFO 3, (b) APFO-Green 2 and (d) APFO-Green 1 films casted on a platinum disk electrode in Bu_4NBF_4/AcN supporting electrolyte/solvent system.*

We also investigated in some detail selectively for three of the polymers (APFO 5, APFO Green 2 and APFO Green 1) to see how the sweep rate affects the estimated HOMO-LUMO values. The sweep rate was varied from 100 mV/s down to 1.0 mV/s. Estimation was made in both cases from the first scans. For APFO 5, which gives good performance in solar cell devices, the onset reduction and oxidation potentials change randomly with sweep

rate up to 60 mV. The random change is mainly due to the difficulty in estimating the ill-defined onset potential values and the difficulty in getting exactly similar film morphology by casting the polymer films on the electrode surface. Nevertheless, as shown in Table 2.3, these changes do not significantly affect the HOMO-LUMO values for the polymer. For APFO Green 2, however, the onset reduction potentials show a random change up to 110 mV (Table 2.4). APFO Green 1 also shows a significant change in the onset reduction potentials up to 180 mV (Table 2.5). These values have impacts on the LUMO values, where the LUMO values for APFO Green 2 varies between about 3.4 – 3.5, and that of APFO Green 1 varies between about 3.8 – 4.0 eV.

Table 2.3 *The onset-potentials and the corresponding LUMO and HOMO values as a function of sweep rate for APFO 3.*

Sweep rate (mV/s)	E^{red}_{on}/V (*vs* Ag/AgCl)	-LUMO (eV)	E^{ox}_{on}/V (*vs* Ag/AgCl)	-HOMO (eV)
1	-1.14	3.26	0.95	5.3
10	-1.09	3.3	0.91	5.3
50	-1.16	3.24	0.92	5.3
100	-1.15	3.25	0.91	5.3

Table 2.4 *The onset-potentials and the corresponding LUMO and HOMO values as a function of sweep rate for APFO-Green 2.*

Sweep rate (mV/s)	E^{red}_{on}/V (*vs* Ag/AgCl)	-LUMO (eV)	E^{ox}_{on}/V (*vs* Ag/AgCl)	-HOMO (eV)
1	-1.03	3.4	0.65	5.0
5	-1.01	3.4	0.65	5.0
10	-1.00	3.4	0.60	5.0
20	-0.93	3.5	0.57	5.0
50	-0.96	3.4	0.62	5.0
100	-0.92	3.5	0.58	5.0

Table 2.5 *The onset-potentials and the corresponding LUMO and HOMO values as a function of sweep rate for APFO-Green 1.*

Sweep rate (mV/s)	E^{red}_{on}/V (*vs* Ag/AgCl)	-LUMO (eV)	E^{ox}_{on}/V (*vs* Ag/AgCl)	-HOMO (eV)
1	-0.53	3.9	0.65	5.1
5	-0.53	3.9	0.65	5.1
10	-0.55	3.8	0.66	5.1
20	-0.55	3.8	0.65	5.1
50	-0.60	3.8	0.66	5.1
100	-0.42	4.0	0.73	5.1

Semi-empirical SCF MO calculations were carried out to show how the HOMO and LUMO positions are affected by electron-donating and electron-withdrawing groups. The polymer that has the lowest optical band gap of 1.3 (APFO Green 1) is compared with APFO 3, which has an optical band gap of 2.0. Accordingly, after optimising the different repeating units whose structures are shown in Figure 2.11 using the AM1 method, the HOMO-LUMO values were calculated at MNDO level. When an electron-donating thiophene (FT) is added to the fluorene (F) unit, the LUMO level is stabilized by 0.39 eV while the HOMO is destabilized by 0.23 eV. However, when the quinoxaline and benzothiadiazole units are added to the fluorene structure (FC), the LUMO is highly stabilized by 1.21 eV, while the HOMO is slightly destabilized by 0.22 eV. Further introduction of the electron-donating thiophene units on both sides of the qunoxaline and benzothiadiazole units (FTCT) stabilized the LUMO level by up to 1.6 eV, while the HOMO level is not very much affected. Therefore, the lowering in the optical band gap from 2.0 eV in APFO 3 (FTBT) to 1.3 in APFO Green 1 (FTCT) is mainly due to the stabilization of the LUMO level by the donor-acceptor-donor units in the repeating units of APFO Green 1. The calculation at MNDO level also shows that the stabilization of the LUMO level in APFO Green 1 is higher than that of the stabilization in the repeating unit of APFO 3 (Figure 2.12). These predictions are in agreement with the significantly lower onset of the reduction potential of APFO Green 1 compared to APFO 3.

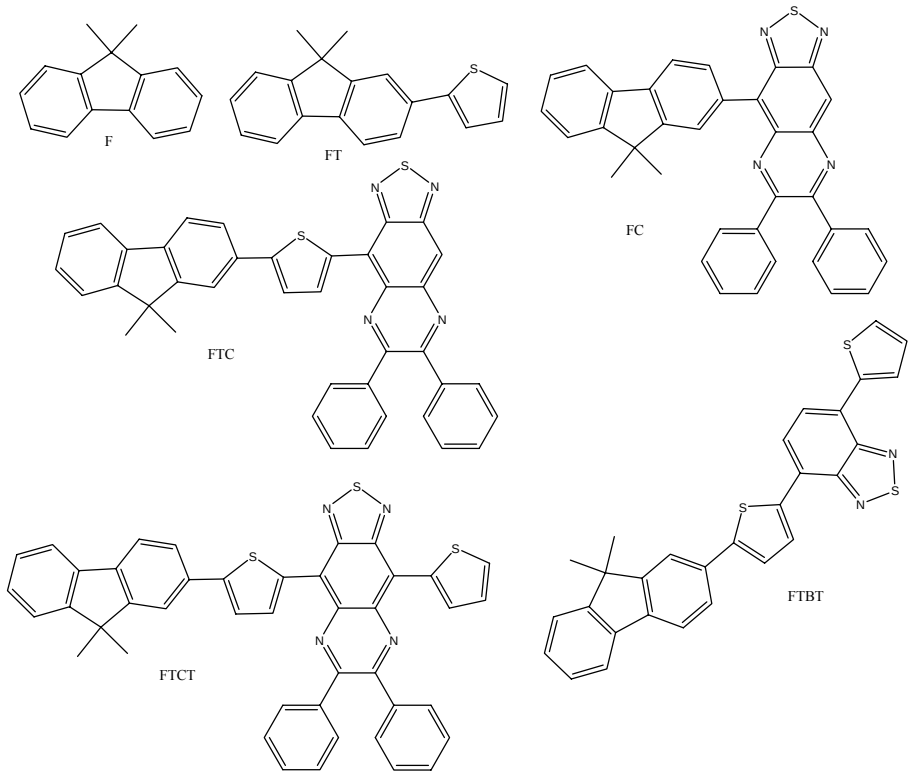

Figure 2.12 *Repeating units used in the MNDO calculations.*

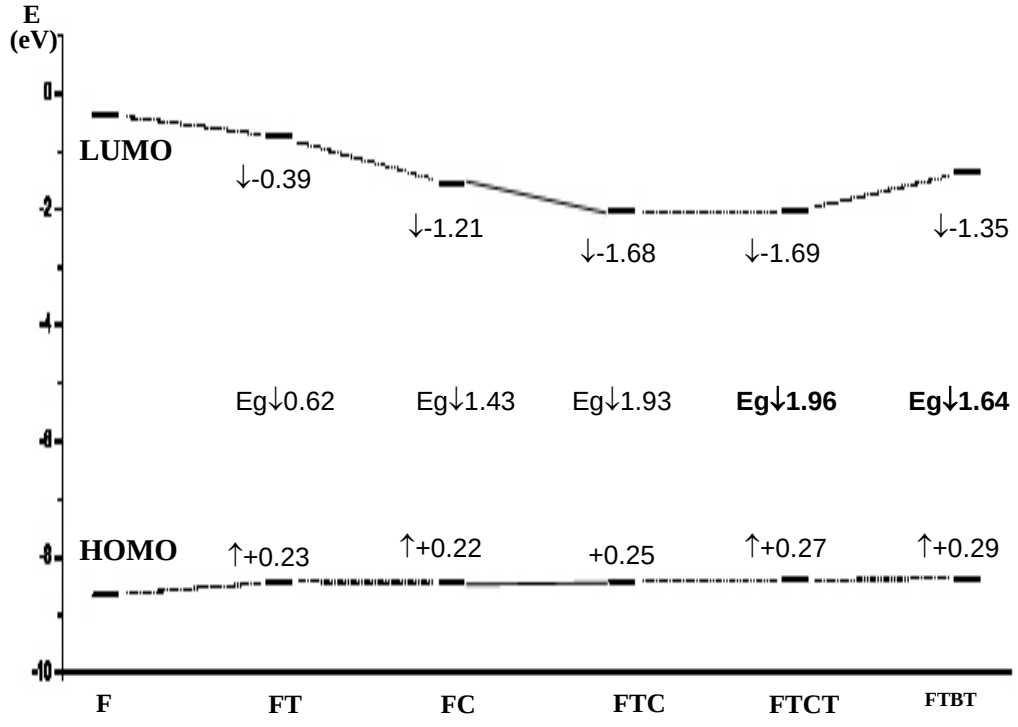

Figure 2.13 *MNDO calculated energies of HOMO and LUMO of the various repeating units.*

2.4.2 Characterization of Electroactive Conjugated Polymers Designed for Photovoltaic Cells

2.4.2.1 Structure-property relationships in low band gap alternating polyfluorene copolymers designed for photovoltaic cells.

The chemical structures of the alternating polyfluorene copolymers characterized for structure-property relationships are shown in Figure 2.14.

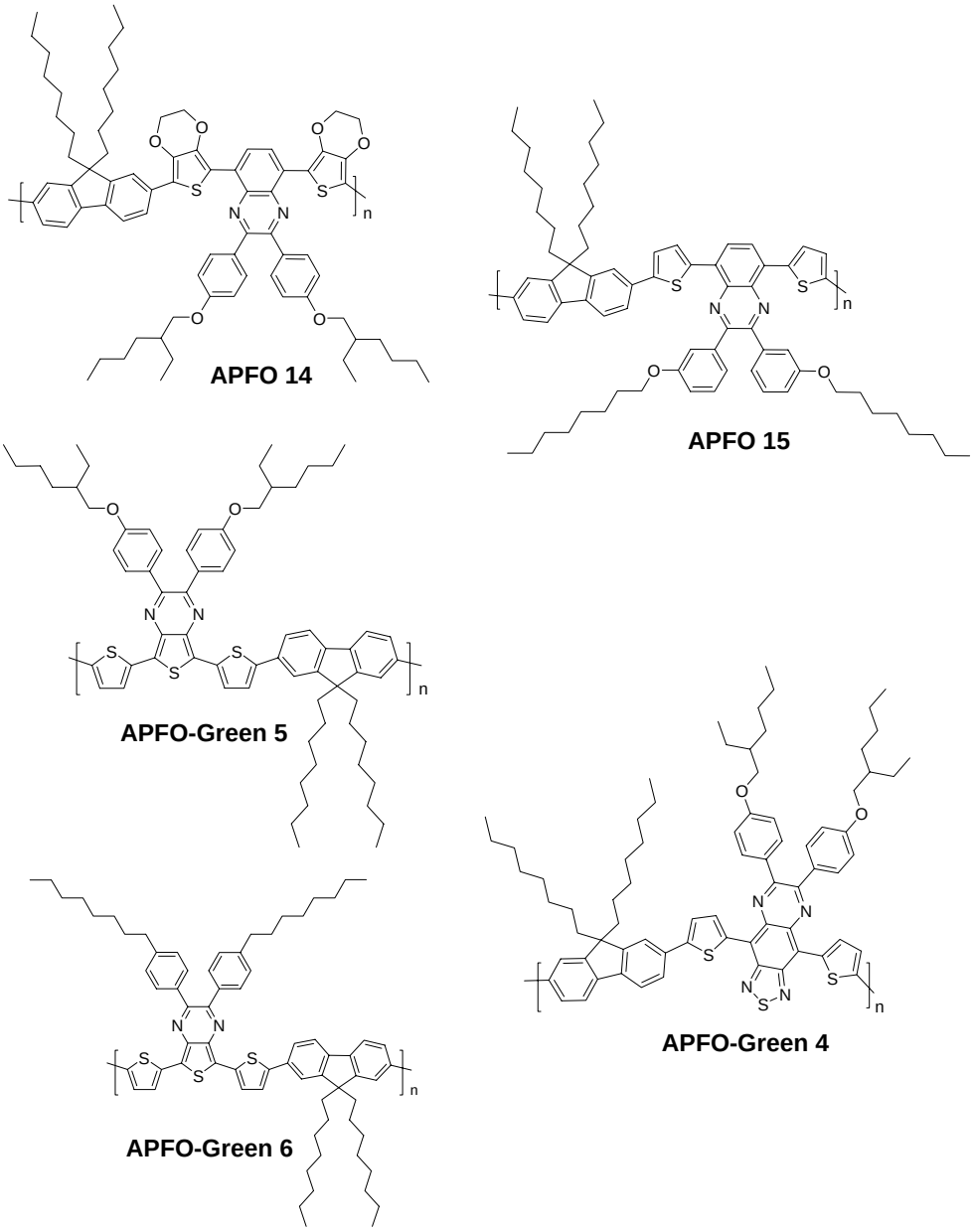

Figure 2.14 *The chemical structure of the low band gap alternating polyfluorene copolymers* ***APFO 14, APFO 15, APFO-Green 4, APFO-Green 5, and APFO-Green 6 .***

Figure 2.15 shows the UV-Vis spectra of the polymers in the solid state. The maximum absorption wavelength of the polymers ranges from 555 – 823 nm. The optical band gap determined from the onset of absorption varies between 1.3 – 2.0 eV (Table 2.6).

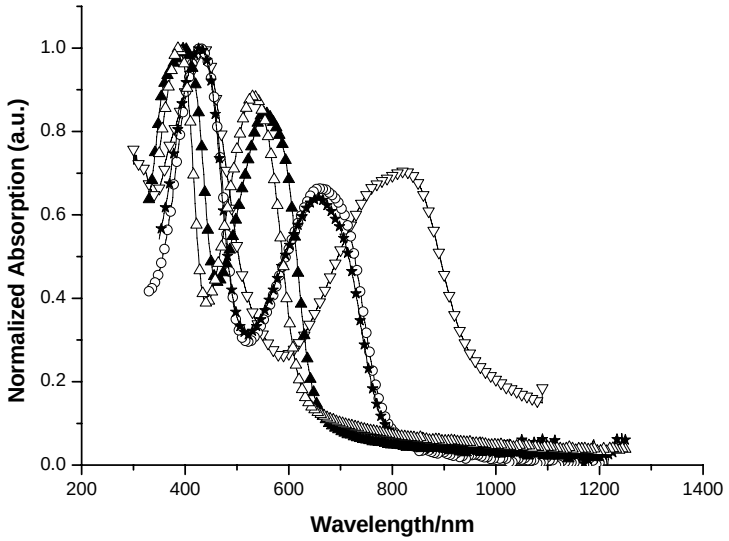

Figure 2.15 *The optical absorption spectrum of the low band gap polymers (▲)**APFO 14**, (○)**APFO-Green 5**, (★)**APFO-Green 6**, (△)**APFO 15**, and (▽)**APFO-Green 4**.*

Table 2.6 *Optical properties of polymers **APFO 14, APFO 15, APFO-Green 4, APFO-Green 5, and APFO-Green 6**.*

Polymer	λ_{max}/nm	E_g^{p}/eV	λ_{on}/nm	E_g^{on}/eV	$E_{g(EC)}^{on}$/eV
APFO 14	555	2.2	662	1.9	1.7
APFO-Green 5	658	1.9	796	1.6	1.6
APFO-Green 6	658	1.9	786	1.6	1.7
APFO 15	532	2.3	635	2.0	1.9
APFO-Green 4	823	1.5	952	1.3	1.4

The cyclic voltammograms of ***APFO 14, APFO 15, APFO-Green 4, APFO-Green 5, and APFO-Green 6*** polymers solvent casted on platinum disk electrodes are shown in Figures 2.16-2.17.

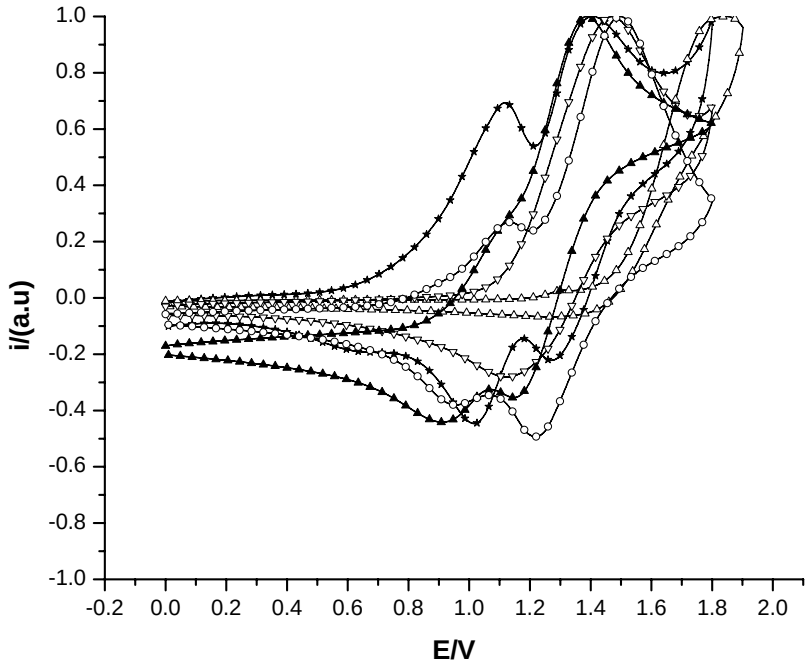

Figure 2.16 *Cyclic voltammograms for the p-doping region of polymers (▲)* ***APFO 14****, (○)* ***APFO-Green 5****, (★)****APFO-Green 6****, (△)****APFO 14****, and (▽)****APFO-Green 4*** *films solvent casted on Pt disk electrode in 0.1 M* Bu_4NBF_4*/AcN supporting electrolyte.*

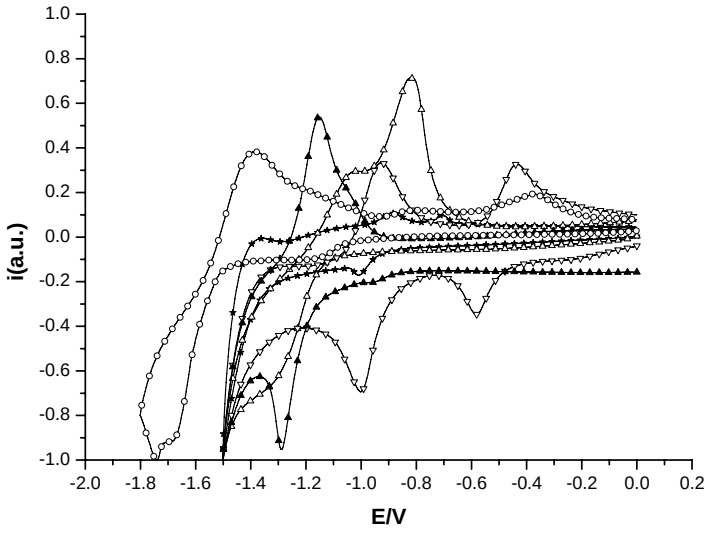

Figure 2.17 *Cyclic voltammograms for the n-doping region of polymers (▲)* ***APFO 14****, (○)* ***APFO-Green 5****, (★)****APFO-Green 6****, (△)****APFO 14****, and (▽)****APFO-Green 4*** *films solvent casted on Pt disk electrode in 0.1 M* Bu_4NBF_4*/AcN supporting electrolyte.*

Square wave voltammetry is much more sensitive to determine the half-wave potential values. The square wave voltammograms are shown in Figure 2.18. The relevant information are summarized in Tables 2.7 and 2.8.

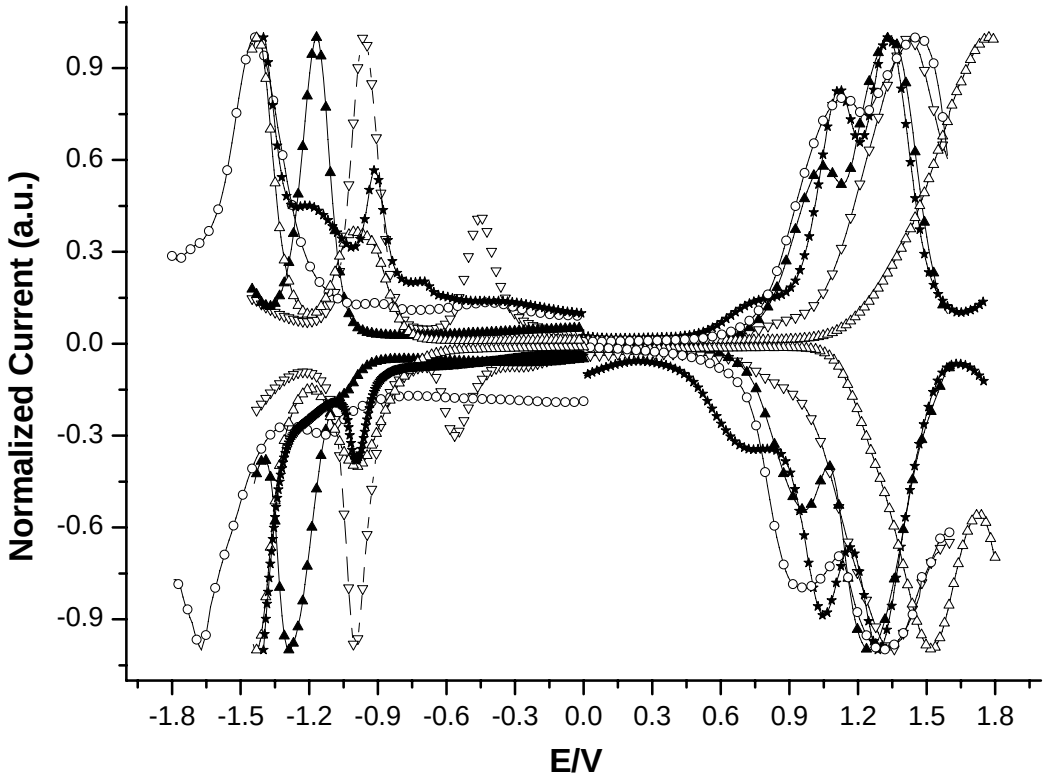

Figure 2.18 *Square wave voltammograms of polymers (▲) **APFO 14**, (○) **APFO-Green 5**, (★)**APFO-Green 6**, (△)**APFO 14**, and (▽)**APFO-Green 4** films solvent casted on Pt disk electrode in 0.1 M Bu_4NBF_4/AcN supporting electrolyte.*

In Table 2.7 comparison has also been made between the HOMO values estimated from the electrochemical studies with the open circuit potential (V_{OC}) values determined from photovoltaic devices [37]. Polymers **APFO 14** and **APFO-Green 5** can be compared with each other. Polymer **APFO 14** has additional electron donating unit from the ethylenedioxy units on the thiophene ring, while polymer **APFO-Green 5** has additional electron donating thiophene unit where the acceptor quinoxaline unit is built. The optical band gap of **APFO-Green 5** (1.6 eV) is lower than that of **APFO 14** (1.9 eV). The electrochemical and optical band gaps for **APFO-Green 5** are the same while for **APFO 14**, the electrochemical band gap is lower by about 0.2 eV. The reduction in the band gap for **APFO-Green 5** as

compared to **APFO 14** is mainly due to the stabilization of the LUMO level of **APFO-Green 5**. The HOMO values for both polymers are almost the same.

Table 2.7 Onset *potential values (vs Ag/AgCl), estimated HOMO and LUMO levels and comparison with open circuit potential for* ***APFO 14, APFO 15, APFO-Green 4, APFO-Green 5, and APFO-Green 6.***

Polymer	E^{on}_{red}/V	-LUMO/eV	E^{ox}_{on}/V	-HOMO/eV	V_{oc}/V
APFO 14	-1.10 (-1.09)	3.30 (3.31)	0.76 (0.66)	5.10 (5.06)	0.57
APFO-Green 5	-1.00 (-0.95)	3.40 (3.45)	0.61 (0.67)	5.00 (5.07)	0.58
APFO-Green 6	-0.92 (-0.90)	3.48 (3.50)	0.69 (0.79)	5.09 (5.19)	0.61
APFO 15	-1.13 (-0.74)	3.37 (3.66)	1.34 (1.16)	5.74 (5.52)	0.98
APFO-Green 4	-0.47 (-0.46)	3.93 (3.95)	1.04 (0.91)	5.44 (5.31)	0.56

Table 2.8 Half-*wave potential values (vs Ag/AgCl) and estimation of HOMO and LUMO levels for* ***APFO 14, APFO 15, APFO-Green 4, APFO-Green 5, and APFO-Green 6****.*

Polymer	$E^{red1}_{½}$/V	$E^{red2}_{½}$/V	-LUMO/eV	$E^{ox1}_{½}$/V	$E^{ox2}_{½}$/V	-HOMO/eV	$E_{g(EC)}{}^{p}$/eV
APFO 14	-1.26	--	3.39	0.98	1.26	5.63	2.2
APFO-Green 5	-1.03	-1.58	3.62	0.99	1.35	5.64	2.0
APFO-Green 6	-0.98	--	3.67	1.05	1.28	5.70	2.0
APFO 15	-1.03	--	3.62	1.61	--	6.26	2.6
APFO-Green 4	-0.54	-1.01	4.11	1.35	--	6.00	1.9

This is also in agreement with almost similar values of the V_{OC} of **APFO 14** and ***APFO-Green 5*** as shown in Table 2.7. These results suggest that the electron-donating ability on both polymers is almost the same. ***APFO-Green 5*** and ***APFO-Green 6***, which have the same backbones, can also be compared with each other. They differ on the substituents

attached to the phenyl rings. ***APFO-Green 5*** has alkoxy substituents while ***APFO-Green 6*** has alkyl substituents. The optical band gaps of both ***APFO-Green 5 and APFO-Green 6*** (1.6 eV) are the same. The electrochemical and optical band gaps for ***APFO-Green 6*** differ by about 0.1 eV. The electrochemical studies show that both the HOMO and LUMO values in ***APFO-Green 6*** are more stabilized than ***APFO-Green 5*** (Table 2.7). This is caused by the stronger electron donating effect of the alkoxy substituent in ***APFO-Green 5*** destabilizing both the HOMO and LUMO values. Hence, as we go from ***APFO-Green 5*** to ***APFO-Green 6*** we observe an increase in the HOMO level, which is also in agreement with the increased V_{OC} values as shown in Table 2. ***APFO-Green 6*** and **APFO 15** can also be compared to each other. The optical band gap of **APFO 15** (2.0 eV) is higher than that of ***APFO-Green 6*** (1.6 eV). The electrochemical and optical band gaps for ***APFO-Green 6*** and **APFO 15** differ by about 0.1 eV. Two factors contribute for the higher optical band gap in **APFO 15**. One is the absence of the additional electron donating thiophene unit on the backbone where the electron accepting quinoxaline unit is built. This is expected to increase both the HOMO level and the value of the Voc. Furthermore, the alkoxy substituents in **APFO 15** are on the *meta* position of the phenyl rings. Hence, in **APFO 15** there is presumably a stronger steric interaction of the *meta*-substituted alkoxy groups of the phenyl rings, which are closer to the main chain. These increased steric interactions could cause a decrease in the effective conjugation length and a shift of the absorption maximum to a lower wavelength. Similar observations were also reported for poly(*p*-phenylene vinylene) derivatives [38]. Hence, from the absence of the additional electron donating thiophene unit and stronger steric interaction, the band gap as well as the HOMO values in **APFO 15** are found to be higher than all the other polymers. Interestingly also this polymer gave the highest V_{OC} values [37]. The additional electron withdrawing thiadiazole unit in ***APFO-Green 4*** gave the lowest band gap of 1.3 eV. The electrochemical data clearly shows that this is mainly due to the stabilization of the LUMO level as a result of the additional thiadiazole unit. Because of the higher LUMO level a different acceptor molecule (a derivative of C_{70}) is used in the solar cell devices [39]. This makes it difficult to compare the V_{OC} values with HOMO levels.

These studies are clearly suggesting that there is a limit to the reduction of the band gap by lowering the HOMO level for such approach clearly reduces the V_{OC} and hence the over all efficiency of solar cells.

2.3.2.2 Structure-property relationships in low band gap homo polymers designed for photovoltaic cells

The chemical structures of the low band gap homo polymers **P1-P5** characterized in the course of this work are shown in Figure 2.19.

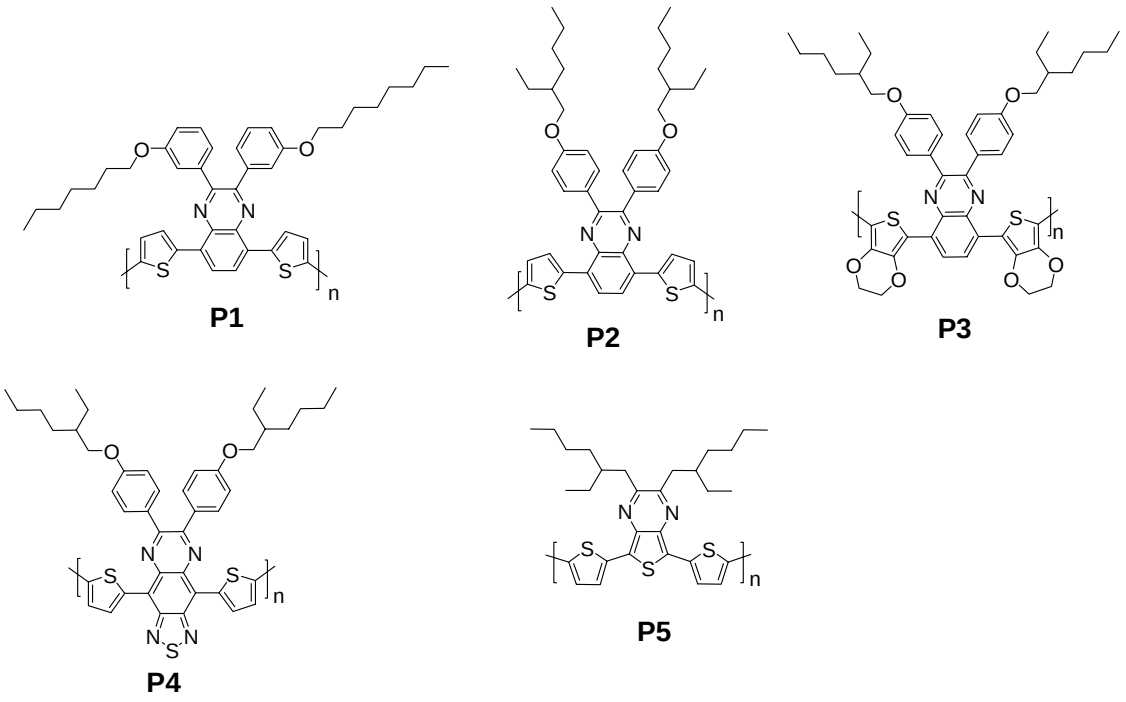

Figure 2.19 *The chemical structures of the low band gap homo polymers **P1-P5**.*

The UV-Vis spectra of the polymers in the solid state are shown in Figure 2.20. The maximum absorption wavelength of the polymers ranges from 605 – 943 nm. The optical band gap determined from the onset of absorption varies between 0.8 – 1.6 eV (Table 2.9).

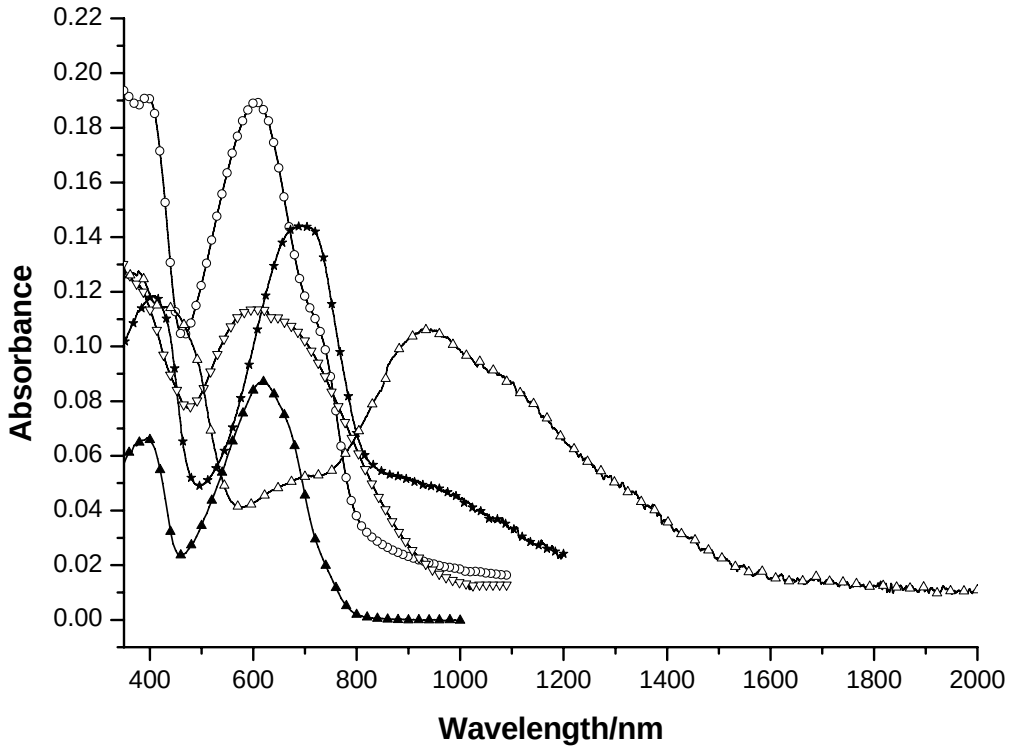

Figure 2.20 *The optical absorption spectrum of the low band gap polymers (▲) **P1**, (○) **P2**, (★) **P3**, (△) **P4**, and (▽) **P5**.*

Table 2.9 *Optical properties of polymers **P1-P5**.*

Polymer	λ_{max}(nm)	E^g_{peak}(eV)	λ_{onset}(nm)	E^g_{onset}(eV)
P1	620	2.0	776	1.6
P2	605	2.1	817	1.5
P3	696	1.8	815	1.5
P4	943	1.4	1553	0.8
P5	608	2.0	933	1.3

The cyclic voltammograms of the polymers **P1-P5,** solvent casted on platinum disk electrodes, are shown in Figure 2.21. The peak and half-wave potentials values are given in Table 2.10.

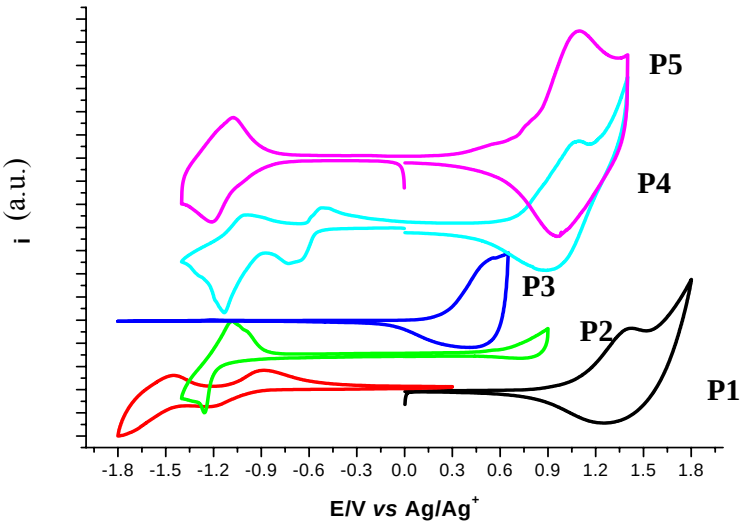

Figure 2.21 *Cyclic voltammograms of polymers **P1-P5** films solvent casted on Pt disk electrode in 0.1 M Bu_4NBF_4/AcN supporting electrolyte.*

Table 2.10 *Peak and half wave potentials (vs Ag/AgCl) of polymers **P1-P5**.*

Polymer	$E^{red}{}_p$(V)	$E^{reox}{}_p$(V)	$E_{½}{}^{red}$(V)	$E^{ox}{}_p$(V)	$E^{rered}{}_p$(V)	$E_{½}{}^{ox}$(V)
P1	-1.27	-0.94	-1.11	1.36	1.19	1.28
P2	-1.29	-1.12	-1.21	0.87	0.69	0.78
P3	---	---	---	0.51	0.37	0.44
P4	-0.75	-0.54	-0.64	1.07	0.85	0.96
P5	-1.25	-1.11	-1.18	1.06	0.92	0.99

Table 2.11 *Onset potential values (vs Ag/AgCl), estimation of HOMO and LUMO levels and comparison with open circuit potential for polymers **P1-P5**.*

Polymer	$E^{red}{}_{on}$ (V)	$E^{ox}{}_{on}$ (V)	-LUMO[a] (eV)	-LUMO[b] (eV)	-HOMO[c] (eV)	-HOMO[d] (eV)	$E_g{}^e$ /eV	Voc/V
P1	-0.97	0.89	3.43	3.54	5.29	5.93	1.7	0.64
P2	-0.99	0.47	3.41	3.44	4.87	5.43	1.5	0.50
P3	---	0.14	---	---	4.54	5.09	---	0.0
P4	-0.57	0.62	3.83	4.01	5.02	5.61	1.2	0.14
P5	-0.83	0.46	3.57	3.47	4.86	5.64	1.3	0.30

[a,c]determined from the onset of reduction and oxidation potentials. [b,d]determined from the half-wave potentials.
[e]band gap determined from the onset of the electrochemical values.

The correlation between the HOMO and Voc values observed in these series of homo-polymers is similar to the alternating polyfluorenes discussed above. The trends in the experimental HOMO values were also confirmed by quantum chemical calculations. Polymers **P1** and **P2** are similar except for the difference in the position and nature of the substituent on the phenyl rings. Polymer **P2**, the one with branched alkoxy substituent on the *para* position, gave a decrease of the optical band gap from 1.6 eV for polymer **P1** to 1.5 eV. The electrochemical and optical band gaps for polymer **P2** differ very slightly while for polymer **P1**, the electrochemical band gap is higher by about 0.26 eV. The reduction in the band gap for polymer **P2** as compared to polymer **P1** is mainly due to the destabilization of the HOMO level of polymer **P2**. In polymer **P1** there is presumably a stronger steric interaction of the *meta*-substituted alkoxy groups on the phenyl rings, which are closer to the main chain. These increased steric interactions could cause a decrease in the effective conjugation length and a shift of the absorption maximum to a lower wavelength. Similar observations were also reported for poly(*p*-phenylene vinylene) derivatives [36]. Polymers **P2** and **P4** can also be compared with each other. The additional electron withdrawing thiadiazole unit in polymer **P4** gave a decrease in the optical band gap by about 0.7 eV. The electrochemical data clearly shows that this is mainly due to the stabilization of the LUMO level as a result of the additional thiadiazole unit. The optical band gaps for polymers **P2** and **P3** are about the same. The electrochemical data shows that the HOMO level of **P3** is destabilized by about 0.33 eV compared to polymer **P2**. Polymer **P3** is an easily p-dopable polymer and we also observed a very weak electrochemical signal in the n-doping region which makes it difficult to estimate the LUMO level. However, by comparing the optical band gap and the HOMO value obtained electrochemically, one can expect the LUMO level to be around –3.0 eV. Hence, there is no net decrease in the band gap by adding a strong electron-donating group. The optical band gap of polymer **P5** is about 1.3 eV, which is in good agreement with the electrochemical band gap. It is known that with increasing number of thiophene units, the oxidation potential is decreased [38]. Hence, the lower value of the band gap in this polymer is due to the presence of more electron donating thiophene units along with the electron acceptor quinoxaline unit in the repeating structures. The presence of both units also makes this polymer easily p- and n-dopable.

2.3.2.3 Optical and Electrochemical Properties of Conjugated Polymers Incorporating Oxadiazole Units.

The chemical structures of the polymers **P6-P9** characterized are shown in Figure 2.22.

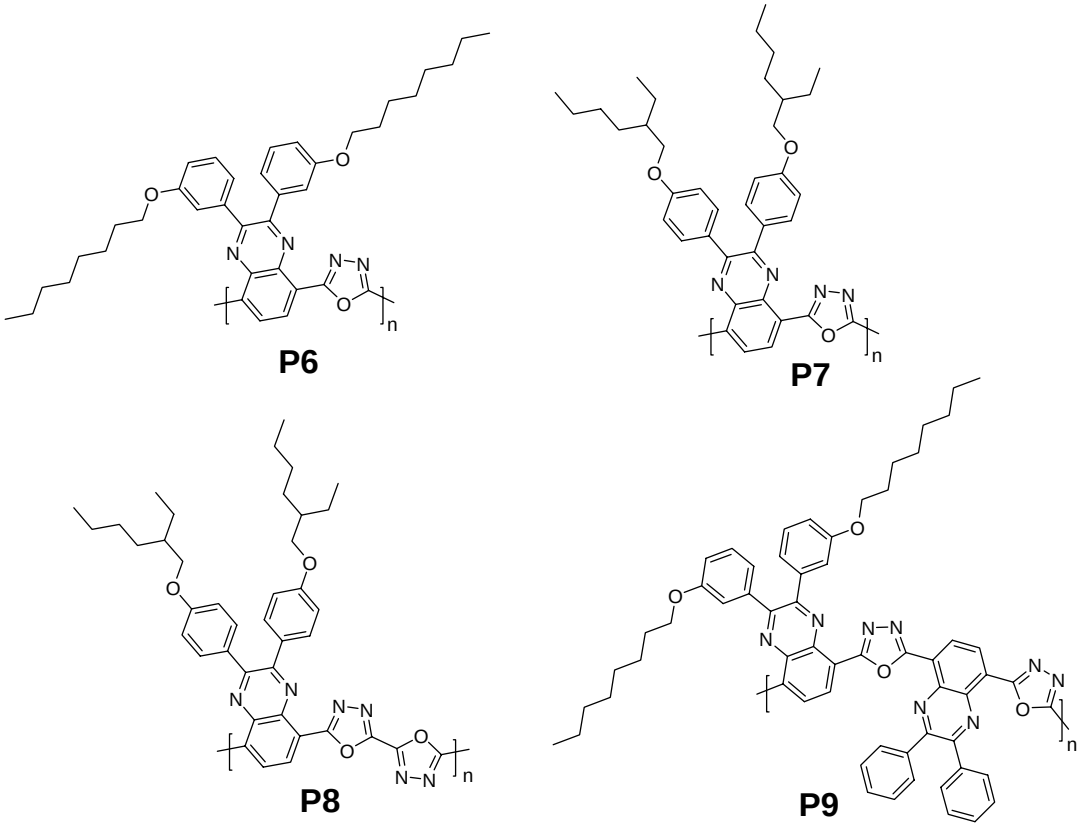

Figure 2.22 The *chemical structures of oxadiazole containing polymers* **P6-P9**.

Figures 2.23 shows the UV-Vis and PL spectra of the polymers **P6-P8** both in chloroform solution and in films. The relevant information of absorption and emission maxima of the polymers **P6-P8** are summarized in Table 2.12. All three polymers show absorption between 385-415 nm and emission between 500-522 nm both from chloroform solutions and from solid films. Both the absorption and emission spectra taken from solution and film do not show significant shifts in the maxima indicating the non-flexibility of the backbone of the polymer chain upon aggregation in the solid film.

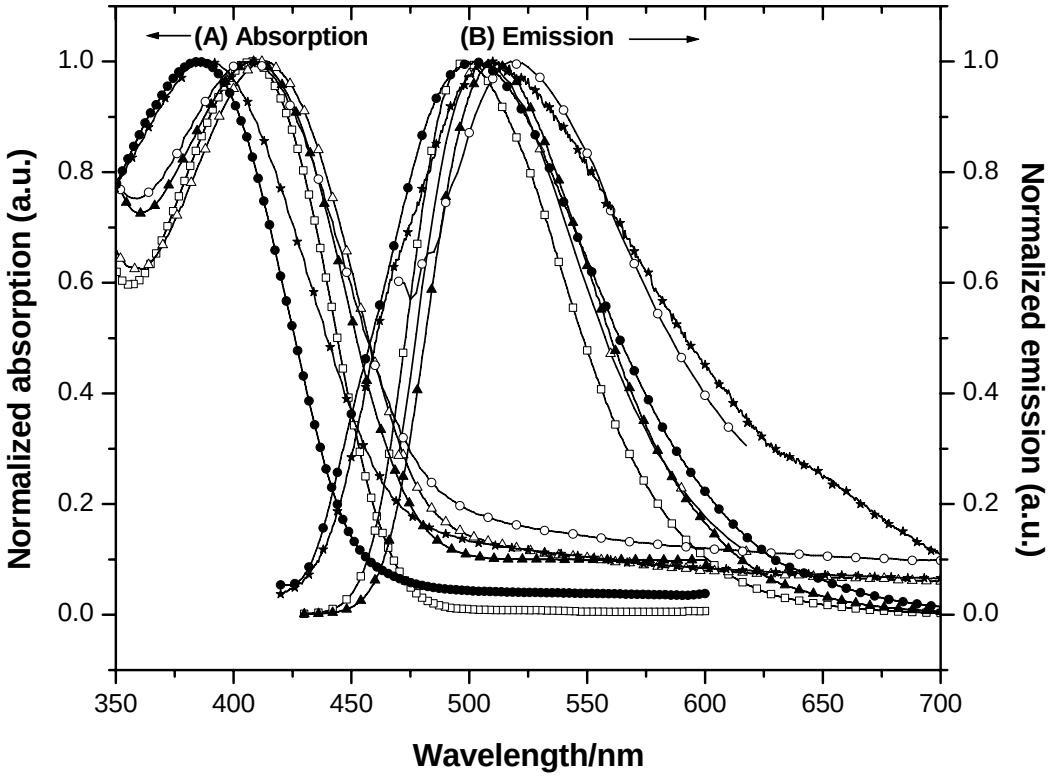

Figure 2.23 *Absorption and emission spectra for polymers (●) **P6**, (□) **P7**, (▲) **P8** from chloroform solution and (★) **P6**, (△) **P7**, (○) **P8** from films casted on glass from a chloroform solution.*

Table 2.12 *Absorption and emission maxima of the polymers **P1-P4** in solution and films.*

Polymer	λ_{max} (abs)/nm		λ_{max} (emiss)/nm	
	Solution	Film	Solution	Film
P6	385	388	504	510
P7	408	414	499	508
P8	408	407	511	522

The cyclic voltammograms of the polymers **P6-P9**, solvent casted on platinum disk electrodes, are shown in Figure 2.24. All polymers show an irreversible oxidation in the p-doping region. Polymers **P6-P8** show very good reversibility in the n-doping region while polymer **P9** shows irreversible behavior in the n-doping regions as well. The relevant data

are summarized in Table 2.13-2.14. The half-wave potentials of the polymers **P6-P8** are around –1.0 V.

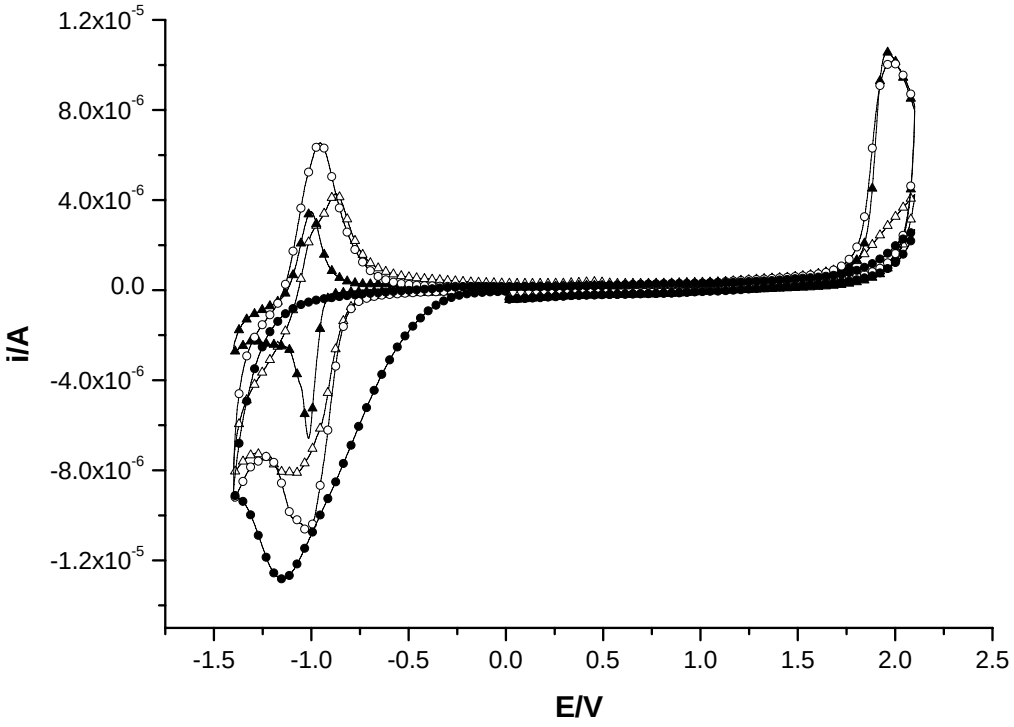

Figure 2.24 *Cyclic voltammograms of polymers (△)* ***P6****, (▲)* ***P7****, (○)* ***P8*** *and (●)* ***P9*** *films solvent casted on Pt disk electrode in 0.1M* Bu_4NBF_4*/AcN supporting electrolyte.*

Table 2.13 *Peak and half-wave potentials (Ag/AgCl) of polymers* **P6-P9**.

Polymer	E^{red}_p (V)	E^{reox}_p (V)	$E_{½}$ (V)	E^{ox}_p
P6	-0.91	-1.12	-1.02	---
P7	-1.04	-1.05	-1.045	1.92
P8	-0.99	-1.05	-1.02	1.95
P9	-1.14	---	---	---

Table 2.14 *Onset potential values (vs Ag/AgCl) and estimation of HOMO and LUMO levels for polymers* **P6-P9**.

Polymer	E^{red}_{on} (V)	E^{ox}_{on} (V)	-LUMO[a] (eV)	-LUMO[b] (eV)	-HOMO[a] (eV)	Band gap[c] (eV)	Band gap[d] (eV)
P1	-0.79	1.67	3.6	3.6	6.1	2.5	2.6
P2	-0.93	1.72	3.5	3.6	6.1	2.6	2.5
P3	-0.82	1.67	3.6	3.6	6.1	2.5	2.5

[a]determined from the onset of reduction and oxidation potentials. [b]determined from the half-wave potentials. [c]band gap determined from the onset of the electrochemical values. [d]band gap determined from the onset of optical absorption of the polymer films.

Among the polymers investigated in this work, **P7** shows less broadening of the reduction and reoxidation peaks as the sweep rate is increased as shown in Figure 2.25. The peak current is also plotted as a function of sweep rate (Figure 2.25 insert) and gives a straight line as expected for surface bound electroactive materials.

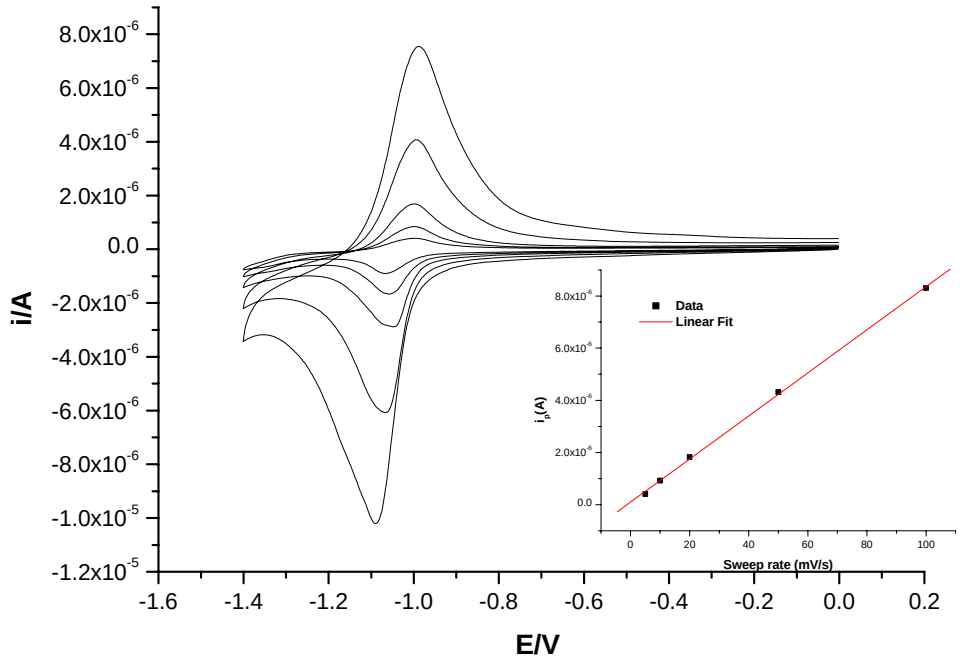

Figure 2.25 *Cyclic voltammograms of* ***P7*** *on Pt disk electrode in 0.1 M* Bu_4NBF_4*/AcN supporting electrolyte at a sweep rate of 5, 10, 20, 50 and 100 mV/s. The insert shows a plot of the peak current as a function of sweep rate.*

2.3.3 Characterization of Electronically Conducting Polymers designed for Polymer Light Emitting Diodes

2.3.3.1 Characterization of alkoxyphenyl-substituted polyfluorenes with hole transporting triphenyl amine units.

The chemical structures of the alkoxyphenyl-substituted polyfluorenes with various composition of the triphenylamine units are shown in Figure 2.26.

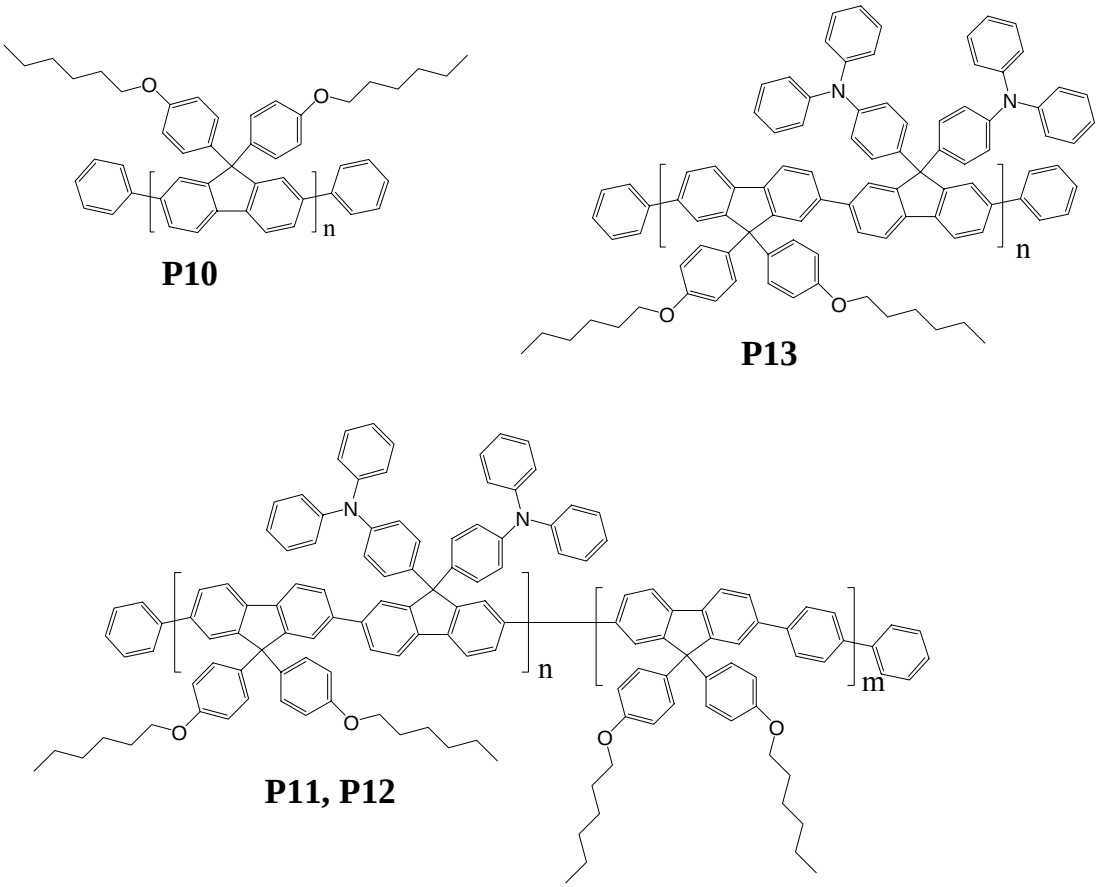

Figure 2.26 *Chemical structures of polymers **P10-P13**. Polymers **P11, P12 and P13** contains 10, 25% and 50% of the triphenylamine-substituted fluorene units, respectively.*

The UV-Vis absorption, photoluminescence (PL) and electroluminescent (EL) spectra of polymer **P11** are shown in Figure 2.27. The corresponding spectra for polymers **P10**, **P12** and **P13** are comparable.

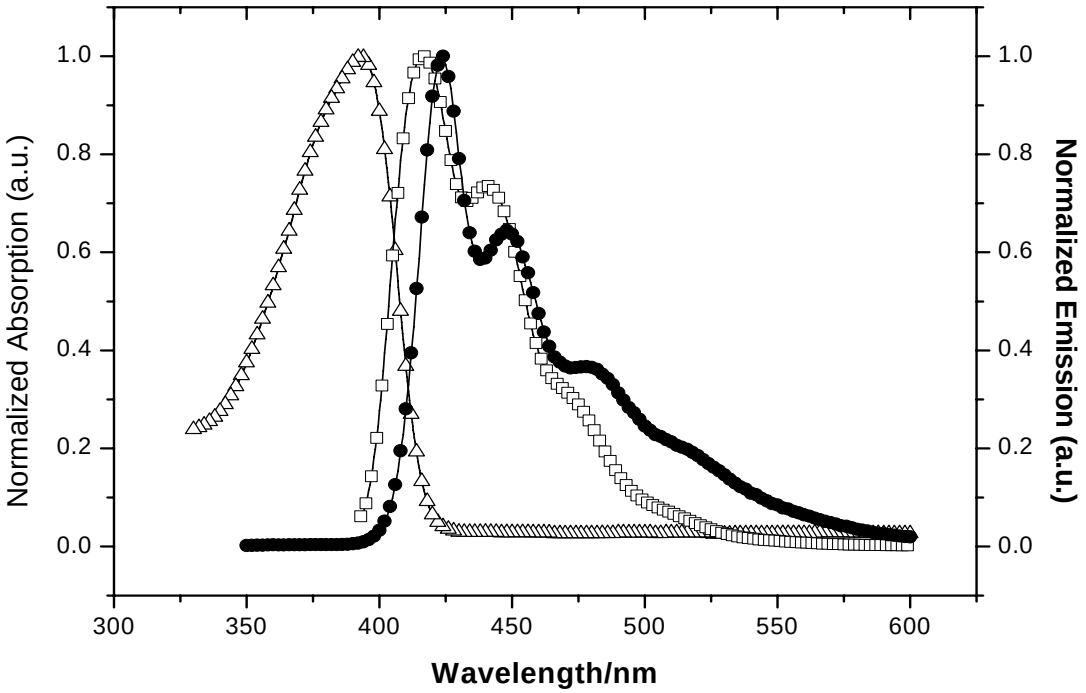

Figure 2.27 *UV-Vis absorption together with PL- and EL-emission spectra for* ***P11***.

The polymers were characterised using cyclic voltammetry using the onset method. Data from this study are summarised in Table 2.15 and clearly show that as the ratios of the triphenylamine units are increased, the HOMO levels of the polymers are reduced.

Table 2.15 *Electrochemical properties of polymers* ***P10-P13***.

Polymer	E^{ox}_{on} (V *vs* Ag/AgCl)	E^{red}_{on} (V *vs* Ag/AgCl)	HOMO (eV)	LUMO (eV)	E_g (eV)
P10	1.30	-1.80	-5.70	-2.60	3.10
P11	1.03	-1.71	-5.43	-2.69	2.74
P12	0.86	-1.55	-5.26	-2.85	2.41
P13	0.86	-1.49	-5.26	-2.91	2.35

The external quantum efficiencies (EQEs) of the PLEDs, fabricated from the polymers [40], are listed in Table 2.16 together with the PL efficiencies in chloroform solution.

Table 2.16 *Photoluminescence efficiencies (ϕ_{PL}) in chloroform solution and external quantum efficiencies (EQE) of the devices.*

Polymer	ϕ_{PL}	EQE (%)
P10	0.95	0.05
P11	0.73	0.32
P12	0.81	0.19
P13	0.52	0.03

Compared with **P10**, improved EQEs were observed in PLEDs made of **P11** and **P12**. When using **P13** the efficiency is much lower, which is in agreement with the PL yields. However, the highest EQE is obtained for polymer **P11**, which indicates a favourable balance between charges in the diode. Furthermore, the thresholds of PLEDs based on polymer **P10**, **P12** and **P13** are 3 V, whereas that of **P11** is 2.5 V, which confirms better hole and electron balance with **P11** [40].

2.3.3.2 Characterization of anthrancene and benzothiadiazole containing polyfluorene copolymers.

The chemical structures of the polymers investigated are shown in Figure 2.28.

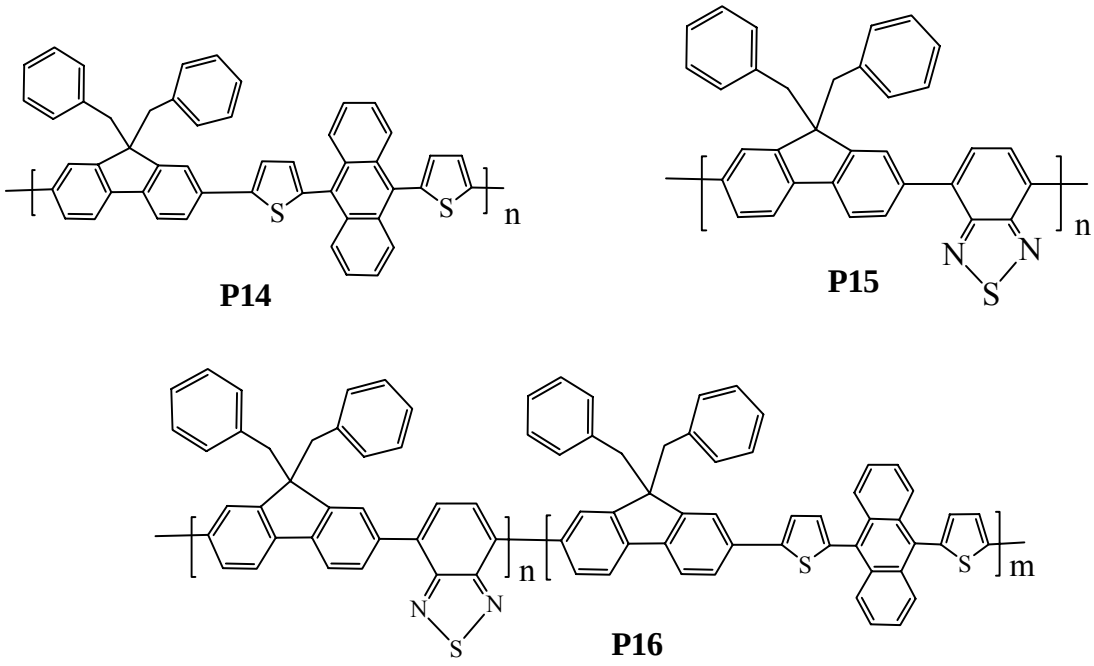

Figure 2.28 *Chemical Structures of Polymers **P14-P16**.*

The UV-Vis absorption, photoluminescence (PL), electroluminescent (EL) spectra and CVs of polymers **P14-P16** are shown in Figures 2.29 and 2.30, respectively. The absorption and emission maxima, the band gaps and PL efficiencies from a chloroform solution of the polymers and the electrochemical data of **P14-P16** are summarized in Tables 2.17 and 2.18. The data show that the absorption maximum of polymers **P15** and **P16** is more red-shifted than polymer **P14**. Moreover, polymer **P14** shows lesser photoluminescence quantum yield as compared to polymers **P15** and **P16**.

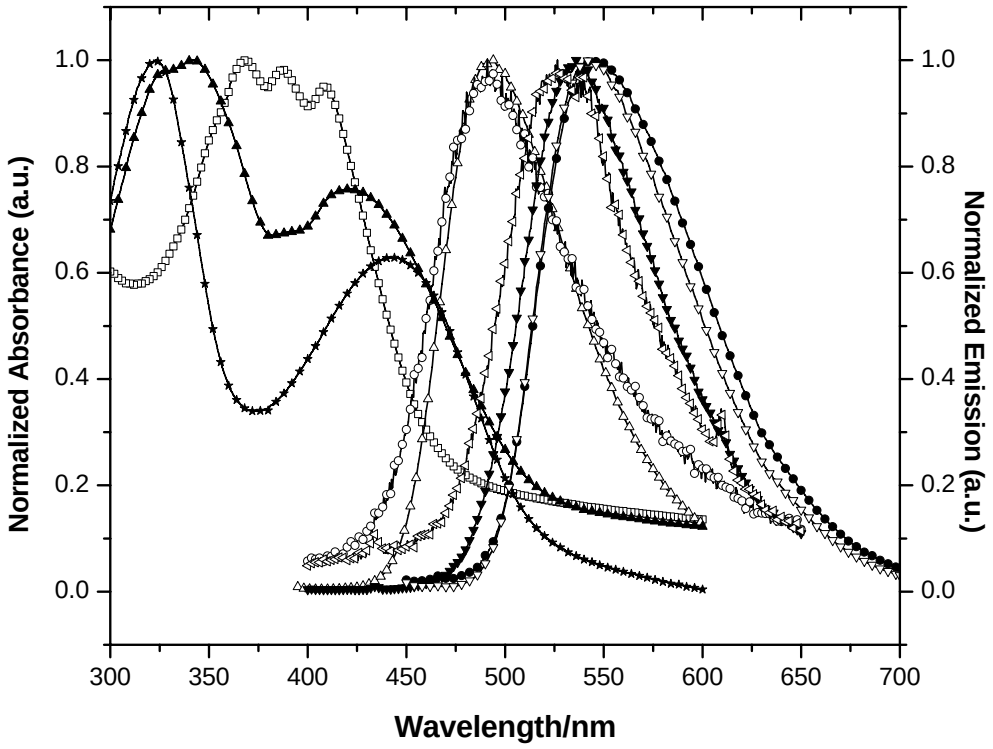

Figure 2.29 *UV-Vis absorption spectrum of polymers (□)* ***P14****, (★)* ***P15*** *and (▲)* ***P16;*** *photoluminescence emission of polymers (△)* ***P14****, (▽)* ***P15*** *and (●)* ***P16;*** *and electroluminescence emission of polymers (○)* ***P14****, (◁)* ***P15*** *and (▼)* ***P16****.*

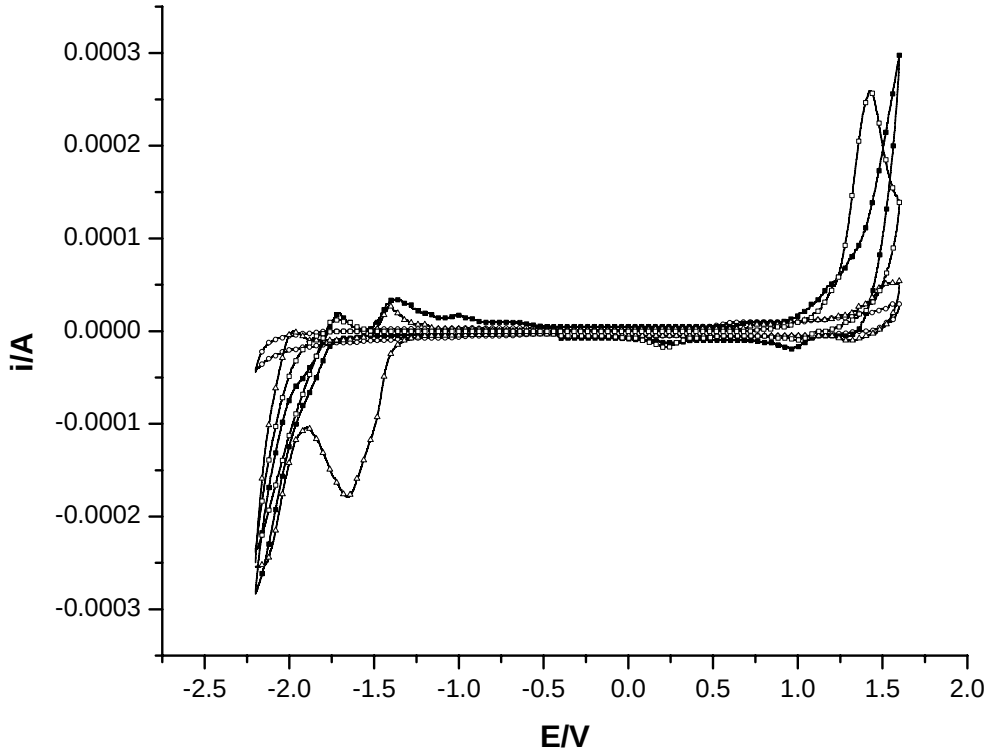

Figure 2.30 *Cyclic voltammogram of (○) background, polymers (□) **P14**, (△) **P15** and (■) **P16** casted on a glassy carbon disk electrode in Bu_4NFB_4/AcN supporting electrolyte/solvent system at 100 mV/s.*

Table 2.17 *Optical absorption and emission properties of polymers **P14-P16**.*

Polymer	λ_{on}/nm	E_g^{op}/eV	λ_{exc}/nm	λ_{max}^{PL}/nm	λ_{max}^{EL}/nm	Φ_{PL}
P14	473	2.62	387	492	492	0.02
P15	544	2.28	440	544	528	0.50
P16	519	2.39	420	547	533	0.42

Table 2.18 *Summary of the electrochemical data for polymers **P14-P16**.*

Polymer	E^{red}_{onset}/V	E^{ox}_{onset}/V	$-E_{LUMO}$/eV	$-E_{HOMO}$/eV	E_g^{ec}/eV
P14	-1.87	1.05	2.63	5.55	2.92
P15	-1.32	1.12	3.18	5.62	2.50
P16	-1.73	1.00	2.77	5.50	2.73

The current density-voltage (J-V) characteristics of the PLED devices (ITO/PEDOT-PSS/polymer/LiF(0.5 nm)/Al(60 nm)) are shown in Figure 2.31. The experimental details of device fabrication are described elsewhere [41]. Polymers **P14** and **P16** show typical diode characteristics with blue light emission at about 3.5 V. Figure 2.32 shows the emission light intensity *versus* the applied potential. Polymer **P16** shows a more pronounced increase in light intensity after 3.5 V than polymer **P14**. Polymer **P15** does not show any significant light emission up to 8 V. This could be due to the imbalance of electron and hole injection as a result of the more stabilized LUMO value of **P15** as shown in Table 2.18.

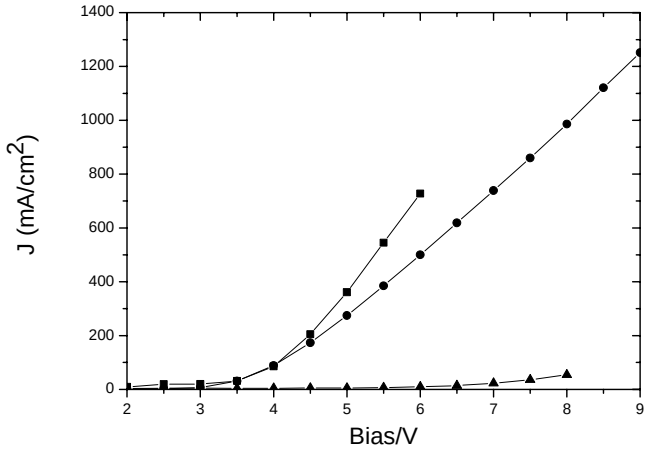

Figure 2.31 *Current density-voltage characteristics of polymers (■) **P14**, (▲) **P15** and (●) **P16**.*

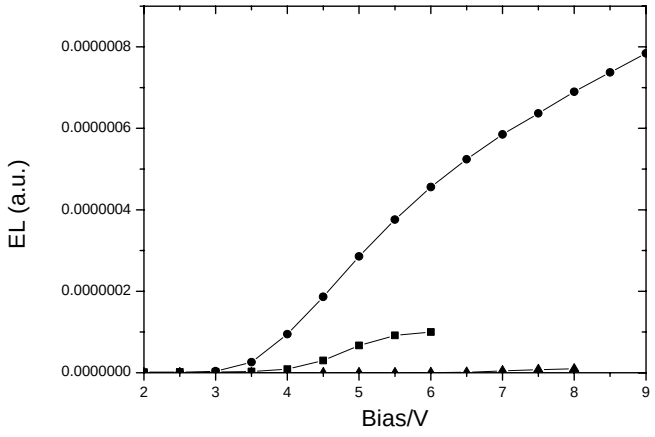

Figure 2.32 *Electroluminescence intensity versus the applied potential of polymers (■) **P14**, (▲) **P15** and (●) **P16**.*

2.4 Conclusion

The energies of HOMO and LUMO of a series of newly synthesized low band gap alternating polyfluorene copolymers were determined using cyclic and square wave voltammetric experiments under ordinary laboratory conditions. Comparison of the electrochemical and optical band gaps show that in most cases the electrochemical band gap was slightly higher, but the differences do not exceed ± 0.15 eV. A band gap as low as 0.8 eV was reached using the DAD strategy. In the structure-property studies the HOMO values obtained from the electrochemical studies were compared with the V_{OC} values determined from photovoltaic studies. The comparison clearly shows that the V_{OC} is decreased as the HOMO level is lowered. The structure-property correlations observed will give insights to further design more efficient polymers for solar cell applications.

High electron affinity n-type oxadiazole containing conjugated polymers were also optically and electrochemically characterized. These polymers were found to have high electron affinities (3.5-3.6) and are highly electrochemically reversible in the n-doping region.

A series of fluorene-based copolymers, containing different molar fractions of a hole-transporting, triphenylamine-substituted fluorene unit (**P10-P13**) were characterized. Absorption and emission properties were similar for all polymers, whereas the PL-efficiencies were affected by the composition of the polymer. Furthermore, the external quantum efficiencies of light-emitting devices from the polymers show a maximum for polymer **P11**. This indicates the presence of an optimal polymer composition between 10 and 50% of the triphenylamine moiety, where the charge carrier mobilities in the PLED are balanced.

The optical, electrochemical and light emitting characteristics of three copolymers (**P14-P16**) containing anthracene and benzothiadiazole units have been investigated. Blue light emissions were observed at about 3.5 V in polymers **P14** and **P16** with a more pronounced intensity for polymer **P14**.

2.5 References

1. R.H. Friend, R.W. Gymer, A.B. Holmes, J.H. Burroughes, R.N. Marks, C. Taliani, D.D.C. Bradley, D.A. Dos Santos, J.L. Bredas, M. Logdlund and W.R. Salaneck, *Nature,* **397** (1999) 121.
2. B.C. Thompson, L.G. Madrigal, M.R. Pinto, T.-S. Kang, K.S. Schanze and J.R. Reynolds, *J. Polymer Science, Part A: Polymer Chem.,* **43** (2005) 1417.
3. W. Ma, P.K. Iyer, X. Gong, B. Liu, D. Moses, G.C. Bazan and A.J. Heeger, *Adv. Mater.,* **17** (2005) 274.
4. M. Chen, E. Perzon, M.R. Andersson, S. Marcinkevicius, S.K.M. Jonsson, M. Fahlman and M. Berggren, *Appl. Phys. Lett*., **84** (2004) 3570.
5. X.Wang, M.R. Andersson.; M.E. Thompson and O. Inganäs, *Thin Solid Films,* **468** (2004) 226.
6. C.J. Brabec, N.S. Sariciftci and J.C. Hummelen, *Adv. Funct. Mater*., **11** (2001) 15.
7. N.S. Sariciftci, *Materials Today,* **7** (2004) 36.
8. H.J. Snaith, N.C. Greenham and R.H. Friend, *Adv. Mater.,* **16** (2004) 1640.
9. Y. Kim, S. Cook, S.A. Choulis, J. Nelson, J. R. Durrant and D.D. C. Bradley, *Chem. Mater.,* **16** (2004) 4812.
10. N.-K. Persson, H. Arwin and O. Inganäs, *J. Appl. Phys*., **97** (2005) 34503.
11. E.J. Meijer, D.M. De Leeuw, S. Setayesh, E. van Veenendaal, B.-H. Huisman, P.W.M. Blom, J.C. Hummelen, U. Scherf and T.M. Klapwijk, *Nature Materials,* **2** (2003) 678.
12. P. T. Nguyen, U. Rammelt, W. Plieth, S. Richter, M. Ploetner, W.-J. Fischer, N. Kiriy, K.P. Kamloth and H.-J Adler, *Electrochim. Acta,* **50** (2005) 1757.
13. A. Babel and S. A. Jenekhe, *J. Am. Chem. Soc*., **125** (2003) 13656.
14. A. Babel and S. A. Jenekhe, J. *Phys. Chem. B,* **107** (2003) 1749.

15. H. Sirringhaus, N. Tessler and R. H. Friend, *Science,* **280** (1998) 1741.

16. H. Meng, D. Tucker, S. Chaffins, Y. Chen, R. Helgeson, B. Dunn and F. Wudl, *Adv. Mater.,* **15** (2003) 146.

17. A. A. Argun, P.-H. Aubert; B. C. Thompson, I. Schwendeman, C. L. Gaupp, J. Hwang, N. J. Pinto, D. B. Tanner, A. G. MacDiarmid, and J. R. Reynolds, *Chem. Mater.,* **16** (2004) 4401.

18. F. Fungo, S. A. Jenekhe and A. J. Bard, *Chem. Mater.* **15** (2003) 1264.

19. P. R. Somani and S. Radhakrishnan, *Mater. Chem. and Phys.,* **77** (2003) 117.

20. R. J. Mortimer, *Electrochim. Acta,* **44** (1999) 2971.

21. C. Winder and N. S. Sariciftci, *J. Mater. Chem.*, **14** (2004) 1077.

22. X. Wang, E. Perzon, J. L. Delgado, P. De la Cruz, F. Zhang, F. Langa,; M.R. Andersson, and O. Inganäs, *Appl. Phys. Lett.,* **85** (2004) 5081.

23. M. Svensson, F. Zhang, S. C. V. Veenstra, J. H. Wiljan, J. C. Hummelen, J. M. Kroon, O. Inganäs and M. R. Andersson, *Adv. Mater.,* **15** (2003) 988.

24. H. Huang and P. G. Pickup, *Chem. Mater.,* **11** (1999) 1541.

25. J. Roncali, *Chem. Rev.,* **97** (1997) 173.

26. H. Meng; D. Tucker, S. Chaffins, Y. Chen, R. Helgeson, B. Dunn and F. Wudl, *Adv. Mater.,* **15** (2003) 146.

27. P. Schottland, K. Zong, C. L. Gaupp, B. C. Thompson, C. A. Thomas, I. Giurgiu, R. Hickman, K. A. Abboud, and J. R. Reynolds, *Macromolecules,* **33** (2000) 7051.

28. G. Zeng, S.-Jin Chua and W. Huang, *Thin Solid Films*, **417** (2002) 194.

29. F. Wudl, M. Kobayashi and A.J. Heeger, *J. Org. Chem.,* **49** (1984) 3382.

30. C. Kitamura, S. Tanaka and Y. Yamashita, *Chem. Mater*., **8** (1996) 570.

31. T. Yamamoto, Z.-H. Zhou, T. Kanbara, M. Shimura, K. Kizu, T. Maruyama, Y. Nakamura, T. Fukuda, B.-L. Lee, N. Ooba, S. Tomaru, T. Kurihara, T. Kaino, K. Kubota, and S. Sasaki, *J. Am. Chem. Soc.,* **118** (1996) 10389.

32. Q. T. Zhang and J. M. Tour, *J. Am. Chem. Soc.,* **120** (1998) 5355.

33. O. Inganäs, M. Svensson, F. Zhang, A. Gadisa, N.K. Persson, X. Wang and M.R. Andersson, *Appl. Phys. A,* **79** (2004) 31.

34. G. Hughes and M.R. Bryce, *J. Mater. Chem*., **15** (2005) 94.

35. A.P. Kulkarni, C.J. Tonzola, A. Babel and S.A. Jenekhe, *Chem. Mater.,* **16** (2004) 4556.

36. Gaussian 98, Revision A. 6.

37. F. Zhang, W. Mammo, S. Admassie, M. R. Andersson and O. Inganäs, *Adv. Mater.*, accepted.

38. J.Y. Kim, S.H. Park, I.S. Yum, S.H. Jin and K. Lee, *Synth. Met.,* **137** (2003) 1011.

39. X. Wang, E. Perzon, F. Oswald, F. Langa, S. Admassie, M. R. Andersson, and O. Inganäs, *Adv. Funct. Mater.,* **15** (2005) 1665.

40. X. Wang, E. Perzon, W. Mammo, F. Oswald, S. Admassie, N. K. Persson , F. Langa, M. R. Andersson, and O. Inganäs, *Thin Solid Films*, in press.

41. L. J. Lindgren, F. Zhang, S. Admassie, X. Wang, M. R. Andersson, and O. Inganäs, *J. Photoluminescence*, in press.

42. S. Admassie, Z. Yacob, F. Zhang, W. Mammo, T. Yohannes and T. Solomon, *Bull. Chem. Soc. Ethiop.,* accepted.

3 Vapour Phase Polymerised PEDOT as Electrode Material for Polymer Solar Cells

3.1 Background

Conjugated polymers like polypyrrole, polythiophene, polyaniline, polyphenylenes, and poly(*p*-phenylene vinylene)s have attracted a great deal of attention because of their great potential of application in a number of electronic devices like displays, smart windows, sensors, capacitors, batteries, and photovoltaic devices[1-2]. Among the various organic conducting polymers, poly(3,4-ethylenedioxy)thiophene (PEDOT) is one of the most widely studied conducting polymer because of its unique properties like high electrical conductivity, almost transparent thin film in the oxidized state and excellent stability at ambient and elevated temperatures [3].

For large area electronics it is desirable to use flexible transparent and conducting electrodes. For photovoltaic energy conversion devices, the large active area is a necessity to compensate for the lower energy conversion efficiencies still found in these systems. Deposition of the transparent electrode material should preferably be done by reel-to-reel methods. Also, the difficulties of using transparent oxides on flexible supports during reel-to-reel processing are considerable, arguing the use of flexible metallic polymer conductors. The commercially available polyelectrolyte complex poly(3,4-ethylenedioxy)thiophene: poly(styrene sulphonate) (PEDOT-PSS) can be easily spin-coated resulting in a highly transparent and conducting (0.05 –10 S/cm) polymer film. To use this polymer as an anode material in flexible polymeric devices, higher values of conductivities are needed. Electrochemical polymerization is widely used to get high conductivity. However, the method is restricted to depositing the polymer only on conducting substrates. For applications of such materials in large area electronics, deposition must be done over very large areas, and it is preferable if the deposition methods exclude electropolymerisation.

Very recently several groups have been working to improve the conductivity of PEDOT using different approaches. Jönsson *et al.* significantly improved the conductivity of the commercially available PEDOT-PSS up to 48 S/cm for a film thickness of about 110 nm by mixing the polymer solution with sorbitol as a secondary dopant [4]. Similar works using blending with polyethylene oxide [5] or using other secondary dopants like dimethyl

sulfoxide, N,N´-dimethyl formamide, tetrahydrofuran and 2,2'-thiodiethanol also significantly improved the conductivity of PEDOT-PSS in thin films up to 98 S/cm and optical transmission to 84% [6-7].

PEDOT-PSS modified by glycerol treatment has been reported as anode material for polymer light emitting diodes [8]. Inganäs and co-workers [9] also reported polymeric photovoltaic cells using polymer anodes made of PEDOT-PSS and PEDOT-PSS modified with sorbitol treatment on a glass substrate, which demonstrated the possibility of using flexible polymer anodes in plastic solar cells.

Others have used the chemical oxidative polymerization of PEDOT from its monomer (3,4-ethylenedioxythiophene) by optimizing the ratio of the monomer, the oxidant (iron(III)p-toluenesulfonate ($Fe(OTs)_3$), and a weak base (imidazole) [10 - 12]. With this method, conductivity as high as 750 S/cm and 81% transparency have been reported. Further enhancement of the conductivity up to 900 S/cm and 82% transparency has been achieved by using methanol substituted EDOT [13].

Another approach is to use the vapour phase polymerization (VPP). Mohammadi *et al.* [14] first reported this method as chemical vapour deposition (CVD) using $FeCl_3$ and H_2O_2 as oxidants for polymerizing polypyrrole films. The VPP method to produce conducting polymers like polypyrrole and PEDOT has been reported by Kim *et al.* [15-16] using the $FeCl_3$ as oxidant. The conductivity of PEDOT obtained by this method reached up to 70 S/cm. Winther-Jensen *et al* further developed the method of de Leeuw to improve the conductivity by using base-inhibited VPP of EDOT and reported conductivities as high as 1025 S/cm for a film thickness of 250 nm [17 -18]. Other studies showed that PEDOT could further be electrochemically oxidized to modify its work function and also further enhance the electrical conductivity for improved performance [19-21].

From all these studies, so far it is the VPP that gives the highest conductivity of PEDOT. Therefore, the first part of this chapter demonstrates the possible use of the base-inhibited VPP method to produce highly conducting anodes for photovoltaic devices. We also made devices from PEDOT-PSS and PEDOT-PSS modified with sorbitol on glass substrate for comparison. Further attempts were also made to enhance the open circuit potential by electrochemically depositing a very thin layer of Prussian blue on top of the VPP PEDOT.

In all the devices, a polyfluorene copolymer **APFO 3** mixed with [6,6]-phenyl-C_{61}-butyric acid methylester (PCBM) in 1:4 ratio was used as the active layer.

Commonly, polymer solar cells are constructed by sandwiching an active layer between two electrodes. The anode is usually made of a transparent substrate (glass) coated with a conducting film such as indium-tin-oxide (ITO). In many cases, a thin film of a conducting polymer PEDOT: PSS is spin coated on top of ITO to improve the interface conditions in order to facilitate charge injection and extraction. The cathode is usually formed by evaporation of metals like aluminum on top of the active layer. The thermal evaporation processes in most cases destroy the polymer/metal interface, and consequently alter the transport and/or the charge injection condition at the polymer/cathode interface.

Quite recently, noninvasive techniques, termed soft contact lamination, have emerged as an alternative method for formation of electrodes [22-23]. Soft contact lamination exploits the good adhesion property of soft elastomeric materials put in conformal contact with smooth surfaces. The adhesion of such elastomeric materials is attributed to Van der Waals forces facilitating good electrical contact when conducting materials are applied on the elastomer. This technique has been effectively used in organic light emitting diodes (OLED) [24-25] that generate uniform and stable light. Moreover, it has been shown that such devices are as efficient as the traditional OLEDs with evaporated cathode electrodes. The noninvasive technique, therefore, in combination with high-resolution printing and lamination techniques, can also be considered as an alternative way to fabricate contacts for OLEDs and organic photovoltaic devices. The later method can, in particular, assist to avoid direct evaporation of metals on top of the active layer, which in turn allows formation of smooth and well-defined interfaces. M. Granström and coworkers, [26] were able to demonstrate laminated devices that rely on fusing of two half cells, electrode/photoactive blend and photoactive blend/electrode together at elevated temperature. Such lamination processes may not be applied for all materials as, for example, the optical behavior and morphology of most polymer films are quite sensitive to temperature changes. Soft contact lamination does not rely on the melting of layers in order for surfaces to achieve contact.

The second part of this chapter demonstrates a polymer based solar cell, which is constructed by sandwiching an active layer between two conducting polymer electrodes. The anodes of the solar cells were constructed from ITO/PEDOT:PSS films that are

supported by glass substrates while the cathodes were made from a highly conducting VPP PEDOT on a flexible elastomeric substrate. The devices have shown good electrical and optical responses.

3.2 Experimental

A microscope glass slide was cut in to four pieces and cleaned with a 5:1:1 mixture of deionized H_2O, 25% NH_3 and 28% H_2O_2 at 85^oC for 5 minutes to remove organic contaminants. It was further washed with distilled water several times and dried followed by oxygen plasma treatment. The polydimethylsiloxane (PDMS) substrate was initially prepared and cured as described elsewhere [27] on a silicon wafer, to achieve a smooth surface. The thickness of the PDMS layer was about 1mm. The PDMS slab was exposed to oxygen plasma for few seconds. A 40% solution of Fe(III) tosylate ($Fe(OTs)_3$) in butanol (Baytron C) is used as an oxidizing agent. 0.5 mol of pyridine per mole of oxidant was used for base inhibited vapour phase polymerisation. In the case of PDMS substrate, 1.0 mL of toluene was added for every 2.0 mL of the oxidant. The mixture of pyridine and $Fe(OTs)_3$ were spin coated on the previously cleaned glass substrate at a speed of 3000 rpm. The film was allowed to dry in air until the solvent (butanol) evaporates. It was further dried in an oven at 75^oC for three minutes.

The films were then transferred to a reaction chamber containing the monomer, 3,4-ethylenedioxythiophene (Baytron M). The vaporization reaction was carried out at 30^oC for 1 hour and allowed to stay in air for 30 minutes. The films were then thoroughly rinsed for ten minutes twice in ethanol. The morphology of the films was recorded using atomic force microscopy in a tapping mode using the SFM-Nanoscope III, Digital Instrument.

Prussian blue was deposited onto the VPP PEDOT by potentiostatic method at a potential of +0.3 V, from an aqueous solution containing 2 mM $K_3[Fe(CN)_6]$ and 2 mM $FeCl_3$ in 0.1 M KCl + 0.01 M HCl. The electrolysis was prolonged for 15 seconds. After the deposition, the modified anode was rinsed with distilled water. Optical transmissions were measured using Lambda 9 Spectrophotometer (Perkin-Elmer). Film thicknesses were measured using a Sloan DEKTAK 3030 surface profilometer. The conductivities of the films were measured using the four-point probe technique, both with four point-like contacts in line, as well as with four parallel gold lines deposited on the insulating samples support. Solar cell devices

where VVP PEDOT was used as anode, were fabricated by spin-coating the active layer, consisting of a blend of chloroform solution of APFO 3 and PCBM (Figure 3.1) on top of each PEDOT electrodes followed by depositing LiF (0.6 nm) and Al (60 nm) by evaporation in vacuum (Figure 3.2).

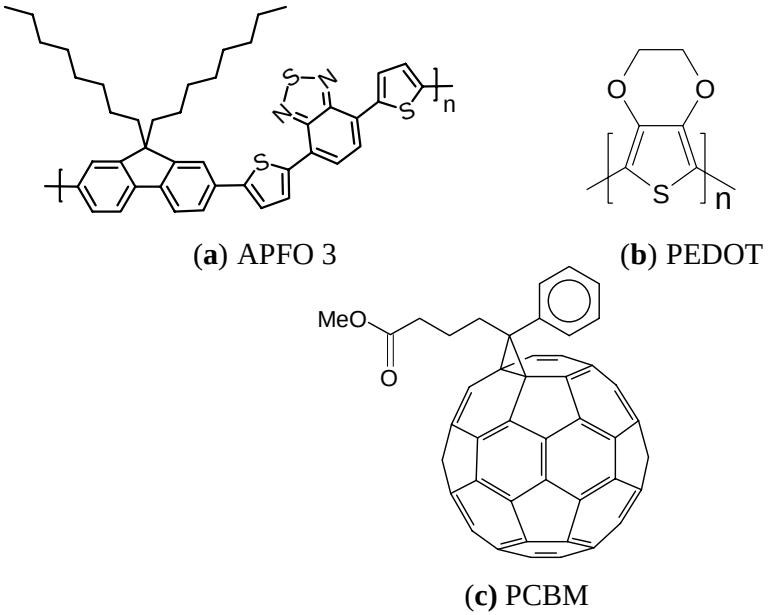

(**a**) APFO 3 (**b**) PEDOT

(**c**) PCBM

Figure 3.1 *The chemical structures used in the device fabrication.*

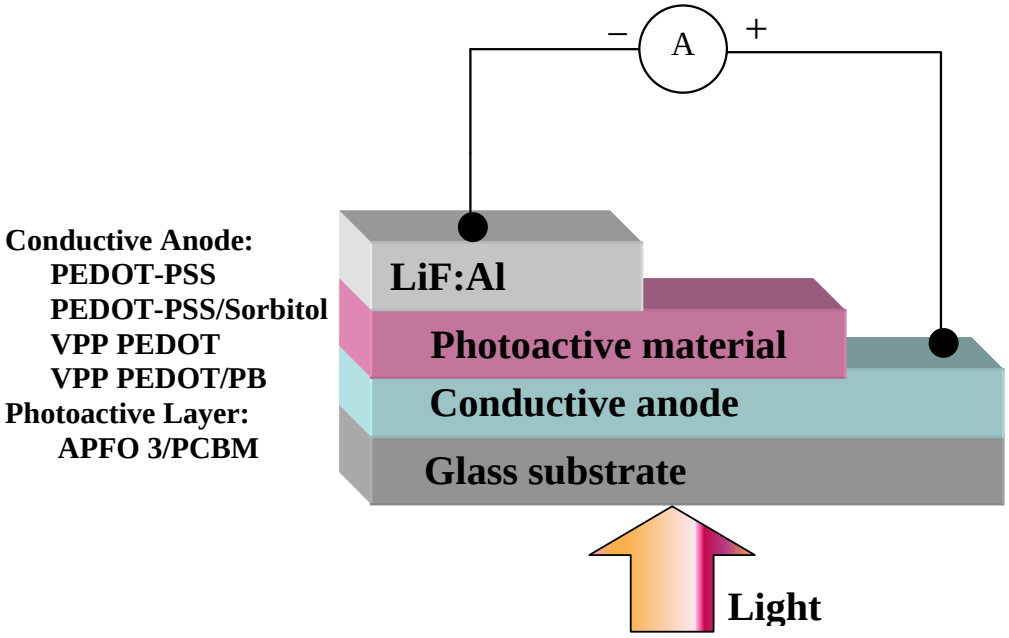

Figure 3.2 *Solar cell device structure made of glass/conductive anode/active layer/LiF/Al*

In the solar cell devices, where the VPP PEDOT was used as cathode, the VPP PEDOT film on PDMS was patterned by using sodium hypochlorite (NaOCl), to define suitable electrode

geometries. The active layer was spin coated on the anode electrode made of ITO/PEDOT:PSS. The solar cells are completed by bringing anode and cathode components in contact using soft lamination technique (Figure 3.3).

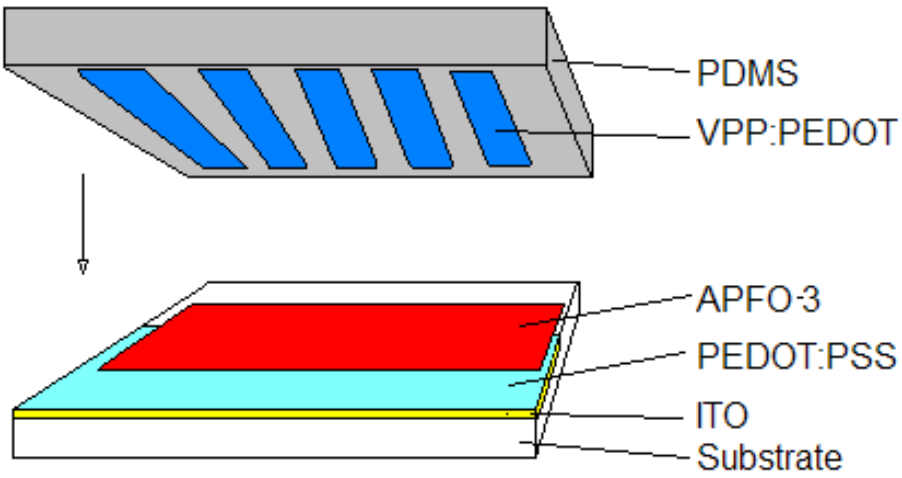

Figure 3.3 *The schematic illustration of the top and bottom components of the solar cells device where VPP PEDOT is used as a cathode.*

Current density-voltage (J-V) measurements were done under white light illumination of intensity 100 mW/cm^2 using a xenon lamp regulated by an Oriel power supply (Model 68911) and recorded by Keithley 2400 Source Meter. The spectral response was measured using a Keithley 485 picoammeter under short circuit condition. The general schematic diagram is shown in Figure 3.4.

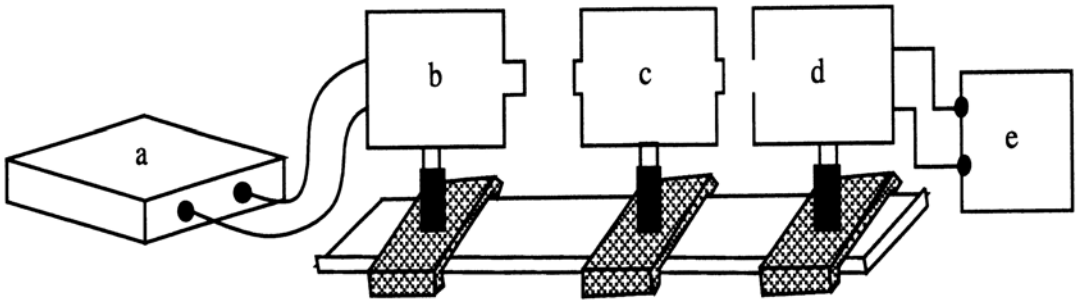

Figure 3.4 *General schematic diagram for photovoltaic measurements. (a) Power supply, (b)lamp housing, (c) monochromator, (d) sample holder and (e) an output measuring instrument.*

3.3. Results and Discussion

3.3.1 A Polymer Photodiode Using Vapour Phase Polymerised PEDOT as An Anode.

The VPP-PEDOT, and PEDOT:PSS doped with sorbitol provide highly conducting anodes. The conductivity values for different anodes made on glass substrate are summarized in Table 3.1. The transmission properties of the anodes were also studied (Figure 3.5) and are summarized in Table 3.1.

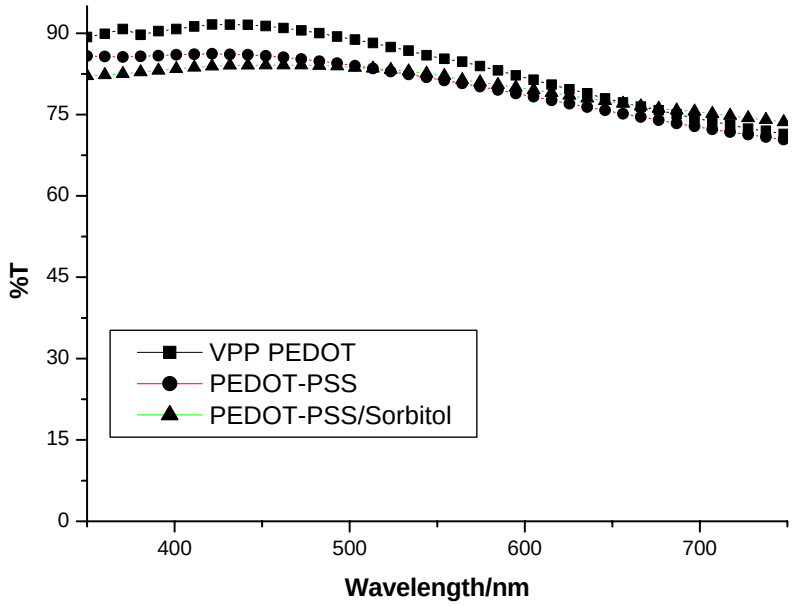

Figure 3.5 *Transparencies of the various anodes used in the device in the range 350-800 nm.*

Table 3.1 *Summary of the anode conductivities and transmission values.*

Electrode	Film thickness (nm)	%T	Surface resistance (ohm)	Conductivity (S/cm)
PEDOT-PSS	190	80	$307x10^3$	0.17
PEDOT-PSS/Sorbitol	190	81	629	84
VPP PEDOT	60	84	215	775

The single transmission values refer to the averages of the RGB transmission at λ = 700, 520 and 480 nm. The morphology of the film was studied by AFM (Figures 3.6) and the surface showed rough nanostructure features. This can influence the free charge carrier transfer to the anode at high incident light intensities as a result of the increased surface area between the PEDOT electrode and the active polymer, possibly also due to the roughness causing scattering of light.

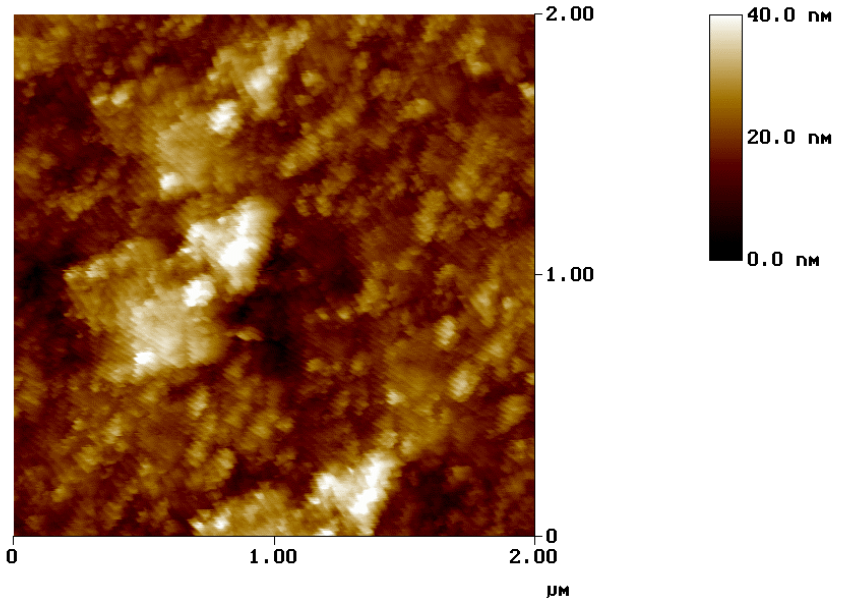

Figure 3.6 *AFM image of VPP PEDOT films.*

The photocurrent spectral responses of the device with different anodes were similar in IPCE for low incident light intensities as shown in Figure 3.7. The photocurrent is a result of (1) photoinduced exciton dissociation at the polymer/PCBM interface, (2) free charge carriers transport through the active layer and (3) transfer of the free charge carriers to the electrode. At low photocurrent densities, due to low incident light intensity, the IPCE is not significantly influenced by the conductivity of the anodes. At high light intensities a highly conducting electrode is needed to extract maximum power output from the device.

Current-voltage characteristics of the diodes with different anodes, without and with LiF layer, are shown in Figures 3.8-3.11 under white light illumination of intensity 100 mW/cm^2 and in the dark, respectively.

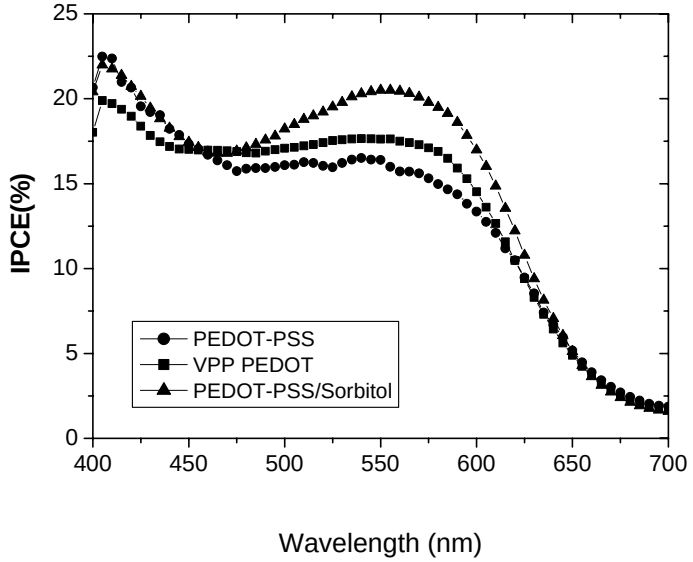

Figure 3.7 *IPCE of photodiodes with different anode materials.*

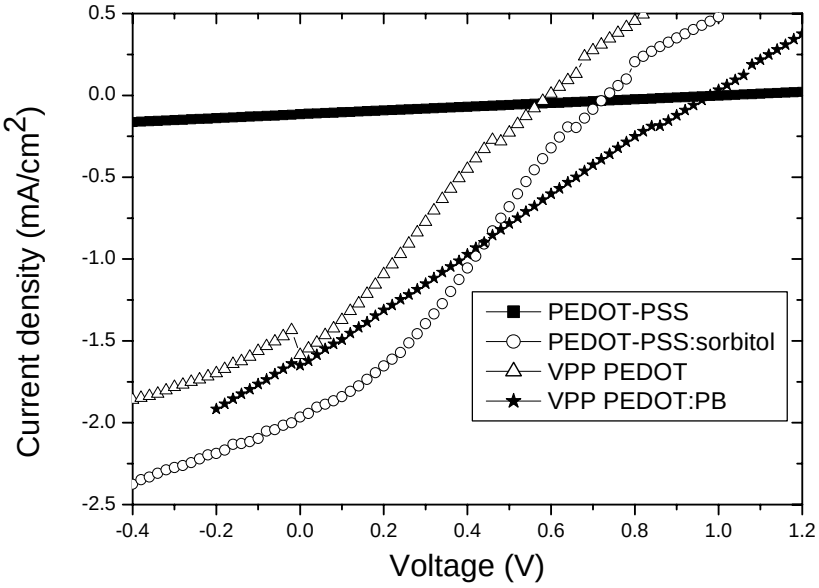

Figure 3.8 *I-V characteristics of photovoltaic devices with different anodes under AM1.5 illumination without LiF layer.*

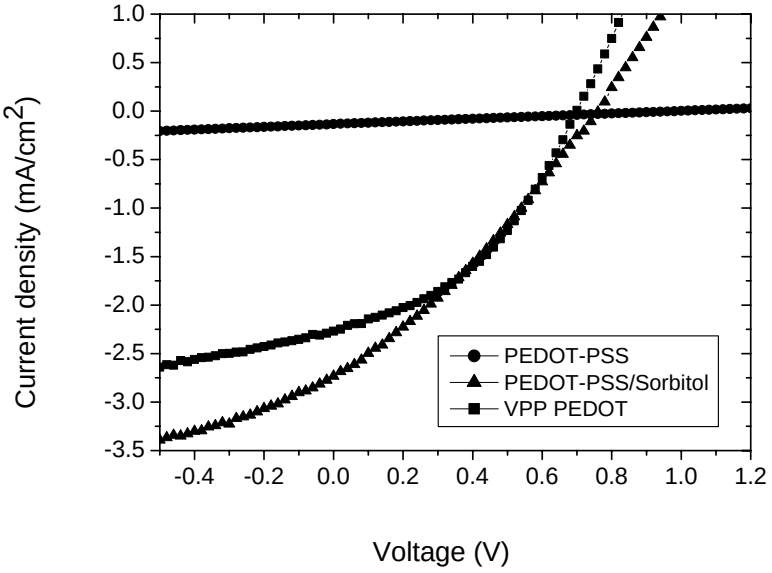

Figure 3.9 *I-V characteristics of photovoltaic devices with different anodes under AM1.5 illumination with LiF layer.*

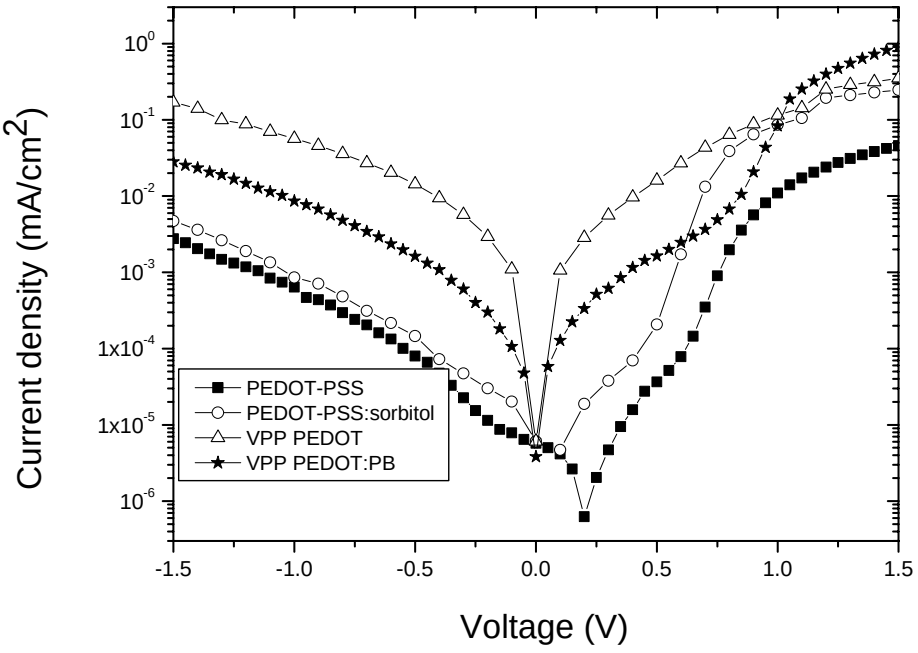

Figure 3.10 *Semi-log of I-V characteristics of photovoltaic devices with different anodes in the dark without LiF layer.*

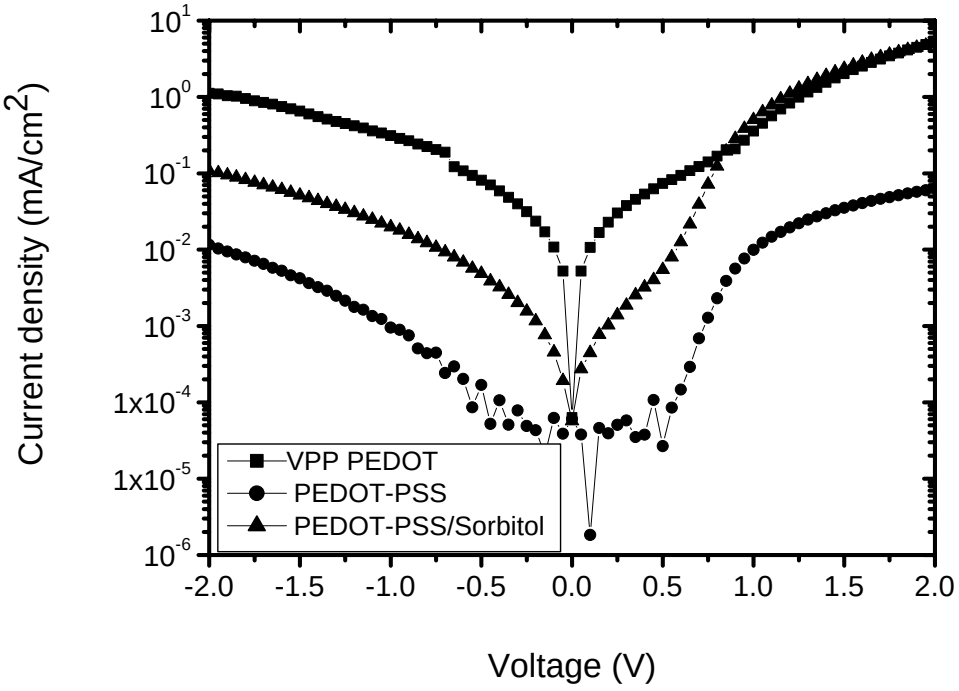

Figure 3.11 *Semi-log of I-V characteristics of photovoltaic devices with different anodes in the dark with LiF layer.*

The fill factor and power conversion efficiencies were calculated from I-V curves, which are summarized in Tables 3.2 and 3.3.

Table 3.2 *Summary of the photovoltaic characteristics of the devices made without LiF.*

Electrode	Jsc	Voc	FF	PCE(%)
PEDOT-PSS	0.11	1.01	0.26	0.03
PEDOT-PSS/Sorbitol	1.97	0.73	0.30	0.43
VPP PEDOT	1.59	0.60	0.25	0.24
VPP PEDOT-PB	1.65	0.98	0.24	0.40

Table 3.3 *Summary of the photovoltaic characteristics of the devices made with LiF.*

Electrode	J_{sc}(mA/cm^2)	V_{oc}(V)	FF	PCE(%)
PEDOT-PSS	0.13	0.98	0.26	0.03
PEDOT-PSS/Sorbitol	2.73	0.76	0.30	0.63
VPP PEDOT	2.27	0.70	0.41	0.65

The devices with highly conducting anodes showed an order of magnitude increase in the power conversion efficiencies. The low value of the open circuit voltage can be attributed to the low work function of VPP PEDOT and has been confirmed with photoelectron spectroscopy data. The data showed a work function of 4.3 eV. This can be a cause of the observed low rectification property of devices made with VPP PEDOT. We note that the work function of VPP PEDOT is close to the LUMO of PCBM, causing a low barrier for electron injection. This would cause the almost symmetric dark I-V characteristics of the diode to show a space charge limited current due to electron transport in PCBM [29]. The devices with VPP PEDOT showed enhanced power conversion efficiency, which is comparable with that of PEDOT-PSS doped with sorbitol. An order of increase in J_{sc} and PCE of such devices compared with that of PEDOT-PSS electrode can be attributed to the increased conductivity of the anode.

3.3.1 A Polymer Photodiode Using Vapour Phase Polymerised PEDOT as a Cathode.

The estimated thickness of VPP PEDOT used as a cathode on top of PDMS was 130 to 150 nm and the surface conductivity as measured by a four-point probe was 330 to 385 S/cm. Figure 3.12 shows the photocurrent image of one of our devices whose active area amounts to 8 mm^2.

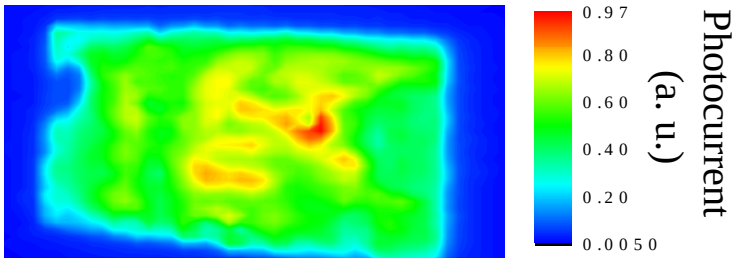

Figure 3.12 *The photocurrent image of a typical device.*

The sample was scanned under an illumination of a focused pulsed laser (635 nm) with a spot radius of about 21 μm, and intensity 21 kW/m^2. This technique helps us to investigate the degree of contact between the bottom and top layers by tracing the surface distribution of the generated photocurrents. The technique can also be used to study the extent of uniformity of the photocurrent that is generated from the whole active area of the devices. As can be seen from Figure 3.12, the image of the photocurrent is quite uniform throughout the active region (2 mm × 4 mm) except for tiny high current generating spots, which are located close to the central region. For all the devices measured, no dark spot was observed indicating that interface contacts are well established. The incident photon to current conversion efficiency (IPCE), which was recorded under illumination of monochromatic light, is depicted in Figure 3.13. The IPCE of the device is well correlated to the absorption of the active layer.

The I-V characteristics measured under dark conditions also give information, including rectification and injection conditions. From a typical I-V curve (Figure 3.14) we extracted a rectification ratio of over 10^3 at ± 2 V.

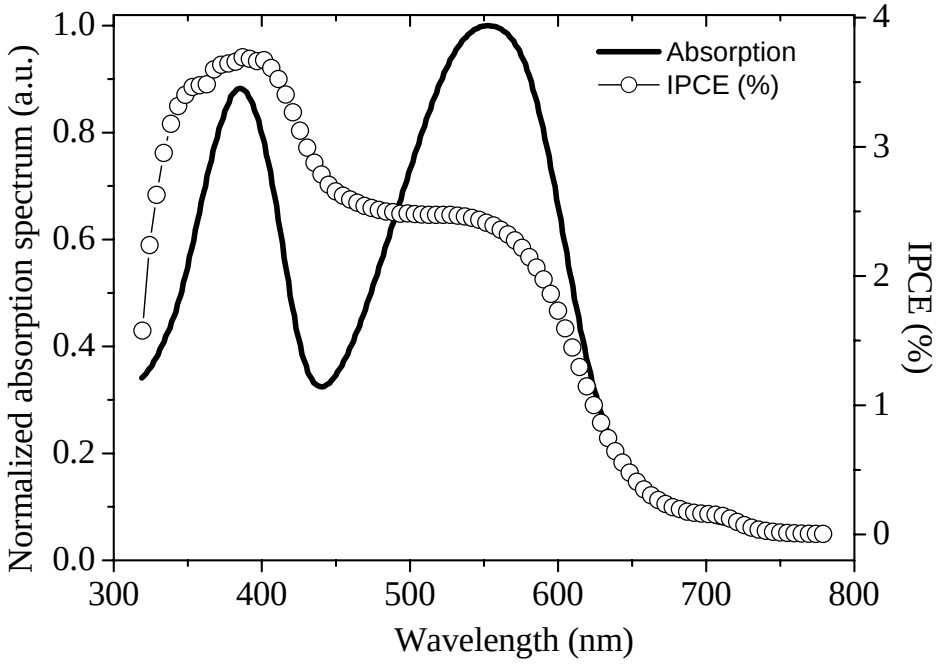

Figure 3.13 *The incident photon to current conversion efficiency (IPCE) of a typical device.*

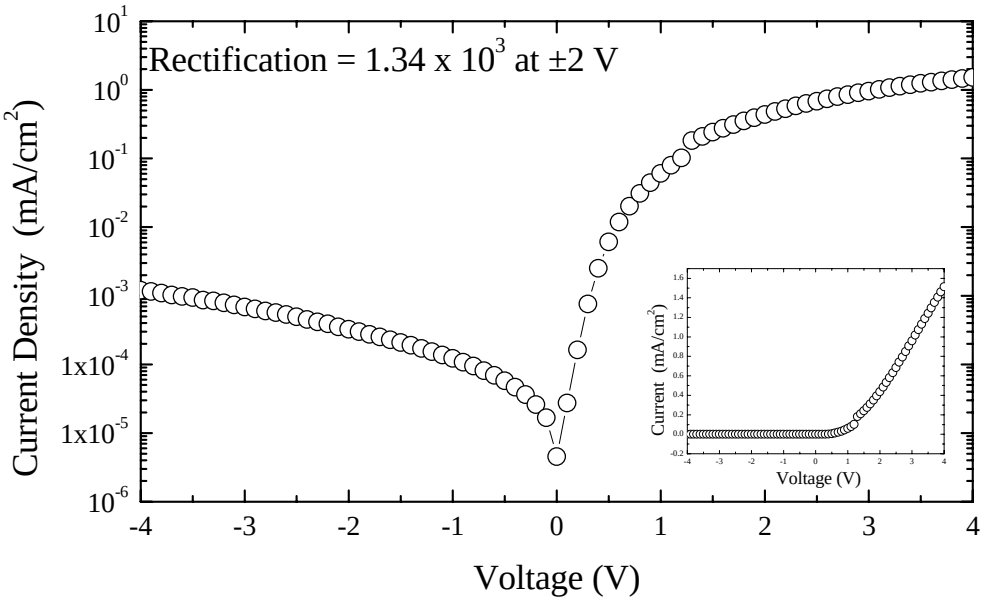

Figure 3.14 *The current-voltage characteristics measured under dark conditions.*

The devices investigated here are based on an ITO/PEDOT-PSS bottom electrode (WF = 5.1 ± 0.1 eV) and a VPP PEDOT top electrode (WF = 4.3 ± 0.1 eV). From electrochemical measurements (see Chapter 2) we have extracted the highest occupied molecular orbital (HOMO) of APFO-3 to be 5.3 ± 0.1 eV and the lowest unoccupied molecular orbital (LUMO) of PCBM to be 3.7 eV ± 0.1 eV. Accordingly, the barrier to hole injection at each electrode amounts to about 0.2 eV and 1.0 eV for ITO/PEDOT-PSS and VPP PEDOT, respectively. Hence, the ITO/PEDOT:PSS electrode definitely serves as an anode. Similarly, the barrier to electron injection at each electrode, namely 1.4 eV at the ITO/PEDOT-PSS and 0.7 eV at the VPP PEDOT interface, leads us to conclude that VPP PEDOT is more suitable for electron injection. Thus, we have concluded that the unmodified VPP PEDOT well serves as a cathode for all the devices investigated here. The same devices were also characterised under white light illumination of intensity 100 mW/cm^2. We extracted short circuit current density (J_{sc}) of 0.074 mA/cm^2, open circuit voltage(V_{oc}) of 320 mV, fill factor of 0.35 and a power conversion efficiency of 0.008%. Both J_{sc} and V_{oc} of the laminated devices are less than that of similar devices with evaporated lithium fluoride (LiF)/aluminium (Al) cathode. The surface roughness of the VPP PEDOT film is non-

negligible. Thus, surface effects in conjunction with various contaminations (processing in open air) can be considered as the main source of device performance degradation.

3.4 Conclusion

The photovoltaic devices with VPP PEDOT and PEDOT-PSS doped with sorbitol anodes showed an order of increase in power conversion efficiency under sunlight illuminations conditions compared to devices with anodes made of PEDOT-PSS. The anodes showed high conductivity and transmission properties, which can be used to replace the indium tin oxide as anodes. The AFM studies showed that the anode surfaces were nanostructured.

We have also demonstrated solar cells that use a highly conducting polymer electrode as a cathode. A soft lamination technique enabled us to construct the solar cells. Further development of the devices using the state of the art printing and lamination techniques may lead to the fabrication of cheap and large area opto-electronic devices.

3.5 References

1. Handbook of Conducting Polymers, 2nd ed. Marcel Dekker, New York, 1998.
2. Handbook of Organic Conductive Molecules, Vols 1-4, Wiley, New York, 1997.
3. L. B. Gorenendaal, F. Jonas, D. Freitag, H. Pielartzik and J. R. Reynolds, *Adv. Mater.*, **12** (2000) 481.
4. S. K. M. Jönsson, J. Birgerson, X. Crispin, G. Greczynski, W. Osikowicz, A.W. Denier van der Gon, W. R. Salaneck and M. Fahlman, *Synth. Met.*, **139** (2003) 1.
5. S. Ghosh and O. Inganäs, *Electrochem. Sol. St. Lett.*, **3** (2000) 213.
6. B.D. Martin, N. Nikolov, S.K. Pollack, A. Saprigin, R. Shashidhar, F. Zhang and P.A. Heiney, *Synth. Met.*, **142** (2004) 187.
7. J. Y. Kim, J. H. Jung, D. E. Lee, and J. Joo, *Synth. Met.*, **126** (2002) 311.
8. S.L. Lai, M. Y. Chan, M. K. Fung, C. S. Lee and S. T. Lee, *Mater. Sci. and Eng. B,* **104** (2003) 26.
9. F. Zhang, M. Johansson, M.R. Andersson, J. C. Hummelen, and O. Inganäs, *Adv. Mater.*, **14** (2002) 662.

10. D.M. de Leeuw, P.A. Kraakman, P.F.G. Bongaerts, C.M.J. Mutsaers and D.M. Klassen, *Synth. Met.*, **66** (1994) 263.
11. L.A.A. Pettersson, F. Carlsson, O. Inganäs and H. Arwin, *Thin Solid Films*, **313-314** (1998) 356.
12. K.E. Aasmundtveit, E.J. Samuelsen, L.A.A. Pettersson, O. Inganäs, T. Johansson and R. Feidenhansl, *Synth. Met.*, **101** (1999) 561.
13. Y.-H. Ha, N. Nikolov, S.K. Pollack J. Mastrangelo, B.D. Martin and R. Shashidhar, *Adv. Func. Mater.*, **14** (2004) 615.
14. A. Mohammadi, I. Lundström, W. R. Salaneck and O. Inganäs, *Chemtronics*, **1** (1986) 171.
15. J. Kim, D. Sohn, Y. Sung, E.R. Kim, *Synth. Met.*, **132** (2003) 309.
16. J. Kim, E. Kim, Y. Won, H. Lee and K. Suh, *Synth. Met.*, **139** (2003) 485.
17. B. W. Jensen and K. West, *Macromolecules*, **37** (2004) 4538.
18. B. W. Jensen, J. Chen, K. West and G. Wallace, *Macromolecules*, **37** (2004) 5930.
19. A. Petr, F. Zhang, H. Peisert, M. Knupfer, and L. Dunsch, *Chem. Phys. Lett.*, **385** (2004) 140.
20. H. Frohne, C. R. McNeill, G.G. Wallace and P. C. Dastoor, *J. Phys. D: Appl. Phys.*, **37** (2004) 165.
21. H. Frohne, S.E. Shaheen, C.J. Brabec, D.C. Müller, N.S. Sariciftci and K. Meerholz, *Chem. Phys. Chem.*, **9** (2002) 795.
22. Y.-L. Loo, R. L. Willett, K. W. Baldwin, and J. A. Rogers, *App. Phys. Lett.*, **81** (2002) 562.
23. J. Zaumseil, T. Someya, Z. Bao, Y.-L. Loo, R. Cirelli, and J. A. Rogers, *App. Phys. Lett.*, **82** (2003) 793.
24. D. A. Bernards, T. Biegala, Z. A. Samuels, J. D. Slinker, and G. G. Malliaras, *App. Phys. Lett.*, **84** (2004) 3675.
25. T.-W. Lee, J. Zaumseil, S. H. Kim, and J. W. P. Hsu, *Adv. Mater*., **16** (2004) 2040.
26. M. Granström, K. Petritsch, A. C. Arias, A. Lux, M. R. Andersson, and R. H. Friend, *Nature*, **395** (1998) 257.
27. S. Admassie and O. Inganas, *J. Electrochem. Soc*., **151** (2004) H153.
28. T. Yohannes, F. Zhang, M. Svensson, J. C. Hummelen, M. R. Andersson and O. Inganäs, *Thin Solid Films*, **449** (2004) 152.

29. V.D. Mihailetchi, J.K.J. van Duren, P.W.M. Blom, J.C. Hummelen, R.A.J. Janssen, J.M. Kroon, M.T. Rispens, W.J.H. Verhees and M.M. Wienk, *Adv. Funct. Mater*., **13** (2003) 43.

4 Chromism in Electronically Conducting Polymers

4.1 Background

Different methods are being used to tailor the electrochromic properties of conducting polymers. New materials may be synthesised to produce the desired colours. Reynolds' group [1-3] synthesized several new conducting poly(3,4-alkylenedioxythiophene) derivatives and alkyl substituted poly(3,4-ethylenedioxythiophenes) as fast electrochromics with high contrast ratios. Co-polymers are also used as chemical method for improving the electrochromic properties of conducting polymers [4]. Blends and bilayer devices are used by other groups as physical methods to combine the electrochromic properties of conducting polymers [5-7].

Creating micro and nanostructured surfaces to control the flow of photons through polymer devices is well demonstrated. Different soft lithographic techniques [8] have been used to imprint structure in polymer films, for instance to improve the efficiencies of photodiodes [9] and in making conducting polymer nanowires and nanodots [10]. It has been shown that the diffracted light in a grating structure is much more affected by changes of both the real and complex components of the refractive index in an active grating, than is the zeroth order beam [11-17]. Optical analyses show that the diffractive efficiency of a modulated grating – a measure of the amount of energy carried in the diffracted beams - is proportional to the sum of the square of the changes of the parameters n and k, where n and k are the real and the imaginary part of the refractive index and where the dielectric function $\varepsilon = (n+ik)^2$**.** Electrochromic gratings show the expected property [11,13]. It is therefore of interest to evaluate the contribution that diffractive gratings may have in forming the active element in displays, such as in electronic paper [17].

In this chapter we present a study of the performance of the electrochromic properties of PEDOT-PSS film patterned with a liquid printing soft lithographic technique and oligoethylene oxide and alkoxy substituted polythiophenes with and without PEDOT-PSS.

On the other hand several groups have investigated the chromic properties of neutral conjugated polymers in order to explain the relationship between optical properties and chemical structure [18-23]. These studies have also opened new possibilities for applications in chemical and biochemical sensors [24-27]. The chromic behaviours of substituted polythiophenes depend on conformational transitions of the polythiophene backbone caused by changes in temperature (thermochromism) or solvent (solvatochromism). The transitions are believed to be between a coplanar (highly conjugated) form and a nonplanar (less conjugated) conformational structure of the backbone [28].

In order to understand the effect of substituents on molecular conformations and subsequently on their physical properties, theoretical calculations have been of great importance. *Ab inito* calculations performed at the HF/3-21G* level on many substituted bithiophenes have provided rotational barriers that have been correlated with the thermochromism and solvatochromism observed in the parent polymers. It was reported that polymers that show chromic behaviours had a flexible backbone with relatively smaller energy barrier against planarity (for example $\leq$ 2.2 – 2.3 kcal/mol per repeat unit for conjugated oligothiophenes). On the other hand, nonchromic polymers have a large energy barrier between the planar and twisted conformations. To get such barrier to rotation using *ab inito* method, the 3-21G* basis set was shown to be the minimum level of calculation that gives results in close agreement with those obtained from more elaborate basis sets [29-33].

The electrochemical activity, photovoltaic and optical properties of different kinds of 3-phenyl-substituted polythiophenes have been reported [34-35]. However, to the best of our knowledge *ab initio* calculations on phenyl-substituted polythiophenes and their correlation with the experimentally observed thermochromic and solvatochromic properties have not been reported in the literature. Therefore, this chapter also deals with the study of the thermochromic and solvatochromic properties of different kinds of phenyl-substituted polythiophenes and correlates the results with the values of the barrier to rotation against planarity obtained using *ab initio* calculations.

4.2 Experimental

Cleaning ITO: The ITO coated glass was cleaned with distilled water and acetone and further treated in a 5:1:1 mixture of deionized H_2O, 25% NH_3 and 28% H_2O_2 at 85^oC for 5 minutes. It was washed with distilled water several times and dried.

Making the Rubber Stamps: To make the rubber stamps, ten parts of polysiloxane pre polymer (Sylgard 184) and one part of a curing agent were mixed. After the mixture was degassed to avoid bubbles in the stamp, it was poured on to commercial gratings and heated in oven for 40 minutes at 140^oC. After allowing it to cool to room temperature the stamp was peeled off from the gratings and cut into pieces of about 1.0 cm by 2.5 cm area to completely cover the surface of the polymer coated on the ITO.

Patterning of PEDOT-PSS by soft lithographic technique: The conducting polymer, PEDOT-PSS, obtained in the form of an aqueous dispersion (1.2% by weight), under the trade name Baytron-P from Bayer AG, Germany was filtered and spin-coated on a pre-cleaned ITO at 1000 rpm. The rubber stamp was then put on top of the PEDOT-PSS film immediately while there is still some liquid on the surface of the film. A small pressure was applied on top of the stamp to force it to make good contact with the film. After letting the film to dry the stamp was carefully removed from the film.

For samples made from gratings of 300 and 600 lines/mm the images of both the stamp replicated from the commercial gratings and the patterned PEDOT-PSS were taken using Axiovert 200M inverted microscope equipped with an Axio Cam HRC CCD camera. Before running each spectroelectrochemical experiments, the transfer of the gratings to the PEDOT-PSS was checked by shining a HeNe laser light, while the patterned film was in the dry state as well as after dipping it in the supporting electrolyte/solvent system. Several diffraction maxima were observed in both cases showing the transfer of the gratings to the polymer.

Preparation of the bilayer films: PEDOT-PSS was spin-coated on a pre-cleaned ITO at 1500 rpm and annealed for 2 min at 80^oC. After cooling the film, the polymers used to form the bilayer were spin coated from a 5 mg/ml solution of chloroform at 1500 rpm.

Spectroelectrochemical measurements: 0.1 M tetraethylammoniumtetrafluoroborate (TEATFB) in acetonitrile was used as a supporting electrolyte. Ex-situ spectroelectrochemical experiments were carried out by taking the polymer film out of the electrochemical cell and placing it into the spectrophotometer sample holder using Autolab PGStat 10 (EchoChemie, the Netherlands) and Lambda 9 Spectrophotometer (Perkin-Elmer). A conventional three-electrode system consisting of the PEDOT-PSS coated ITO/glass or glass/ITO/PEDOT-PSS/Polymer as a working electrode, a Ag/Ag+ quasi reference electrode and a platinum foil as counter electrode were used. A waiting time of 2 minutes were used at each potential. In-situ spectroelectrochemical experiments were carried out by measuring the optical absorption while the polymer film is inside the electrochemical cell using Autolab PGStat 10 (EchoChemie, the Netherlands) and Lambda Polynom UV-1601 PC Spectrophotometer (Shimadzu) inside a hood-system. A three-electrode system consisting of the PEDOT-PSS coated ITO/glass or glass/ITO/PEDOT-PSS/Polymer as a working electrode, a Ag/Ag^{+} quasi reference electrode and a platinum wire counter electrode fitted to a quartz cuvette were used for simultaneous chronoampereometric and absorbance-time measurements. A general schematic diagram for the spectroelectrochemical measurement is shown in Figure 4.1.

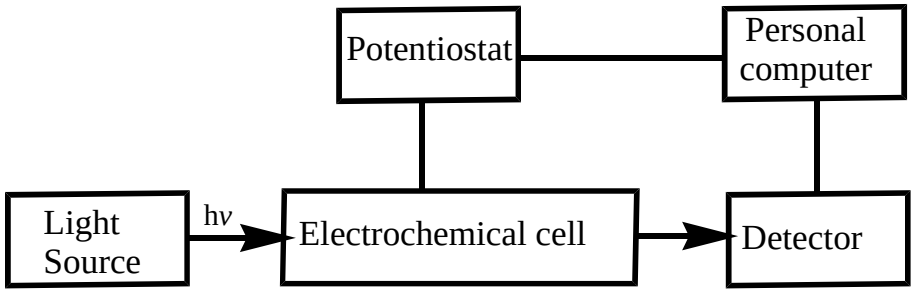

Figure 4.1 *Schematic diagram of apparatus used for spectroelectorchemical switching measurements.*

Ultraviolet-visible absorption spectroscopy measurements: UV-Vis spectra were recorded from dilute solutions or films of the polymers cast on a glass substrate. The spectra were obtained with Spectronic Genesys 2PC Spectrophotometer fitted with a temperature regulating system.

Theoretical calculations: Ab initio calculations were performed on a personal computer using Gaussian 98W program [36]. The dimeric structures of the monomers used to

synthesize the polymers were drawn using Chem Draw Ultra 7.0 of the Chem Office 2001 package. The structures were then imported to Chem3D. Gaussian 98 was used from the Chem3D interface to optimize the structures, vary the dihedral angles and calculate the energies at each dihedral angle. The conformational analyses of all the dimeric compounds were done by changing the torsional angle θ by 15^{o} steps. The geometries were then optimised at the HF level with the 3-21G* basis set.

4.3 Results and Discussions

4.3.1 Electrochromism in diffractive polymer gratings

For samples made from gratings of 300 and 600 lines/mm the images of the patterned PEDOT-PSS are shown in Figure 4.2. The transfer of the gratings to the PEDOT-PSS can be clearly seen from these images, as well as some defects in the pattern. The heights of the ridges were found to be about 410 nm for 300 lines/mm and about 140 nm for 600 lines/mm from AFM measurements (Figure 4.3).

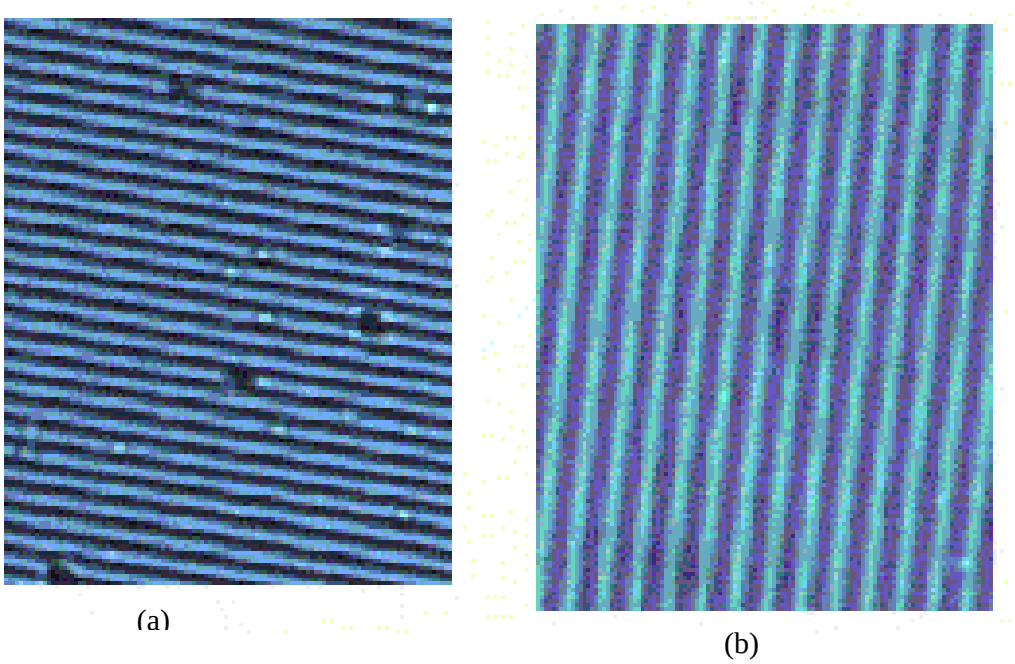

Figure 4.2 *Inverted microscopic images of (a) patterned PEDOT-PSS film formed with the 300 lines/mm gratings with 4.3 μm gap width, (b) patterned PEDOT-PSS film formed with the 600 lines/mm gratings with 1.6 μm gap width.*

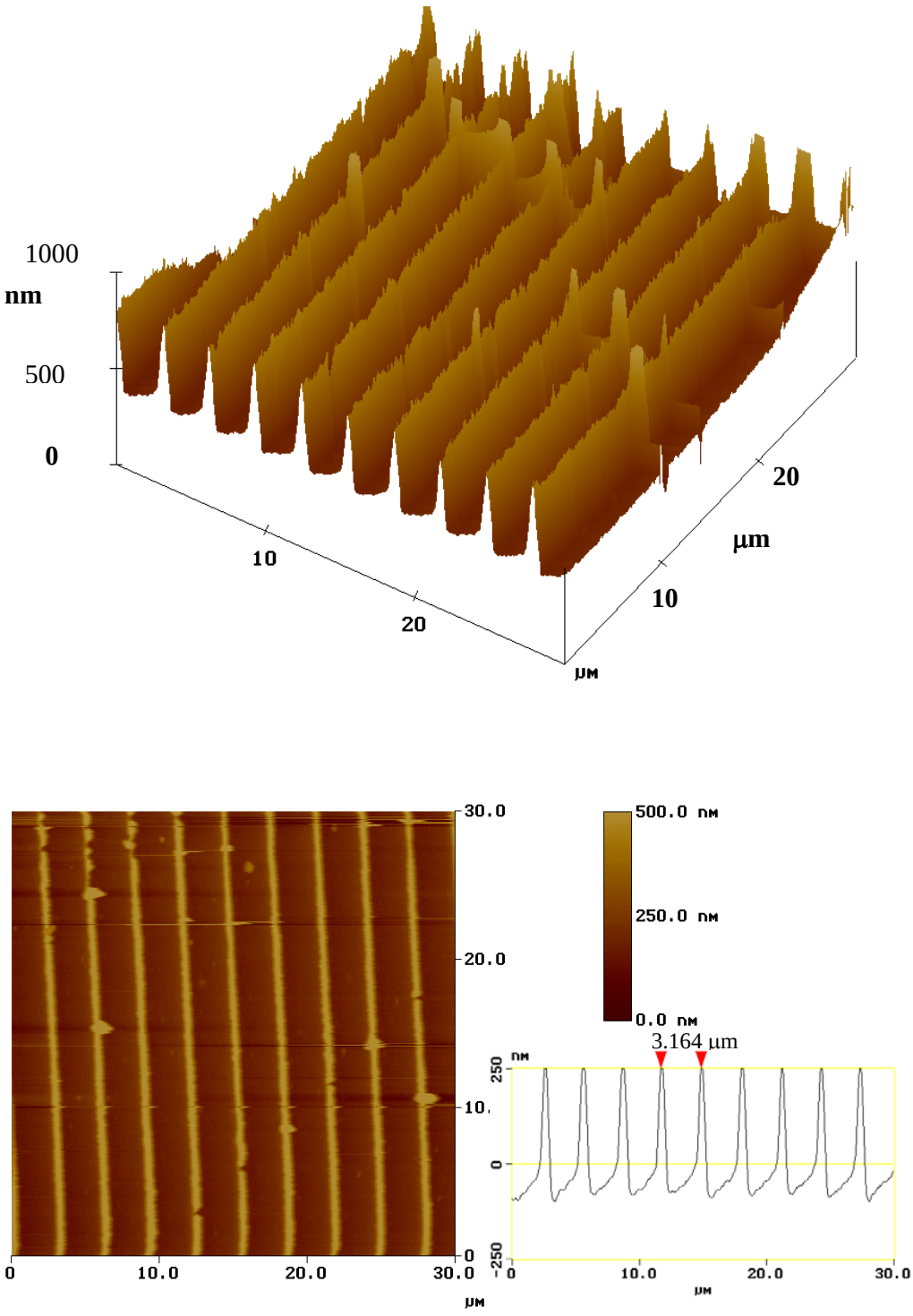
1000
nm
500
0
10
20
µm
10
20
µm
30.0
20.0
10.
0
0
10.0
20.0
30.0
µm
500.0 nm
250.0 nm
0.0 nm
3.164 µm
nm
250
0
-250
0
10.0
20.0
30.0
µm

(a)

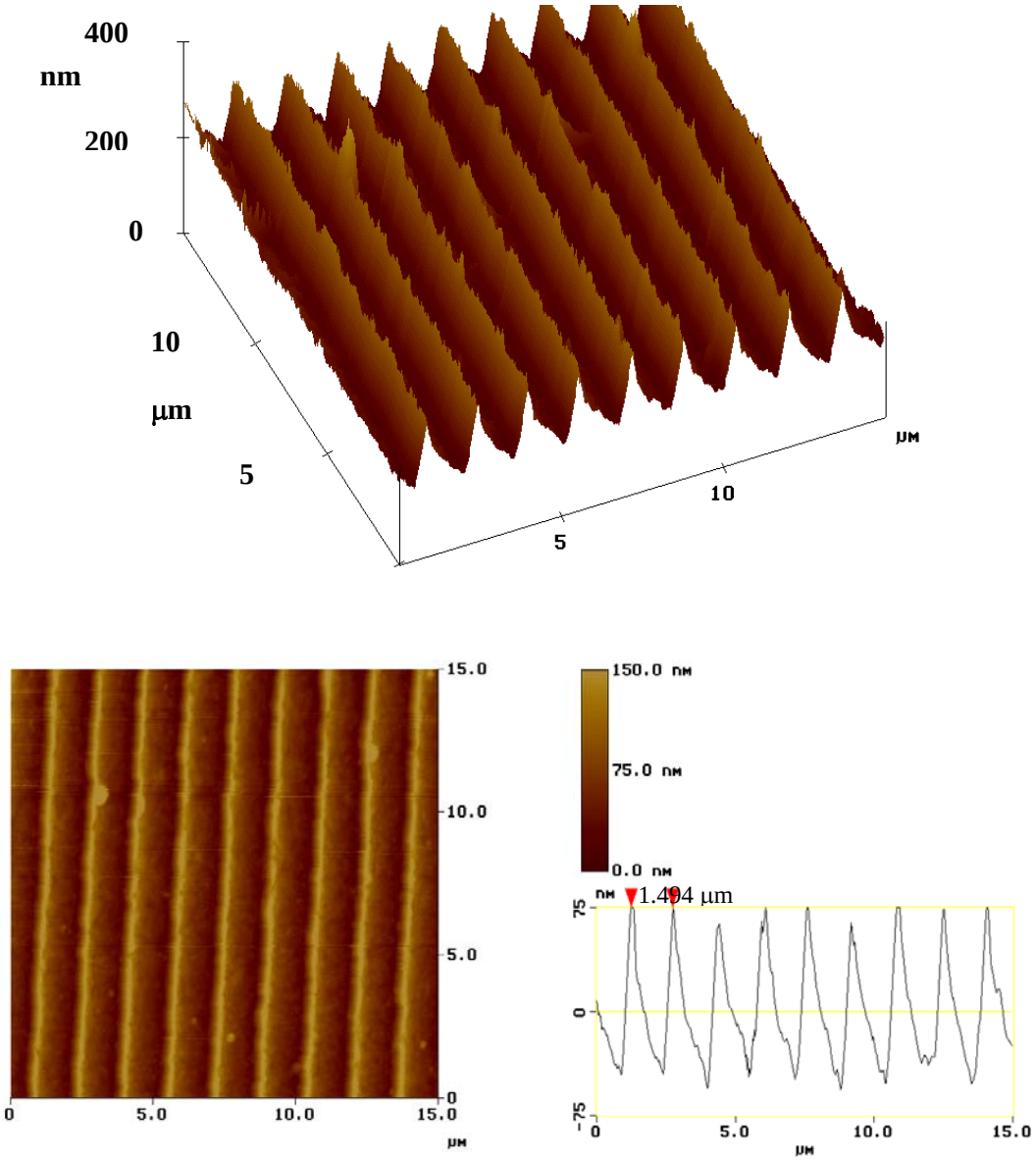

(b)

Figure 4.3 *AFM images of patterned PEDOT-PSS film formed with the (a) 300 lines/mm: height of the ridges about 410 nm and the period is about 3.164 µm, (b) 600 lines/mm: height of the ridges about 140 nm and the period is about 1.494 µm.*

The static spectroelectrochemistry of the PEDOT-PSS film on ITO glass electrode at different potentials in 0.1 M TEATFB without pattern and with pattern are shown in Figure 4.4 and 4.5, respectively.

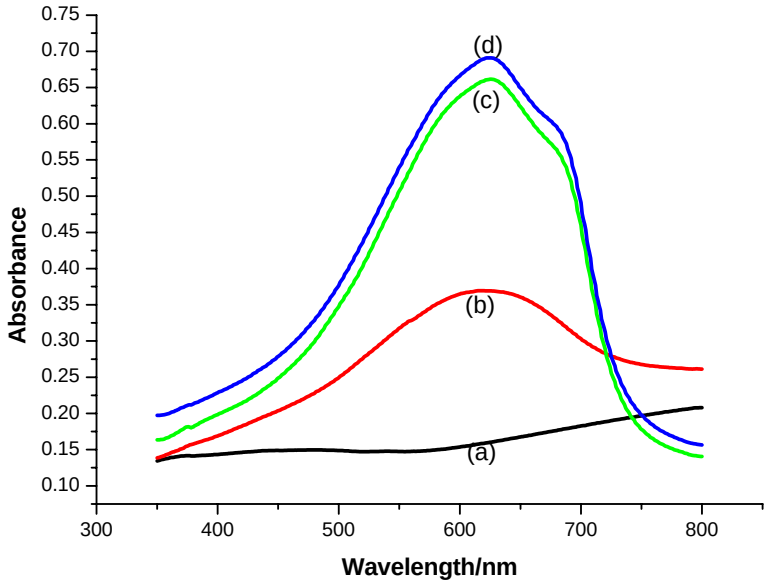

Figure 4.4 *Ex-situ static spectroelectrochemistry of unpatterned PEDOT-PSS film on ITO/glass electrode in 0.1 M TEATFB in acetonitrile at (a) +0.2, (b) –0.2, (c) –0.6 and (d) –1.2 V.*

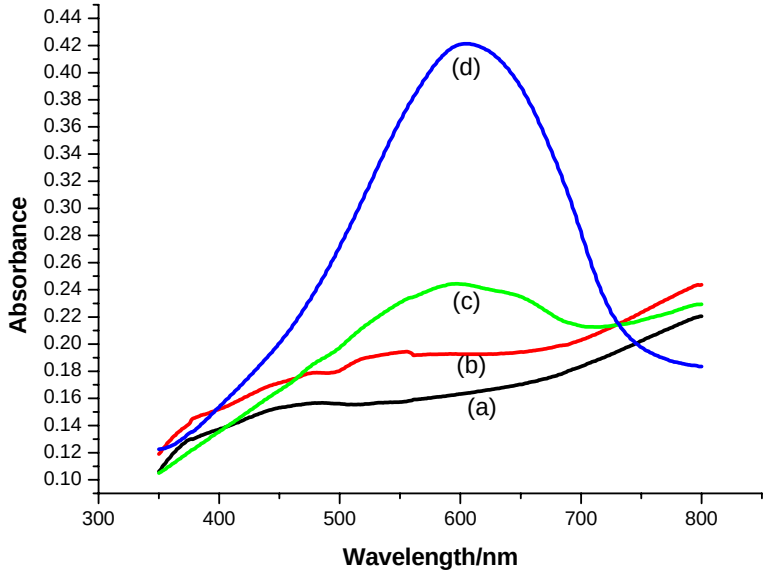

Figure 4.5 *Ex-situ static spectroelectrochemistry of patterned PEDOT-PSS film on ITO/glass electrode in 0.1 M TEATFB in acetonitrile at (a) +0.2, (b) –0.2, (c) –0.6 and (d –1.2 V.*

As the applied potential is increased from +0.2 V to -1.2 V vs the Ag/Ag^+ quasi reference electrode, the color of the film is changed from transparent blue to deep blue color, as indicated by the increased broad peak at a maximum wavelength of around 610 nm for both the unpatterned and patterned films. A significant increase in the absorption peak for the patterned films was observed, which is even more pronounced at less negative potentials. Several experiments done using different patterned gratings showed a similar enhancement of the absorption peak. Figure 4.6 shows the comparison of the absorption peak for the unpatterned and patterned films at +0.2 and –0.6 V.

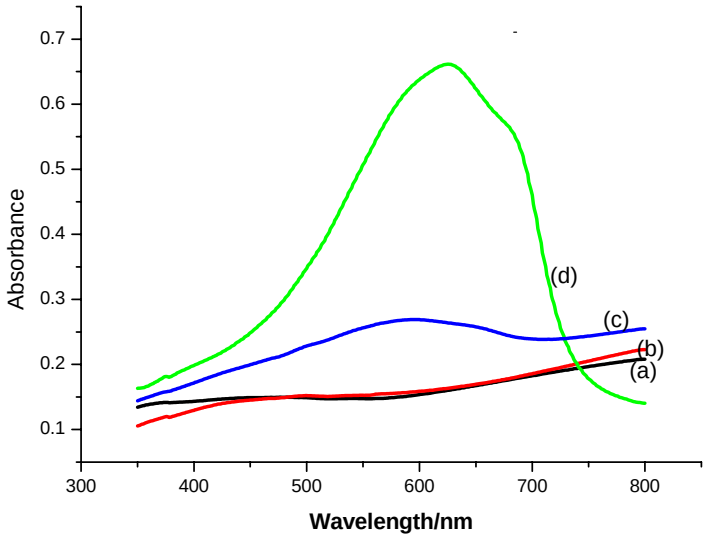

Figure 4.6 *Comparison of the ex-situ static spectroelectrochemistry of unpatterned and patterned PEDOT-PSS film on ITO/glass in 0.1 M TEATFB in acetonitrile: (a) patterned film at +0.2 V, (b) unpatterned film at +0.2 V, (c) unpatterned film at –0.6 V and (d) patterned film at –0.6 V.*

Figure 4.7 shows the comparison of the in-situ static spectroelectrochemical measurement for the unpatterned and patterned films. These results indicate that the gratings formed as a result of the patterning of the PEDOT-PSS film can be used to influence the light absorption, as measured for normal transmission. Part of the impinging light is diffracted by the grating, and therefore is not accounted for in the transmission spectra. The enhanced absorption is due to this contribution. The wavelength dependence of transmission spectra are complex, and it must be emphasized that only transmitted light on the zeroth order diffraction peak is recorded. As the wavelength of light is varied, we see a dramatic

difference between patterned and unpatterned films, in particular in the near infrared range of the spectrum (see Fig 4.7, d,e).

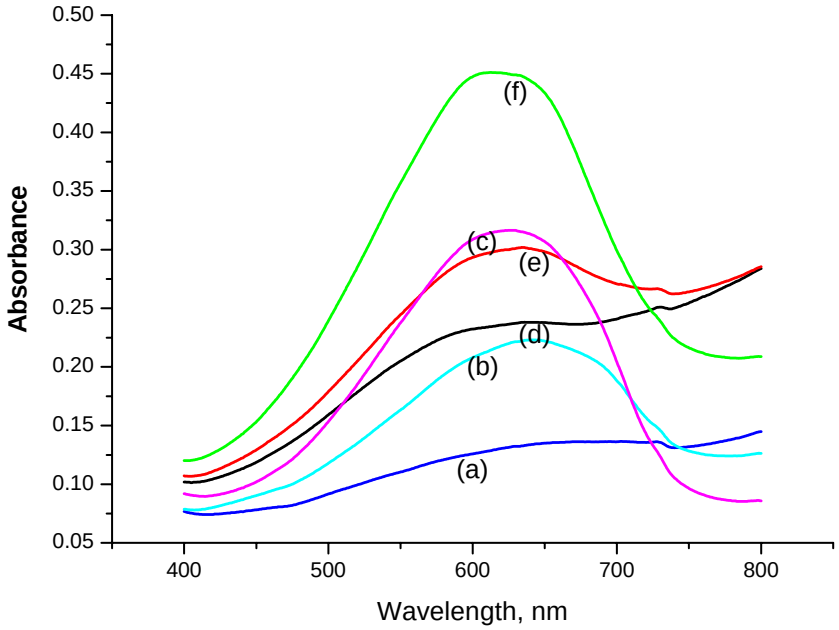

Figure 4.7 *Comparison of the in-situ static spectroelectrochemistry of PEDOT-PSS film on ITO/glass electrode in 0.1 M TEATFB in acetonitrile (i) unpatterned at (a) +0.2 V, (b) –0.2 V, (c) –0.6 V and (ii) patterned at (d) +0.2 V, (e) –0.2 V, (f) –0.6 V.*

The results observed in the static spectroelectrochemistry data of increased absorption peaks by patterning the PEDOT-PSS film, could improve the coloration efficiency of electrochromic devices. Dynamic spectroelectrochemical experiments were carried out, to further investigate this observation in detail. Simultaneous absorption or % transmittance *vs* time and chronoamperometery techniques were used for unpatterned and patterned PEDOT-PSS films. A square wave potential with different switching potentials were used for the dynamic spectroelectrochemical measurement. The % transmittance *vs* time plots for unpatterned and patterned PEDOT-PSS film are compared in Figure 4.8.

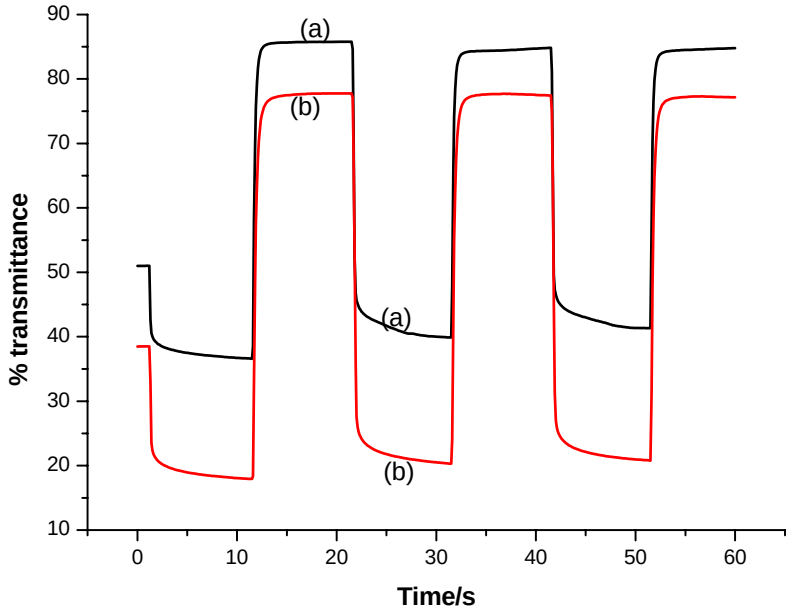

Figure 4.8 *Comparison of the change in % transmittance vs time of (a) unpatterned and (b) patterned PEDOT-PSS film on ITO/glass in TEATFB in acetonitrile when the potential is stepped between –0.6 and +0.6 V. at 610 nm.*

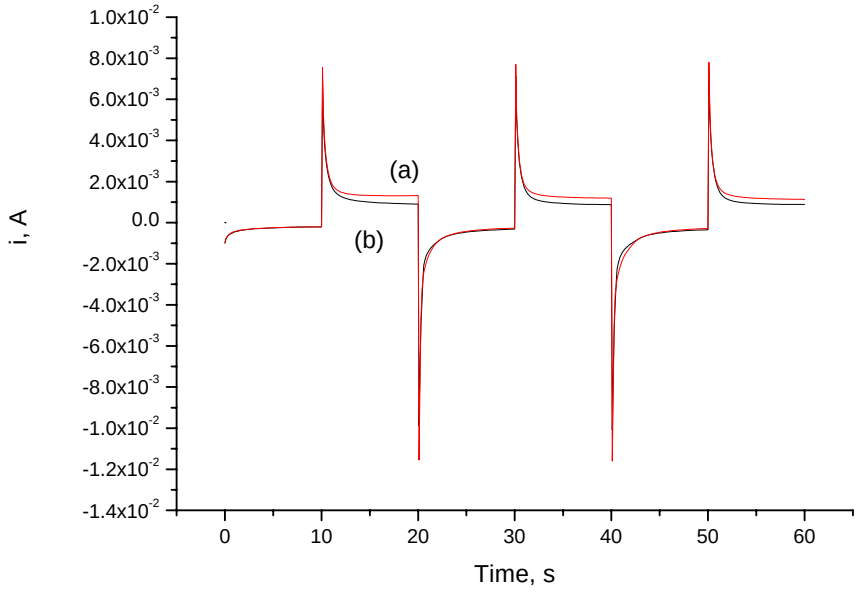

Figure 4.9 *The change in current vs time of (a) unpatterned and (b) patterned PEDOT-PSS film on ITO/glass in TEATFB in acetonitrile when the potential is stepped between –0.6 and +0.6 V, simultaneously measured with the optical measurement shown in Figure 4.8.*

Several experiments were performed to compare the coloration efficiencies of unpatterned and patterned films. To find the best potential window both chronoamperometric and absorption *vs* time studies were performed at different potential limits for the patterned PEDOT-PSS film. The results are shown in Table 4.1. The results show that the coulombic efficiency significantly increased from 56% to 96.7% when the potential window is changed from –0.6 - +0.6 to –1.0 - +0.6 V.

Table 4.1 *Effect of Potential Limits on the Electrochromic Properties for Patterned PEDOT-PSS Film.*

Potential Limit/in V.	Q_{ox} (mC/cm^2)	Q_{red} (mC/cm^2)	η' (%)	T_{ox}	T_{red}	ΔOD	η (cm^2/C)
-0.6 - + 0.6	2.5	-1.4	56	61.98	18.65	0.52	371
-1.0 - + 0.6	2.17	-2.1	96.7	61.67	12.99	0.68	324
-1.0 - + 0.8	3.84	-2.78	70.31	64.25	11.17	0.76	273
-1.0 - + 1.0	6.15	-3.3	53.65	65.1	12.47	0.72	218

However, there is a decrease in the coloration efficiency from 371 to 324 cm^2/C as a result of the increase in the amount of charge injected/ejected when going to the more negative potential. The potential range that gives a reasonable contrast with small amount of charge injected/ejected seems to be between –0.6 to +0.6 V. Using this potential range the electrochromic properties between unpatterned and patterned PEDOT-PSS films are compared in Table 4.2.

The change in optical densities, ΔOD, for three unpatterned films varies between 0.32 and 0.33, whereas for the three patterned films higher values ranging from 0.36 to 0.59 were obtained. The large gap in the change in optical densities in the patterned films may be due to incomplete or unequal transfer of the gratings from the stamps on to the PEDOT-PSS films. Values of coloration efficiency varying from 107 to 174 cm^2/C were obtained for three different unpatterned PEDOT-PSS films. These values are the best values we have obtained after several experiments in order to make a realistic comparison with the patterned films. The values we found are also in agreement with a value of 183 cm^2/C reported by Reynolds and co-workers [38] for the electrochemically polymerized PEDOT. For three different patterned PEDOT-PSS films higher electrochromic efficiency values ranging from 211 to 371 cm^2/C were found.

Table 4.2 *The electrochromic properties of spin-coated PEDOT-PSS on ITO glass without patterning and patterned PEDOT-PSS film when the potential is scanned between –0.6 to + 0.6 V.*

Film No.	Q_{ox} (mC/cm^2)	Q_{red} (mC/cm^2)	T_{ox}	T_{red}	η' (%)	ΔOD	η (cm^2/C)
Unpatterned Film 1	7.83	-2.99	81.68	38.67	38.18	0.32	107
Unpatterned Film 2	5.39	-2.81	85.77	40.01	52	0.33	117
Unpatterned Film 3	5.05	-1.89	77.69	36.66	37.42	0.33	174
Patterned Film 1	2.5	-1.4	61.98	18.65	56.00	0.52	371
Patterned Film 2	4.30	-2.79	77.75	20.05	65	0.59	211
Patterned Film 3	2.71	-1.43	71.08	31.12	68.10	0.36	252

For the three-unpatterned PEDOT-PSS films where the electrochromic efficiencies were calculated, the columbic efficiencies vary between 37 and 52, while both the three patterned PEDOT-PSS films show higher coulombic efficiencies varying between 56 to 68 as shown in Table 4.2.

4.3.2 Electrochromism in conducting polymer bilayer system

The electroactivity of different polythiophenes including polymer I and II (Figure 4.10) have been reported recently by Inganäs, *et al.* [14] where the onset potential for the oxidation of polymer II was –0.13 V much lower than that of polymer I which was about 0.39 V *vs* Ag/AgCl. In this section, we present the electrochromic properties of PEDOT-PSS film by forming a bilayer device with polymers. Polymer I was found to be solvatochromic, where the wavelength corresponding to the maximum absorption is blue shifted by about 20 nm upon dipping the film into $LiClO_4$/MeOH supporting electrolyte/solvent system.

The blue shift is more pronounced in TEAP/AcN system, where a shift of about 40 nm and a splitting of the peak were observed as shown in Figure 4.11. Similar behavior was not observed for polymer II, where the purple color still persists when dipped in to the same supporting electrolyte-solvent system (see Figure 4.12).

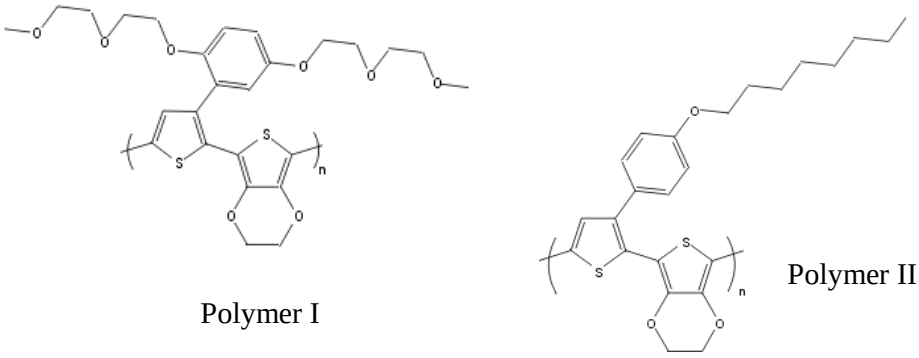

Figure 4.10 *Chemical structures of the polymers used to make bilayer*.

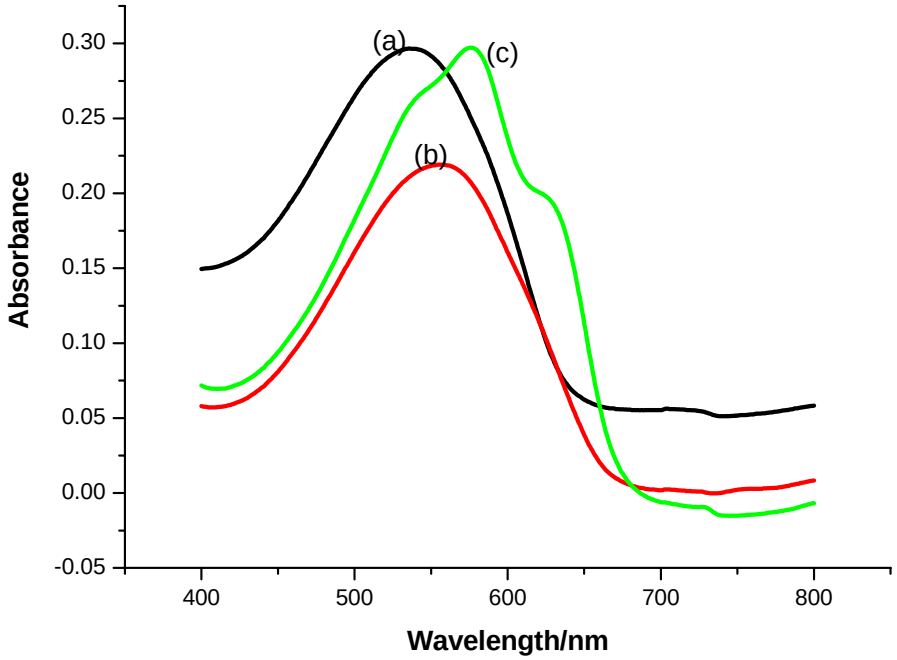

Figure 4.11 *Effect of supporting electrolyte/solvent system on the absorption behavior of polymer I coated on ITO: (a) in the dry state, (b) dipped into $LiCLO_4$/MeOH, (c) TEAP/AcN supporting electrolyte/solvent system.*

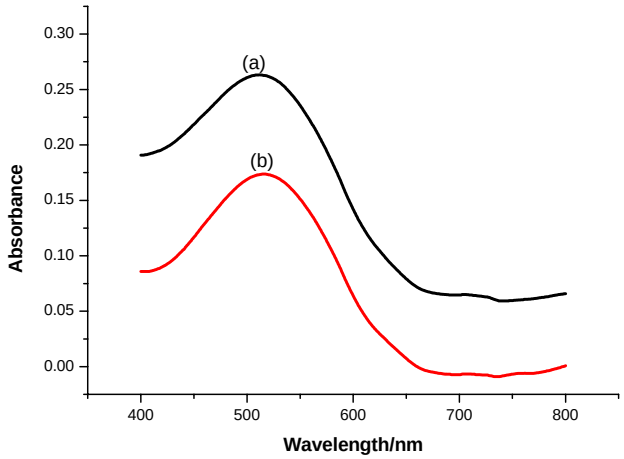

Figure 4.12 *Effect of supporting electrolyte/solvent system on the absorption behavior of polymer II coated on ITO: (a) in the dry state, (b) dipped into $LiClO_4$/MeOH supporting electrolyte/solvent system.*

The static *ex-situ* spectroelectrochemistry of the glass/ITO/PEDOT-PSS/polymer (I and II) films at different potentials in 0.1 M TEATFB are shown in Figure 4.13 and 4.14.

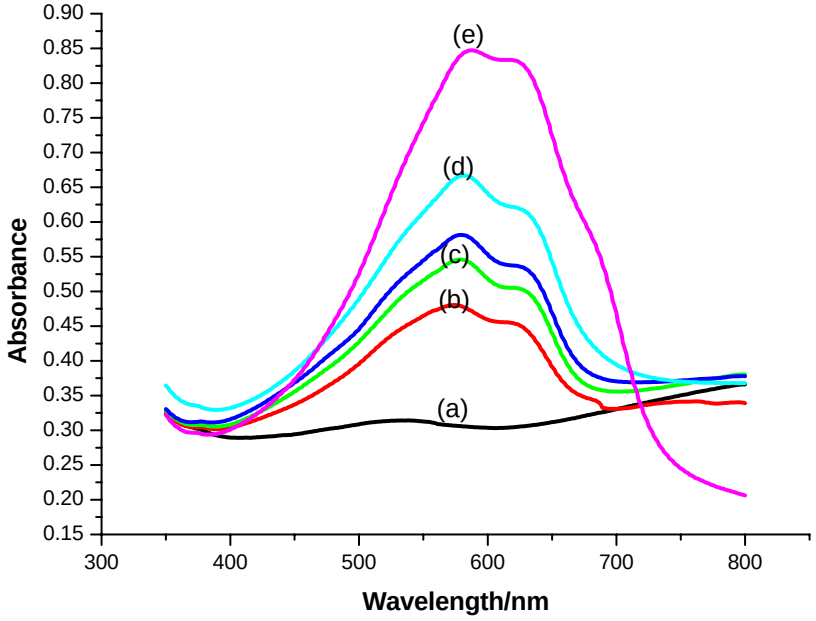

Figure 4.13 *Static ex-situ spectroelectrochemistry of polymer I spin-coated on PEDOT-PSS/ITO/glass electrode in 0.1 M TEATFB in acetonitrile at (a) +0.8 V (b) +0.4 V, (c) 0.0 V, (d) –0.4 V (e) –1.2 v and (f) –1.8 V.*

For polymer I, as the applied potential is increased anodically from +0.8 V to –1.8 V *vs* the Ag/Ag^+ quasi reference electrode, the color of the film is changed from violet to deep blue color, as indicated by the increased broad peak at a maximum wavelength of around 620 nm. For polymer II, as the applied potential is increased anodically from +0.4 V to –1.8 V *vs* the Ag/Ag^+ quasi reference electrode, the color of the film is changed from purple to deep blue. Corresponding to the increased absorption peak upon doping, a shift in the maximum absorption wavelength from about 520 nm to 570 nm was also observed for polymer II. The peak seen at about 620 nm in polymer I was not observed for polymer II.

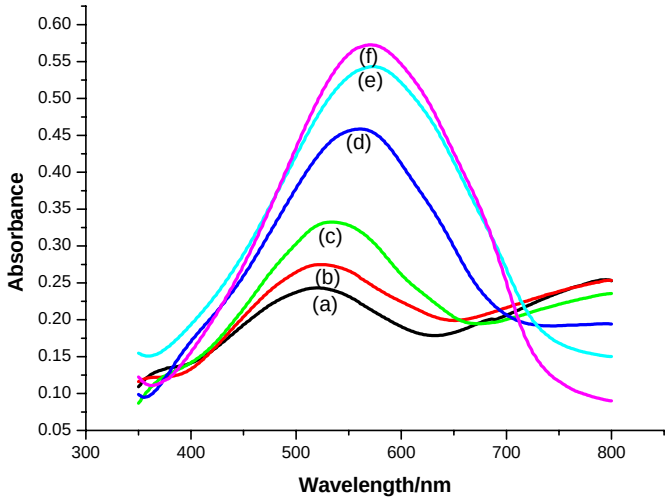

Figure 4.14 *Static ex-situ spectroelectrochemistry of polymer II spin-coated on PEDOT-PSS/ITO/glass electrode in 0.1 M TEATFB in acetonitrile at (a) +0.4 V (b) +0.0 V, (c) –0.4 V, (d) –1.0 V (e) –1.4 V and (f) –1.8 V.*

The reversibility of the electrochromic behavior of the bilayer device was also studied by changing the applied potential from +0.8 to –1.8 V and back again to +0.8 V. The results for polymers I and II are shown in Figures 4.15 and 4.16, respectively.

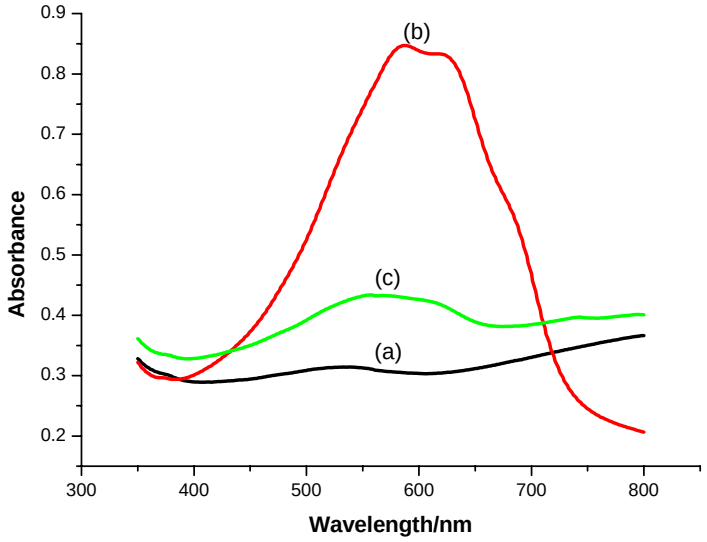

Figure 4.15 *Static ex-situ spectroelectrochemistry of polymer I coated on PEDOT-PSS/ITO/glass at (a) +0.8 V; (b) –1.8 V and (c) +0.8 V after going to –1.8 V showing the reversibility in the color of the polymer.*

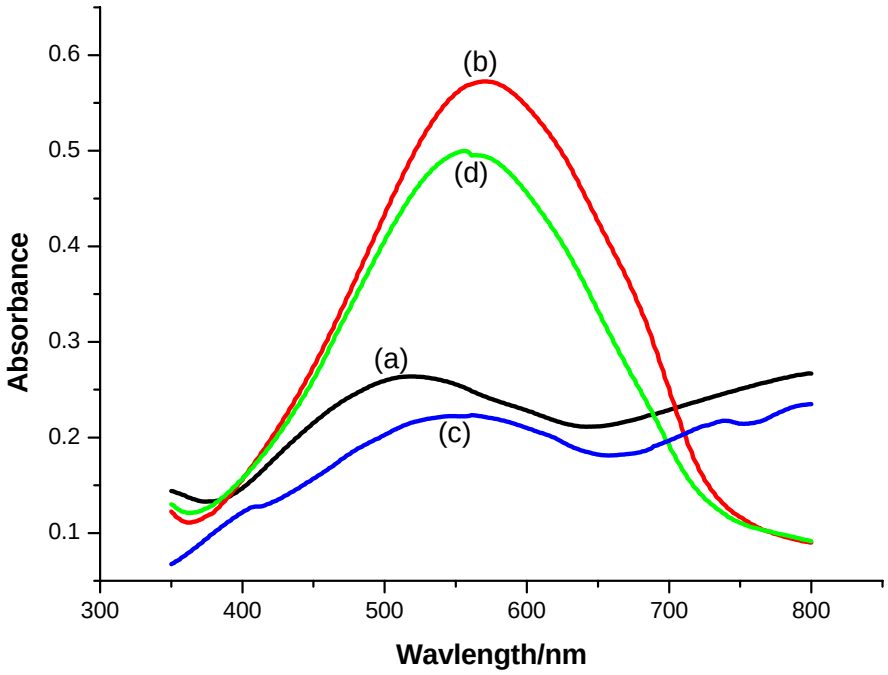

Figure 4.16 *Static ex-situ spectroelectrochemistry of polymer II coated on PEDOT-PSS/ITO/glass at (a) +0.8 V; (b) –1.8 V, (c) +0.8 V after going to –1.8 V and (d) –1.8 V after going to +0.8 V, showing the reversibility.*

Polymer I show reversibility in the color with light bluish color persisting after going to more negative potentials. The peak that is observed at about 520 nm at +0.8 V in polymer II was not observed in polymer I. *In-situ* absorption spectra of single layers of PEDOT-PSS, Polymer I and the bilayer film of glass/ITO/PEDOT-PSS/Polymer I at different potentials were measured and compared in Figure 4.17. The color of the neutral state of Polymer I and the doped state of PEDOT-PSS gives a higher absorption at the negative potential with a deep blue color for the bilayer film, while at positive potentials; the color of the film is that of the neutral Polymer I (violet) since PEDOT-PSS becomes transparent blue. For the single layer of polymer II, at positive potentials the peak at about 515 nm disappeared giving rise to a broad peak above 650 nm, where the film changes its color from red to blue as shown in Figure 4.18.

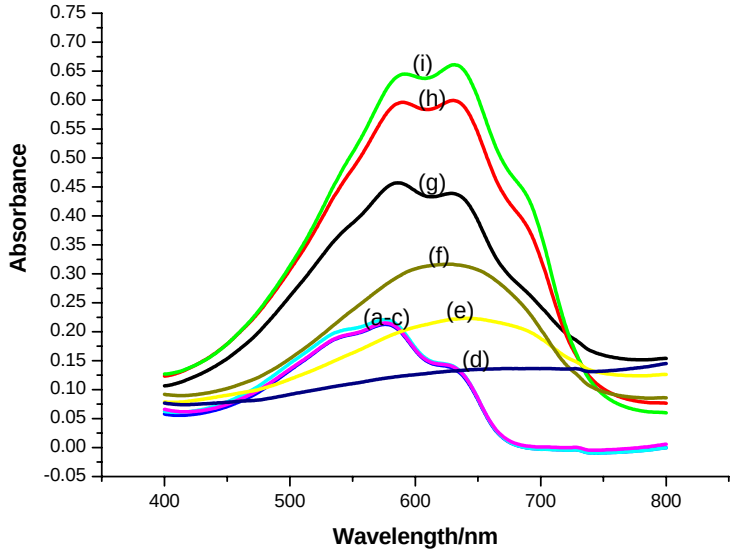

Figure 4.17 *Comparision of the Absorbance vs wavelength for (i) single layer of polymer I at (a) +0.2 V, (b) –0.2 V, (c) –0.6 V; (ii) single layer of PEDOT-PSS at (d) +0.2 V, (e) –0.2 V, (f) –0.6 V; (iii) bilayer of PEDOT-PSS with Polymer I at (g) +0.2 V, (h) –0.2 V, (i) –0.6 V.*

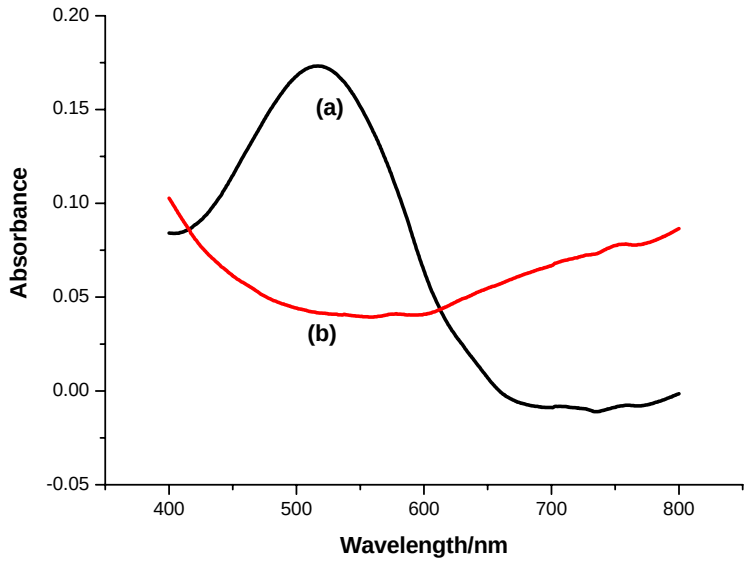

Figure 4.18 *Absorbance vs wavelength plot for glass/ITO/polymer II in $LiClO_4$/MeOH at two different potentials showing (a) the neutral and (b) doped state.*

The switching properties of the bilayer film of polymer I and II with PEDOT-PSS and the single layer of polymer II were investigated by simultaneous % transmittance *vs* time and chronoamperometery techniques. A square wave potential with different switiching potentials were used for the dynamic spectroelectrochemical measurement. Figure 4.19 compares the switching property of polymer I and II in the bilayer structure.

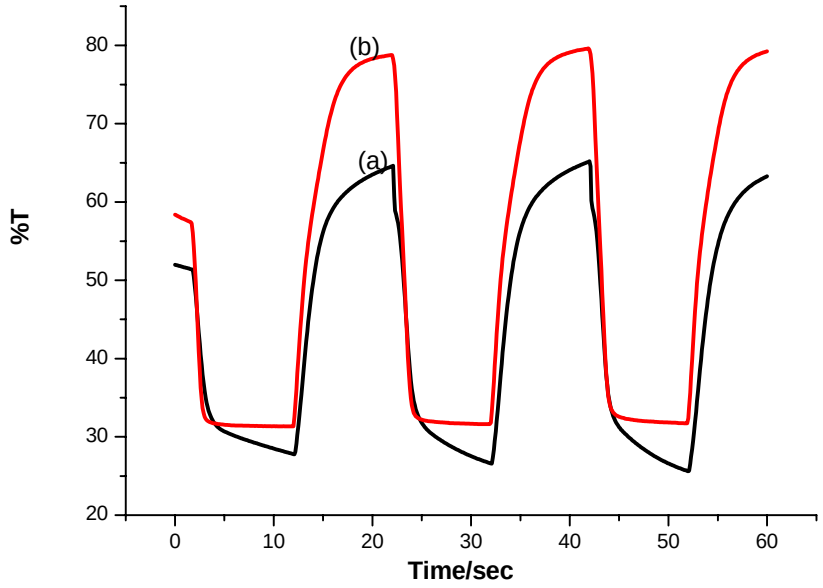

Figure 4.19 *Comparison of the % transmittance vs time plots for (a) glass/ITO/PEDOT-PSS/ Polymer II, (b) glass/ITO/PEDOT-PSS/Polymer I bilayer in TEATFB/acetonitrile.*

It was found that polymer I show better contrast and switching characteristics than polymer II. However, polymer II, which has lower oxidation potential, switches from red to blue in the single layer structure as shown in Figure 4.20. For two different films, when the potential is cycled between +0.6 and –0.6 V at 630 nm, the change in optical density, ΔOD, was found to vary between 0.49 – 0.53. The Δ%T was also found to vary between 51 – 55%. The coulombic efficiency was about 95% and the electrochromic efficiency varies between 90 – 106 C/cm^2. The % transmittance *vs* time plot for the film that shows larger contrast is shown in Figure 4.21.

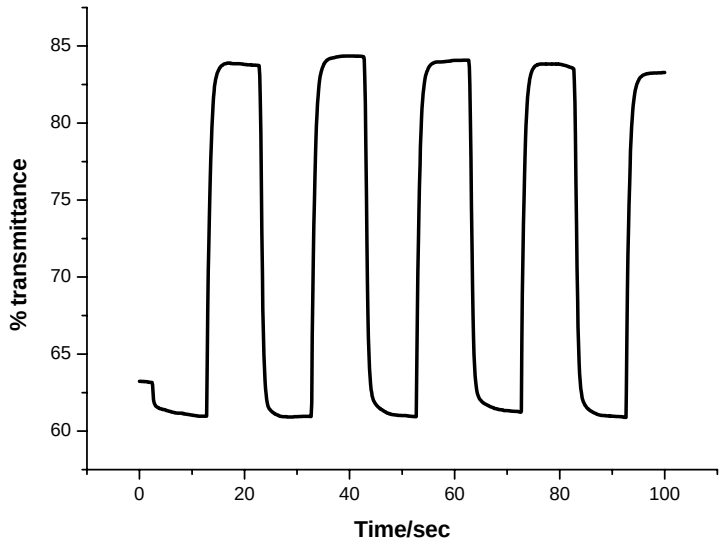

Figure 4.20 *% transmittance vs time plots for glass/ITO/polymer II, in $LiClO_4$/MeOH supporting electrolyte/solvent system when the potential is switched between –0.2 and +0.8 V vs Ag/Ag^+ at 515 nm.*

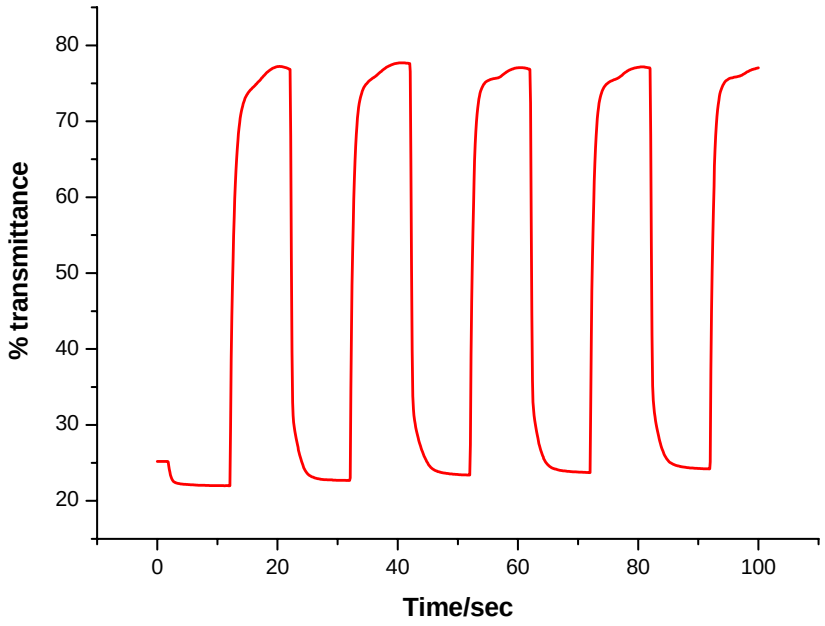

Figure 4.21 *% transmittance vs time plots for glass/ITO/PEDOT-PSS/polymer I, in TEAFB/AcN supporting electrolyte/solvent system when the potential is switched between –0.6 and +0.6 V vs Ag/Ag^+ at 630 nm.*

Polymer II, which switches from red to blue in the single layer structure when the potential is cycled between between –0.2 and +0.8 V vs Ag/Ag^+ at 515 nm, the change in optical density, ΔOD, was 0.14 and the Δ%T was 23%. The coulombic efficiency was about 42% and the electrochromic efficiency was about 55 C/cm^2.

4.3.3 Chromic transitions in phenyl-substituted polythiophenes

The polymers investigated in the course of this study were phenyl-substituted polythiophenes with different side chains whose chemical structures are shown in Figure 4.22. The UV-Vis spectra of polymer **1** in chloroform solution (Table 4.3) at room temperature shows absorption maximum (λ_{max}) around 347 nm. When a solution of this polymer is cast on a glass substrate there is no shift in the maximum absorption wavelength indicating that there is no aggregation of the polymer film in the condensed phase. On the other hand, the other polymers studied showed red shifts by upto 37 nm (Table 4.3).

Table 4.3 *Comparison of the absorption maxima in the solution and condensed phase for the polymers investigated.*

Polymer	λ_{max}(nm) in solution	λ_{max}(nm) in film	$\Delta\lambda_{max}$(nm)
1	347	347	0
2	498	513	15
3	468	496	28
6	487	518	31
7	483	520	37
8	446	463	17
9	497	508	11

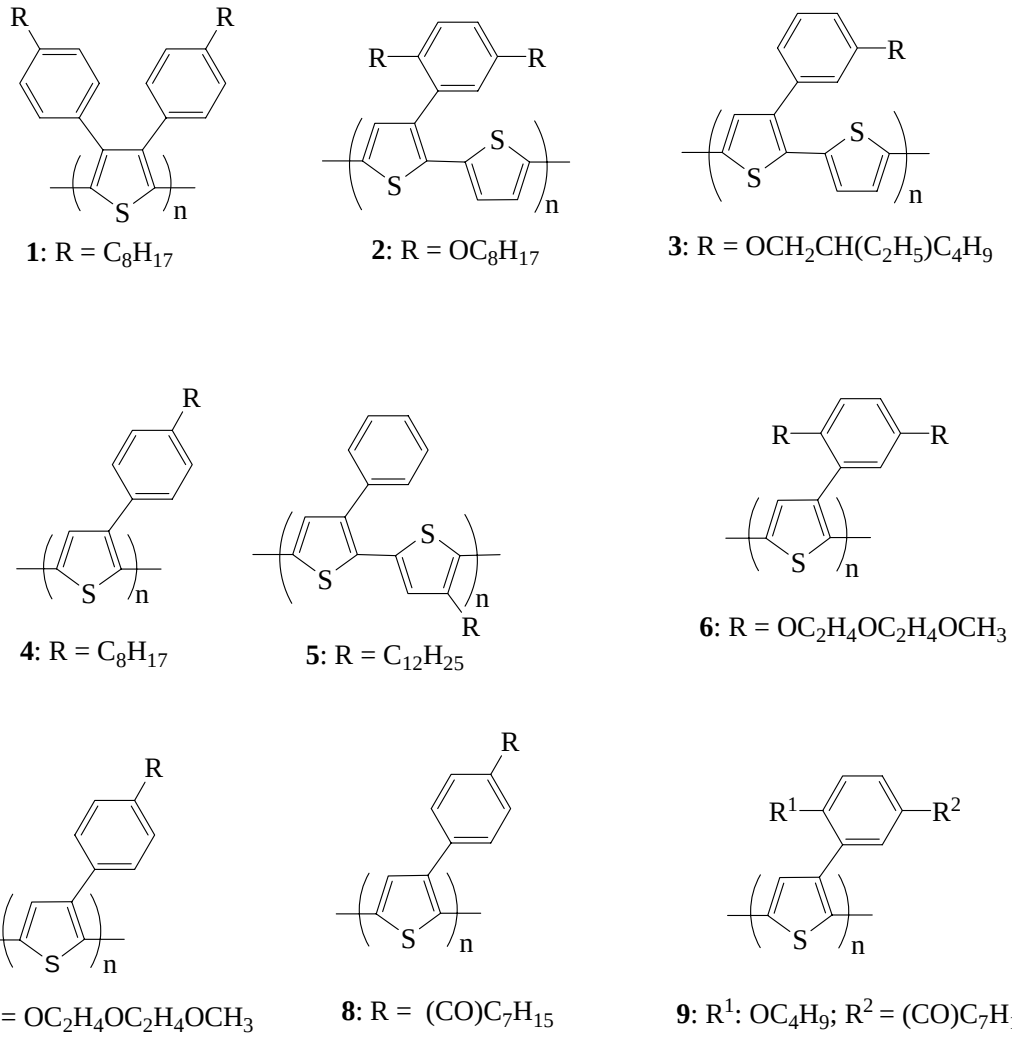

Figure 4.22 *Chemical structures of polymers **1-9.***

The symmetrically substituted polymer, polymer **1**, remains yellow when heated from room temperature up to 150^{o}C. The UV-Vis absorption spectrum does not also reveal any significant change in the maximum absorption. On the other hand, the other polymers undergo a continuous red or blue shift solid-state thermochromic transitions. When heated, the colours of most of the polymers change from red to yellow, returning to red when cooled to room temperature. For the polymers investigated, the changes in the absorption maxima at two different temperatures are summarized in Table 4.4.

Table 4.4 *Comparison of the absorption maxima at two different temperatures for the polymers investigated.*

Polymer	λ_{max}(nm) at 25°C	λ_{max}(nm) at 150°C	$\Delta\lambda_{max}$(nm)
1	347	347	0
2	515	491	24
3	497	463	34
6	518	473	45
7	494	553	59
8	461	545	84
9	505	467	38

Typical absorption spectra for the polymers that show some significant blue-shifted and red-shifted absorptions are shown in Figures 4.23 and 4.24.

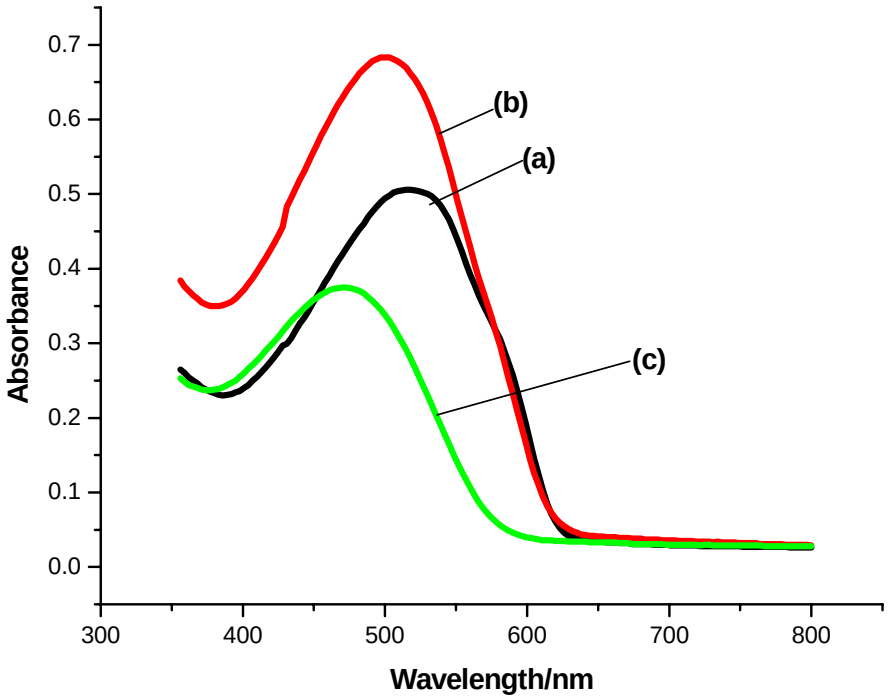

Figure 4.23 *UV-Vis optical absorption spectra of polymer **6** at: (a) 18°C, (b) 85°C, and (c) 150°C.*

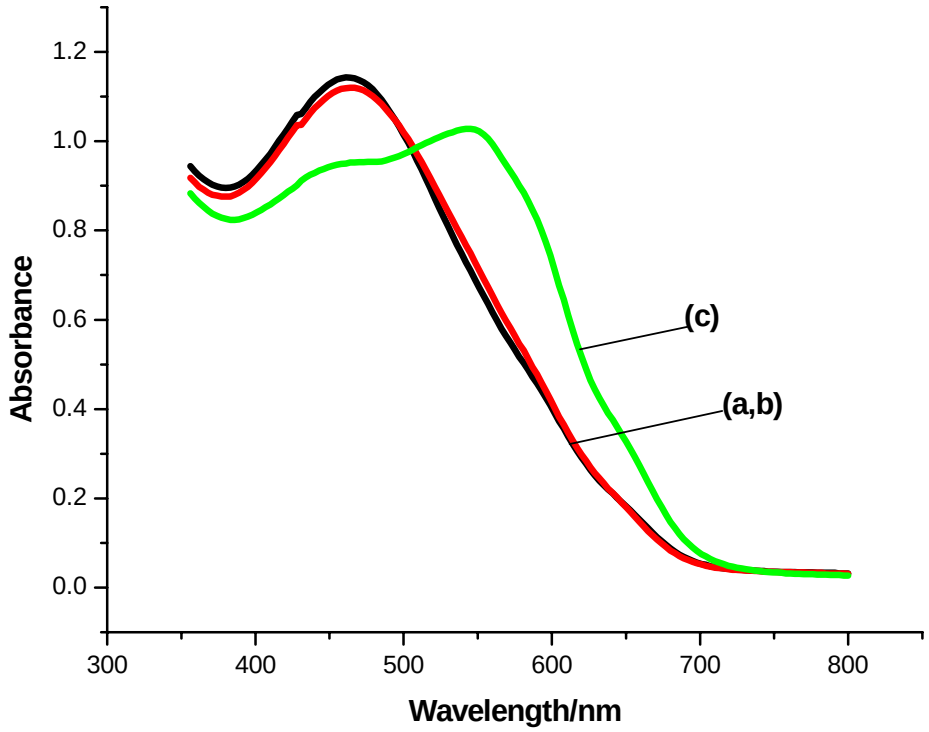

Figure 4.24 *UV-Vis optical absorption spectra of polymer **8** at: (a) 18°C, (b) 85°C, and (c) 150°C.*

Similarly, solvatochromic studies in mixtures of chloroform and methanol have revealed up to about 90 nm red shift in the maximum absorption, where the colour is changed from red to violet, as the mole fraction of methanol is increased, while there is no change in the maximum absorption wavelength for polymer **1**. Figure 4.25 shows some typical absorption spectra for polymer **1**, the polymer that does not show any chromic transition, while Figure 4.26 shows the absorption spectra for polymer **7**, the one that shows significant red shift. In order to understand the behaviour of these chromic transitions, theoretical quantum chemical calculations were carried out. The energy barrier for rotation of the dimeric structures of the monomers used to synthesise the polymers shown in Figure 1 are plotted as a function of the dihedral angle in Figures 4.27 and 4.28. The energy barriers for rotation to a planar structure are summarized in Table 4.5.

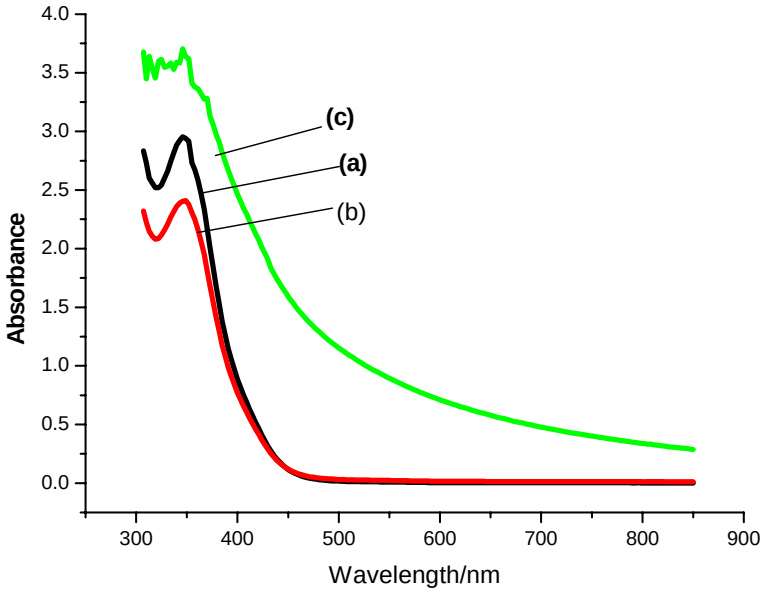

Figure 4.25 *UV-Vis optical absorption spectra of polymer **1** in chloroform/methanol mixtures at different mole fractions of methanol: (a) 0.0, (b) 0.36, and (c) 0.64.*

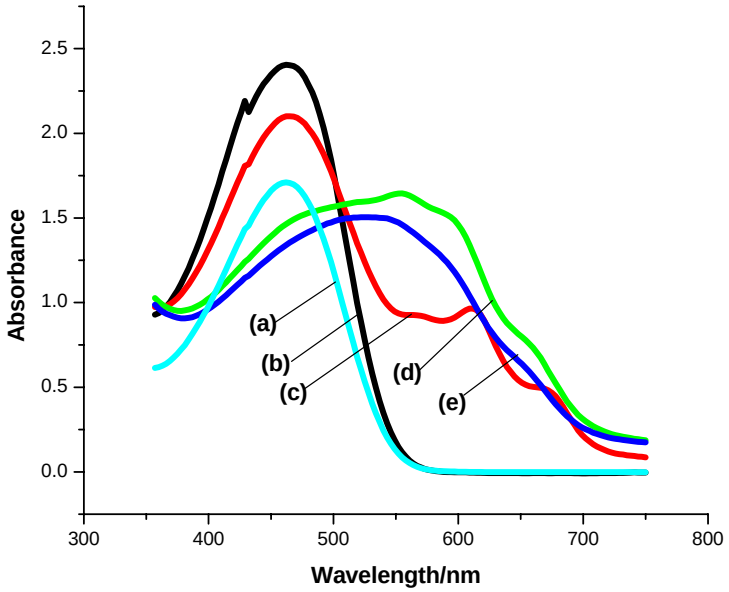

Figure 4.26 *UV-Vis optical absorption spectra of polymer **7** in chloroform/methanol mixtures at different mole fractions of methanol: (a) 0.0, (b) 0.36, (c) 0.64, (d) 0.85, and (e) 0.96.*

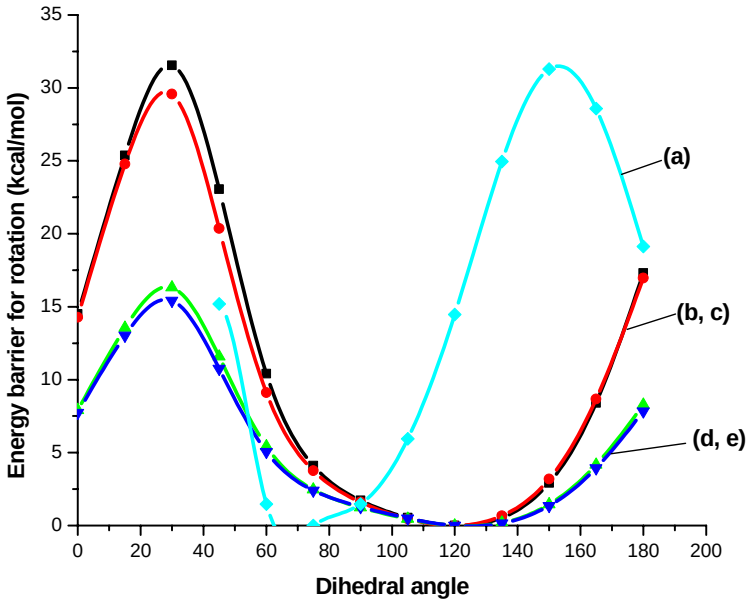

Figure 4.27 *Potential energy curve (a) polymer **1**, (b) polymer **2**, (c) polymer **3**, (d) polymer **4**, and (e) polymer **5**.*

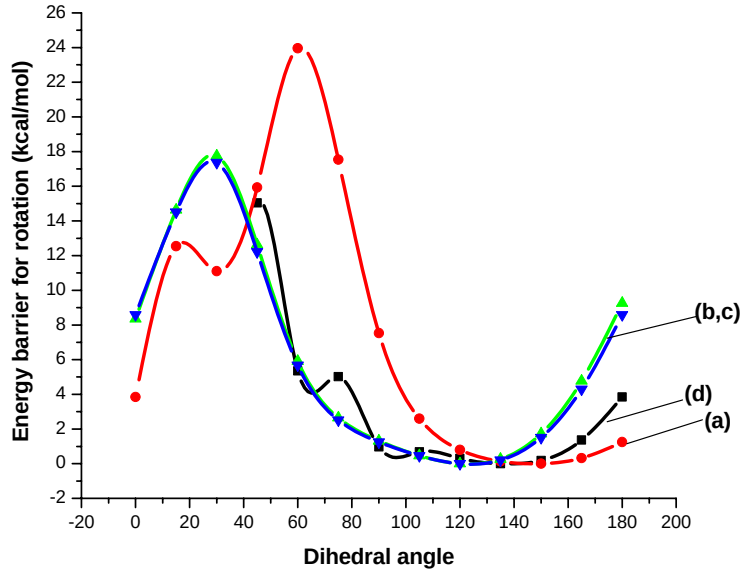

Figure 4.28 *Potential energy curve (a) polymer **6**, (b) polymer **7**, (c) polymer **8**, and (d) polymer **9**.*

The theoretical calculation shows that (see Figure 4.26 and Table 4.5) for polymer **1** the barrier for rotation to a planar structure is much higher than the rest of the polymers investigated, which is in agreement with the nonchromic behaviour of the polymer observed experimentally. On the other hand, polymers **2** and **3**, which show some degree of chromic

behaviour, still have large barrier for rotation as compared to polymers **4** and **5**, whose thermochromic and solvatochromic behaviours are reported in the literature [40-41].

Table 4.5 *Summary of the energy barrier to rotation to a planar structure for the dimer molecules of the polymers whose structures are shown in Figure 4.21.*

Molecule	Energy barrier against rotation (kcal/mol)	
	Syn	Anti
Polymer **1**	---	19.13
Polymer **2**	14.5	17.31
Polymer **3**	14.28	16.97
Polymer **4**	7.9	8.28
Polymer **5**	7.74	7.83
Polymer **6**	3.85	1.25
Polymer **7**	8.59	8.59
Polymer **8**	8.35	9.26
Polymer **9**	---	3.85

We note that the polymers reported in the literature (polymers 4 and 5) are regioregular polythiophenes. Therefore, as can be seen from the results of the theoretical calculations, we conclude that regioregular phenyl-substituted polythiophenes show more pronounced solvatochromic and thermochromic behaviours than the phenyl-substituted polybithiophenes. Both experimental and theoretical calculations on other similar phenyl-substituted regioregular polythiophenes further confirm this conclusion as observed in polymers **6**, **7** and **8**. For polymers **6**, **7** and **8**, the stable conformation is non planar and the barrier against planarity is relatively small as can be seen in Figure 4.28 and Table 4.5. The calculated values of the energy barriers against rotation are close in value with similar phenyl-substituted polythiophenes reported in the literature [40-41].

4.4 Conclusions

In this work we have shown a soft lithographic method for patterning the electrochromic polymer PEDOT-PSS on ITO/glass electrode. With patterned gratings both our *ex-situ* and *in-situ* spectroelectrochemical studies clearly show that one can obtain better coloration efficiency in the electrochromic grating. We have also shown the optical and electrochromic properties of oligoethylene oxide and alkoxy-substituted polythiophenes both in single and

double layer structures using both ex-*situ* and *in-situ* spectroelectrochemical studies. Both polymers are potentially useful in electrochromic devises and further stability studies are being under investigation.

The thermochromic and solvatochromic properties of several phenyl-substituted polybithiophenes and polythiophenes were investigated. We observed that highly sterically hindered phenyl-substituted polythiophenes do not show chromic behaviour. We have also noted that regioregular phenyl-substituted polythiophenes show more pronounced thermochromism and solvatochromism than the phenyl-substituted polybithiophenes. Among the regioregular phenyl-substituted polythiophenes some show blue-shifted absorption band while some show red-shifted absorption band upon heating. Both show red-shifted absorption bands upon increasing the amount of the more polar solvent (methanol) whose dissolving power for the polymers decreases favouring the formation of aggregates and increased effective conjugation. This is explained by the possibility of conformational transition between less conjugated, non-planar and more-conjugated, planar structures upon heating and changing the polarity of the solvent. Attempt has been made to explain these chromic transition by optimizing the dimers of the polymers and calculating the energy barrier for rotation from the most stable conformer to a planar structure using the HF SCF quantum chemical method and 3-21G* basis set.

4.5 References

1. A. Kumar, D. M. Welsh, M. C. Morvant, F. Piroux, K. A. Abboud, J. R. Reynolds, *Chem. Mater.,* **10** (1998) 896.
2. D. M. Welsh, A. Kumar, E. E. Meijer and J. R. Reynolds, *Adv. Mater.,* **11** (1999) 1379.
3. G. A. Sotzing, J. R. Reynolds and P. J. Steel, *Chem. Mater.,* **8** (1996) 882.
4. Y. Ohsedo, I. Imae and Y. Shirota, *Electrochim. Acta,* **45** (2000) 1543.
5. W. A. Gazotti Jr, G. Casalbore-Miceli, S. Mitzakoff, A. Geri, M.C. Gallazi and M. – A. De Paoli, *Electrochim. Acta,* **44** (1999) 1965.
6. J. L. Boehme, D.S.K. Mudigonda and J.P. Ferraris, *Chem. Mater.,* **13** (2001) 4469.
7. D. L. Meeker, D. S. K. Mudigonda, J. M. Osborn, D. C. Loveday and J. P. Ferraris, *Macromolecules,* **31** (1998) 2943.
8. Xia, Y.N. and G.M. Whitesides, *An. Rev. Mater. Sc*., **28** (1998) 153.
9. L.S. Roman, O. Inganäs, T. Granlund, T. Nyberg, M. Svenson, M. R. Anderson and J.C. Hummelen, *Adv. Mater.,* **12** (2000) 189.
10. F. Zhang, T. Nyberg and O. Inganäs, *Nanoletters,* **2** (2002) 1373.
11. K. S. Schanze, T. S. Bergstedt, B. T. Hauser, and C. S. P. Cavalaheiro, *Langmuir,* **16** (2000) 795.
12. X.J. Dang, A.M. Massari, and J.T. Hupp, *Electrochem. and Solid State Lett*., **3** (2000) 555.
13. A.M. Massari, K.J. Stevenson and J.T. Hupp, *J. Electroanal. Chem.,* **500** (2001) 185.
14. T.S. Bergstedt, B.T. Hauser, and K.S. Schanze, *J. Am. Chem. Soc.,* **116** (1994) 8380.
15. K.S. Schanze, T.S. Bergstedt, and B.T. Hauser, *Abstracts of the 209th American Chemical Society*, p**.** 310.
16. K.S. Schanze, T.S. Bergstedt, and B.T. Hauser, *Adv. Mater.,* **8** (1996) 531.
17. P. Anderson, D. Nilson, O. O. Svensson, M. Chen, A. Malmström, T. Remonen, T. Kugler, and M. Berggren, *Adv. Mater.,* **14** (2002) 1460.
18. O. Inganäs, in *Handbook of Organic Conductive Molecules and Polymers,* Vol. 3, *Conductive Polymers: Spectroscopy and Physical Properties*, Nalwa, H.S. (Ed.); Wiley: New York; **1997**; p 787.
19. O. Inganäs, *Trends Polym. Sci.,* **2** (1994**)** 189.
20. P. Blondin, J. Bouchard, S. Beaupre,; M. Belletete, G. Durocher and M. Leclerc, *Macromolecules,* **33** (2000**)** 5874.

21. G. Dufresene, J. Bouchard, M. Belletete,; G. Durocher and M. Leclerc, *Macromolecules* ,**33** (2000**)** 8252.
22. F. Bertinelli, P. Costa-Bizzarri, C. Della-Casa and M. Lanzi, *Spectrochimica Acta Part A*, **58** (2002**)** 583.
23. K.P.R. Nilsson, M.R. Andersson and O. Inganäs, *J. Phys.: Condens. Matter*, **14** (2002**)** 10011.
24. M. Leclerc, *Adv. Mater.*, **11** (1999) 1491.
25. L.M. Goldenberg, M.B. Bryce and M.C. Petty, *J. Mater. Chem.*, **9** (1999) 1957.
26. G. Mauthner, F.P. Wenzl, M. Collon, M. Bougettaya, J.R. Reynolds, G. Leising and E.J.W. List, *Synth. Met.*, **139** (2003) 613.
27. A.A. Ho and M. Leclerc, *J. Am. Chem. Soc.*, **125** (2003) 4412.
28. M. Leclerc and K. Faid, in *Handbook of Conducting Polymers*, 2nd Ed., Marcel Dekker: New York; 1998; p 695.
29. N. DiCesare, M. Belletete, C. Marrano, M. Leclerc and G. Durocher, *J. Phys. Chem. A,* **102** (1998) 5142.
30. N. DiCesare, M. Belletete, C. Marrano, M. Leclerc and G. Durocher, *J. Phys. Chem. A,* **102** (1998) 2700.
31. E. Orti, P.M. Viruela, J. Sanchez-Marin and F. Tomas, *J. Phys. Chem.*, **99** (1995) 4955.
32. H. Hernandez and J.T.L. Navarrete, *J. Chem. Phys.*, **101** (1994) 1369.
33. P.M. Viruela, R. Viruela, E. Orti, J.L. Bredas, *J. Am. Chem. Soc.*, **119** (1997) 1360.
34. T. Johansson, *Electroactivity of Conjugated Polymers*, Ph.D. Thesis, Linkoping University, Sweden, 2003.
35. L.S. Roman, *Organic Photodiodes: Optical, Electric and Morphological Aspects of Polymer Based Devices*, Ph.D. Thesis, Linkoping University, Sweden, 2000.
36. Gaussian 98, Revision A.6, 1998.
37. L.-M. Haung, T.-C. Wen and A. Gopalan, *Synth. Met.*, **130** (2002) 155.
38. C. L. Gaupp, D. M. Welsh, R.D. Rauh and J.R. Reynolds, *Chem. Mater.*, **14** (2002) 3964.
39. J. Roncali and F. Garnier, *J. Phys. Chem.*, **92** (1988) 833.
40. W. Mammo and M.R. Andersson, *Bull. Chem. Soc. Ethiop.*, **12** (1998) 141.
41. D.R. Greve, J.J. Apperloo and R.A. Janssen, *Eur. J. Org. Chem*. (2001) 3437.

Appendix A: Computational Methods Employed

This appendix provides a brief, non-mathematical description of *ab-initio* and semi-empirical quantum mechanical methods used in this thesis.

A.1. *Ab-initio* Methods

The term *ab-initio* is Latin for ``from the beginning." This name is given to computations that are derived directly from theoretical principles with no inclusion of experimental data. This is an approximate quantum mechanical calculation. The approximations made are usually mathematical approximations, such as using a simpler functional form for a function or finding an approximate solution to a differential equation.

Three approximations are required to go from the full many-electron Schrödinger equation to practical *ab-initio* methods:

1. Separation of nuclear and electron motions (the Born-Oppenheimer approximations). In effect, what this says is that “from the point of view of the electrons, the nuclei are stationary”. This is actually quite reasonable; while the nuclei are moving quite fast, their motion is very slow when compared to the motions of electrons. The Born-Oppenheimer approximation eliminates the nuclear kinetic energy in the Hamiltonian and leads to a constant nuclear-nuclear potential energy term. In so doing, it eliminates the mass dependence in what is now referred to as the electronic Schrödinger equation.
2. Separation of electron motions (the Hartree-Fock approximation). What is actually done is to represent the many-electron wavefunction as a sum of products (in the form of a determinant) of one-electron wavefunctions, the spatial parts of which are termed molecular orbitals.
3. Representation of the individual molecular orbitals in terms of linear combinations of atom-centered basis functions or atomic orbitals (the LCAO

approximation). This reduces the problem of finding the best functional form to the much simpler problem of finding the best set of linear coefficients.

These three approximations lead to the Roothan-Hall equations, the computation costs of which scales formally as the fourth power of the total number of atomic orbitals. These equations are not solvable in closed form; rather their solution requires self-consistent-filed (SCF) procedure.

A.2 Basis sets

A basis set is a set of functions used to describe the shape of the orbitals in an atom. All present day molecular orbitals methods make use of Gaussian basis functions, written in terms of polynomials in x, y, z multiplying and exponential in r^2:

$$x^l y^m z^n \exp(\alpha r^2)$$

α is a constant which controls the radial extent of the function. These functions are by convention named s, p, d, etc, depending on the order of the polynomial. The sum of the integrals l, m, n is 0 for an s function, 1 for a p function, 2 for a d function, etc.

The simplest (smallest) possible atomic orbital representation is termed a minimal basis set. This comprises only that number of functions required to accommodate all of the electrons of the atom, while still maintaining overall spherical symmetry. This requires a single (1s) function for hydrogen, five functions (1s, 2s, $2p_x$, $2p_y$, $2p_z$) for first-row elements carbon to fluorine, and nine functions (1s, 2s, $2p_x$, $2p_y$, $2p_z$, 3s, $3p_x$, $3p_y$, $3p_z$) for second-row elements silicon to chlorine, and so forth.

Minimal basis sets are not capable of adequately describing non-spherical (anisotropic) electron distributions in molecules. This is because the individual basis functions are either themselves spherical (s functions), or come in sets of equivalent functions which uniformly span a spherical space (p functions). The simplest remedy for any problems such a restriction might cause is to “split” the valence description into “inner” and “outer” components.

Among the most simple split-valence basis set is 3-21G. This uses three Gaussian functions to represent each non-valence atomic orbital, and two and one Gaussians, respectively, to represent the "inner" and "outer" components of each valence shell orbital. While 3-21G performs quite well for structure and energetic comparisons involving molecules comprising hydrogen and first-row elements only, it often performs poorly in the description of molecules incorporating second-row and heavier main-group elements. Adequate descriptions here have been found to require incorporation of unoccupied (in the atom) but energetically low-lying d-type functions. A very simple representation of this type is the 3-21G* basis set. The "*" indicates addition of d-type functions to second-row (and heavier) elements.

A.3 Semiempirical Methods

A major drawback with *ab-initio* HF calculations is the number of two-electron integrals that have to be calculated. If K is the number of basis set functions used, the number of two-electron integrals that have to be calculated is of the order of $K^4/8$. Hence, for large systems, *ab-initio* HF calculations become impractical to perform. Semiempirical methods make it possible to calculate very large systems yet obtain near *ab-initio* quality results. Approximations used in these methods include evaluation of certain integrals by use of empirical data, neglect of some types of one- and two-electron integrals, and restricting the wavefunctions to include only the valence electrons. In this thesis the modified neglect of diatomic overlap (MNDO) and the Austin Model 1 (AM1) methods which are incorporated into several popular semiempirical programs are used for qualitative results.

A.4 References

1. PC SPARTAN plus, Tutorial and User's Guide, Wavefunction, Inc., USA, 1997.
2. J.B. Foresman and E. Frish, Exploring Chemistry with Electronic Structure Methods, 2nd Ed., Gaussian, Inc., USA, 1996.
3. D.C. Young, Computational Chemistry, John Wiley & Sons, New York, 2001.
4. M. Fahlman, PhD Thesis, Linköping University, Linköping, 1995.

ADDIS ABABA UNIVERSITY
GRADUATE STUDIES

Electrochemical and Optical Studies of Electronically Conducting Polymers for use in Electronic Devices

BY: Shimelis Admassie Molla

Department of Chemistry
Faculty of Science

Approved by the Examining Board

Prof. Dr. Lothar Dunsch _____
External Examiner

Prof. Theodros Solomon _____
Advisor

Dr. Teketel Yohannes _____
Advisor

Dr. Ahmed Mustefa _____
Examiner

Dr. Mesfin Redi _____
Examiner

Dr. Wendimagegn Mammo _____
Examiner

This is what the LORD says:

"Let not the wise man boast of his wisdom
or the strong man boast of his strength
or the rich man boast of his riches,
but let him who boasts boast about this:
that he understands and knows me,
that I am the LORD, who exercises
kindness,
justice and righteousness on earth,
for in these I delight,"
declares the LORD
Jer. 9:23-24

DECLARATION

This thesis is my original work and has not been presented for a degree in any other university, and that all sources of material used for the thesis have been duly acknowledged.

Name: Shimelis Admassie

Signature:

Place and date of submission:

School of Graduate Studies

Addis Ababa University

May 2006

The thesis has been submitted for examination with our approval as university advisors.

Theodros Solomon

Professor of Chemistry

Addis Ababa University

Teketel Yohannes

Associate Professor of Chemistry

Addis Ababa University